Climatic, environmental changes and human impacts in Central Africa over the last 10 ka inferred from organic biomarkers

Valentine Schaaff

THESE

en vue de l'obtention du grade de Docteur, délivré par

l'ECOLE NORMALE SUPERIEURE DE LYON

Ecole Doctorale N° 341
Ecosystèmes Evolution Modélisation Microbiologie (E2M2)

Discipline : Sciences de l'univers

Soutenue publiquement le 22/11/2023, par :

Valentine Schaaff

Climatic, environmental changes and human impacts in Central Africa over the last 10 ka inferred from organic biomarkers

Changements climatiques, environnementaux et impacts anthropiques en Afrique Centrale durant les 10 derniers ka à partir de l'étude des biomarqueurs lipidiques

Devant le jury composé de :

ALEXANDRE, Anne	Directrice de recherche, Aix-Marseille Université	Rapporteure
DUBOIS, Nathalie	Professeure, ETH-EAWAG Zurich	Rapporteure
COFFINET, Sarah	Maitresse de conférences, Université de Rennes	Examinatrice
JACOB, Jérémy	Directeur de recherche, Université Paris Saclay	Examinateur
MONTADE, Vincent	Chargé de recherche, Université de Montpellier	Examinateur
RUSH, Darci	Chercheuse, NIOZ	Examinatrice
GROSSI, Vincent	Directeur de recherche, Université Lyon 1	Examinateur
MENOT, Guillemette	Professeure, ENS de Lyon	Directrice de thèse

Remerciements

Je teins tout d'abord à remercier tous les membres de mon jury de thèse : Anne Alexandre, Nathalie Dubois, Sarah Coffinet, Jérémy Jacob, Vincent Montade et Darci Rush pour avoir accepté d'évaluer ma thèse. Merci pour vos retours et pour les discussions que nous avons pu avoir le jour de la soutenance.

Ensuite, je voudrais remercier mes directeurs.trices/encadrants de thèse : Guillemette Ménot, Vincent Grossi et Matthew Makou pour tout ce que vous m'avez apporté durant cette thèse. Merci beaucoup pour toutes les opportunités et le soutien que vous m'avez offert durant ma thèse que ce soit au labo, de pouvoir aller sur le terrain ou en conférences ou encore pour tout le bagage scientifique que m'avez transmis durant ces 3 derniers années. Merci à tous les trois pour votre bienveillance au quotidien. Guillemette, merci pour m'avoir fait confiance avec ce projet malgré les petites mais nombreuses digressions par rapport au sujet initial ! Merci aussi de m'avoir donné l'opportunité d'aller sur le terrain et merci d'avoir toujours le bon mot dans les bons moments mais aussi les moments de stress ou de doute. Vincent, merci de m'avoir fait découvrir la diversité de la géochimie organique et de m'avoir poussé à sortir des sentiers battus, ma thèse serait bien triste sans les hopanes, les botryo, et tous ces petits composés qui n'attendent encore que d'être mieux compris… Matt, merci de m'avoir transmis tes connaissances sur l'analyse des alcanes depuis la préparation des échantillons jusqu'à l'interprétation en passant par les analyses.

Je tiens aussi à remercier toutes les personnes de l'ANR Tapioca pour avoir suivi ce projet de thèse et les résultats avec attention ! Un grand merci donc à Pierre Deschamps, David Sebag, Yannick Garcin, Bruno Hamelin et Geoffroy de Saulieu pour toutes les discussions passées et à venir sur ce projet et pour votre aide à différents niveaux et moments de ma thèse. Merci David pour ton aide sur l'écriture du premier article sur la tourbière de NGaoundaba. Merci à Pierre pour cette expérience inoubliable qu'a été le carottage de la tourbière en 2023. Merci à Geoffroy et Pascal Nlend pour m'avoir transmis un peu de la culture camerounaise lors du terrain au Cameroun. Merci à tous de m'avoir transmis une part de votre expertise pendant ces trois dernières années !

Je remercie également Salomé, Ingrid et Balkis pour votre aide au labo car un labo ne serait pas grand-chose sans les personnes qui participent tous les jours à le faire tourner. Merci pour votre aide et vos conseils sur l'analytique. Merci Salomé pour ton écoute et ton soutien que ce soit dans la vie pro ou perso. Merci à Nour et Sébastien pour votre aide lors de vos stages, je suis très contente d'avoir pu vous faire découvrir un petit peu de NGaoundaba même pour un petit mois.
Merci à Louis Rouyer d'avoir ressorti ton travail de master pour retravailler sur des composés au nom obscur mais sommes toutes intéressants !

Je remercie toutes les personnes qui nous ont aidé lors de notre terrain au Cameroun en Mars 2023 et notamment le Professeur NGounou NGatcha de l'université de NGaoundéré pour son accueil et son aide à NGaoundéré ainsi que la délégation IRD au Cameroun. Merci aux étudiants de l'université de NGaoundéré qui nous ont aidé lors du carottage quelle que soit les conditions météo ! Merci à Aboukar de me faire découvrir ta culture et ton pays ☺, pour ton soutien et pour tous les updates sur la tourbière de NGaoundaba !

Merci à tous les membres du laboratoire de Géologie de Lyon que j'ai pu croiser lors de mon parcours que ce soit pendant ma thèse ou avant. Je remercie notamment toutes les personnes du R6 pour votre présence au quotidien ainsi que les nombreux doctorants, post-doctorants, permanents dont j'ai pu croiser la route au bâtiment Géode à l'occasion d'un repas, d'un goûter ou autre et notamment Anastasis, Laëtitia, Elena, Selma, Antoine M., Matthieu V. et Nicolas P. Merci à Alex, co-bureau du R6 de partager ta passion des orogenèses varisques et anté-varisques avec moi bien que je ne sois pas un public très qualifié en la matière et merci pour ces bons moments partagés autour de gâteaux ou à observer des faucons crécerelles depuis la fenêtre de notre bureau (et ca c'est quand même la classe) (et merci pour ce très bel échantillon de BIF qui rend jaloux tous mes camarades d'agreg !!!). Côté ENS, je remercie également toutes les personnes que j'ai pu croiser tout au long de ma thèse. Du côté des « anciens » thésards merci notamment à Pierre-Jean, Delphine, Thibault C. et Sam. Merci à mes super co-bureaux du M8 : Alexandra, Enguerrand et Marwane, merci pour nos discussions au quotidien sur tout et n'importe quoi, pour les fous rires, les râlages. Merci Alexandra pour nos petites pauses goûters, nos échanges de thés et de biscuits, pour ta bonne humeur et ta gentillesse, à tous les cookies passés et à venir ! Merci Marwane pour ta bonne humeur (promis c'est pas écrit sous la contrainte), de partager avec moi le côté bordélique du bureau et pour la petite dose de sarcasme dont on a tous besoin dans la vie (même si parfois ca me fait marmonner). Merci Enguerrand pour les updates politiques twitters et pour toutes les discussions et débats politico-sociaux et fait divers pour se rendre compte qu'au final, la plupart du temps on est du même avis. Merci à Valentin, co-thésard de 2020-2023 pour avoir rendu moins solitaire cet été de rédaction au labo. Merci aussi à Cécile, Danaé, Asma, Line, Laëtitia, Marianne, Marine, Laura, Clothilde, Camille et Mathias, etc.

Merci à tous mes ami.e.s en dehors du labo d'égayer le quotidien ! Merci à mes amies de lycées et de prépa pour les bons moments partagés au cours de ces dernières années. Merci à Aurélie et Marilou pour votre bonne humeur et nos rencontres fortuites ou pas. Merci à la prépamour, la meilleure promo d'agreg qui soit, merci pour toutes nos retrouvailles au cours de ces dernières années à travers la France, merci de partager vos tips pour réussir à comprendre quelque chose aux mutations de l'EN et de partager vos passions pour la botanique, l'ornitho, le palet vendéen, la crème de Bresse et j'en passe ! Merci au groupe des bios d'avoir adopté une géologue dans vos rangs et pour les bons moments qu'on a pu partager au cours de ces dernières années ! Merci aux gônes pour tout ce qu'on a vécu ensemble pendant ces trois années de thèse à Lyon car elles auraient été bien tristes sans vous ☺, merci pour toutes ces moments partagés entre repas/gâteau, film et sieste sur le canapé (avec un plaid de préférence), danse (pas souvent ok…), partie de jeu de société (de préférence coop), week-end rando … Merci Nico, co-TP, acolyte de toutes les sorties bota, co-chef pâtissier à de nombreuses reprises. Merci Adèle d'avoir été une des forces motrices de notre groupe même pendant le covid, pour ces batailles de boules de neige, ces balades dans les calanques et à la montagne, merci pour ta bonne humeur et ton énergie sans faille ! Merci Alice, d'être une superbe personne à la fois à l'écoute et attachée de tes convictions ! Merci Justine pour ta gentillesse, on a tous besoin d'un.e breton.ne dans sa vie ! Merci Nicolas L. d'avoir été un si bon amateur de gâteau, merci pour ces soirées jeu et crêpes ! Merci Octave pour supporter nos arrêts multiples lors des randos à chaque être vivant qui croise notre route…

Enfin, merci à mes sœurs, Camille et Myrtil, pour votre soutien de près ou de loin ces dernières années et d'être venues partager ma soutenance de thèse avec moi, la sororité vaincra :p !

Contents

Introduction

Why reconstructing past climate? Well, one of the most common answers to that question might be: “We need to understand the past in order to be able to plan the future” and I will come to that later on. Aside from this very pragmatic answer, reconstructing past climates and past environments provide us pictures of landscapes and places that are no longer existing. Each lake, peatland or speleothem is like a book that has been slowly written over thousands of years and is waiting for someone to read it. It has already taken several generations of scientists to learn how to unravel the paleoclimatic signal preserved in sediments and there is still many questions remaining and new questions coming up as we go into more and more detailed analyses of paleoclimatic archives. Paleoclimatology is gathering many disciplines focusing on pollen, lipids biomarkers, climate modeling, dust source tracing, etc.

In the present context of anthropogenic global warming, understanding how climate changes at different temporal and spatial scales become more and more important. Paleoclimate studies are necessary to understand climate forcing and are used to predict the future climatic changes and to calibrate and test the simulation of future climate change. In addition, understanding past changes in ecosystems can guide politic and economic decisions to help human population to face climate change and protect biodiversity endangered by climate disruption. Countries with high demography are particularly threaten by rapid climate changes.

Sub-Saharan Africa counts many countries topping the list of highest demographic development and present key environments that need to be protected (e.g., Feka and Ajonina, 2011; Abernethy et al., 2016). 7000 years ago, most of the Sahara was covered by savannas triggered by increased precipitation during the so-called “Holocene African Humid Period” (AHP) (e.g., DeMenocal et al., 2000; Claussen et al., 2017; Tierney et al., 2017b). This period had many consequences on human population and human evolution (e.g., Dunne et al., 2012; Larrasoaña et al., 2013; Larrasoaña, 2021). At lower latitude, increase in precipitation have been reported together with an extension of biome farther north and south from the equator (e.g., Gasse, 2000; Schefuß et al., 2005; Vincens et al., 2010). In addition to the African Humid Period, shorter scale events such as drying event or forest crises are recorded but not widespread in tropical Africa (Gasse, 2000). In West and Central Africa, pioneer works, mainly based on pollen, diatoms and sedimentological analyses, have revealed the complexity of climate changes, with different timings for the beginning and end of the AHP and/or short events such as the Younger Dryas recorded unevenly between sites (e.g., Gasse et al., 1990;

Maley, 1991; Reynaud-Farrera et al., 1996; Salzmann et al., 2002). Since then, new proxies have been applied such as the isotopic composition of n-alkanes (e.g., Shanahan et al., 2015; Garcin et al., 2018) and new sites have been explored (e.g., Nguetsop et al., 2013; Vincens et al., 2010; Garcin et al., 2022) to improve our understanding of climate variation during the Holocene in West and Central Africa. However, records spanning nearly the entire Holocene are still sparce and sometimes discontinuous or with poor time resolution.

This thesis focuses on tropical Africa and presents a new paleoclimatic and paleoenvironmental record from North East Cameroon. The aim is to use lipid biomarkers to propose new high-resolution records of precipitation, temperature and environmental changes over the past 10 ka. Until now, most work in West and Central Africa have focused on lake and marine records (e.g., Gasse, 2000; Garcin et al., 2018; Schefuß et al., 2005; Yacoub et al., 2023). This study is based on a peatcore from the NGaoundaba peat deposit, a sedge-dominated peat deposit from the Adamawa Plateau.

This work is part of the ANR project TAPIOCA "Temperature and Precipitation reconstructions in Central Africa and recently developed organic biomarkers" regrouping collaborator with various expertise (organic and inorganic geochemistry, sedimentology, archeology, palynology, etc). A 10-meter core provide a continuous, high-resolution records of the end of the African Humid Period and of short climatic events during the Holocene. Based on lipid biomarkers data, this study further benefited from discussion with all the members of the TAPIOCA project, and complementary studies performed by collaborators of the project (pollen analyses, levoglucosan analyses, hydrological survey of the peat deposit) are still ongoing and will enrich the paleoclimatic record of the NGaoundaba peat deposit and our understanding of the site evolution throughout the Holocene.

In addition to paleoclimatic and paleoenvironmental interpretation, this thesis describes a large panel of lipid biomarkers to test recently developed proxies and expand the panel of lipid biomarkers that are commonly used in paleoclimatic reconstruction. Peat sediment contain a large amount and a huge diversity of lipid biomarkers and have great potential in paleoclimatic and paleoenvironmental reconstructions (Naafs et al., 2019). However, very few tropical peat deposits have been investigated, in particular those with settings similar to the NGaoundaba peat deposit (e.g., Aucour et al., 1996; Coffinet, 2015). For example, in the global calibration of temperature and pH reconstruction based on lipid biomarkers, African tropical peat deposits are barely represented (Inglis et al., 2018; Naafs et al., 2017b). Therefore, the specificities of these sites still need to be assessed and biomarkers distribution, abundance and isotopic composition need to be reported.

Structure of the manuscript:

Except for the “state of the art” and “study site” chapters, each chapter is in an article format with its own abstract, introduction and methods. The method sections may be redundant from one chapter to the other, but I tried to limit repetition and highlight the unique aspects of each chapter. The state of the art is kept (relatively) brief on purpose as some chapters include their own detailed “state of the art” section.

The manuscript is organized into 8 chapters. The first chapter briefly reviews the present and past climatic and environmental features of tropical Africa with a focus on West and Central Africa and introduces the lipid biomarkers that will be used in this manuscript. The second chapter briefly presents the study site. The third chapter is a published article (Schaaff et al., 2023) presenting the bulk organic data as well as a simple model to remove the decomposition signal from these data. Chapter 4 focuses on hopanes and brGDGTs and their use as pH proxies in peat by applying and comparing two recently published pH calibrations. Based on the carbon isotopic composition of hopanes, we also propose new constraints on the origin of C_{31} hopanes in peat. Chapter 5 covers the temperature and precipitation reconstructions based on brGDGTs and n-alkanes, respectively, from proxy validation to the presentation of the main paleoclimatic features. In chapter 6, we focus on two 1-ka climatic events observed at the NGaoundaba peat deposit. Starting from a local approach focusing on the environmental and ecological changes associated with these two events, we then try compare our observations with others records from tropical Africa and around the world. Chapter 7 presents a record of past methane cycling at the NGaoundaba peat deposit. We use the carbon isotopic composition of hopanes to trace methanotrophic activity in the NGaoundaba peat deposit and the distribution of isoGDGTs to track changes in past methanogenesis and we discuss the limits of these proxies in peat deposits. Finally, chapter 8 presents preliminary results on other lipid biomarkers (Des-A-triterpenoids and 5-n-alkylresorcinols) still rarely considered and which deserve further consideration.

Chapter 1: State of the art

Part 1: West and Central African climate: past and present dynamics

1. Essential features of present African climate

1.1. Climate zones of Africa

Contrasting climates are present in Africa, ranging from tropical rainforests to arid deserts (Figure 1). Climate zones form a global latitudinal gradient that is primarily determined by rainfall amounts. Western Central Africa has tropical climates from tropical rainforest to tropical monsoon and tropical savannah, with the coldest month's air temperature exceeding 18°C and high mean annual precipitation. Tropical rainforest is the climate zone closest to the Equator, with precipitation exceeding 60 mm during the driest month. The tropical monsoon climate is characterized by intermediate precipitation during the driest month, whereas the tropical savannah is characterized by low precipitation during the driest month.

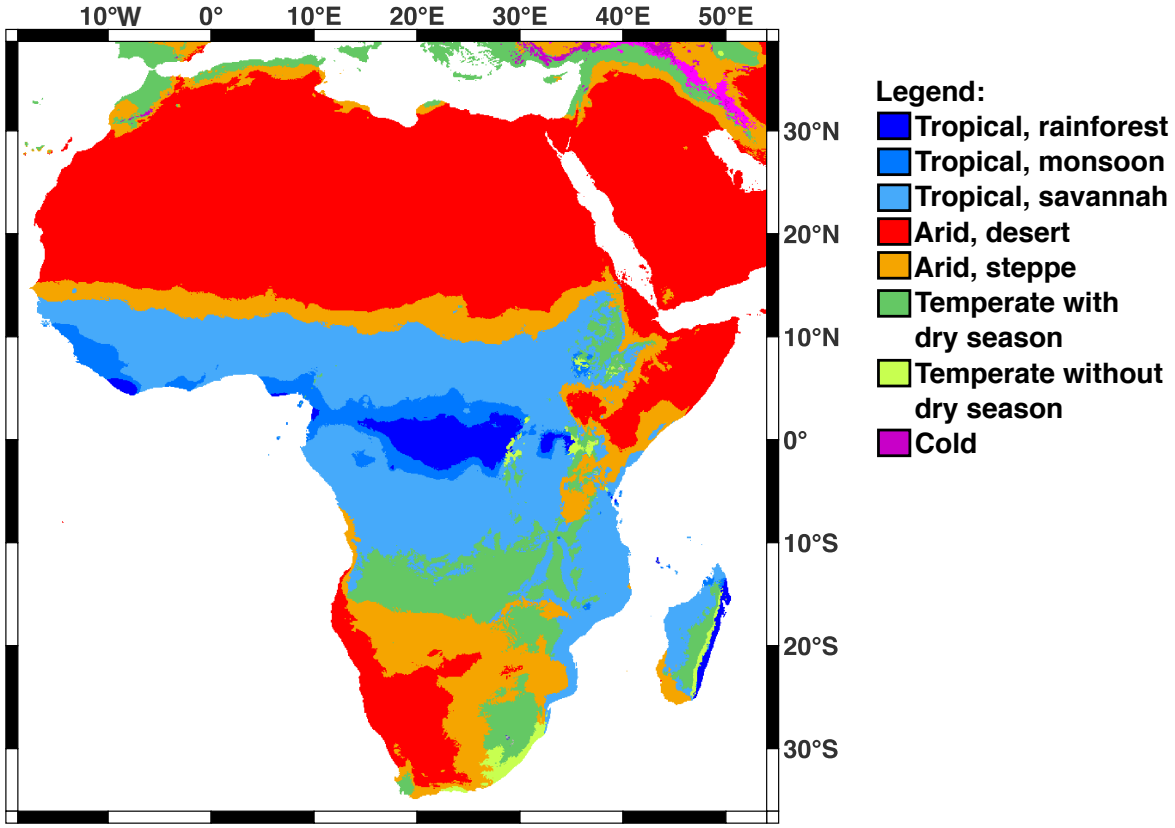

Figure 1: Simplified climate zones of Africa based on Köppen-Geiger climate classification for the present-day (1980-2016) after Beck et al. (2018). The Köppen-Geiger classification is based on patterns of seasonal precipitation and temperature corrected for topographic effect. The original classification from Beck et al. (2018) was simplified by merging some temperate climate zones together as they are not the focus of this study.

Temperate climates are uncommon but can be found at high elevations or in the continent's north and south, where they are influenced by extratropical atmospheric circulations. In response to these many contrasted climates, Africa has many different environments/biomes.

Briefly, in tropical and subtropical Africa, major biomes are tropical rainforest characterized by tropical evergreen trees, tropical seasonal forest are characterized by a mix of tropical evergreen and raingreen trees and tropical dry forest and savannah, which are characterized by different taxa of raingreen trees (Jolly et al., 1998 and references therein).

1.2. The classical picture of the ITCZ and of the West African Monsoon system

1.2.1. General circulation model and Hadley-cell

The greatest heating of air masses in the tropics is due to radiation and latent heat in the form of water vapor (Giannini et al., 2008). This warm and/or moistened air is light enough to rise (low pressure). During this process, the majority of the water vapor is lost through precipitation, releasing its latent heat and contributing to the rise of the air mass. Trapped at the top of the troposphere, the air masses move towards the subtropics and sink towards the surface near 30° latitude. This thermally-direct circulation pattern associated with tropical and subtropical heating is called the Hadley cell (Figure 2).

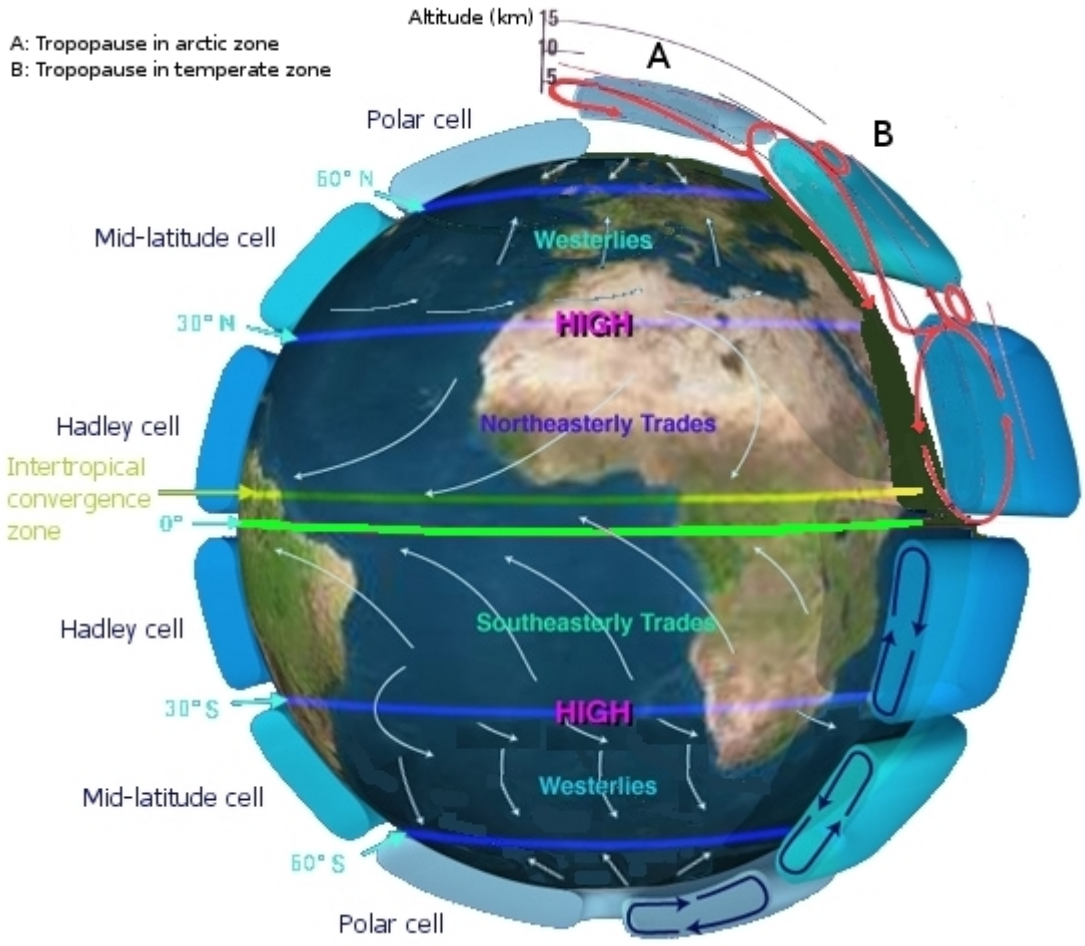

Figure 2: General circulation of the Earth's atmosphere created by the NASA and downloaded from Wikipedia Commons.

To supplement the Hadley cell circulation at the Earth's surface, trade winds blow from the high pressure of the subtropics to the low pressure of the tropics. Deviated by the Coriolis force, these winds blow from northeast in the Northern Hemisphere and southeast in the Southern Hemisphere and are this also known as Easterlies. In West Africa, the trade winds are known as the Harmattan. The northern and southern trade winds converge near the Equator to form the Intertropical Convergence Zone (ITCZ), forming the ascending branch of the Hadley cell. It is also sometimes defined as the region of maximum cloudiness (Holton et al., 1971) and is associated with the maximum rainfall (Sultan and Janicot, 2000).

1.2.2. Seasonality of precipitation in West Africa

Seasons in Africa are driven by the annual cycle of insolation and result from complex interactions between the atmosphere, land and oceans. Over the course of a year, the Northern and Southern Hemispheres experience variations in the intensity of sunlight due to the Earth's rotation around the Sun and the inclination of the Earth's rotational axis. In the tropics, this annual fluctuation is small but is enough to cause a seasonal shift of the ITCZ. The ITCZ moves north during Northern Hemisphere's summer and south during the Southern Hemisphere's summer (Figure 3). During the Northern Hemisphere's winter, the ITCZ is at its southernmost position and the Harmattan blows from the Sahara over West Africa. This dry wind brings fine dust and sand particles from the Sahara. The maximum solar heating occurs during summer. The high heat capacity and high thermal inertia of ocean water causes the ocean to warm slowly, while lands and soils have lower heat capacity and thermal inertia, resulting in rapid warming. This contrasting response to solar heating generates a tropical summer land-sea circulation, called the monsoon. As continents heat up quickly, the warm, dry air rises, creating low pressure zone over the land. This low-pressure area forces cooler moist air from the ocean to the land. As moist air rises over the land, it cools, reducing its ability to hold water resulting in heavy precipitation over the land. The air then returns to the ocean, completing the cycle of circulation. The winter monsoon circulation is the opposite of the summer monsoon, driving dry air from the continent to the ocean.

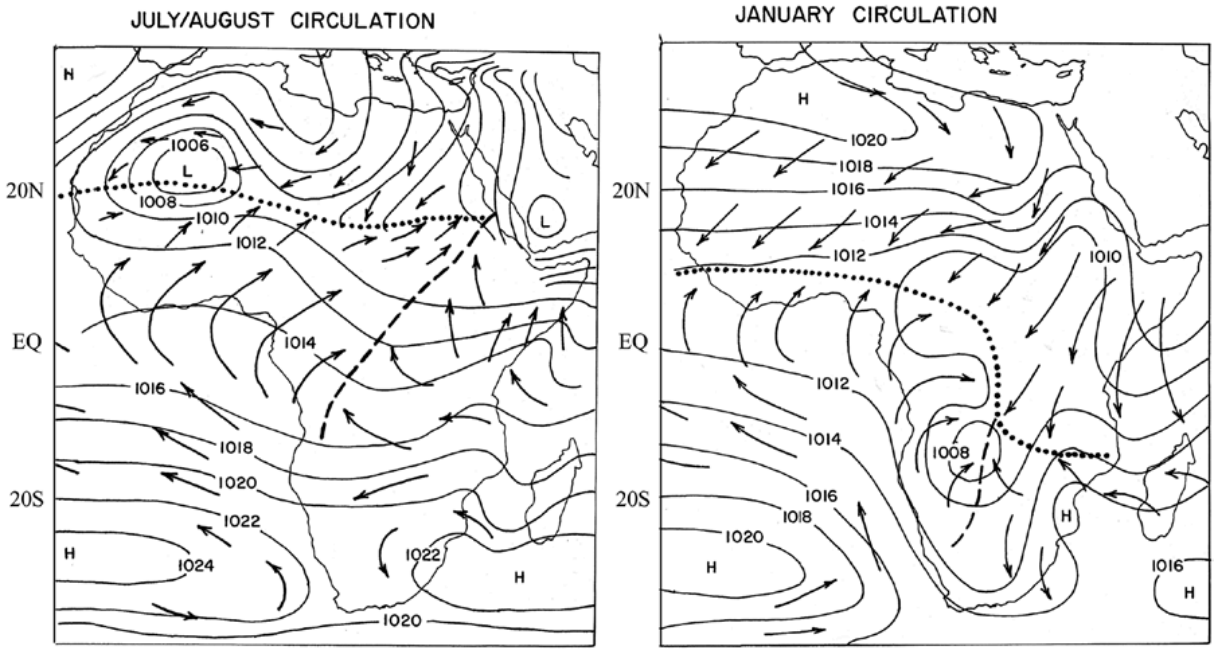

Figure 3: Seasonal changes of the position of the ITCZ resulting from the tilted rotation axis of the Earth around the Sun. During Northern Hemisphere's summer, the solar radiation is maximal in the Northern tropics and subtropics while during the Southern Hemisphere's summer, the solar radiation is maximal in the Southern tropics and subtropics. This seasonal shift of the solar radiation drives the migration of the ITZC. From Nicholson (2018).

As a result of the migration of the ITCZ, there are two belts of tropical zone with a single monsoon season, which are bracketing the equatorial zone characterized by two seasonal rainfall maxima. In paleoclimatic studies, the expansion of the ITZC further north and south may have modified not only the amount of precipitation but also the seasonality of rainfall, shifting from a single to a double maximum rainfall.

1.3. Revision of the classical model of the ITCZ

1.3.1. Limits of the classical model

At least in West Africa, the model described above is oversimplified, especially on land. Several meteorological observations contradict with the above-described model (Grist and Nicholson, 2001).

First, the zone of maximum cloudiness and precipitation zone does not coincide with the zone of winds convergence with a 500 km displacement. In the classical model, convection cannot be sustained when the depth of humid air is too shallow. However, Nicholson et al. (2009) show that this is not the case because the amount of vapor in the atmosphere is quite constant from 5 to 18°N in August.

Trade winds are typically weak over the continent. The ITCZ is rarely a continuous cloud line, but rather an ensemble of "cloud clusters" (Holton et al., 1971).

1.3.2. Revised picture of the Western and Central African monsoon

According to Nicholson (2009), the ITCZ in West Africa is decoupled from rainfall amount and distribution, and is instead controlled by the dynamics of the Easterly Jet (mid- and upper-level winds). The classic Hadley-type circulation model was reevaluated, and a more complex picture with two meridional overturning circulations was proposed (Figure 4) (Zhang et al., 2006; Nicholson, 2009).

Several studies also suggested that a significant part of moisture over West Africa may be recycled from local evaporation over the continent (Brubaker et al., 1993; Savenije, 1995).

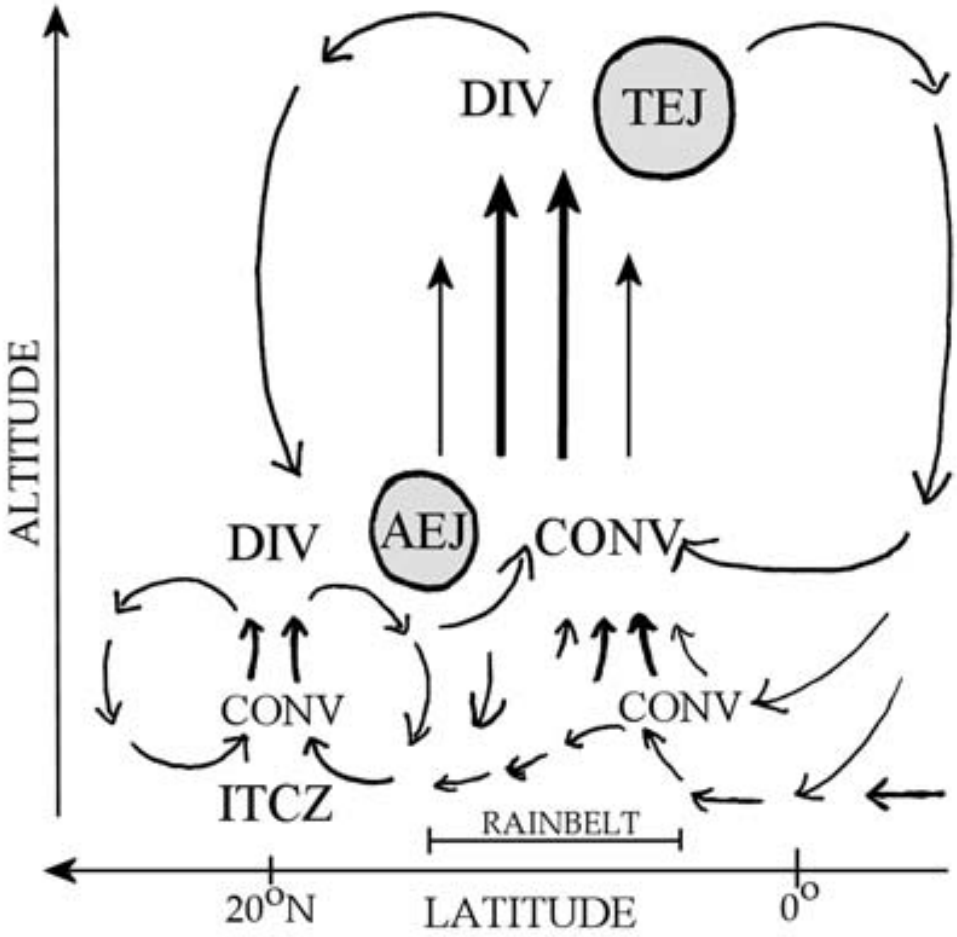

Figure 4: Revised picture of the West African monsoon from Nicholson (2009). Abbreviations: TEJ: Tropical Easterly Jet, AEJ: African Easterly Jet, Conv: Wind convergence, Div: Wind divergence.

In addition to these general models, local topography and coastal effects have a significant impact on circulation pattern and precipitation spatial distribution (Zhang et al., 2006). In Cameroon, the Cameroon mountain chain has a significant impact on rainfall distribution, and downscaling approaches of GCMs are required to evaluate the effects of large-scale climate forcing on local precipitation (Penlap et al., 2004). The complexity of atmospheric circulation

and rainfall distribution is reflected in the difficulty of obtaining accurate weather predictions in Cameroon (Igri et al., 2018).

1.4. Interannual and multidecadal climate variation over West Africa

Aside from the annual monsoonal system, Africa encounters significant interannual and multi-decadal rainfall variability as measured by rainfall stations over the last century. The 1950s were unusually wet, while the 1980s were unusually dry (Nicholson, 1981, 1993).
The characteristics of this multi-decadal variability are contrasted across Africa's different regions. Several causes have been proposed, including a dipole mode of variability in the Indian (Indian Ocean Dipole or IOD) and the influence of ENSO (El Niño-Southern Oscillation), particularly in equatorial east Africa and southern Africa (Nicholson and Selato, 2000; Hulme et al., 2001). In West and Central Africa, this interannual variability has been linked to variations in the intensity or latitudinal location of the easterly jets (AEJ and TEJ) (e.g., Fontaine and Janicot, 1992; Long et al., 2000; Grist and Nicholson, 2001). The relationship between this interannual rainfall variability, and the ITCZ is still controversial (e.g., Lamb, 1978; Nicholson, 1981; Fontaine and Janicot, 1992; Sultan and Janicot, 2000)

1.5. Implications for paleoclimatic and paleoenvironmental studies

While the old model of a unique Hadley cell and precipitation controlled by ITCZ displacement is still used in paleoclimatic and paleoenvironmental reconstructions in Western central Africa (e.g., Vincens et al., 2010; Nguetsop et al., 2013), the impact of Nicholson (2009)'s revised model must be evaluated.
The distance between the ITCZ (zone of trade winds convergence) and the tropical rainbelt is not constant (Grist and Nicholson, 2001), so the two terms cannot be switched. Among the paleoclimatic proxies that will be mentioned in this manuscript, hydrogen isotopic data records changes in precipitation (Sachse et al., 2012 and references therein) and thus is related to tropical rainbelt variation rather than the ITCZ directly. Similarly, pollen reflects changes in vegetation in the studied area that are primarily governed by modulating precipitation amount and seasonality or temperature (e.g., Lézine and Casanova, 1989; Vincens et al., 1998). However, many proxies are influenced by wind strength and direction as it modulates the inputs of pollen (e.g., Hooghiemstra et al., 1986; Autio and Hicks, 2004) and of lipid biomarkers such as n-alkanes partially transported in dust (e.g., Gagosian and Peltzer, 1986; Huang et al., 2000; Schefuß et al., 2003). Dust inputs record changes in wind trend and direction and are thus related to the ITZC rather than the tropical rainbelt (e.g., Gillette and Passi, 1988; Rea, 1994). Microbial biomarkers or diatoms are produced in situ or within the

catchment area; the production of these compounds is influenced by temperature, moisture content, pH, nutrient availability, and other factors. The production of these compounds is more likely to be influenced by precipitation rather than winds, but nutrient availability may be strongly dependent on dust input. Interannual variability in the distance between the rainbelt and the ITCZ has been reported associated with the displacement of jet winds which are modulated by sea-surface temperature gradient (Nicholson, 2009). Sea-surface temperature gradient present long-term variations that are modulated by millennial-scale trends (Cohen and Tyson, 1995).
In the remaining part of the manuscript, we will prefer to use the term tropical rainbelt instead of ITCZ.

1.6. Environmental response to present and future climate variability

Climate models predict changes in rainfall amount and seasonality associated as a result of global warming (Hulme et al., 2001). Furthermore, modeling studies indicate that human pressure through forest loss and degradation will superimpose to climate change and have a significant impact on vegetation by 2050 (Heubes et al., 2011). Degradation of soils, water resources, vegetation and fauna were reported by Mertz et al. (2012) over the past 20 years, while rainfall did not decrease during this period, but the seasonality of precipitation was affected.
Changes in ENSO-related rainfall variability are also suggested in response to climate warming, with more intense ENSO events (Timmermann et al., 1999; Collins, 2000). However, Collins 2000) highlights the complexity of ENSO response to climate changes with different climate models simulating different response of ENSO which may be associated with non-linear response increase greenhouse gases.

2. The Holocene African Humid Period

2.1. The three orbital parameters and the changes in insolation

The Earth's orbit changes over time. In the 1920s, Milankovitch proposed that the long-term climate of the Earth is determined by its position relative to the Sun. These long-term variations, the Milankovitch cycles, are defined by three parameters: eccentricity, obliquity or tilt, and precession (Milanković, 1920).
The eccentricity is defined as the elliptical shape of the Earth's orbit compared to a perfect circle. The eccentricity periods are estimated to be between 100 and 400 ka (Berger, 1977). Currently, the Earth is closest to the Sun on January 3 and farthest from the Sun on July 4, close to the Northern Hemisphere' winter and summer solstices respectively. This position

makes winter radiations slightly stronger and summer radiations slightly weaker in the Northern Hemisphere than a perfectly circular orbit, and vice versa for the Southern Hemisphere. The effect of Earth's eccentricity on seasonal contrast, on the other hand, is minor.

Obliquity or tilt is defined as the angle between the Earth's axis of rotation and a line perpendicular to the plane of the ecliptic. The obliquity has a periodicity of 41 ka (Berger, 1977). An increase in obliquity strengthens of the seasons in both hemispheres, especially at the poles.

The axial precession is the wobbling motion of the Earth on its axis. The precession of the equinoxes is formed by combining the precession of the ellipse and the rotation of the elliptical orbit of the Earth around the Sun. Changes in precession affect the position of the equinoxes and solstices around the Earth's orbit and, as a result, the seasonal contrast. The strongest precession cycle occurs around 23 ka (Berger, 1977).

Changes in the orbital parameters affect the amount of solar radiation received at the Earth's surface, as well as the distribution of solar radiation received by latitude and season. The amount of solar radiation is referred to as insolation.

2.2. Impact of change in orbital parameters on African climate

The control of the African monsoon by insolation was proposed by John Kutzbach in the 1980s (Kutzbach, 1981). During periods of high insolation, land heating and the associated land-sea circulation are stronger, resulting in an increase in rainfall. Furthermore, the tropical rain belt moves north and south in response to changes in the maximum solar heating location (Gasse, 2000). As a result, the precipitation seasonality is altered, with changes in rainy season length and possibly even a shift from a single to a double monsoon maximum.

Countless studies indicate that Africa experienced periods of increased precipitation due to monsoon strengthening : the African Humid Periods (AHP) (e.g., DeMenocal et al., 2000; Gasse, 2000; Shanahan et al., 2015; Skonieczny et al., 2015; Yacoub et al., 2023). The term AHP was proposed by deMenocal et al. (2000) to describe the more recent AHP: the Holocene AHP. The latter occurs between approximatively 15 and 5 ka (DeMenocal et al., 2000; Gasse, 2000), with a maximum humidity recorded between 9 and 6 ka (e.g., Leblanc, 2022). Throughout the rest of the manuscript the term AHP will refer to the Holocene AHP. The timing of the onset and termination of the AHP has been widely debated and is still debated, as is the abruptness of the AHP's termination (e.g., DeMenocal et al., 2000; Renssen et al., 2006; Shanahan et al., 2015). Precipitation changes during the AHP are closely related to changes in insolation (DeMenocal et al., 2000; Garcin et al., 2018).

Reconstructing precipitation changes is critical to understand the timing and termination of the African Humid Period, and many proxies were used to quantitatively or qualitatively reconstruct past precipitation changes. Reconstructions of lake levels were among the first techniques used to estimate the precipitation change in Africa (see Gasse, 2000 for a review). On the other hand, lake level variations are an indirect indicator of past changes in precipitation because they are also impacted by other parameters, particularly evaporation, which is strongly influenced by temperature (e.g., Gasse, 2000; Shanahan et al., 2007; Forman et al., 2014) and can present a significant response time to climatic changes (e.g., Sene and Plinston, 1994; Lézine et al., 2011). Hydrogen isotopic composition of leaf waxes δD_{wax} is a paleohydrological proxy (see Sachse et al., 2012 for a review). In tropical Africa, the δD_{wax} is primarily affected by the amount effect (Dansgaard, 1964; Rozanski et al., 1993) and has been proposed as quantitative proxy for rainfall (Niedermeyer et al., 2016). However, and specifically in continental settings, other parameters such as changes in the moisture sources can influence the δD_{wax} (Costa et al., 2014). Changes in moisture sources are more of a concern in East Africa than in West Africa, as the displacement of the Congo Air Boundary (CAB) during the African Humid Period may have altered the relative contribution of precipitation sources (Congo Basin/Atlantic Ocean or Indian Ocean) (Tierney et al., 2011b; Costa et al., 2014). Pollen or phytoliths can be used to trace past precipitation changes or as a proxy for water stress (Bonnefille and Chalié, 2000; Gajewski et al., 2002; Bremond et al., 2005)

The AHP had a variety of environmental effects, including:

- *Changes in vegetation.* The increased precipitation causes a greening of the Sahara. Pollen records and quaternary plants fossils show grasslands in what is now desert (Wickens, 1975; Neumann, 1989; Lézine, 2017), as well as a shift in biome limit further north (Amaral et al., 2013; Salzmann, 2000; Vincens et al., 2010).
- *Increased lake level and river flow.* Increases in lake level have been reported all over Africa during the AHP (Street-Perrott et al., 1989; Gasse, 2000; Tierney et al., 2011a, and reference therein) as have paleolakes and paleowetlands that dry out completely after the AHP (e.g., Gasse et al., 1990; Junginger and Trauth, 2013; Yacoub et al., 2023). For example, the lake Chad, covering a surface of 25 10^3 km^2 for a volume of water around 40-100 km^3 in the 1960s (Yunana et al., 2017), reached a surface of 340 10^3 km^2 for a volume of water around 7000km^3 during the Holocene AHP, similar to the modern Caspian Sea, and therefore called Lake Mega-Chad (Bouchette et al., 2010; Ghienne et al., 2002). Several studies (e.g., Skonieczny et al., 2015; Depreux et al., 2021; van der Lubbe et al., 2017) report changes in river system and increased river flow during this time period.

- *Impact on fauna and on human population migration and evolution.* The greening of the Sahara is thought to have played a significant role in hominin migration and evolution (e.g., Drake et al., 2011; Larrasoaña et al., 2013; Tierney et al., 2017a).
- *Reduced dust emissions due to increased vegetation cover.* Wind strength weakening associated with increased vegetation cover were responsible for a reduction in dust emission and deposition in the Atlantic ocean (e.g., DeMenocal et al., 2000; McGee et al., 2013), the Mediterranean Sea (Ehrmann et al., 2017) and the Red Sea and Gulf of Aden (Palchan and Torfstein, 2019). Numerous model simulations support the interpretations based on marine dust records (e.g., Schepanski et al., 2009; Egerer et al., 2016).

3. Short timescale climatic events

In the northern monsoon domain, two dry events have been reported around 8.4-8 ka and 4.2-4 ka cal BP (Gasse, 2000). In equatorial West Africa and in the Sahelian belt, lake level drops have been reported around 8.3-8 ka cal BP and 4.2-4 ka cal BP (Gasse and Van Campo, 1994; Gasse, 2000 and reference therein). However, in hydrogen isotopic composition of leaf waxes, these events are not widely reported in leaf waxes hydrogen records (e.g., Schefuß et al., 2005; Garcin et al., 2018). A more in-depth examination of these two events will be provided in chapter 6.

In central African rainforest, two climatic crises were reported around 4.0 and 2.5 ka cal BP, resulting in forest contraction and savannah southward expansion or rainforest fragmentation (Maley et al., 2018). The geographical, temporal extension and causes of these forest crises are still being debated. While some authors argue that these events are caused by climatic changes (e.g., Ngomanda et al., 2009; Giresse et al., 2018; Bayon et al., 2019), others argue that human population has a significant impact on the environment (e.g., Bayon et al., 2012; Garcin et al., 2018) because it occurs at the same time as Bantu expansion (Bostoen et al., 2015)

Furthermore, a savanna corridor (located in Ghana, Togo and Benin) began around 4.5 ka cal BP, most likely as a result of drier climatic conditions (Maley, 1989; Salzmann and Hoelzmann, 2005; Tossou et al., 2008; Demenou et al., 2016). This corridor, also known as the Dahomay Gap, may have been interrupted around 3.3 ka cal BP by a return to wetter conditions, which ended around 1.1 ka cal BP, leading to a return to open savanna vegetation (Salzmann and Hoelzmann, 2005), but this interruption is not reported everywhere (Tossou et al., 2008).

4. Human impact on African environment

The impact of humans on their environment in West and Central Africa has been the focus of many debates over the last few decades, most notably around the late Holocene rainforest crisis (Bayon et al., 2012; Neumann et al., 2012; Garcin et al., 2018; Clist et al., 2018). Bantu population expansion coincides with rainforest crises, and the role of land use and deforestation has been called into question (e.g., Bayon et al., 2012; Garcin et al., 2018; Giresse et al., 2020; Maley et al., 2018). Bayon et al. (2012) argue that the increase chemical weathering around 3ka ago recorded in a marine sedimentary core record collected off the mouth of the Congo River could indicate deforestation by the Bantu for agriculture and iron metallurgy. Similarly, an abrupt change toward C4 plants inferred from n-alkane carbon isotopic composition was recorded at the Lake Barombi at 2.6 ka cal BP while no hydrological change was recorded during the same period suggesting human impact (Garcin et al., 2018). However, Giresse et al. (2020) argue that because human populations were at low densities at that time, the synchrony of rainforest fragmentation around 2.5 ka cal BP across Central and West Africa is inconsistent with human-driven deforestation.

Similarly, humans have also been proposed as an active agent in the end of the African Human period due to their role in landscape denudation (Wright, 2017), but they have also been proposed to have postponed the end of the green Sahara due to pastoralism (Brierley et al., 2018).

5. Peat deposits, a poorly represented paleoclimatic archive

5.1. Continental archives

Continental archives include lakes, peatlands, soils, speleothems, and so on. Each of these archives has its own set of assets and drawbacks, as well as unique characteristics that must be considered. Strong influence of the hydrological system and feedbacks from vegetation or land complicate interpretation based on continental archives, but they are capable of recording complex environmental and ecological changes. They can be used to investigate the effects of climate change and human activity on the environment. The lack of specific proxies, particularly for paleotemperatures (e.g., Powers et al., 2004), was a limitation for using continental archives compared to marine archives, but several paleotemperature calibrations were developed based on pollen, biomarkers or chironomids (e.g., Brooks and Birks, 2001; Davis et al., 2003; Weijers et al., 2007b; Wilmshurst et al., 2007; Loomis et al., 2012; Longo et al., 2016). Furthermore, in tropical Africa, continental paleoclimatic archives suffer from poor radiocarbon dating, particularly for early studies, as well as frequent discontinuities in records that complicate paleoclimatic interpretations (Gasse, 2000).

5.2. Characteristics of peat deposits in tropical Africa

Peat is defined as partially decomposed biomass and, as such, is an organic rich sediment (Andriesse, 1988). Andriesse (1988) emphasizes the difficulty of defining tropical peat and defines tropical and subtropical peats using arbitrary boundaries between 35 degrees North and South. If boreal and temperate peatlands cover a larger area than tropical peatlands, the latter remain an important component of the terrestrial carbon storage (e.g., Page et al., 2011; Rieley and Page, 2016) and are threatened by human impacts and climate changes through deforestation (Langner et al., 2007; Koh et al., 2011), drainage (Hooijer et al., 2010, 2012) and fires (Turetsky et al., 2015; Konecny et al., 2016; Langner et al., 2007).

In tropical Africa, the largest wetland is the Cuvette Centrale, which is located within the central Congo Basin and is the world's second largest tropical wetland after the Amazon plain river (Keddy et al., 2009). A large proportion of this region is covered by swamp forests (Dargie, 2015; Hughes and Hughes, 1992). Lowland peatlands are mostly found in coastal regions and can be both freshwater and saline (Thompson and Hamilton, 1983). At mid and high elevations, peatlands are dominated by Cyperaceae (Dargie, 2015). Sedge-dominated ecosystems typically have pH ranges between 6 and 7.5 (Thompson and Hamilton, 1983), and the *Cyperus papyrus* can contribute up to 97% of biomass (Thompson et al., 1979). *Sphagnum* bogs are extremely rare, having only been found at high altitudes in Burundi and Uganda (Rwenzori Mountains) (Thompson and Hamilton, 1983).

5.3. Paleoclimatic records based on peat deposit

Peat deposits are common, have relatively fast accumulation rates, and are organic rich sediment, making the ideal for biomarker studies to reconstruct paleoclimate and paleoenvironment (Naafs et al., 2019).

The majority of paleoclimatic research based on peat deposits has focused on temperature and boreal peat deposits, while tropical peat deposits have received far less attention except peat deposits from China with significant contributions to our understanding of lipid biomarkers in tropical peat. However, the climatic conditions are quite different from the study site presented with often colder temperature and strong difference in main vegetation.

Part 2: Biomarkers

1. Introduction: What is a lipid biomarker?

A lipid biomarker is defined as the preserved lipid components found in bitumen, kerogen and more generally in organic matter of sediments, and that can be unambiguously linked with biological precursor compounds (Killops and Killops, 2013). Diagenesis processes such as defunctionalization, hydrogenation or aromatization alter the original structure of the biological precursor compounds (Killops and Killops, 2013). In bitumen and kerogen, many of these processes can be abiotically driven by physico-chemical conditions, whereas in "young" sediments, the majority of these diagenetic modifications are biologically mediated (Killops and Killops, 2013). Biomarkers can be used to track the earliest lifeforms on Earth (Brocks et al., 1999; Knoll, 1999) as well as potentially extraterrestrial life (Georgiou and Deamer, 2014; Vago et al., 2017). They can be used to reconstruct past environmental and climate changes, recording changes in microbial and vegetation communities and allowing the reconstruction of key climatic parameters such as precipitation, temperature or salinity (see Eglinton and Eglinton, 2008; Inglis et al., 2022; Naeher et al., 2022 for reviews).

2. N-alkanes

N-alkanes were among the first lipid biomarkers to be described and can be found in epicuticular waxes of leaves and roots (Eglinton and Hamilton, 1967). Only a few bacteria can also produce long-chain n-alkanes (Han and Calvin, 1969). Plant-derived n-alkanes have a long carbon-carbon chain with no functional groups and are thus resistant to degradation. In plants, they commonly contain between 21 and 37 carbons, with a predominance of odd-numbered n-alkanes (e.g., Ficken et al., 2000; Nott et al., 2000; Diefendorf and Freimuth, 2017). This odd over even predominance is inherited from the biosynthetic pathway of n-alkanes (von Wettstein-Knowles, 1979) and is preserved in sediments with low thermal maturity (Figure 5). Terrestrial vascular plants have usually chain lengths ranging between 25 to 37 (Diefendorf and Freimuth, 2017), whereas aquatic plants have shorter chain lengths (n-C_{23} and n-C_{25}) (Ficken et al., 2000), like mosses (Nott et al., 2000).

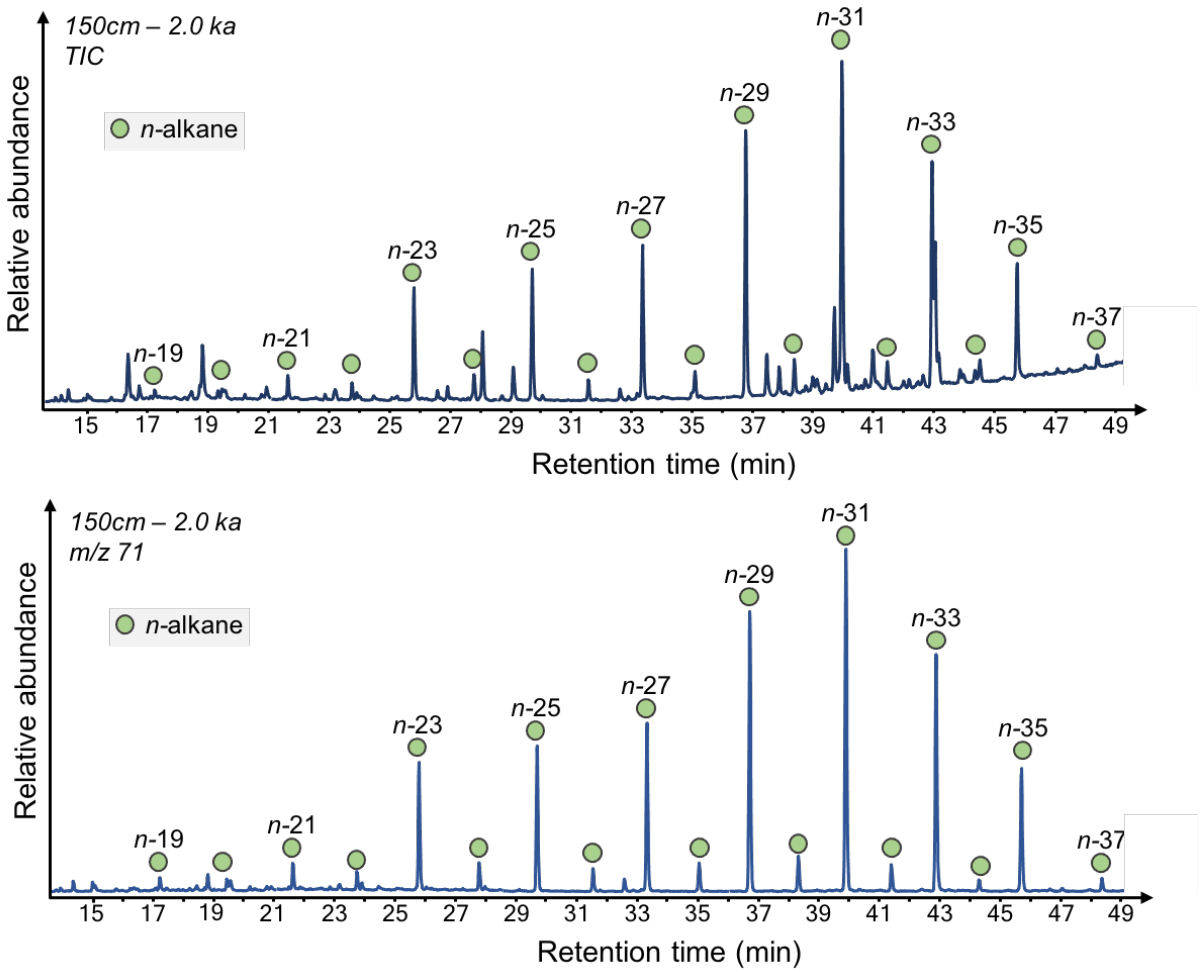

Figure 5: Distribution of n-alkanes in peat sediments illustrating the predominance of odd-numbered chain length n-alkanes. The sample is from the NGaoundaba peat deposit, upper graph corresponds to the Total Ion Chromatogram (TIC) and the lower graph to an extracted ion (m/z 71) for the same sample.

The distribution of n-alkanes differs between plants species and is not specific enough to allow for precise reconstruction (Diefendorf and Freimuth, 2017). Despite this, several n-alkane ratios have been developed to quantify changes in n-alkane distribution in sediment.
The average chain length (ACL) ratio was proposed by Poynter et al. (1989):

$$ACL_{27-31} = \frac{(27 * C_{27} + 29 * C_{29} + 31 * C_{31})}{(C_{27} + C_{29} + C_{31})}$$

There are several versions of this ratio that take longer and/or shorter chain n-alkanes into account (Poynter and Eglinton, 1990; Poynter et al., 1989). The ACL ratio has been used in peat to reconstruct past temperature changes based on studies showing longer chain length in plants growing under warmer climate (e.g., Sachse et al., 2006; Bush and McInerney, 2013). However, the ACL ratio is also influenced by others parameters such as precipitation or

moisture content (Huang et al., 2016), and its relationship with temperature has been called into question (Diefendorf and Freimuth, 2017).

The Carbon Preference Index (CPI) was defined by Bray and Evans (1961) to describe the sources and thermal maturity of crude oil and sediments:

$$CPI = \frac{1}{2}\left[\left(\frac{C_{25}+C_{27}+C_{29}+C_{31}+C_{33}}{C_{24}+C_{26}+C_{28}+C_{30}+C_{32}}\right)+\left(\frac{C_{25}+C_{27}+C_{29}+C_{31}+C_{33}}{C_{26}+C_{28}+C_{30}+C_{32}+C_{34}}\right)\right]$$

Fresh plants have high CPI values, indicating a strong predominance of odd-numbered n-alkanes (Collister et al., 1994), whereas thermally mature sediments have low CPI values (Bray and Evans, 1961). In peat, the CPI ratio has been used to reconstruct changes in humification (Lehtonen and Ketola, 1993) or past changes in climate and environment, but the numerous factors influencing its variations such as vegetation (Diefendorf and Freimuth, 2017) or moisture content (Hoffmann et al., 2013), complicate interpretation.

The P_{aq} ratio was proposed by Ficken et al (2000) to assess aquatic plant contribution to lake sediments, based on the higher abundance of mid-chain n-alkanes (C_{23} and C_{25}) in submerged and floating macrophytes compared to terrestrial plants:

$$P_{aq} = \frac{(C_{23}+C_{25})}{(C_{23}+C_{25}+C_{29}+C_{31})}$$

In *Sphagnum*-dominated peat deposits, this ratio has been reinterpreted as a proxy for the contribution of *Sphagnum* sp. (Nichols et al., 2006). Similarly, the C_{23}/C_{31} n-alkane ratio has been used to reconstruct the input of *Sphagnum* sp. in peat (Nott et al., 2000), but it does not always track *Sphagnum* changes because mixed sources can overlap the signal from *Sphagnum* (Schellekens and Buurman, 2011).

The carbon isotopic composition of plants reflects the incorporation of atmospheric CO_2 into leaves and is influenced by the plant's photosynthetic pathway, resulting in a significant difference between the carbon isotopic signature of C_3 plants (between -22‰ and -30‰) and C_4 plants (between -10‰ and -14‰) (Figure 6) (e.g., Bender, 1971; Farquhar et al., 1989). This difference between the $\delta^{13}C$ values of C_3 and C_4 plants is also visible in the $\delta^{13}C$ values of n-alkanes from C_3 and C_4 plants (e.g., Chikaraishi and Naraoka, 2003). The compound specific $\delta^{13}C$ values are slightly offset from the bulk $\delta^{13}C$ values because of the fractionation that occurs during the synthesis of the n-alkane (Chikaraishi et al., 2004). In sediments, the carbon isotopic composition of n-alkanes has been used to infer changes in C_3 and C_4 vegetation in a variety of settings and over time (e.g., France-Lanord and Derry, 1994; Huang et al., 2001; Garcin et al., 2014). Additional environmental and biological controls, such as diagenesis and

aeolian inputs, can also affect the carbon isotopic composition of n-alkane in sediments and must be considered (Diefendorf and Freimuth, 2017).

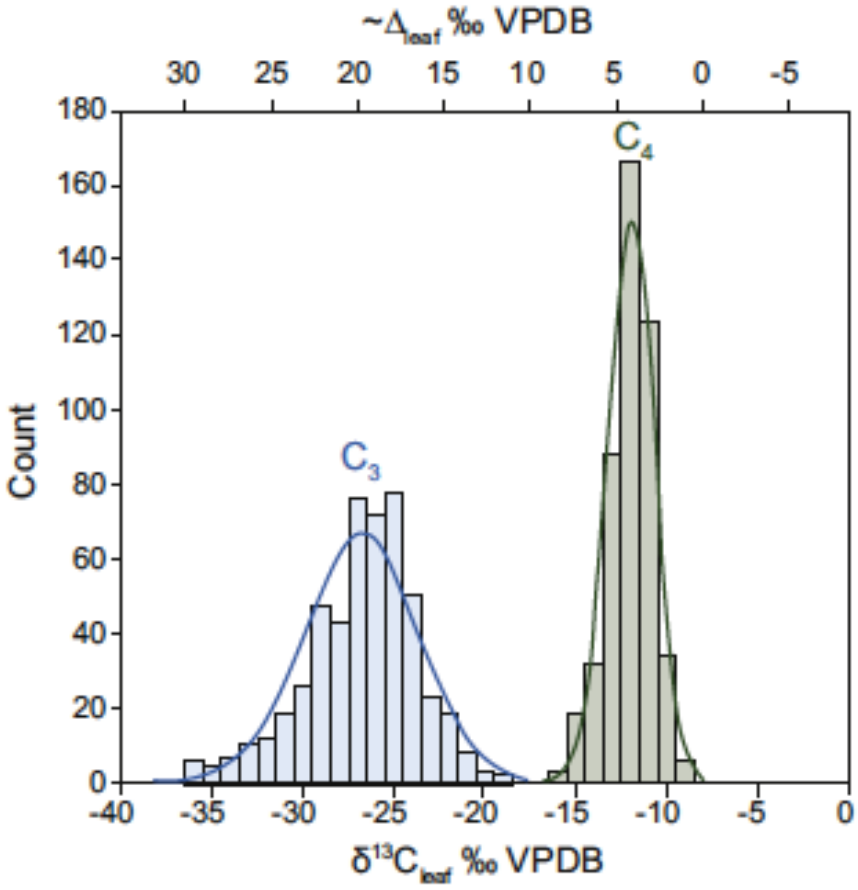

Figure 6: Histogram showing the different carbon discrimination associated with the C_3 and C_4 photosynthetic pathways. From Diefendorf et al. (2017) based on Cerling and Harris (1999) data.

The hydrogen isotopic composition of n-alkanes reflects the hydrogen isotopic signature of the water used by plants during biosynthesis and has been used as a paleohydrological proxy (Sauer et al., 2001; Sachse et al., 2012). Sachse et al. (2012) present a review of the various factors influencing the hydrogen isotopic composition of n-alkanes. Several factors influence the isotopic composition of the source water, including the continental effect, temperature effect, and amount effect (Sachse et al., 2012). In tropical regions, the dominant factor is the amount effect, with greater deuterium depletion as precipitation increases (Bowen, 2008), and the hydrogen isotopic composition of n-alkane has been used to reconstruct past changes in precipitation amount (e.g., Schefuß et al., 2005; Shanahan et al., 2015; Niedermeyer et al., 2016). Hydrogen isotopic composition of leaf wax lipids is also affected by isotope fractionation due to evapotranspiration in soil and leaves as well as during biosynthesis (Figure 7). The impact of the photosynthetic pathway on hydrogen isotopic composition can be

corrected using a binary mixing model with C_3 and C_4 plant end members (e.g., Garcin et al., 2014, 2018).

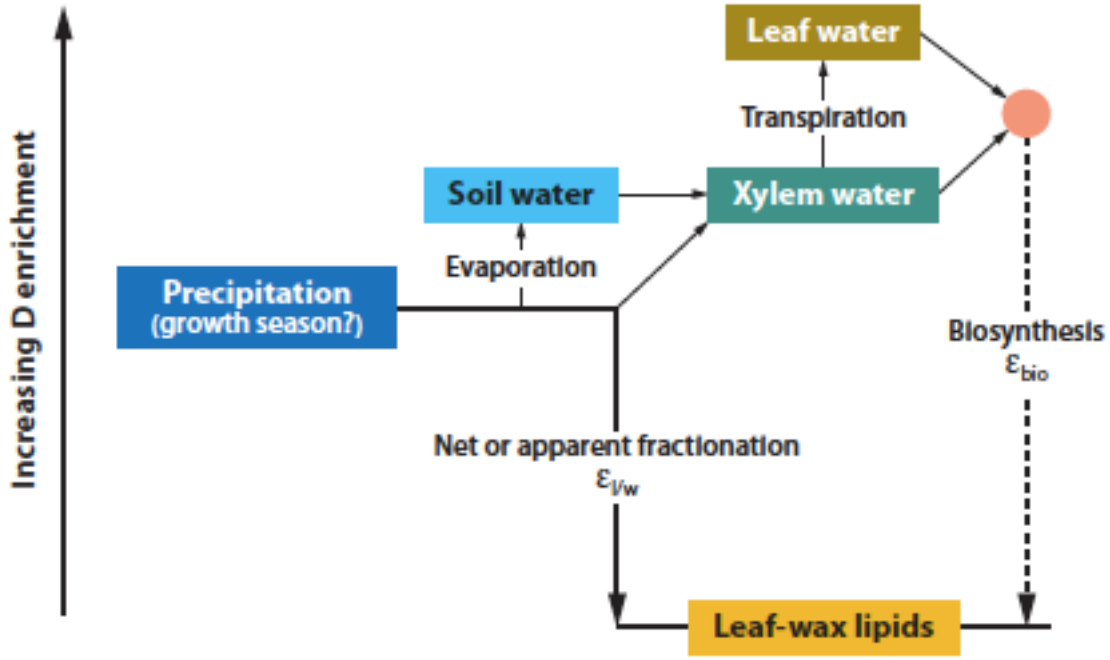

Figure 7: Diagram describing the relationship between the hydrogen isotopic composition of precipitation and of leaf-wax lipids. From Sachse et al. (2012).

N-alkanoic acids and n-alkanols are also common lipid biomarkers in peat sediment and have also been used for paleoclimatic reconstruction (e.g., Naafs et al., 2019) but they will not be investigated here.

3. GDGTs

Glycerol dialkyl glycerol tetraethers (GDGTs) are membrane-spanning lipids forming monolayers. GDGTs are classified into two types: isoprenoid GDGTs (isoGDGTs) based on isoprenoid units and branched GDGTs (brGDGTs) (Figure 8). IsoGDGTs were the first to be discovered and described, and they are common in Archaea (de Rosa et al., 1977). brGDGTs were discovered in a peat deposit (Sinninghe Damsté et al., 2000) and are of bacterial origin (Weijers et al., 2006, 2009). Acidobacteria have been proposed as main producers of these compounds, even if other sources are not ruled out (e.g., Sinninghe Damsté et al., 2011, 2018). The main isoGDGTs differ by the number of cyclopentane moieties in their alkyl chains and the presence of a cyclohexane moiety for Crenachaeol (Figure 8). The main brGDGTs differ by the number of cyclopentane moieties and by the numbers and the position of additional methylations in their alkyl chains (Figure 8).

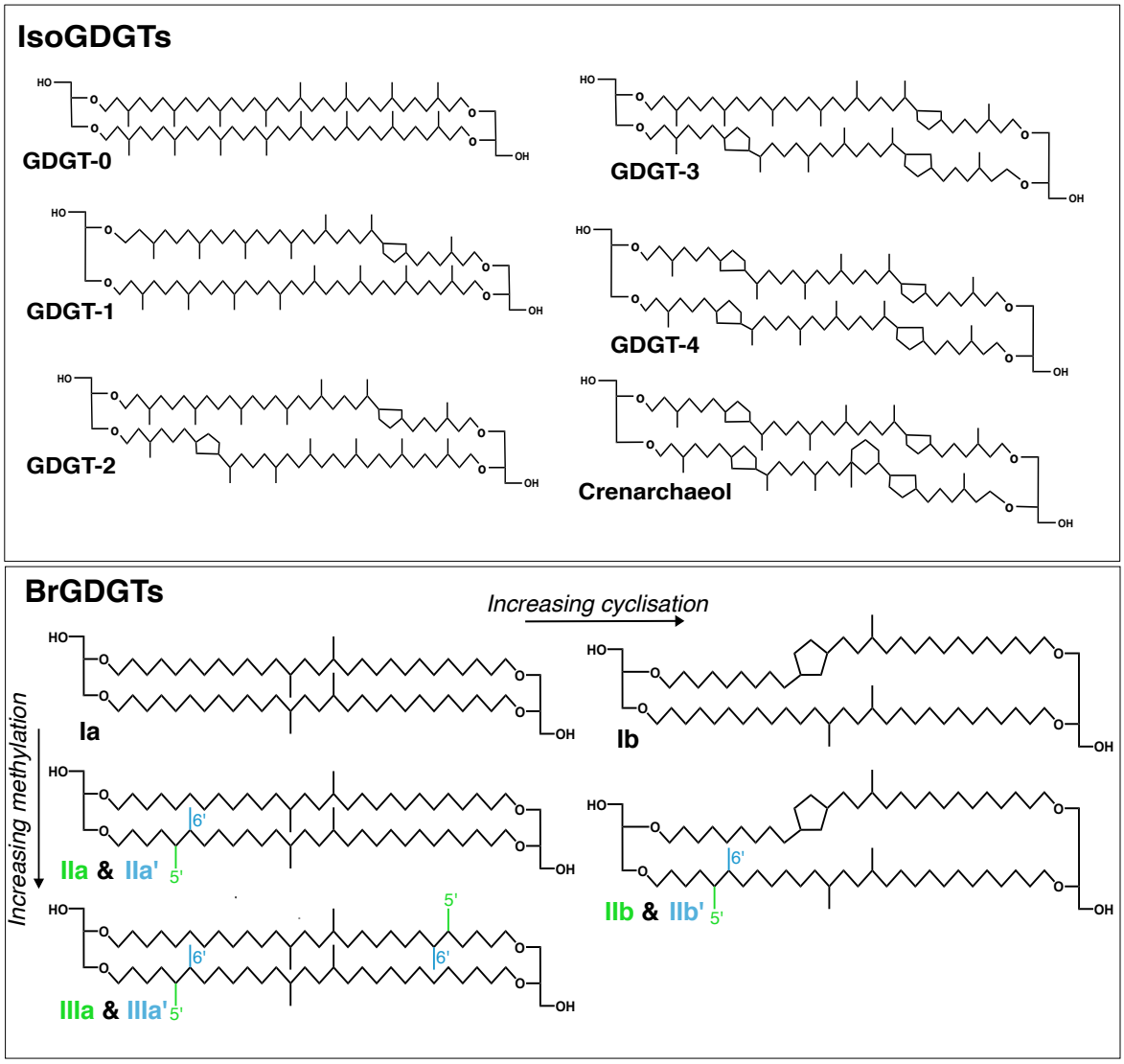

Figure 8: Structures of iso and brGDGTs. brGDGTs with two cyclopentane moieties (one on each alkyl chain), called Ic, IIc and IIIc, also exist but are not represented here.

The distribution of isoGDGTs and brGDGTs in sediments records past changes in paleoenvironmental and paleoclimatic conditions such as temperature, pH, water column stratification, and changes in microbial community (Schouten et al., 2013; Naafs et al., 2019 and references therein). In peats, isoGDGT-0 has been used to trace past changes in methanogenesis (Pancost et al., 2003). Weijers et al. (2007b) show that the number of methylations and cyclizations of brGDGTs was significantly correlated with temperature and pH, respectively. Based on a database of more than 130 soils from various settings, Weijers et al. (2007b) defined two ratios: the methylation of branched tetraethers (MBT) and the cyclization of tetraethers (CBT), and proposed empirical calibration to reconstruct temperature and pH in soils based on these ratios:

$$MBT = \frac{Ia + Ib + Ic}{Ia + Ib + Ic + IIa + IIb + IIc + IIIa + IIIb + IIIc}$$

$$CBT = \frac{Ib + IIb}{Ia + IIa}$$

Since then, new calibrations were proposed using different statistical approaches (Peterse et al., 2012), refining analytical methods (De Jonge et al., 2013, 2014), increasing the size of the calibration dataset or proposing local calibrations (Loomis et al., 2012; Pérez-Angel et al., 2020) and based on different type of sediments (e.g., Peterse et al., 2012; Naafs et al., 2017b; Martínez-Sosa et al., 2021). Several peat-specific temperature and pH calibrations have been developed in recent years based on brGDGT new methylation and cyclization ratios (Naafs et al., 2017b; Dearing Crampton-Flood et al., 2020; Véquaud et al., 2022):

$$MBT'_{5ME} = \frac{Ia + Ib + Ic}{Ia + Ib + Ic + IIa + IIb + IIc + IIIc}$$

$$CBT_{peat} = log\left(\frac{Ib + IIa' + IIb + IIb' + IIIa'}{Ia + IIa + IIIa}\right)$$

4. Hopanes

Geohopanes (hereafter called hopanes) are degradation products of biohopanoids, which are pentacyclic triterpenes produced by a variety of bacteria (Ensminger et al., 1974; Peiseler and Rohmer, 1992). Hopanes are abundant and diverse in peat and soil sediments (Quirk et al., 1984; Ries-Kautt and Albrecht, 1989). Different isomers can be found in sediment, for example the C_{31} homohopanes have three major configurations: 17β,21β(H) (ββ), 17β,21α(H) (βα) and 17α,21β(H) (αβ) (Figure 9), with the latter being especially abundant in peats (Quirk et al., 1984). Isomerization at the C_{22} position also occurs. The last two configurations are related in crude oils to sediment thermal maturation (Ensminger et al., 1974; Mackenzie and McKenzie, 1983). The reason for the high proportion of αβ hopanes in peat sediments is still unknown, as ββ appears to be the main configuration in living organisms and these sediments have a low thermal maturity. Although a role of peat pH has been proposed, the precise mechanism underlying the formation of αβ hopanes remains unknown (Quirk et al., 1984; Huang et al., 2015; Inglis et al., 2018).

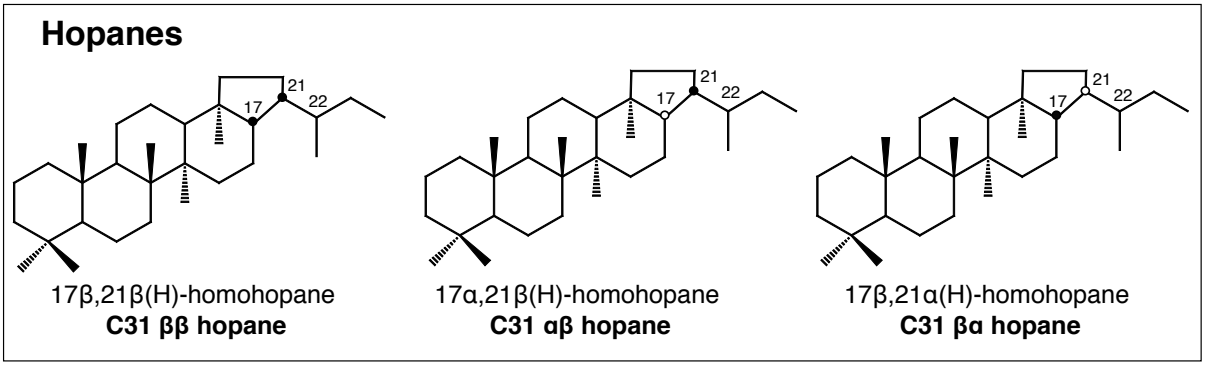

Figure 9: The structure and different isomers of C_{31} hopane

Based on the ββ/(αβ+ββ) index proposed by Mackenzie et al. (1980), Inglis et al. (2018) demonstrated a significant correlation between this ratio and pH in peat and proposed a pH calibration based on a global peat dataset.

The carbon isotopic composition of hopanes has been proposed to track changes in bacterial communities' metabolic pathways (Inglis et al., 2019). Hopanes with fewer than 30 carbons have a depleted carbon isotopic signature when compared to n-alkane and other hopanes, implying that some of these compounds are produced by methanotrophic bacteria (methane is a depleted carbon source) (Inglis et al., 2019). Hopane has the potential to be used a proxy for past methanotrophic activity in peat deposits (Zheng et al., 2014; Elvert et al., 2016; Huang et al., 2018).

5. Other biomarkers

A few other biomarkers were studied at the NGaoundaba peat deposit and are briefly summarized below.

Botryococcenes are triterpenoid hydrocarbons synthesized by the race B of the green colonial alga, *Botryococcus braunii* (Metzger et al., 1985b, 1985a, 1988). Botryococcenes have been found in both temperate and tropical lake and wetland sediments (Huang et al., 1999; Gao et al., 2007; Grossi et al., 2012; Atahan et al., 2015). They have been used to track ecological changes in aquatic environments based on changes in their structure and carbon isotopic composition (Huang et al., 1999; Grossi et al., 2012; Atahan et al., 2015).

Des-A-triterpenoids are diagenetic products of pentacyclic triterpenoids derived from plants (Trendel et al., 1989). des-A-triterpenoids have rarely been studied in sediments and little is known about their origin and diagenetic pathways. They appear to be derived primarily from C_3 plants (van Bree et al., 2016). Changes in des-A-triterpenoid distribution in sediments have

been linked to changes in paleoenvironment (Jacob et al., 2007; Regnery et al., 2013) or diagenetic conditions (Huang et al., 2008).

5-*n*-alkylresorcinol is a type of phenolic lipids founds in many plants, particularly cereals (Ross et al., 2003). They have been found in peat sediments (e.g., Avsejs et al., 2002; Xie et al., 2004; McClymont et al., 2008). Based on the analysis of peat forming plants, Avsejs et al. (2002) suggest that 5-*n*-alkylresorcinol can be used as a proxy for sedges in peat. This study is based on an ombrotrophic temperate peat deposit dominated by Sphagnum sp. and sedges, but the conclusions have not yet been tested on a tropical peat deposit with different peat forming plant species.

Chapter 2: Study site: the NGaoundaba peat deposit and the Adamawa Plateau

1. Geology and climate on the Adamawa Plateau

The NGaoundaba peat deposit is located on the Adamawa Plateau in Northeastern Cameroon. The Adamawa Plateau is the eastern end of the Cameroon Volcanic Line (CVL), an intraplate volcanic province active since the Cenozoic (Figure 10) (Nono et al., 1994). The Adamawa Plateau has altitudes ranging from around 800 m to 1200 m (e.g., Poudjom Djomani et al., 1997; Nguetsop et al., 2011). The basement is Precambrian (Poudjom Djomani et al., 1997), with numerous extinct volcanoes hosting lakes and peatlands (Abba et al., 2023). The studied site is located 25 km south-east of the town NGaoundéré in a maar crater (N7.13542°, E13.69009°, 1175 m above sea level). The peat deposit has an approximative surface area of 18 000 m^2 and an unknown maximum depth. The catchment area is constrained by the rim of the crater and thus extremely small. The NGaoundaba peat deposit is a rain-fed ombrotrophic bog.

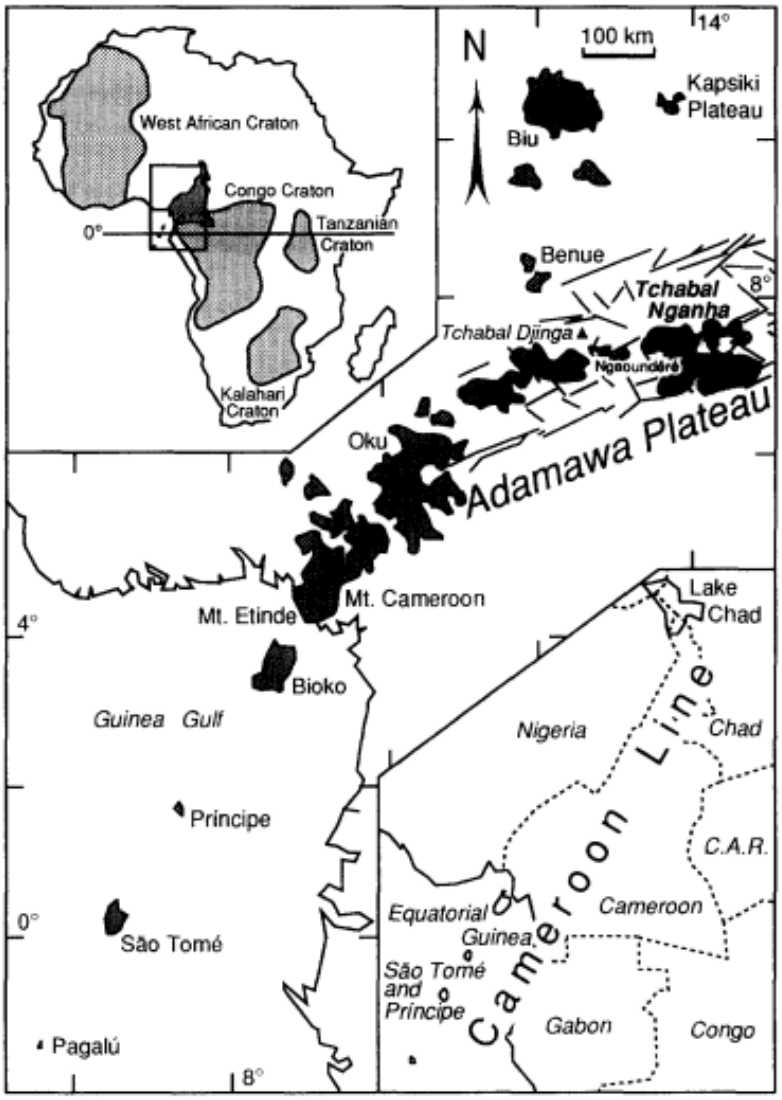

Figure 10: The Cameroon volcanic Line and the Adamawa plateau. From Nono et al.(1994).

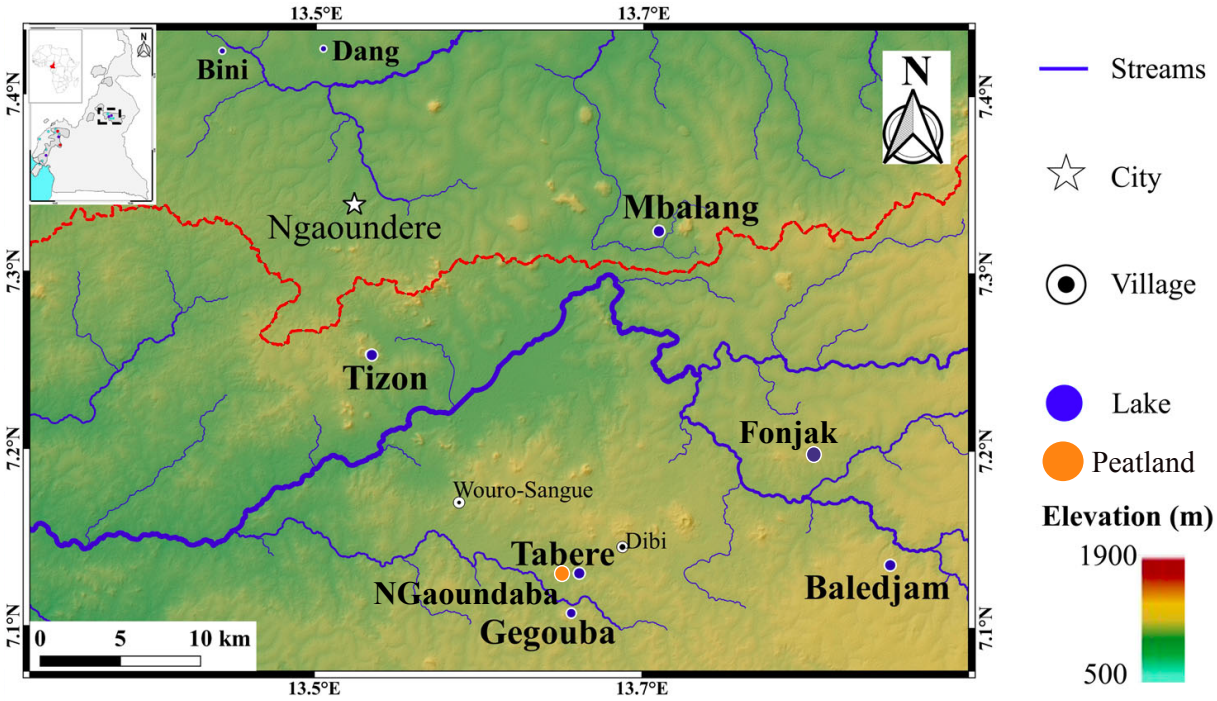

Figure 11: Topographic map of the Adamawa plateau and lakes location modified after Abba et al. (2023). The NGaoundaba peat deposit is indicated by an orange circle. The lake Tabere is also referred as lake NGaoundaba in the literature.

A recent hydrological and geochemical investigation of nearby lakes (Figure 11) by Abba et al. (2023) highlights the distinct geochemical characteristics and isotopic signature of each lake, despite similar crater area morphology and climatic conditions. The study emphasizes the complex balance between watershed inflow and evaporation. A hydrological survey of the NGaoundaba peat deposit is currently underway (A. Abdou – PhD student supervised by Prof. NGounou NGatcha - University of NGaoundéré in collaboration with IRD).

The current climate has a 5 to 6-month rainy season from April to September and a dry season from October to March (Figure 12). The mean annual precipitation (MAP) is approximatively 1480 mm/year and the mean annual air temperature (MAAT) approximatively 22.2°C (Harris et al., 2014).

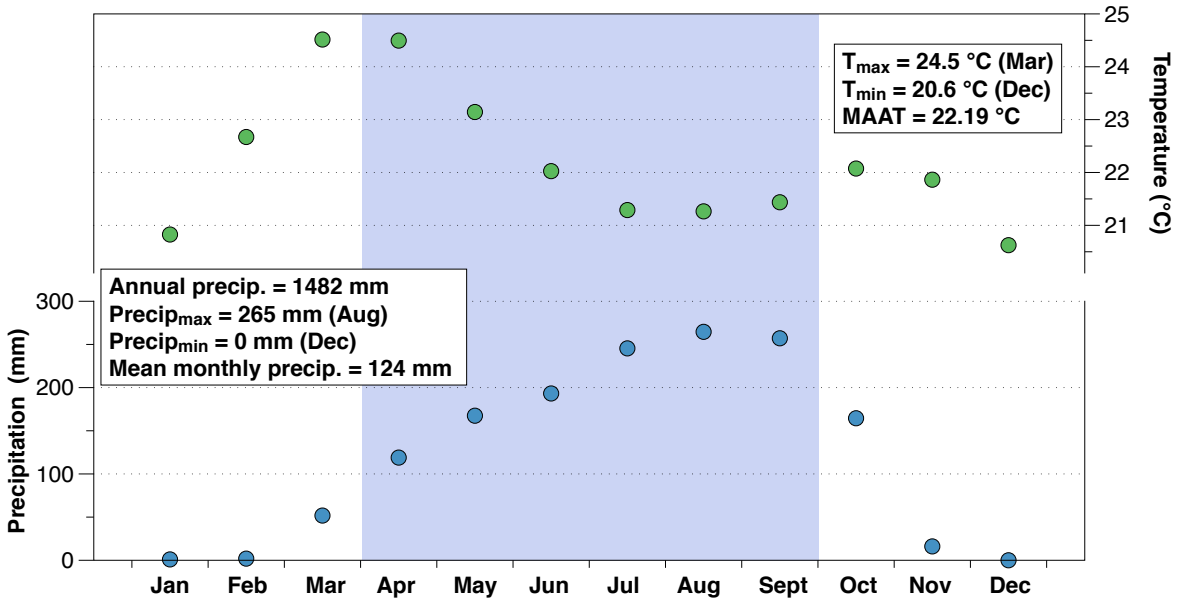

Figure 12: Monthly temperature and precipitation at the NGaoundaba peat deposit based on data from the CRU database (Harris et al., 2014). The rainy season is highlighted in blue.

2. Published paleoclimatic and paleoenvironmental studies on the Adamawa Plateau

The basement of the Adamawa Plateau is made up of plutonic and metamorphic rocks (mostly granites) and recent volcanic formations. The region's recent volcanism has not been extensively studied, but many paleoclimatic records present volcanic pyroclastic and ash layers (Ngos and Giresse, 2012; N'nanga et al., 2019, 2021b). However, the timing of volcanic events even for nearby lakes does not always coincide, implying local eruptions (Ngos and Giresse, 2012). Volcanic activity was recorded at lake Fonjak and lake Tizon (or Tizong) around 4 ka cal BP (Ngos and Giresse, 2012; N'nanga et al., 2019, 2021b). The majority of the lakes on the Adamawa plateau are maars. Following the dramatic CO_2 outgassing at Lake Nyos and Lake Monoun in 1984 and 1986, several studies and surveys of lakes on the Adamawa Plateau were conducted (e.g., Kling et al., 1987; Sigurdsson et al., 1987; Issa et al., 2014; Tanyileke et al., 2019). Furthermore, Abba et al. (2023) documents the hydrological functioning of five lakes on the Adamawa Plateau near NGaoundéré (Mbalang, Tabere, Tizon, Gegouba, and Baledjam). To date, many of the paleoclimatic records of the Adamawa Plateau present reworked material and discontinuous age model complicating paleoclimatic interpretations (e.g., Ngos III et al., 2003; Nguetsop et al., 2013). All sites on the Adamawa Plateau are located in the wooded Sudano-Guinean savannah zone (Letouzey, 1958). The Table 1 present the existing paleoclimatic records from the Adamawa Plateau and the proxies that were applied for each site.

Table 1: Published paleoclimatic and paleoenvironmental studies based on lake on the Adamawa Plateau. The lakes are listed in order of distance from NGaoundaba peat deposit (Figure 11).

Site	Period (ka cal BP)	Tools	References
Lake Tizong	4.0 - 0	Sedimentology, bulk organic analyses, diatom, pollen	Ngos and Giresse (2012) Nguetsop et al. (2013) Lebamba et al. (2016)
Lake Mbalang	7.2 - 0	Sedimentology, pollen, diatom	Vincens et al. (2010) Nguetsop et al. (2011) Ngos and Giresse (2012)
Lake Fonjak	13.5 - 0 (mostly 4.4 - 0)	Sedimentology, mineralogy, diatom	N'nanga et al. (2019) N'nanga et al. (2021a) N'nanga et al. (2021b)
Lake Assom	2.8-0	Sedimentology	Ngos et al. (2003)

3. Present-day vegetation at the NGaoundaba peat deposit

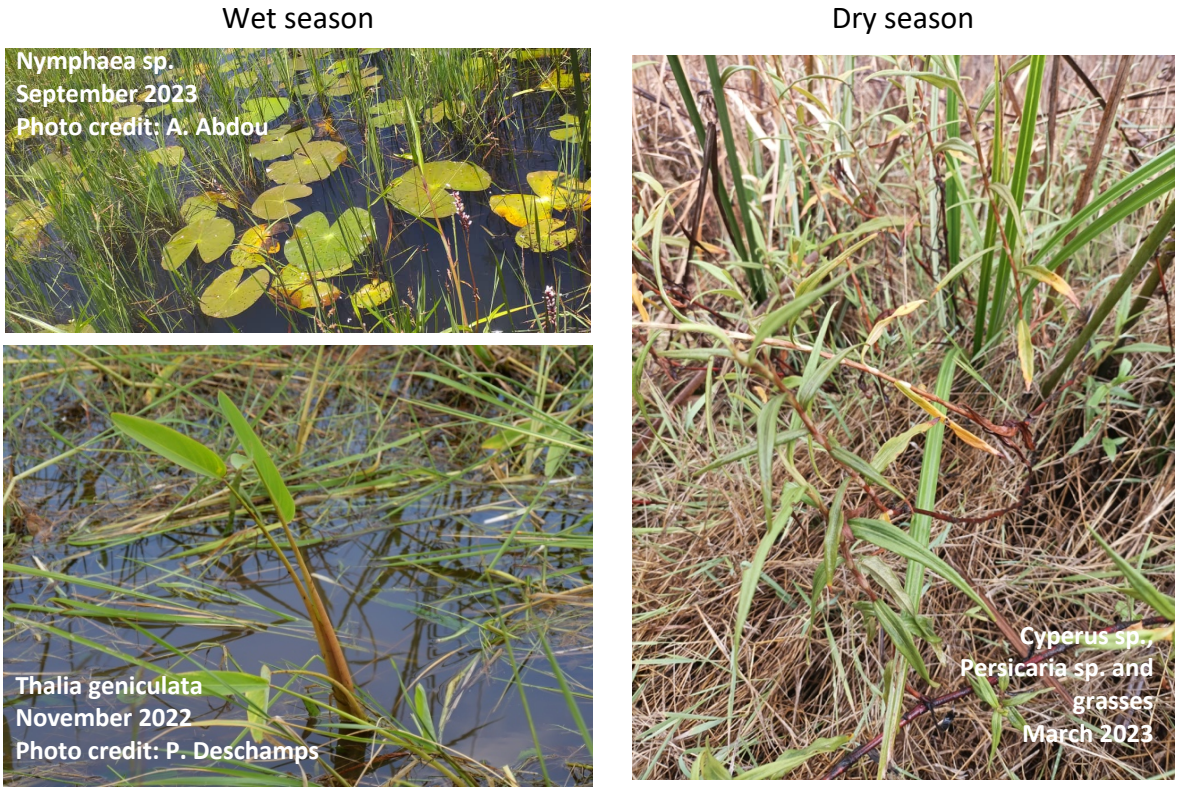

Figure 13: Images of the NGaoundaba peat deposit's vegetation during the rainy and dry seasons. During the wet season, sedges (Cyperus sp.) are the dominant vegetation, but submerged and floating macrophytes are also growing. Note that the southern part of the peatland is more flooded than the northern part.

The inner peatlands' vegetation is dominated by sedges (Cyperaceae, *Cyperus* sp.) with grasses (Poaceae, unknown genus) and *Persicaria* (Polygonaceae, *Persicaria* sp.) (Figure 13). Floating (*Nymphaea* sp.) and submerged macrophytes are also present, primarily during the rainy season. The crater's slopes are partially cultivated and frequently burned. When the water level is low enough, the fire reaches the inner part of the peatlands. The peat deposit's shore remains wet even during the dry season and is used for vegetable cultivation by nearby villagers.

4. Coring and sampling at the NGaoundaba peat deposit

The core analyzed in this thesis was cored using a Russian peat corer in February 2019 (end of the dry season) (NGBA19) by Y. Garcin, B. Hamelin and G. Ménot. The peat's surface was burned shortly before coring (Figure 14 A).

Plant samples presented in chapter 8 were collected in November 2022 (beginning of the dry season) inside the peatland and on the slope of the crater by P. Deschamps and S. Abba.

In March 2023, a second coring was performed using a Livingstone peat corer by P.Deschamps, G. Ménot, V. Schaaff with the help of PhD and master students from the university of NGaoundéré. These cores are not studied here. The site's slopes were burned shortly before the coring by villagers for cultivation (Figure 14 C).

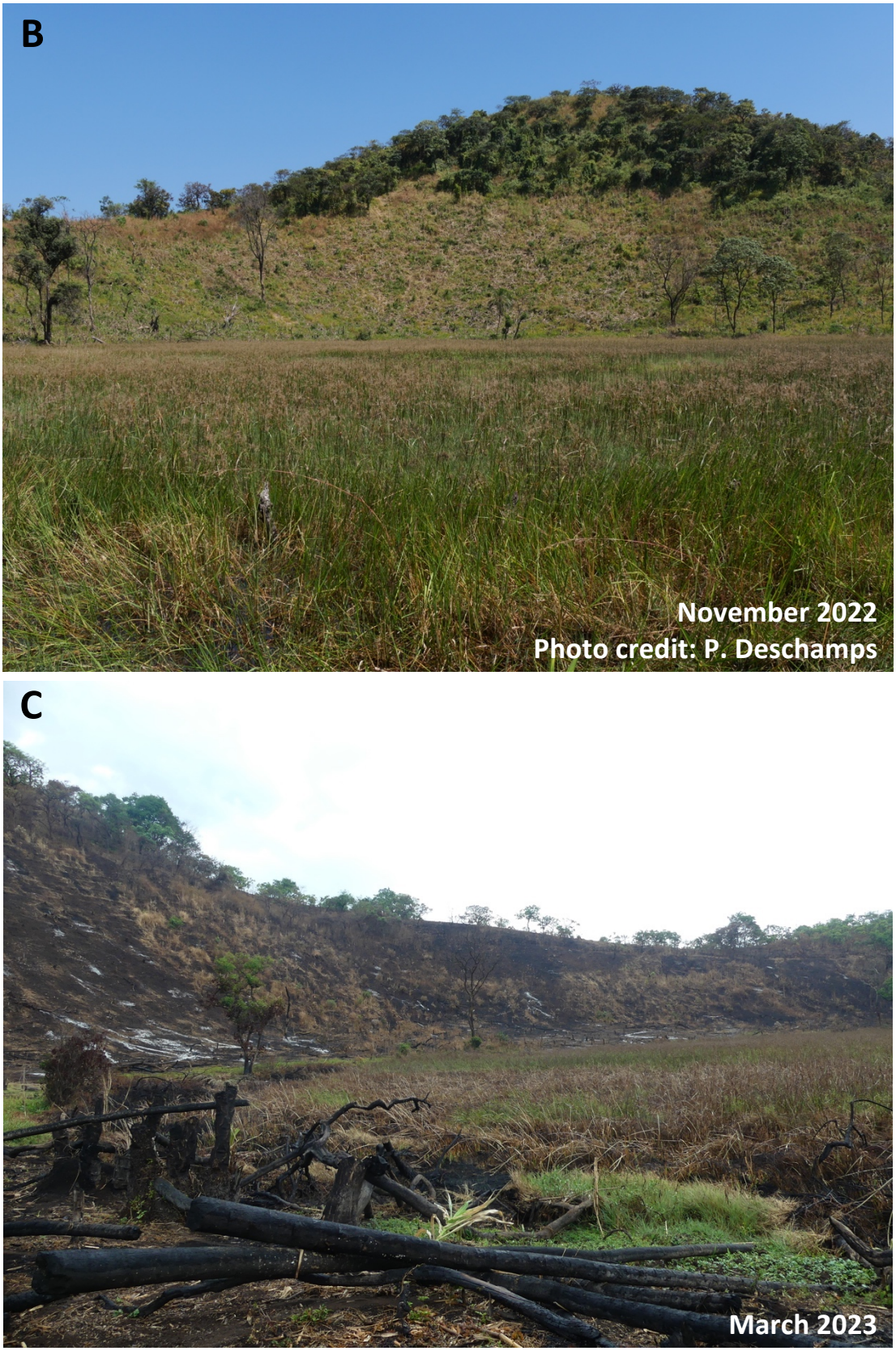

Figure 14: Images of the NGaoundaba peat deposit taken at various times: (A) in February 2019 during the coring of the peat core studied in this thesis, (B) in November 2022 when plant samples were collected and (C) in March 2023 during the second coring.

The NGBA19 core is a 6-meter-long core composed of twelve 50-centimeter-long sections. The coring was limited. The sediment is a dark brown peat, slightly reddish in the lower part of the core (Figure 15). There are no discernable clay, sand or volcanic layers.
After coring, sections were packed and transported to the CEREGE (Aix en Provence, France) were they were kept in cold storage. The subsampling was performed at CEREGE. All samples were then transported to the LGL-TPE (ENS de Lyon, Lyon) and keep in the freezer until freeze-drying.

Figure 15: A section of the NGBA19 peat core just after coring in February 2019. Photo credit: Y. Garcin

Chapter 3: Modeling the decomposition signal and correcting bulk organic data from a peat deposit, a case study at low latitudes (Cameroon)

Published in Organic Geochemistry (179), May 2023 as *Modeling the decomposition signal and correcting bulk organic data from a peat deposit, a case study at low latitudes (Cameroon)*, Valentine Schaaff, David Sebag, Matthew Makou, Vincent Grossi, Ingrid Antheaume, Bruno Hamelin, Yannick Garcin, Benjamin Ngounou Ngatcha, Pierre Deschamps, Guillemette Ménot. DOI: https://doi.org/10.1016/j.orggeochem.2023.104589

Abstract:
Organic compounds are widely used for paleoclimatic and paleoenvironmental reconstructions. Bulk organic proxies, however, are more complicated to interpret due to the multiple causes of variation in climatic and environmental conditions and the degree of diagenetic alteration. As labile compounds, rich in easily degradable function and generally richer in heteroatoms such as oxygen and nitrogen, decompose, the remaining organic matter becomes progressively richer in refractory carbon and its carbon content increases. Thus, in a peat deposit composed almost entirely of organic matter, total organic carbon (TOC) is expected to increase with time and depth, which could mask the paleoclimatic signal. We propose a simple model for peat sediments to remove the decomposition signal based on a logarithmic function fitted with a partial dataset where decomposition is the main parameter. The subtraction of the obtained logarithmic function to the raw data (i.e., measured data) leads to "residual" data. We discuss the influence of different parameters (water table depth, vegetation, microbial community) on the "residual" data and their possible link to paleoclimatic and paleoenvironmental variations. This method is tested on bulk elemental and isotopic data obtained from a new peatcore from the Adamawa Plateau (North-East Cameroon) covering nearly 10 ka cal BP. Comparison with Rock-Eval® parameters highlights similar variations between the Hydrogen Index and residual TOC variations, supporting the interpretation based on residual TOC. Our approach allows to extract paleoenvironmental information from decomposition-prone bulk organic proxies and can be generalized to peat deposits where decomposition plays a major role in controlling bulk data.

Key words: Peat deposit, Decomposition model, Bulk organic data

This chapter has been published in 2023 in Organic Geochemistry.

1. Introduction

Paleoclimatic proxies based on organic compounds rely on the assumption that these compounds are resistant to diagenesis. Many organic compounds can record pre-depositional and syn-depositional information such as climatic conditions (e.g., temperature, hydrology) or environmental conditions (e.g., major vegetation types, pH, methanogenesis) (Sachse et al., 2012; Diefendorf and Freimuth, 2017; Inglis et al., 2019; Naafs et al., 2019). This signal can, however, be overprinted by post-depositional processes such as decomposition (Gupta and Kawahata, 2006) or contamination by other reservoirs (Makou et al., 2018).

Peat deposits have been successfully used to reconstruct past climatic variations at all latitudes using diverse proxies such as pollen, plant macrofossils or biomarkers (e.g., Pancost et al., 2003; Booth et al., 2004; Baker et al., 2014). Bulk analysis of organic matter such as Rock-Eval® or elemental analysis are routine techniques in paleoenvironmental studies. These non-specific analyses give first insights into the sources, nature and decomposition stage of organic matter (e.g., Talbot and Johannessen, 1992; Kuhry and Vitt, 1996; Baker et al., 2014). However, in bulk organic data, the paleoclimatic or paleoenvironmental signal is often hidden by the signal of decomposition (Kuhry and Vitt, 1996; Drollinger et al., 2019). Some proxies were specifically developed to reconstruct the peat decomposition stage such as colorimetric determination (Chambers et al., 2011; Biester et al., 2014) or thermal analyses (Upton et al., 2018; Cooper et al., 2019), while others such as the C/N ratio are sometimes used as an indicator of organic matter decomposition (Kuhry and Vitt, 1996) or of organic matter sources (Baker et al., 2014). In intertropical regions, peat deposits have a large paleoclimatic potential especially when applying organic geochemistry techniques (e.g., Sukumar et al., 1993; Bonnefille et al., 1995; Aucour et al., 1996, 1999; Behling and Safford, 2010). Until now, no study has specifically focused on correcting bulk organic data in tropical peat.

Peatlands are highly impacted by organic matter decay (Clymo, 1984). Peats are usually divided in two distinct layers: the upper layer (the acrotelm), above the mean water table depth and exposed to oxic conditions, and the lower layer (the catotelm) situated under the mean water table depth and dominated by anoxic conditions (Ingram, 1978; Clymo, 1984). Clymo (1984) and Clymo et al. (1998) focused on models of peat mass accumulation and decay rules and indicated that about 90% of the original biomass is lost in the upper oxic part of the peat within an indicative period of 10 to 100 years but selective decay continues in the anoxic layer.

Peat organic matter is often mainly composed of different pools of organic compounds with different sensitivities to decomposition (Dodla et al., 2012) and different $\delta^{13}C$ composition

(Benner et al., 1987). The labile organic compounds such as carbohydrates and proteins composed of easily hydrolyzable functions rich in oxygen and nitrogen rapidly decompose after deposition while recalcitrant organic compounds such as lignin and lipids, having long carbon chains and aromatic structures rich in carbon, can be selectively preserved (Dodla et al., 2012; Wang et al., 2015). Thus, despite global mass loss and carbon loss during organic matter decomposition (Clymo, 1984), the remaining organic matter, mainly composed of recalcitrant compounds, becomes more and more concentrated in carbon with increasing time and depth (Figure 16). In the oxic layer, aerobic decomposers preferentially use ^{12}C, resulting in an increase in ^{13}C content (Ågren et al., 1996; Drollinger et al., 2019). The mineral fraction in the peat is a key point to understand the variations in TOC. If the mineral component is very low, the TOC will follow the trend of the organic matter and increase with depth and time (e.g., Upton et al., 2018). In mineral-rich peat, or when mineral fraction supply varies, the increasing trend will no longer be visible because the increasing proportion of the mineral fraction due to the decomposition of the organic matter will mask the evolution of the carbon in the organic matter (e.g., Baker et al., 2014; Njagi et al., 2021).

While the effects of early diagenesis on $\delta^{13}C$, $\delta^{18}O$ or Mg/Ca of foraminifera and carbonate sediments have been studied for decades (Berner, 2020), and several corrections of these proxies from diagenetic overprint have been proposed (e.g., Schrag et al., 1995; Rosenthal and Lohmann, 2002), only a few studies exist on the diagenetic effects of organic matter decomposition on bulk parameters used for paleoenvironmental studies. The importance of TOC corrections for petroleum studies is well known and several corrections specific to source rocks are available but they have not been applied to paleoenvironmental reconstructions until recently (Hart and Hofmann, 2022). In a marine core from the Timor Sea, Gupta and Kawahata (2006) observed a high impact of diagenesis on labile components (amino acids) and proposed a correction of the measured total organic carbon (TOC) using a linear equation. They suggest that corrected organic carbon more accurately reflects the original organic carbon deposited on the sea floor and thus is more appropriate for primary productivity estimates.

In this paper, we focus on bulk organic data from a peatcore situated on the Adamawa Plateau in Cameroon. Several maar lakes from the Adamawa Plateau have been studied for paleoclimatic and paleoenvironmental reconstruction (e.g., Ngos III et al., 2003; Vincens et al., 2010; Nguetsop et al., 2011; Lebamba et al., 2016; N'nanga et al., 2021a) but until now no peat deposit has been investigated. We propose a method to deconvoluate the diagenetic signal from the climatic signal in peat. We develop a model that allows subtraction of a mean decomposition signal from bulk parameters such as TOC, $\delta^{13}C$ and C/N. Residual data provide a robust means of interpreting palaeoclimatic and palaeoenvironmental variations in

parameters for which the decomposition signal is the main mode of variability (in particular TOC).

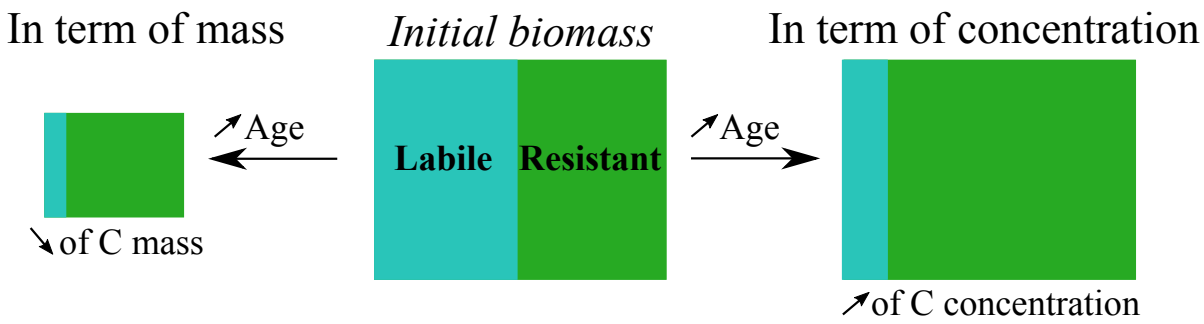

Figure 16: Evolution of carbon mass and carbon concentration with time in OM-dominated sediment reflecting the progressive mineralization of organic matter. Labile compounds are richer in heteroatoms than resistant compounds, leading to an increase in C concentration as labile compounds decompose while the global mass of carbon decreases.

2. Study site and materials

2.1. Study site

The NGaoundaba peat deposit (N7.13542° E13.69009°, 1175m above sea level) is located in North Cameroon near the city of NGaoundéré on the Adamawa Plateau, occupying a volcanic crater situated next to Lake Tabéré. Its current surface area covers ~18 000 m^2, and the maximum depth is still unknown. According to Letouzey (1958), the peat deposit is situated in the soudano-guinean shrubs savannas from the Adamawa Plateau. Nowadays, the peat is covered by sedges (Cyperaceae), that are annually burned. Tropical peatlands of Africa from similar settings are largely sedge-dominated and peat composition is a mix of sedges and woody remains from the surrounding forests (Dargie, 2015).

2.2. Sampling

A 6-meter-long core was collected on February 2019 using a Russian peat corer. The core is composed of twelve consecutive 50-cm sections and consists of dark brown peat containing plant debris. The color is consistently dark brown over the whole core. The NGaoundaba peat deposit is continuous and essentially composed of peat without sandy or clayey zones. The core was subsampled at 2.5-cm intervals corresponding to a resolution of around 40yr. Samples were freeze-dried prior to analysis.

3. Analytical methods

3.1. Dating

The chronological framework of NGaoundaba sequence is based on 30 radiocarbon dates carried out at the LMC14 Laboratory (Saclay, France) following the procedure from Dumoulin et al. (2017) and Moreau et al. (2013). Measurements were performed on bulk peat sediment. Data were compiled using the R-software Bacon v2.5 (Blaauw and Christen, 2011) and calibrated using the SHCal20 calibration curve (Hogg et al., 2020) and postbomb calibration curve NH3 (Hua et al., 2013).

3.2. Rock-Eval® thermal analysis

Rock-Eval® analyses were performed on 69 samples using 10 mg of ground peat and a Rock-Eval® 6 (Vinci Technologies, France). The Rock-Eval® thermal analysis is based on continuous measurement of effluents, i.e., hydrocarbons (HC), carbon monoxide (CO), and carbon dioxide (CO_2), released during the thermal cracking of organic compounds under pyrolytic conditions (from 200 to 650°C at 25°C min^{-1} in an inert atmosphere), followed by the combustion of residual organic compounds (from 200 to 850°C in an oxidative atmosphere). The resulting thermograms were used to calculate the standard parameters by integrating the amounts of HC, CO, and CO_2 within the defined temperature limits (Lafargue et al., 1998; Behar et al., 2001). The Total Organic Carbon (TOC parameter) is calculated as the sum of all C effluents (i.e., HC, CO, and CO_2) under a temperature limit (Lafargue et al., 1998) and usually represents the amount of organic C. When inorganic carbon forms are negligible, the percent C is calculated as the sum of organic carbon (TOC) and MinC parameter. The Hydrogen Index (HI) corresponds to the amount of HC released during pyrolysis relative to percent C. In organic samples with the same source of organic inputs, a decrease in HI is usually related to the decomposition of H-rich organic compounds (dehydrogenation), leading to an enrichment of aromatic compounds during diagenesis in lake deposits (Meyers and Lallier-Vergès, 1999) or pedogenesis in soils (Disnar et al., 2003; Barré et al., 2016). In addition to the above standard parameters, Disnar et al. (2003) proposed using the shape of thermograms to obtain additional information about OM quality. In the present study, we used the I index to quantify the preservation of the thermolabile C pool (Sebag et al., 2016). This index is derived from the integrated S2 areas in specific temperature ranges (200--400 °C, 400--460 °C, and > 460 °C), and is usually interpreted in terms of specific thresholds of the thermal stability of organic compounds, separating the thermolabile, thermoresistant, and thermorefractory C pools (Disnar et al., 2003; Sebag et al., 2006; Saenger et al., 2013). The I-index has recently been used to measure the degree of decomposition of a tropical peat to identify an event of increased decomposition of organic matter after deposit (Garcin et al., 2022).

While it is well calibrated for sedimentary organic matter (i.e., kerogens), Rock-Eval® percent C needs to be corrected in soils and litters (Disnar et al., 2003). The correction factor

calculation depends on an estimation of the decomposition state of the sediment. As decomposition state is a focus of this study, we chose to use elemental and stable isotope analyses rather than Rock-Eval® analyses for data processing to avoid the use of any pre-processing assumption of decomposition state.

3.3. Elemental and stable isotope analyses

A total of 66 samples was ground and homogenized, then measured for TOC, total nitrogen, and $\delta^{13}C$ composition of TOC. Between 2 and 4 mg of non-acidified sediment were combusted in tin capsules using an elemental analyzer (Vario Micro Cube Elementar) coupled to a thermal conductivity detector and an isotope ratio mass spectrometer IRMS (Elementar Vision). The carrier gas was helium.

Samples were first passed through a combustion furnace at 950°C under an excess of oxygen with copper oxide as an oxidation catalyst, producing CO_2, N_xO_x, and H_2O. Then, a reduction furnace at 550°C reduced N_xO_x to N_2 and removed excess O_2 using reduced copper. H_2O was trapped and removed using a phosphorous pentoxide chemical trap. N_2 and CO_2 were separated using a purge and trap desorption column. The C/N ratio was calculated as the ratio between TOC and wt%N.

A working standard (IVA sediment) was analyzed every 10 samples and used to normalize the mass spectrometer signals. Triplicates were analyzed every 3 samples and standard deviations were calculated. The absence of carbonates in the samples was confirmed by acid-treating 6 samples (1 every meter) using vapor of 12N hydrochloric acid for 72 hours and then performing a comparative analysis.

4. Data processing

4.1. General information

The method proposed in this study is divided into 4 steps (Figure 17) and described in detail below.

Kinetics of organic compound degradation follow a simple first order equation (Westrich and Berner, 1984; Grossi et al., 2003) with different reactivity depending on the compounds. The increase in the proportion of recalcitrant compounds leads to a progressive increase in carbon concentration despite the total mass loss (Figure 16). Using a different approach, Clymo (1984) and Clymo et al. (1998) developed models of peat accumulation. Based on equation 1, α denotes the manner of decay and constant, linear and quadratic rules were tested by Clymo et al. (1998). Using a linear decay rule α_L*, the plot of peat growth (cumulative carbon M_t)

follows the logarithmic equation (2) with p* the rate of addition of dry mass at the top of the peat deposit (Clymo et al., 1998).

$$\frac{d\mu}{dt} = -\alpha \times \mu \; with \; \mu = \frac{m_t}{m_0} \qquad (1)$$

$$M_t = \frac{p^*}{\alpha_L^*} \times \ln(1 + \alpha_L^* \times t) \qquad (2)$$

Based on these observations and on the logarithmic trend followed by TOC with age and depth in our dataset and in several others (e.g., Upton et al., 2018; Wei et al., 2012; Garcin et al., 2022), we chose to use a natural logarithmic function (noted "ln") in two possible forms presented in equations 3 and 4 using age as the variable. The parameter c can be linked to the initial C content in freshly deposited organic matter, while a and b are related to the kinetic constants and the proportion of labile versus recalcitrant organic matter.

$$f(x) = a \times \ln(b \times t) + c \quad \forall t \in \Re^{+*} \qquad (3)$$

$$f(x) = a \times \ln(b \times t + d) + c \quad \forall t \in \;]-d/b, +\infty[. \qquad (4)$$

Data processing was performed using the Python software. The different parameters a, b, c and d of each function are optimized using the curve.fit() function of the SciPy Python library. The difference between the two forms is slight; equation 4 allows an offset on the t axis of the data and the domains of the function defined as the set of *t*-values accepted by the function are slightly different for the two functions. By definition, the ln function is only defined for strictly positive values, equation 3 is defined for strictly positive values $\Re^{+*}$, while equation 4 is defined for t above the ratio of d and b parameters -d/b (i.e. for $t \in$]-d/b; +∞[).

The choice of the function for each parameter was determined by comparing the determination coefficient r^2 between the raw data and the curve-fit for each form. We called "raw data" the initial data prior to any data treatment.

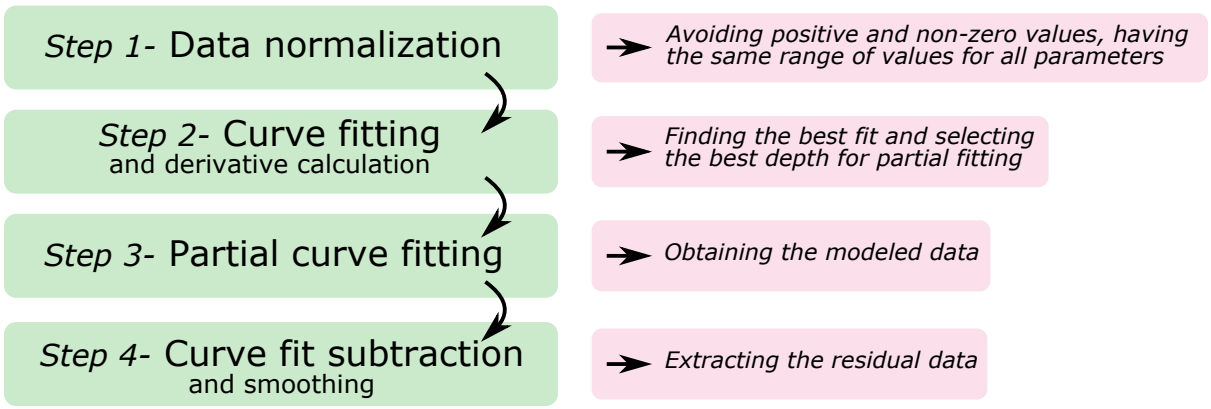

Figure 17: Description of the different steps of the procedure from raw to residual data.

4.2. Data normalization

As logarithmic functions can only be used for positive and non-zero values, raw data were normalized (scaling of all values in the range of 0 and 1) prior to any analysis (Figure 17 - Step1). Practically, all values were normalized using the MinMaxscaler transforms from Python library sklearn.preprocessing based on the following equation 5:

$$x_{scaled} = \frac{x - x_{min}}{x_{max} - x_{min}} \qquad (5)$$

We add 0.001 to all normalized ages to avoid having a zero *t*-value that cannot be used in a logarithmic function.

4.3. Total curve fitting and derivative calculation

The method is based on two successive curve fittings, which are presented in the next two subsections. The objective is to find a curve fit based only on a part of the initial dataset where the decomposition is predominant.

A first option would use the upper oxic layer thickness (acrotelm) as most of the decomposition occurs in this layer (Clymo, 1984). However, no measurement of this parameter is available for the NGaoundaba peat deposit. Based on the mean water table depth, upper oxic layer thicknesses between 5 and 35 cm were estimated for several temperate peat deposits (Kuhry and Vitt, 1996; Evans et al., 1999; Weijers et al., 2004, 2006; Liu et al., 2010; Drollinger et al., 2019). In a tropical peat swamp forest, Jauhiainen et al. (2005) reported a water table varying between 80 cm under and 20 cm above the peat sediment surface throughout the year with maximum occurrences of values between 10 and 30 cm under the peat sediment surface. The upper oxic layer thickness is usually on the order of tens of centimeters. In the case of the NGaoundaba dataset, neither measurement of the upper layer thickness nor estimation based on literature can be used for the modeling as it would involve only a few points and would lead to poorly constrained results.

To determine the age where the decomposition is the main parameter controlling bulk organic data, we first fit the logarithmic function *f* using all x-values, then we calculate the derivative of this function *f'* and determine the range of x-values where *f'*(x)>1, thus finding the inflection point of the curve (Figure 17 - Step 2 and Figure 18 - Light colored curves). The value *f'*(x)>1 was fixed arbitrarily. This choice avoids using the whole dataset for the modeling and avoids purely circular reasoning.

4.4. Partial curve fitting

A new function *g* is then fitted based only on the reduced range of x-values (Figure 17- Step 3 and Figure 18). In other words, only a part of the original data is selected for the final curve fitting *g*. For each parameter, the selected x-values are indicated in dark color on Figure 18. A total of 13, 17 and 11 x-values were selected for TOC, $\delta^{13}C_{bulk}$ and C/N, respectively.

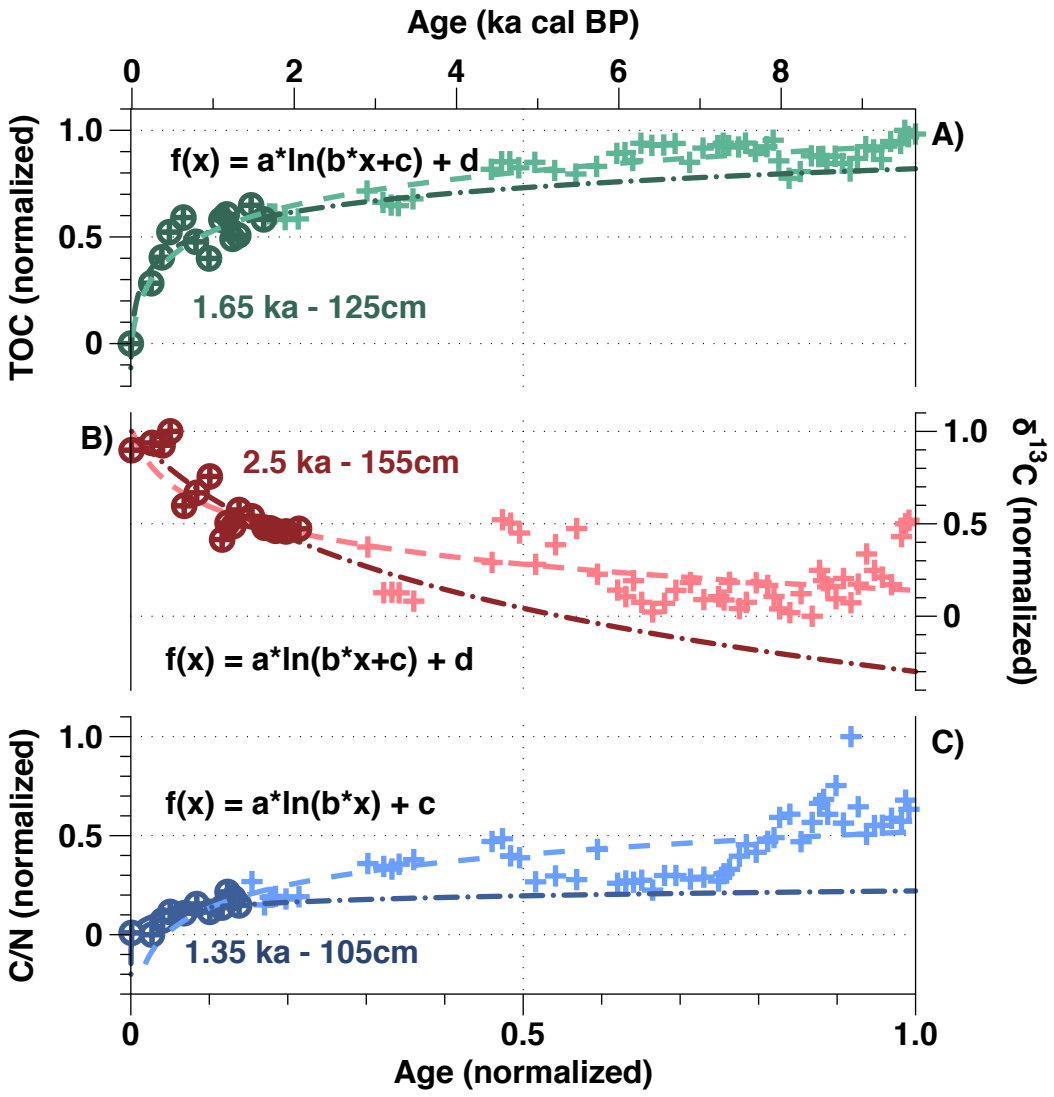

Figure 18: Normalized data of the NGaoundaba peat deposit plotted against age (ka cal BP & normalized): (A) TOC, (B) $\delta^{13}C_{bulk}$ and (C) C/N. The light-colored curves represent the curve fitting based on the whole dataset and the dark colored curves represent the curve fitting based on the partial dataset using only depth with a positive derivative. The function selected for each parameter is indicated on the left of each panel, the constants a, b, c and d are fitted for each parameter and x-range. The selected x-range for each parameter is indicated in dark color (encircled points). The x-range limit is indicated in both age and depth for each parameter.

4.5. Curve fit subtraction

The last step is the subtraction of the function *g* (i.e., the modeled data) to the raw data. The resulting data are named the residual data. Thus, positive residual values indicate that the raw

data values are superior to those of the modeled data, indicating an excess of this parameter compared to the modeled data. Residual data are smoothed (Figure 17 - Step 4) using a moving average method.

5. Results

5.1. Age model

Calibrated ages range from -39 a cal BP at 10 cm depth to 9642 a cal BP at the bottom (590 cm) (Figure 19, Table 2). The age-depth model presents a quite uniform sediment accumulation rate except around 150 cm-depth (2.5 ka cal BP) and 200 cm-depth (4.0 ka cal BP). These two periods are not situated at the limit between two core sections, as indicated on Figure 19.

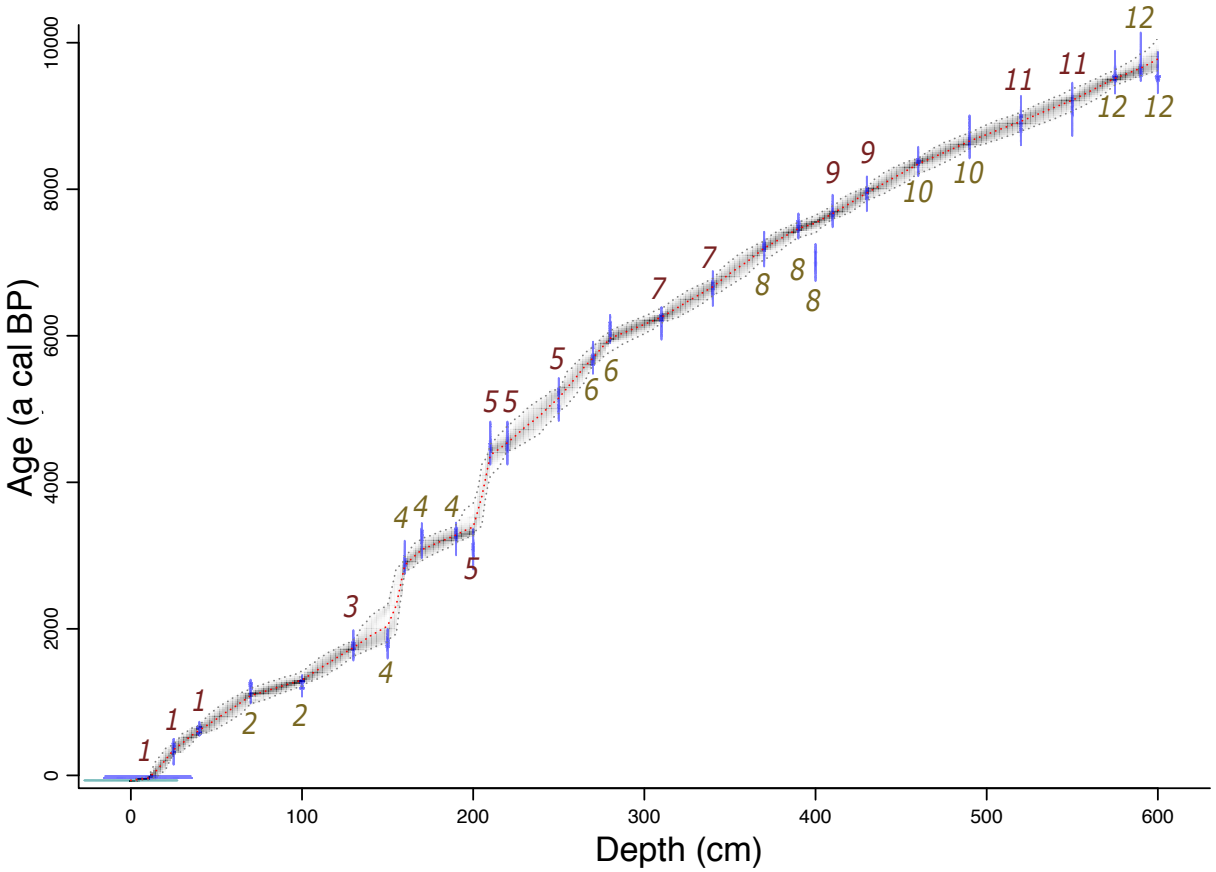

Figure 19: Age-depth model of NGaoundaba peatland core. The corresponding section number is indicated for each ^{14}C sample.

Table 2: Chronology of NGaoundaba peatland with pMC values, uncalibrated AMS 14C ages (BP: before present) and calibrated median 14C age (a cal BP).

Sample code	Depth (cm)	pMC	Uncalibrated Age	Calibrated age (a cal BP)

58976	10	120.49		-39
62587	25	95.95±0.28	330 ± 30 BP	343
58977	40	91.39±0.23	725 ± 30 BP	614
58978	70	84.93±0.22	1310 ± 30 BP	1093
58979	100	84.12±0.23	1390 ± 30 BP	1290
58980	130	79.22±0.22	1870 ± 30 BP	1741
62588	150	78.82±0.26	1910 ± 30 BP	1981
64844	160	70.22±0.21	2840 ± 30 BP	2871
58981	170	68.04±0.20	3090 ± 30 BP	3082
58982	190	67.75±0.22	3130 ± 30 BP	3274
62589	200	69.07±0.23	2975 ± 30 BP	3345
64845	210	60.24±0.21	4070 ± 30 BP	4417
58983	220	60.24±0.20	4070 ± 30 BP	4531
58984	250	57.30±0.19	4475 ± 30 BP	5180
62590	270	53.67±0.23	5000 ± 35 BP	5690
58985	280	51.49±0.19	5335 ± 30 BP	5960
58986	310	50.69±0.18	5460 ± 30 BP	6255
58987	340	48.19±0.18	5875 ± 30 BP	6668
58988	370	45.45±0.18	6335 ± 35 BP	7201
64846	390	43.64±0.18	6660 ± 30 BP	7465
58989	400	46.40±0.18	6170 ± 30 BP	7547
62591	410	42.52±0.20	6870 ± 40 BP	7665
58990	430	40.91±0.19	7180 ± 40 BP	7955
58991	460	38.83±0.17	7600 ± 35 BP	8361
58992	490	37.30±0.18	7925 ± 40 BP	8653
58993	520	36.57±0.17	8080 ± 35 BP	8926
58994	550	35.99±0.17	8210 ± 40 BP	9223
62592	575	34.26±0.19	8605 ± 45 BP	9511
64847	590	33.85±0.16	8700 ± 40 BP	9642
58995	600	34.32±0.17	8590 ± 40 BP	9759

5.2. Elemental raw data

TOC increases with increasing depth and age ranging from 26.76 to 53.5 % for elemental and stable isotope analyses (Figure 20 A).

The C/N ratio roughly increases with depth and age. Until 4.5 ka cal BP, values increase nearly linearly (Figure 20 C). From 4.5 to around 5 ka cal BP, the C/N ratio decreases and then

stabilizes until 7.1 ka cal BP. The bottom of the core is marked by a general increase of the C/N ratio with small-scale variations.

The range of values of elemental raw data is consistent with data reported for other African peat deposits (e.g., Aucour et al., 1999; Baker et al., 2014; Strobel et al., 2019).

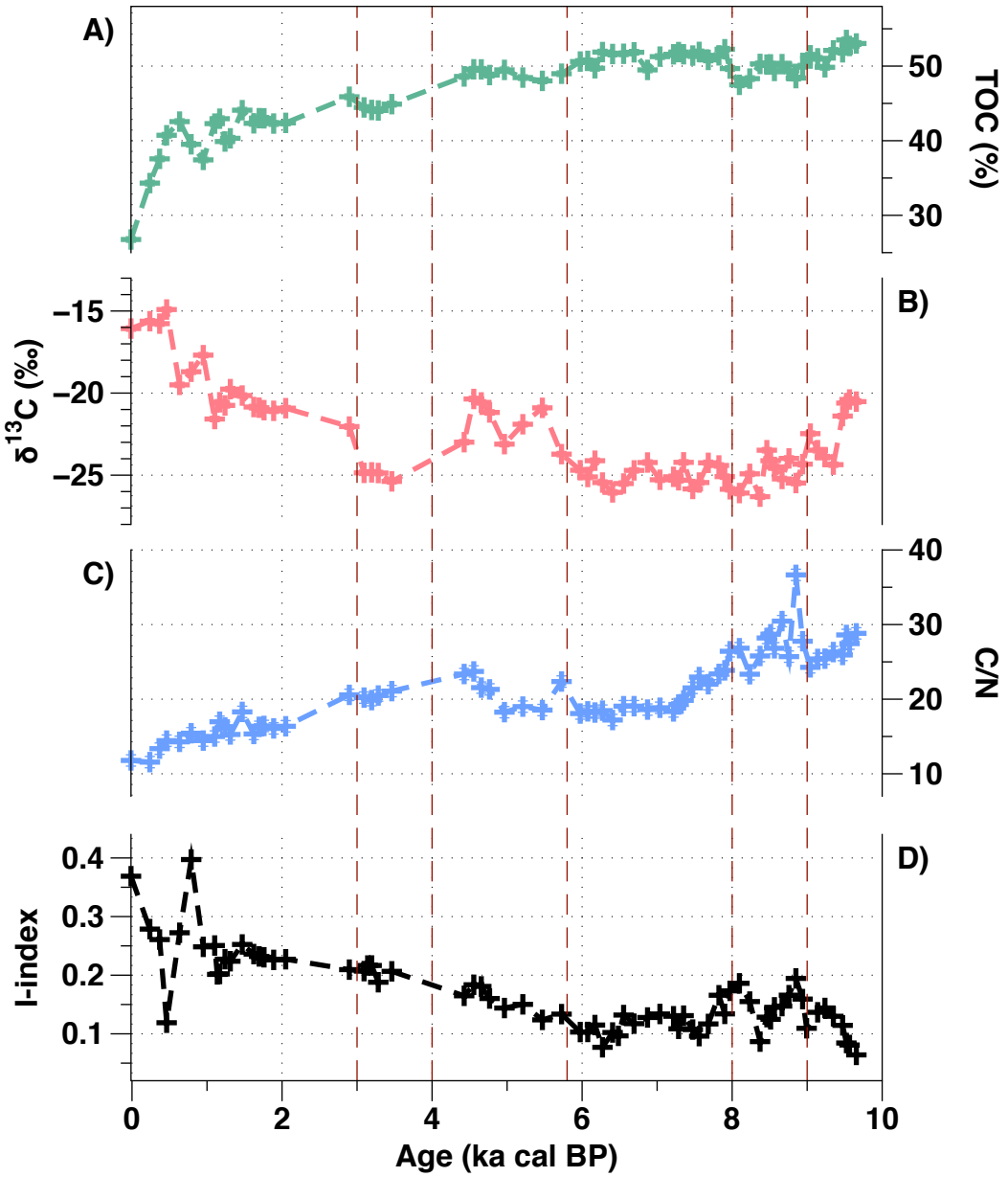

Figure 20: Raw data (i.e., before data processing) from the NGaoundaba peat deposit: (A) TOC (%), (B) $\delta^{13}C_{bulk}$ (‰), (C) C/N from Elemental and stable isotope analysis and the I-index from Rock-Eval® analysis. Visible transitions are indicated with vertical red dashed lines.

5.3. Rock-Eval® I-index and HI

The I-index ranges from 0.06 to 0.37. The I-index variations can be divided into two periods (Figure 20 D). The first period from the present to 6.4 ka cal BP is characterized by a regular decrease in I-index from 0.37 to 0.08. The second period from 6.4 ka cal BP to the bottom of the core presents more variations, but with a narrower amplitude between 0.2 and 0.06 (Figure 20 D).

The HI ranges from 195 to 427 (Figure 21 G). The HI is between 250 and 300 from 5.8 ka cal BP until present except between 4 and 3 ka cal BP where values are around 225. The highest HI values are found from 7.9 to 5.8 ka cal BP and at the bottom of the core. From 9.4 to 7.9 ka cal BP, HI values are under 300 (Figure 21 G).

5.4. Isotopic raw data

The $\delta^{13}C_{bulk}$ presents a general decrease with increasing depth and age ranging from -15.6 to -26.3‰ (Figure 20 B). The $\delta^{13}C_{bulk}$ decreases from the top of the core to 3 ka cal BP from values around -16‰ to values around -22‰. Between 3 and 4 ka cal BP, $\delta^{13}C_{bulk}$ is close to -25‰. The $\delta^{13}C_{bulk}$ increases between 4 ka cal BP and 5.8 ka with most values between -23 and -20.4‰ compared to values around –25 between 5.8 and 9.4 ka cal BP. The $\delta^{13}C_{bulk}$ also increases from 9.4 ka to the bottom of the core ranging from -21.4 to -20.4 ‰ during this period.

5.5. Processed residual data

Processed residual data range from -0.126 to 0.181, -0.189 to 0.815 and -0.090 to 0.782 for TOC, $\delta^{13}C_{bulk}$ and C/N respectively. Both residual TOC, residual $\delta^{13}C_{bulk}$ and residual C/N are mostly positive (Figure 21 C, D and E respectively).

Residual TOC values are decreasing from the bottom of the core until 8 ka cal BP with values close zero between 9 and 8 ka cal BP (Figure 21 D). From 8 to 4 ka cal BP, residual TOC are between 0.1 and 0.2 except around 5.5 ka cal BP where values are slightly lower. From 2.5 ka cal BP until present, TOC values present rapid variations between -0.13 and 0.12.

The residual $\delta^{13}C_{bulk}$ presents a general decreasing trend and positive values from the bottom of the core to around 4 ka cal BP (Figure 21 E). The period of less depleted values from 5.8 to around 4 ka cal BP observed in the raw $\delta^{13}C_{bulk}$ data (Figure 20 B) is still visible in the residual $\delta^{13}C_{bulk}$ with positive residual data ranging from 0.2 to 0.5.

The residual C/N presents similar variations as the raw C/N data with a globally increasing trend with depth and age (Figure 21 F). Values are close to zero until 2.5 ka cal BP and between 5 and 7.5 ka cal BP. The highest values occur between 8.5 and 9 ka cal BP.

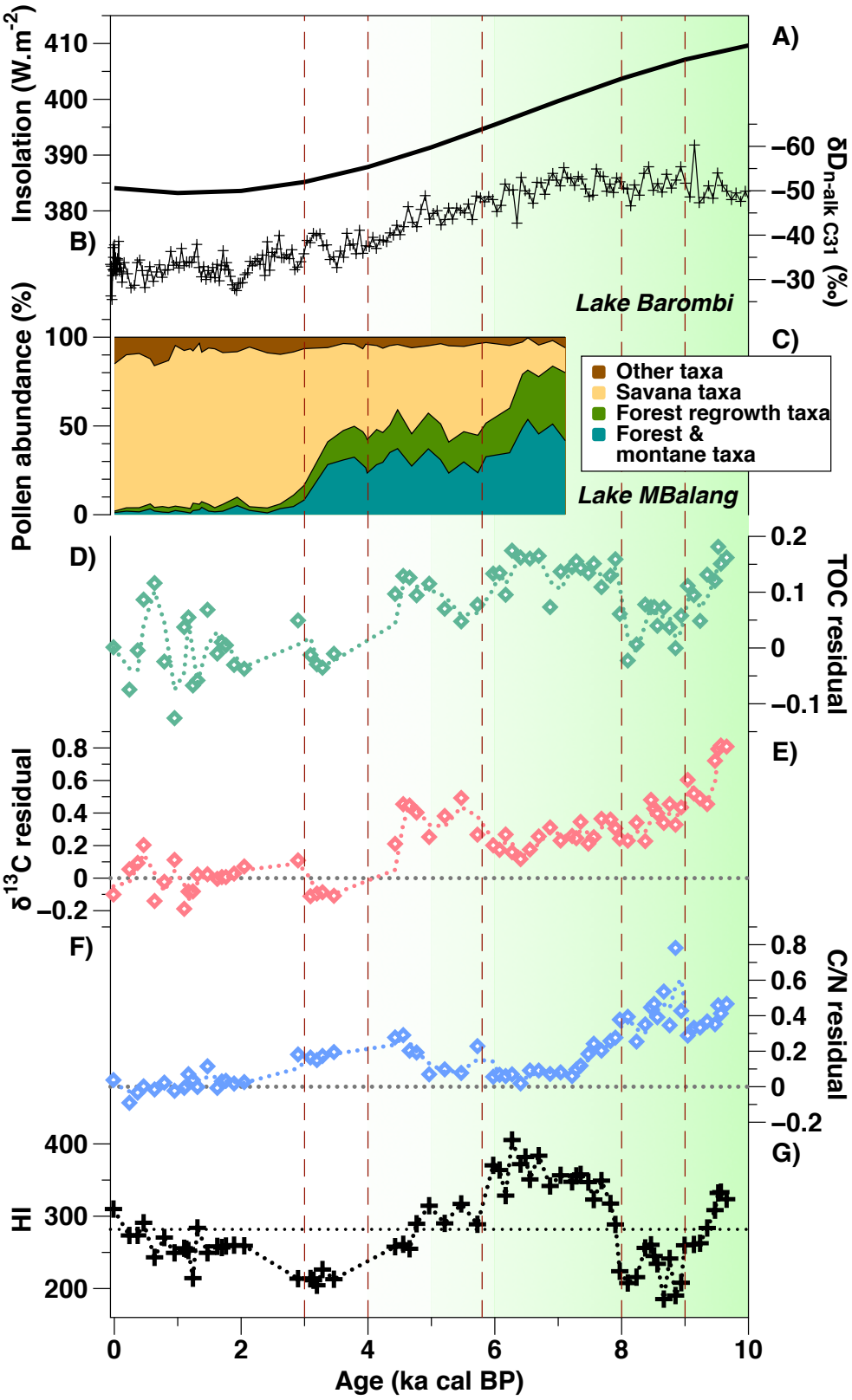

Figure 21: Retreated NGaoundaba peat deposit data and regional climatic and environmental settings: (A) Insolation 0°N ($W.m^{-2}$) from Berger et al. (1981), (B) $\delta D_{n\text{-}alkC31}$ corrected for vegetation changes in Lake Barombi (Southwest Cameroon) (Garcin et al., 2018), (C) Simplified pollen data from Lake MBalang (about 25 km from the NGaoundaba peat deposit) (Vincens et al., 2010) (D) TOC (%), (E) $\delta^{13}C_{bulk}$ (‰) and (F) C/N as well as (G) Hydrogen Index (HI) from Rock-Eval® analysis. The African Humid Period is highlighted in green, the termination of this period has been represented as a color gradient to illustrate the uncertainties and different possible timings of the termination. The mean value of HI is indicated as a dashed line. Visible transitions are indicated with vertical red dashed lines.

6. Discussion

6.1. Interpreting the residual data

The log-generated data represent the part of the signal due to decomposition. Residual values close to 0 indicate a good correspondence between the original data and the log-generated data (Figure 21). Higher values (both positively and negatively) indicate a greater difference between raw data and the model and suggest either a change in the decomposition compared to the model or the influence of other parameters that will be discussed in the next paragraphs.

In a simple approach, the carbon accumulation in peatlands can be described as a balance between vegetation inputs and decomposition (Frolking et al., 2001; Kurnianto et al., 2015). Even if microbial organic matter is generally not considered in the mass balance, microbial activity is a key point of decomposition processes (Moore, 1989). The TOC excess is thus linked to either reduced decomposition or an increase in deposition compared to the mean decomposition signal (and vice-versa). Changes in paleo -climate and -environment exert a strong influence on these parameters.

6.2. Influence of water table depth

An increase in wetness leads to changes in peatland surface structure and an increase in carbon sequestration by increasing litter production and decreasing litter decay losses (Belyea and Malmer, 2004). These changes are driven by an increase in acrotelm thickness due to a rise of the water table (Belyea and Malmer, 2004). Moisture content, redox potential and pH control the microbial community structure and can limit or enhance the presence of key decomposers (Nick T Girkin et al., 2020), even in deep peat deposits (Kluber et al., 2020). Furthermore, Ise et al. (2008) demonstrate the existence of a positive feedback between accumulation of soil organic carbon, water table depth and decomposition rates, highlighting the high sensitivity of peatland to climate variations. Hodgkins et al. (2018) demonstrated that the recalcitrance of tropical peat deposits is higher than that of boreal peat deposits which allows them to persist despite warmer and sometimes drier conditions. Tropical peat also accumulates because of the low decomposition of roots and woods under anoxic conditions when the water table is high (Chimner and Ewel, 2005).

The positive values of residual TOC before ca 4 ka cal BP (Figure 21 D) could indicate a period of increased wetness leading to a rise of the water table favouring preservation of the organic matter. This period is consistent with the timing of the African Humid Period (AHP), beginning around 14.5 ka cal BP and ending between 6 and 4 ka cal BP (among others, DeMenocal et al., 2000; Kröpelin et al., 2008; Amaral et al., 2013). The period between 9 and 8 ka cal BP that

presents residual TOC close to zero could correspond to a relatively drier intermission during the AHP.

6.3. Influence of changes in vegetation

Major shifts in vegetation also have a strong influence on both decomposition and deposition of organic matter (Belyea and Malmer, 2004). Tropical peat deposits may be visually uniform despite considerable changes in vegetation inputs (Page et al., 1999). The visual homogeneity of the NGaoundaba peat deposit does not exclude changes in the vegetation. A reciprocal relation between carbon storage and plant species diversity has been identified in a tropical peat deposit from Sumatra (Shimamura and Momose, 2007). Changes in the sources of organic matter have an influence on the initial proportion of thermo-labile vs thermo-stable organic matter (Wang et al., 2015) and, thus, on the evolution of this organic matter during decomposition. Major changes in vegetation are reported at the end of the African humid period (AHP) (Maley and Brenac, 1998; Vincens et al., 2010) and could explain part of the observed variations in residual TOC by changing the type and amount of vegetation inputs to the peatland.

To identify the period where the signal is most influenced by vegetation changes at the NGaoundaba peat deposit, we use $\delta^{13}C_{bulk}$, both raw and residual (Figure 20 B and Figure 21 E). Skrzypek et al. (2010) demonstrated that the primary $\delta^{13}C$ signal of peat-forming plants is preserved and that decomposition has only a secondary influence on the $\delta^{13}C_{bulk}$ signal. The latter has been directly used to describe changes in C_3/C_4 vegetation (Baker et al., 2014).

The two main periods observed in the residual $\delta^{13}C_{bulk}$ data before and after around 4 ka cal BP are roughly consistent with the timing of the AHP (Figure 21 E). The raw $\delta^{13}C_{bulk}$ values close to -25‰ until 5.8 ka cal BP are consistent with a C_3-dominated environment suggesting predominance of forest taxa (Figure 20 B). The period from 5.8 to around 4 ka cal BP highlighted in both residual and raw $\delta^{13}C_{bulk}$ presents less depleted values. It may suggest a short transition to C_4-dominated savanna taxa followed by a short return of the C_3-dominated environment between 4 and 3 ka cal BP, with raw $\delta^{13}C_{bulk}$ around -25‰. After 3 ka cal BP, the signal is consistent with an increasing influence of C_4-type plants.

Human activities such as turning peatland into cultured field also can have an impact on the accumulation of carbon (Z. Wang et al., 2017) and, consequently, on the $\delta^{13}C_{bulk}$ signature (Lane et al., 2008). The influence of human occupation on sedimentary archives is reported in several studies from West Africa during late Holocene such as around 2.6 ka cal BP at lake Barombi MBo (Cameroon) (Garcin et al., 2018) or after 2.2 ka cal BP in the Congo River Basin (Bayon et al., 2019). It cannot be excluded that the recent history of the NGaoundaba peat deposit was influenced by human occupation.

6.4. Influence of C-cycling and microbial organic matter

Peat deposits can shift from a sink to a source of CO_2 and CH_4 gases reflecting changes in the microbial communities and associated biogeochemical processes such as methanotrophy and methanogenesis (Jauhiainen et al., 2005; Roehm, 2005). Even if the proportion, in terms of the mass of the microbial organic matter, is not large, the specific $\delta^{13}C$ signature of some microbial compounds may not be negligible. Indeed, some carbon sources such as methane can present important variations of their carbon isotopic composition and values as depleted as -110‰ for direct reduction of CO_2 to CH_4 (Whiticar, 1999). The $\delta^{13}C$ of methanotrophs' biomass is generally close to the carbon source signature even if depletion or enrichment of cellular components can be observed depending on metabolic pathway or environmental parameters (Jahnke et al., 1999). Thus, even a small proportion of highly ^{13}C-depleted microbial biomass could significantly modify the $\delta^{13}C_{bulk}$.

Mosses such as Sphagnum spp. can use recycled carbon in wet environments (Price et al., 1997; Nichols et al., 2009). By extension, $\delta^{13}C_{bulk}$ has also been proposed to reflect variations in the uptake of C recycled from methanogenesis with enriched values corresponding to periods of high methanogenesis (Jones et al., 2010). However, Sphagnum are not present at the NGaoundaba peatland, which is dominated by sedges, so $\delta^{13}C_{bulk}$ cannot be interpreted this way.

As an example, if we consider CH_4 with a $\delta^{13}C$ signature close to -60‰, taking into account both direct reduction of CO_2 to CH_4 and acetotrophic methanogenesis (Whiticar, 1999). In a first approximation, we can consider that bulk organic matter produced by consumption of this methane will have a similar $\delta^{13}C$ signature as the source CH_4. Even a 1% input of this microbial organic matter in the bulk will lead to a decrease of more than 0.5‰ of the $\delta^{13}C_{bulk}$. Present bulk data don't give us much information about microbial activity. However, it is important to keep in mind that a microbial signal can superimpose on the primary $\delta^{13}C_{bulk}$ signal and either increase or mask pre-existing variations. Kuhry and Vitt (1996) compared the evolution of bulk C/N in both the acrotelm and catotelm in a Sphagnum peat, suggesting a predominant impact of peat decomposition on C/N values. The increase in acrotelm is interpreted as a preferential N loss in oxic conditions while the decrease in catotelm is consistent with a predominance of methanogenesis affecting C content while N is no longer affected by decomposition and is much less mobile in the sediment under anoxic conditions. These observations are not consistent with the general increase observed in C/N in the NGaoundaba peat deposit (Figure 21 G). This increase follows the general increase observed in TOC and is interrupted by a short interval from 9 to 8 ka cal BP when the C/N increases and might suggest a change in the origin of the organic matter (Talbot and Johannessen, 1992).

6.5. Validation and limits of the approach

The decreasing I-index observed in the NGaoundaba peat deposit from 6.4 ka cal BP to the surface reflects the decrease of thermolabile compounds and the relative increase in thermostable compounds, reflecting the progressive decomposition of labile organic matter and the increase in thermal stability of organic matter from 6.4 ka cal BP until present (Sebag et al., 2016) (Figure 20 D). During this period, raw TOC increases, indicating an enrichment in thermostable C-rich compounds relatively to thermolabile compounds richer in heteroatoms. Between the bottom of the core and 6.4 ka cal BP, the I-index remains rather stable; it is likely that most thermolabile compounds are decomposed and it is consistent with a raw TOC around 50% with limited variations during this period.

Our method is based on the observation that for this particular peat deposit, the TOC increases progressively with depth and follows nearly exactly a logarithmic curve. The function used for the modelling will depend on the dynamics of the system (Clymo et al., 1998). Thus, this method is undoubtedly not applicable to all peat deposits. This increasing trend is expected for peats composed almost entirely of organic matter. The presence of mineral-rich intervals such as clayey or sandy intervals or a steady input of a large amount of mineral matter will affect this trend (Baker et al., 2014; Njagi et al., 2021). Such records are therefore not ideal for the modeling presented in this study. The method gives a lot of weight to the top values of the core and slight analytical errors in these values could have a strong impact on the model. As vegetation may be the primary factor controlling $\delta^{13}C_{bulk}$ (Skrzypek et al., 2010), the curve fitting might be distorted by the primary impact of vegetation changes. It may explain why the curve fitting for $\delta^{13}C$ is not as good as for TOC with the modeling function rapidly diverging from the data (Figure 18). The residual $\delta^{13}C_{bulk}$ (Figure 21 E) erases two periods of relatively enriched $\delta^{13}C_{bulk}$ from 5.8 to 4 ka cal BP and from the bottom of the core to 9 ka cal BP visible in the raw $\delta^{13}C_{bulk}$ record (Figure 20 B).

The comparison between residual TOC and HI from the same peatcore shows striking similarities (Figure 21 D & G). The HI can be controlled by the degree of decomposition but can also reflect changes in the origin of the organic matter (Sebag et al., 2016). The higher values observed between 8 and 6 ka cal BP and at the bottom of the core tend to indicate well preserved terrestrial organic matter that is consistent with the TOC data and the wettest period of the African Humid Period. The decrease in HI between 9 and 8 ka cal BP suggests a change in the origin of the organic matter or in its decomposition and is consistent with the increase in the C/N ratio observed at the same period.

Conclusions

The present case study based on a West-African peat deposit presents several interesting characteristics: it is nearly continuous, macroscopically homogeneous without clayey passages, and some bulk parameters such as TOC present a strong logarithmic trend with age. Thus, it is possible to propose a method to isolate and subtract the part of the variation only due to the decomposition of organic matter and interpret the residual variations as modifications of the environmental conditions.

The residual TOC obtained with our method highlights well-known climatic transitions and variations such as the African Humid Period and presents similar variations as other parameters such as HI. Results obtained from residual C/N and $\delta^{13}C_{bulk}$ are more questionable, suggesting a greater impact of parameters other than decomposition on the variations, such as vegetation shifts (Skrzypek et al., 2010; Baker et al., 2014), changes in microbial processes (Moore, 1989; Nick T Girkin et al., 2020) or detrital input (Amorim et al., 2022) associated with differences in the way the decomposition processes affect these parameters (Ågren et al., 1996). Based only on bulk organic parameters, it is difficult to precisely constrain the origin and timing of the proposed environmental and climatic changes, thus the use of other proxies such as pollen data and biomarkers will help to confirm or infirm the climatic and environmental interpretation proposed here.

This method is certainly not applicable to all peat deposits and we recommend a careful analysis of the data and testing before applying it. We recommend applying this method to records composed almost entirely of organic matter and without significant variation in the mineral fraction. This method is a quick and straightforward way to obtain a first overview of the paleoclimatic and paleoenvironmental variations from a new sediment core based on bulk analytical methods (Elemental Analysis and Rock-Eval®). It can help to identify periods of great interest for more intensive investigations (e.g., pollen, biomarkers), by highlighting the main transitions visible in bulk organic data.

Supplementary material:

Table S 1: Curve fit parameters

	TOC	$\delta^{13}C$	C/N
Curve equation form	**aln(bx+c)+d**	**aln(bx+c)+d**	**aln(bx)+c**
a	**0.182**	**-0.208**	**0.167**
b	**2.267**	**0.931**	**25.612**
c	**0.01217**	**0.01303**	**-0.022**
d	**0.781**	**0.128**	**/**
r^2	**0.909**	**0.63**	**0.59**
Number of values for partial curve fitting	**13**	**17**	**11**
Limit depth (cm)	**125**	**155**	**105**
Limit age (ka cal BP)	**1.65**	**2.5**	**1.35**

The following figure presents the "raw" data depending on depth (cm).

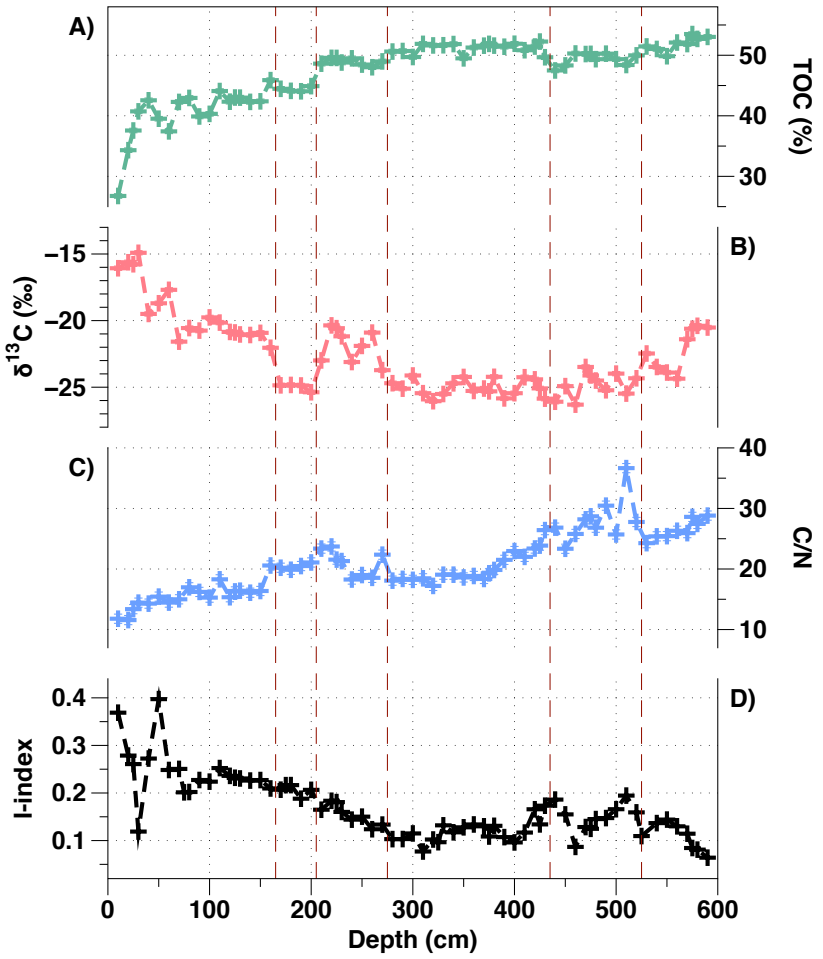

Figure S 1: Raw data (ie before data processing) from the NGaoundaba peat deposit: (A) TOC (%), (B) $\delta^{13}C_{bulk}$ (h), (C) C/N from Elemental and stable isotope analysis and the I-index from Rock-Eval® analysis depending on depth (cm). Visible transitions are indicated with vertical red dashed lines.

Chapter 4: Constraints on hopanes and brGDGTs as pH proxies in peat

Under review at Geochimica Cosmochimica Acta as *Constraints on hopanes and brGDGTs as pH proxies in peat*, Valentine Schaaff, Vincent Grossi, Matthew Makou, Yannick Garcin, Pierre Deschamps, David Sebag, Benjamin Ngounou Ngatcha, Guillemette Ménot.

Abstract:

Bacterial hopanes and branched Glycerol Dialkyl Glycerol Tetraethers (brGDGTs) were investigated in a 10-ka peat record from North-East Cameroon (NGaoundaba, Western Central Africa). Recently developed pH proxies using the hopane ββ/(αβ+ββ) ratio and the brGDGT cyclization ratio (CBT_{peat}) were applied and compared with previously published bulk organic data from the same core. Different hypotheses are usually proposed to explain the high abundance of the "thermally mature" C_{31} αβ hopane in peats: acid-catalyzed isomerization of ββ to αβ isomers with or without biological mediation or the direct input of C_{31} αβ hopanes by bacteria. In the NGaoundaba peat deposit, the opposite variation in the ββ/(αβ+ββ) ratio of C_{30} and C_{31} hopanes and the carbon isotopic composition of C_{31} ββ and αβ hopanes are not consistent with an acid-catalyzed isomerization without biological mediation. A high correlation between hopane- and brGDGT-reconstructed pH is observed, suggesting a similar response to environmental changes for these two independent proxies. Major pH variations coincide with changes in vegetation and precipitation at the end of the African Humid Period (AHP). Lower pH values are observed during the AHP, consistent with increased humification and organic acid production during periods of increased peat wetness. Based on the comparison of several paleo-pH records, we suggest a major influence of catchment lithology on pH variations, as alkaline inputs in a carbonate-dominated environment can significantly influence pH variations.

Keywords: Lipid biomarkers, isomer ratios, ^{13}C composition, pH reconstruction, African Humid Period

This chapter is currently under review for publication at GCA.

1. Introduction

Peat deposits are receiving increasing attention from the scientific community because they are particularly susceptible to be affected by current and future climate warming, which could threaten their ability to store carbon (e.g., Belyea and Malmer, 2004; Leifeld and Menichetti, 2018). Peat deposits also have great potential for paleoclimatic studies, especially those based on organic biomarkers (e.g., Naafs et al., 2019). Continental records can be scarce and discontinuous but peat deposits have great potential to improve our understanding of past climate variations. Developing new proxies based on lipid biomarkers for paleoclimatic and paleoenvironmental reconstructions is limited by our understanding of the origin and diagenesis of these compounds in sediments (e.g., Castañeda and Schouten, 2011; Naafs et al., 2019) and by the lack of records in some areas, especially in the tropics. Recent advances in peat and biomarker proxies are expanding our ability to reconstruct past climates and environments (Naafs et al., 2019 and references therein). Several peat-calibrated proxies based on different classes of compounds, such as hopanoids and branched glycerol dialkyl glycerol tetraethers (brGDGTs) have recently been developed (Naafs et al., 2017b; Inglis et al., 2018; Zhang et al., 2020), extending the possibilities of peat studies for paleoclimatic reconstructions.

Hopanoids are pentacyclic triterpenoids commonly found in diverse geological settings, where they generally occur as hydrocarbons (i.e., geohopanoids) (e.g., Quirk et al., 1984; Ries-Kautt and Albrecht, 1989; Innes et al., 1997; Farrimond et al., 2003). These compounds are produced by a wide range of bacteria, although estimates of the frequency of hopanoid biosynthesis among bacteria are still unclear (Rohmer et al., 1984; Pearson et al., 2007). The role of biological hopanoids is proposed to be similar to that of eukaryotic sterols, which regulate membrane fluidity and permeability (e.g., Ourisson et al., 1987), but a role in protection against pathogens or pH homeostasis has also been reported (Welander et al., 2009; Schmerk et al., 2011). Hopanoids are found in various phylogenetic and metabolic groups of bacteria (e.g., Rohmer et al., 1984; Pearson et al., 2007) and their use as tracers for specific bacterial communities is limited. However, hopanoids are promising biomarkers for the reconstruction of methane cycling in peats based on their carbon isotopic signature (Pancost et al., 2007; Inglis et al., 2019) and their use as proxy for pH variations in peats based on specific ratios of hopane isomers has been suggested (Inglis et al., 2018). Isomerization of biologically-derived 17β,21β(H)-hopanoids (abbreviated ββ in the following text) into the more thermally stable 17β,21α(H) (βα) and 17α,21β(H) (αβ) forms, as well as their isomerization at the C22 position, are well known to occur during the thermal maturation of sediments (Ensminger et al., 1974;

Mackenzie et al., 1980; Mackenzie and McKenzie, 1983). Accordingly, isomer ratios have been used to describe the thermal maturity of sediments (e.g., Farrimond et al., 1996). In peat deposit, high proportions of the αβ stereoisomer have been reported despite the low thermal maturation of these sediments (e.g., Quirk et al., 1984; He et al., 2015; Huang et al., 2015; Inglis et al., 2018). A direct input of αβ hopanes by indigenous bacteria could explain their high abundance (Rosa-Putra et al., 2001). It has also been suggested that these compounds are formed by microbially mediated isomerization (Ries-Kautt and Albrecht, 1989) or by acid-catalyzed isomerization without microbial mediation (Pancost et al., 2003; Inglis et al., 2018). This isomerization reaction may also be influenced by temperature and redox conditions (Huang et al., 2015). To date, the cause of the high abundance of αβ hopanes in peat is still unclear and debated.

Branched glycerol dialkyl glycerol tetraethers (brGDGTs) are membrane-spanning lipids. Unlike isoprenoid GDGTs produced by Archaea, brGDGTs are of bacterial origin (Weijers et al., 2006). BrGDGTs were first identified in a Dutch peat bog (Sinninghe Damsté et al., 2000) and since then, a wide range of brGDGTs with various number of methylation and cyclopentyl moieties have been found in natural environments (Schouten et al., 2000b, 2013). *Acidobacteria* have been proposed as the main producers of brGDGTs since they are abundant in soils and peats and produce isodiabolic acid, a building block of brGDGTs (Weijers et al., 2009; Sinninghe Damsté et al., 2011, 2014, 2018; Chen et al., 2022; Halamka et al., 2023). However, the exact source organisms of brGDGTs in the environment are still unknown, and other producers than *Acidobacteria* cannot be excluded. Environmental parameters exert significant control over brGDGTs distribution, with the cyclization ratio (CBT) primarily dependent on pH and the methylation ratio (MBT) primarily influenced by temperature (Weijers et al., 2007b). Numerous empirical calibrations for temperature and pH have been developed over the past decades as a result of technical improvement and the need for environment-specific (lake, marine, peat, and soil) global and local calibrations.

A statistically significant correlation between brGDGT-based and hopane-based reconstructed pH values was observed in a global peat database, and striking similarities between the two pH reconstructions were obtained in an Early Paleogene lignite deposit from Schöningen (Germany) (Inglis et al., 2018). However, applications of these pH calibrations have remained limited until now (Zhang et al., 2020). Peat brGDGT-based pH reconstructions using a previous soil calibration from Weijers et al. (2007b) showed large pH variations associated with major changes in peat-forming vegetation (Weijers et al., 2011; Nichols et al., 2014) or with changes in humification associated with changes in precipitation (Zheng et al., 2015; M. Wang et al., 2017).

In this study, we further investigate the distribution of hopanes and brGDGTs in peat samples and their respective uses as tracers of pH variations. The results are based on a 10-ka record from the NGaoundaba peat deposit located on the Adamawa Plateau (North East Cameroon, West Africa), already constrained by a study on bulk organic parameters (Schaaff et al., 2023). By comparing various parameters for hopane and brGDGT distributions (relative abundances, specific ratios, and carbon isotopic data for C_{31} hopanes), we propose new constraints on the origin of these compounds. The comparison of hopane- and brGDGT-based pH reconstructions further allowed us to assess the applicability of these reconstructions to Holocene peat records and their potential paleoclimatic and paleoenvironmental interpretations.

2. Material and methods

2.1. Study site

The NGaoundaba peat deposit is located in a volcanic crater on the Adamawa Plateau in Northeast Cameroon (N7.135° E13.690°, 1175 m above sea level). The vegetation at the NGaoundaba peat deposit is dominated by sedges (*Cyperus* spp) while the site lies in the Soudano-Guinean shrubs savannas zone (Letouzey, 1958). Present day climate is characterized by two contrasting seasons: a 7-month rainy season from April to October, and a 5-month dry season from November to March. The mean annual air temperature (MAAT) is 22.19°C and the mean annual precipitation (MAP) is 1482 mm (CRU database, Harris et al., 2014).

2.2. Sediment core and ^{14}C dating

A 6-meter-long core (named NGBA19) was collected in February 2019 using a Russian peat corer. The core is composed of dark brown peat without visible sandy or clayey zones. The core was then sub-sampled at 2.5-cm intervals. Organic geochemical analyses were performed on 73 samples.

The age model of the NGaoundaba peatcore is based on 30 radiocarbon dates carried out at the LMC14 Laboratory (Saclay, France). Details on the dating and calibration of the age model are given in Schaaff et al. (2023) (see Chapter 3).

2.3. Organic geochemical analyses

2.3.1. Sample preparation

All samples were freeze-dried, ground and homogenized. Extraction was performed two times for 0.3g of each sample with 10mL of dichloromethane (DCM)/methanol (3:1, v/v) using a MARS 6 CEM microwave extraction system. Following each extraction, the supernatant was filtered through a sintered Teflon filter. Synthetic C_{46} GDGT was added to the combined extracts of each sample as an internal standard (Huguet et al., 2006). The total lipid extract was separated by column chromatography on silica gel into three fractions. The hydrocarbon fraction containing hopanes was eluted first with 8mL of hexane. A second fraction was eluted with 5mL of hexane/DCM (1:1, v/v). BrGDGTs were eluted in a third fraction with 10mL of DCM/methanol (1:1, v/v).

2.3.2. Hopane identification and analyses

Copper curls activated with HCl were added to the hydrocarbon fractions to remove elemental sulfur. After a first GC-FID analysis (HP 6890A), GC-MS analyses (Agilent 6890N GC coupled to an Agilent 5975C MSD and Agilent 7890B GC coupled to an Agilent 5977B MSD) were performed for identification and quantification of the different compounds. Both GC-MS instruments provided comparable data. Hopanes were identified based on their retention time and mass spectrum. The identification of hopane isomers is consistent with published literature (Naafs et al., 2019). Semi-quantification was performed using the TIC by comparison with an external standard solution containing cholestane.

Prior to carbon isotopic measurements, the hydrocarbon fractions were separated into a saturated and an unsaturated fraction by column chromatography using silica gel impregnated with $AgNO_3$ (10 % wt). Saturated fractions containing hopanes were eluted with 3 to 4 mL of n-heptane. Unsaturated fractions were eluted with 3 to 4 mL of ethyl acetate. Carbon isotopic compositions were measured at the LGL-TPE (Université Claude Bernard Lyon 1) using an Agilent 7890B GC coupled to an Isoprime visION Isotope Ratio Mass Spectrometer via an Isoprime GC-5 combustion interface (Elementar). The GC-5 furnace was operated at 850 °C. An autotune and tests of stability and linearity of the signal were performed daily using the software ionOS. Stable carbon isotopic compositions (expressed as $\delta^{13}C$ values) were calibrated using a reference CO_2 gas reported to VPDB scale. Two Mix hydrocarbon B4 standards (A Schimmelmann, Indiana University) were measured every 4 to 5 samples and used to correct the $\delta^{13}C$ values. Samples were analyzed in duplicates when the quantity of samples allowed it.

2.3.3. brGDGT analyses

Fractions containing brGDGTs were filtered using 0.45 µm PTFE filters. BrGDGT analyses were performed using High Performance Liquid Chromatography Mass Spectrometry (HPLC-APCI-MS, Agilent 1200) at the LGL-TPE (ENS de Lyon). Separation was achieved on two silica columns in series (ACQUITY UPLC BEH HILIC, WATERS) following the procedure of Hopmans et al. (2016) slightly modified (i.e. using hexane/isopropanol (98.2:1.8, v/v)). Peaks corresponding to brGDGTs were manually integrated and quantified using the peak area of C_{46}. The selected m/z values are 743.9, 1050.2, 1048.2, 1046.2, 1036.2, 1034.2, 1032.2, 1022.2, 1020.2 and 1018.2.

2.3.4. Hopane- and brGDGT-based ratios and pH reconstructions

The degree of hopane isomerization was calculated using the ββ/(αβ+ββ) and 22S/(22S+22R) indices developed by Mackenzie et al. (1980). The ββ/(αβ+ββ) ratio was calculated for both C_{30} and C_{31} hopanes. The C_{31} αβ hopane was considered as the sum of the 22S and 22R isomers. The hopane-based pH reconstruction uses the C_{31} ββ/(αβ+ββ) index and was calculated using the following equation proposed by Inglis et al. (2018) for peats:

$$pH = 5.22 * \frac{\beta\beta}{\alpha\beta + \beta\beta} + 3.11 \; (n = 94, r^2 = 0.64, RMSE = 1.4)$$

The GDGT-based pH reconstruction is based on the CBT_{peat} index using the following equation developed by Naafs et al. (2017b) for peats:

$$CBT_{peat} = \log\left(\frac{Ib + IIa' + IIb + IIb' + IIIa'}{Ia + IIa + IIIa}\right)$$

$$pH = 2.49 * CBT_{peat} + 8.07 \text{ (n=51, } r^2\text{=0.58, RMSE=0.8)}$$

Compound structures (with numbering) are presented in Figure 22.

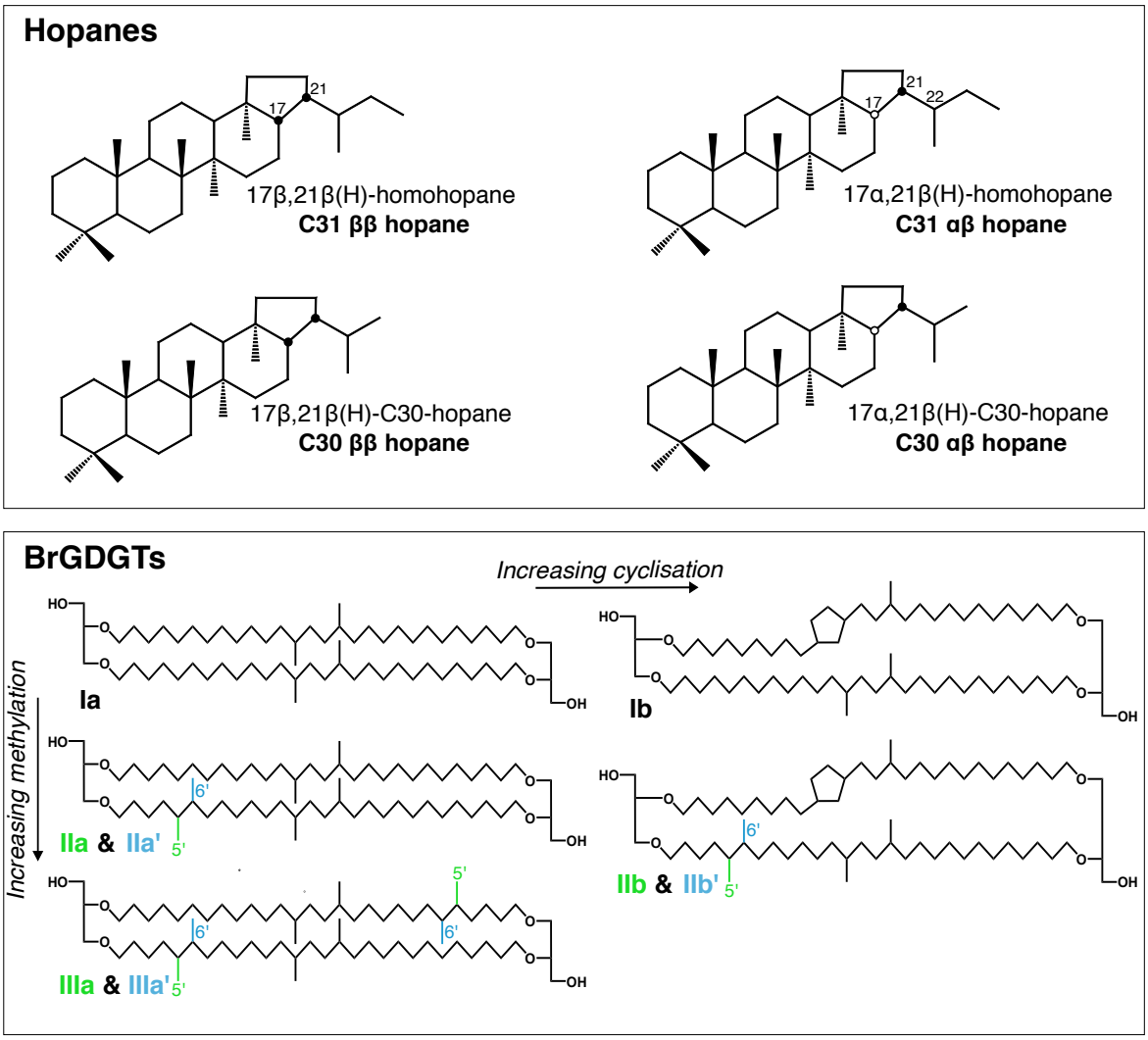

Figure 22: Structures of hopanes and brGDGTs analyzed in this study. C_{31} 22S and 22R hopane isomers are not discriminated.

3. Results

3.1. Relative abundance and concentration of biomarkers

3.1.1. Hopanes

In the peat samples investigated, C_{31} hopanes are present in three different configurations: ββ, αβR and αβS isomers (Figure 23). The C_{31} αβS hopane is present only between 8.4 ka cal BP and 6.0 ka cal BP, and its concentration ranges from 0 to 32.0 µg/g_{TOC} (Figure 24 A). The concentration of C_{31} αβR hopane ranges from 0 to 44.4 µg/g_{TOC} (Figure 24 A). From 9.7 to 9.4 ka cal BP, the concentration of C_{31} αβR hopane ranges from 10.6 to 16.4 µg/g_{TOC}. The concentration decreases to values of around 5 µg/g_{TOC} between 9.4 and 8.5 ka cal BP, and then increases to values above 10 µg/g_{TOC} during the 8.5 to 7.3 ka cal BP interval. Concentration remains between 4.1 and 10.9 µg/g_{TOC} until 5.8 ka cal BP. The concentration is low from 5.8 ka cal BP to the surface except during a 0.6 ka interval centered at 4.4 ka cal BP when a slight

increase is recorded. The concentration of the C_{31} ββ hopane varies from 1.2 to 12.1 µg/g_{TOC} (Figure 24 B). Variations of the C_{31} ββ hopane are similar to those of the C_{31} αβR hopane with the highest values observed between 9.7 and 9.4 ka cal BP and between 8.4 and 5.8 ka cal BP. The C_{31} αβR hopane is more abundant than the C_{31} ββ hopane from 9.7 until 5.8 ka cal BP as well as between 4.8 and 3.0 ka cal BP.

C_{30} hopanes are dominated by ββ isomers in most samples (Figure 23). The concentration of C_{30} ββ hopane ranges from 0.1 to 3.5 µg/g_{TOC}, while the concentration of the C_{30} αβ isomer ranges from 0 to 1.8 µg/g_{TOC}. The concentration of C_{30} ββ hopane presents its maximum from the bottom of the core to 9.4 ka cal BP and from 8.1 ka cal BP to 5.8 ka cal BP (Figure S 2).

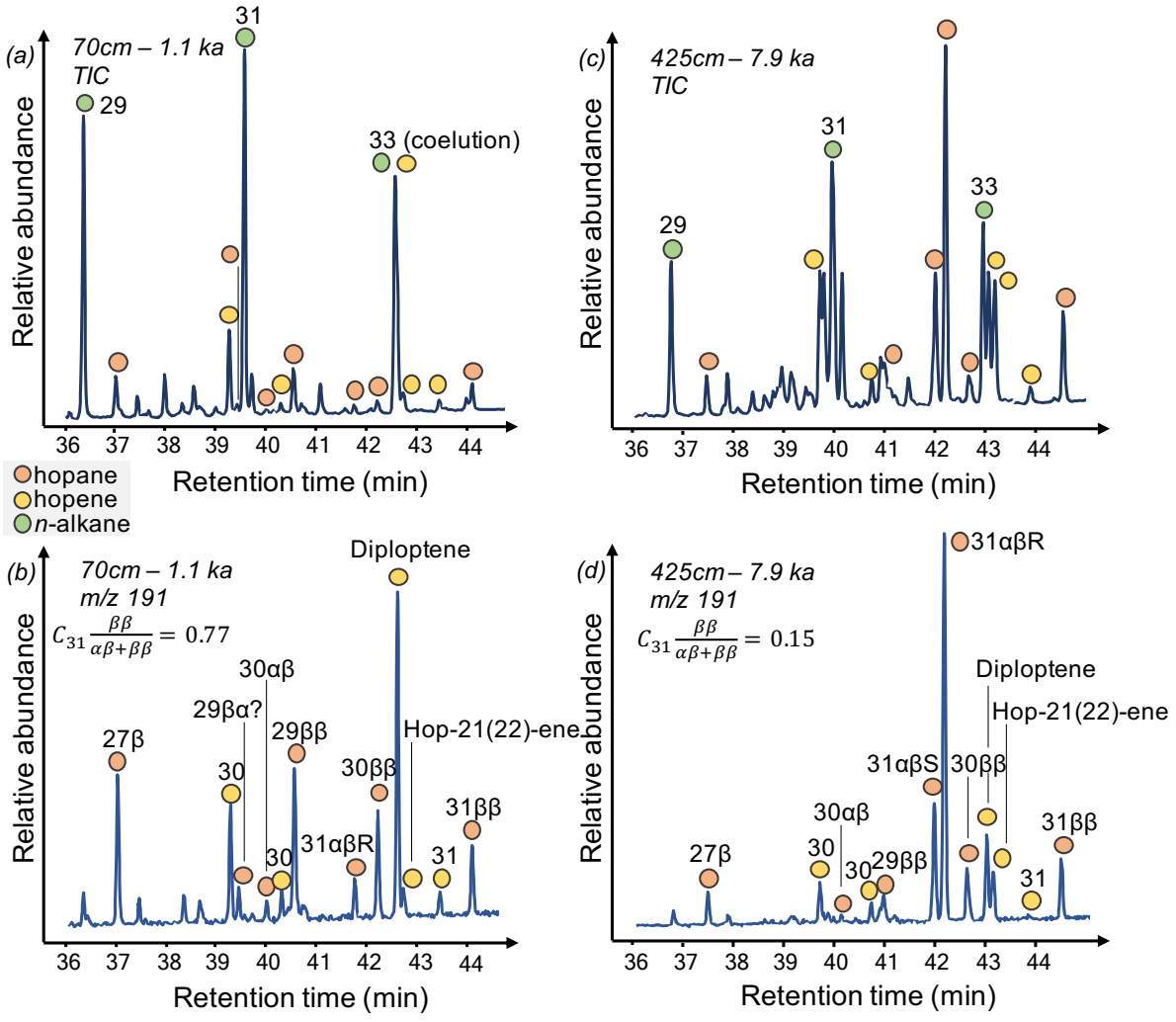

Figure 23: GC-MS partial chromatograms of the hydrocarbon fractions of two samples with distinct hopanoid distribution: 70 cm-depth Total Ion Chromatogram (TIC) (a) and m/z 191 (b) and 425 cm-depth TIC (c) and m/z 191 (d). Ages of the samples are in ka cal BP.

3.1.2. brGDGTs

The brGDGT assemblage is dominated by brGDGT-Ia, which represents between 52.4 and 77.6 % of it (calculations include OH, H and all isomers) (Table 3). The concentration of the brGDGT-Ia ranges from 45.4 to 194.0 µg/g_{TOC}. The relative abundance and concentration of brGDGTs decrease with increasing number of methylation (Ia to IIIa) and degree of cyclization (Ia to Ic) (see Table 3 for more detail). The 6-methyl brGDGTs (IIa', IIb' and IIIa') exhibit lower relative abundance and concentration than their 5-methyl counterparts.

Table 3: Relative abundance (%) and concentration (µg/g_{TOC}) of brGDGTs discussed in this paper. Tr = Traces are for values under 0.05

brGDGT	Abundance (%)				Concentration (µg/g_{TOC})			
	Mean	Min	Max	Median	Mean	Min	Max	Median
Ia	64.8	52.4	77.6	65.9	96.0	45.4	194.0	90.3
Ib	3.6	1.7	7.4	3.2	5.0	1.8	12.1	4.8
IIa	11.9	6.3	18.3	11.4	16.4	8.3	26.7	16.1
IIa'	2.6	0.6	6.1	2.4	3.6	0.7	9.7	3.6
IIb	0.5	0.2	1.3	0.4	0.7	0.3	2.2	0.6
IIb'	0.2	Tr	0.7	0.1	0.3	Tr	0.8	0.2
IIIa	1.0	0.3	2.0	0.9	1.3	0.5	2.7	1.2
IIIa'	0.6	0.2	1.3	0.5	0.8	0.3	2.0	0.7

3.2. Carbon isotope composition of C_{31} ββ and αβR hopanes

The $\delta^{13}C$ isotopic composition of the C_{31} αβR and C_{31} ββ hopanes could be measured for 42 and 43 out of 73 samples, respectively, most of them in duplicates. The $\delta^{13}C$ of the C_{31} αβR hopane ranges from around -25.8 to -18.7 ‰ with a mean standard deviation of 0.24 ‰ (min: 0, max: 0.87) (Figure 24 C). The most ^{13}C-depleted values of the C_{31} αβ isomer are recorded between 8.1 and 5.9 ka cal BP and between 3.5 and 3.1 ka cal BP. More ^{13}C-enriched values are recorded around 9.7, 8.5 and 4.6 ka cal BP (Figure 24 C). The $\delta^{13}C$ composition of the C_{31} ββ hopane appears slightly depleted compared with the αβ isomer, ranging from around -36.0 to -22.6 ‰ with a mean standard deviation of 0.24 ‰ (min: 0.01, max: 0.83) (Figure 24 D). The $\delta^{13}C$ value of the C_{31} ββ hopane presents a global decreasing trend towards present day with periods of short increase around 8.5 ka cal BP and at 4.7 ka cal BP (Figure 24 D).

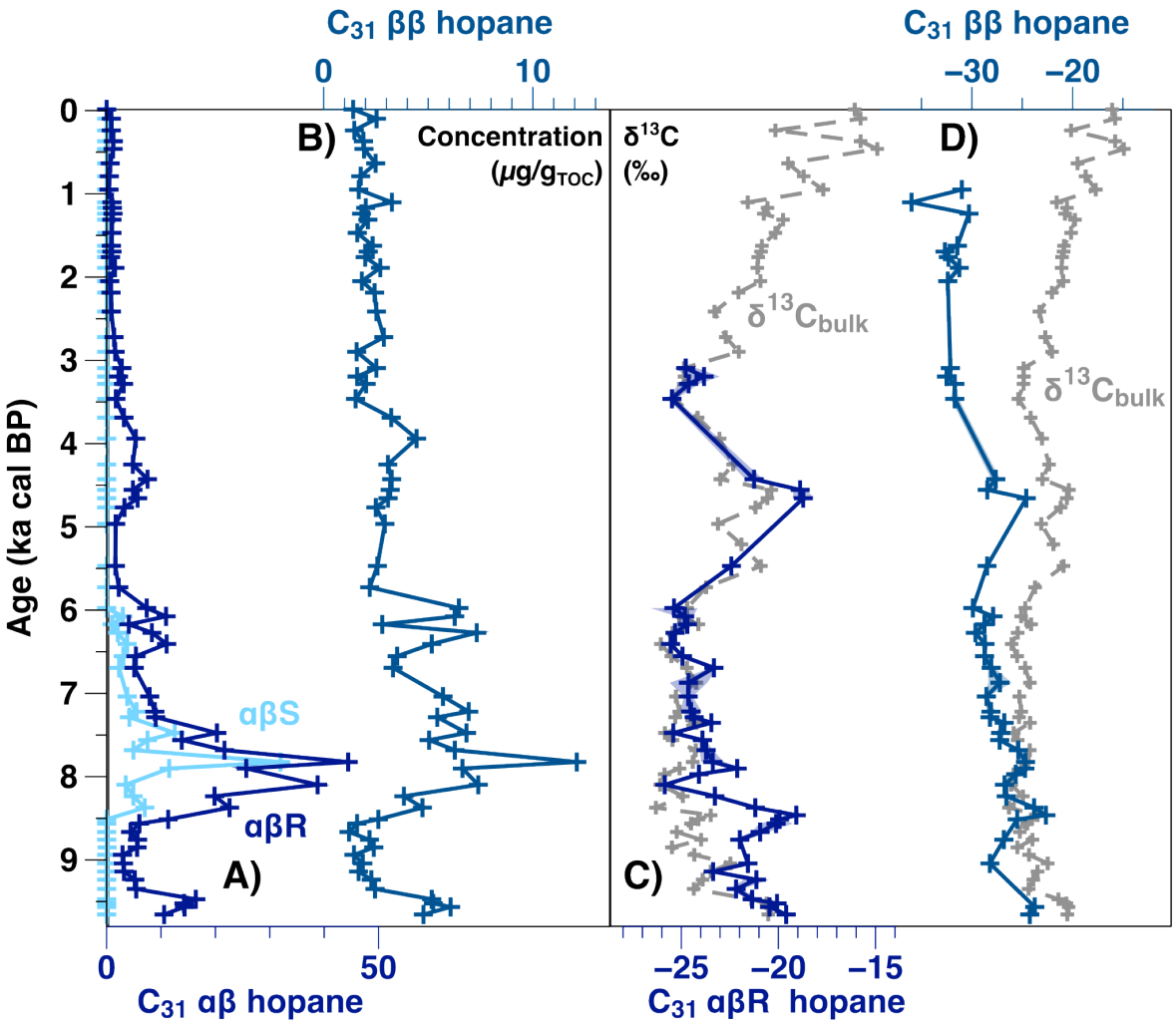

Figure 24: Concentration of (A) C_{31} abR and abS and (B) bb hopanes (μg/g_{TOC}) and carbon isotopic data for (C) C_{31} abR and (D) bb hopanes compared to carbon isotopic data of bulk sediment from Schaaff et al. (2023). The uncertainties for $\delta^{13}C_{bulk}$ values are smaller than the size of the data point, those for $\delta^{13}C_{hopane}$ values are shown on the figure but are, in most cases, smaller than the size of the data point.

3.3. Hopane stereoisomers and CBT ratios

The ββ/(αβ+ββ) indices of C_{31} and C_{30} hopanes were obtained for 67 and 49 samples out of 73, respectively. The C_{31} 22S/(22S+22R) index was only obtained for samples between 8.9 and 6 ka cal BP (Fig. S.3).

The C_{30} ββ/(αβ+ββ) index ranges from 0.4 to 0.9 (Figure 25 A). This index is globally high (around 0.7-0.8) from 9.7 to 6.0 ka except for an isolated sample around 0.53 at 8.8 ka cal BP. The ratio decreases to values around 0.5 between 6.0 and 5.4 ka cal BP and increases again to values around 0.7 between 5.0 and 1.0 ka cal BP. From 1.0 ka cal BP upward, the C_{30} ββ/(αβ+ββ) index shows its lowest values with minima around 0.8 ka cal BP and in the topmost sample corresponding to the post bomb period (Figure 25 A).

The C_{31} ββ/(αβ+ββ) index ranges from 0.1 to 0.8 (Figure 25 B). This index is low until 6.0 ka cal BP with values below 0.42 and presents its lowest values (below 0.2) between 8.5 and 7.4 ka cal BP. The ratio then increases until ca. 4.9 ka cal BP, and after a period of values below 0.5 between 4.9 and 2.8 ka cal BP, the late Holocene is characterized by values above 0.6. Short time-scale variations are recorded between 2.0 and 1.1 ka cal BP (Figure 25 B).

The CBT_{peat} index ranges from -1.4 to -0.7 (Figure 25 C). This index oscillates around -1 from 9.7 to 8.9 ka cal BP, and then progressively decreases to reach its lowest values between 8.4 and 7.4 ka cal BP. The CBT_{peat} index increases between 7.4 and 4.9 ka cal BP, with a short decrease centered at 6.3 ka cal BP. It then decreases from 4.9 to 4.0 ka cal BP and increases again roughly between 4.0 to 0.9 ka cal BP with short time-scale variations. The CBT_{peat} index then decreases until the present day (Figure 25 C).

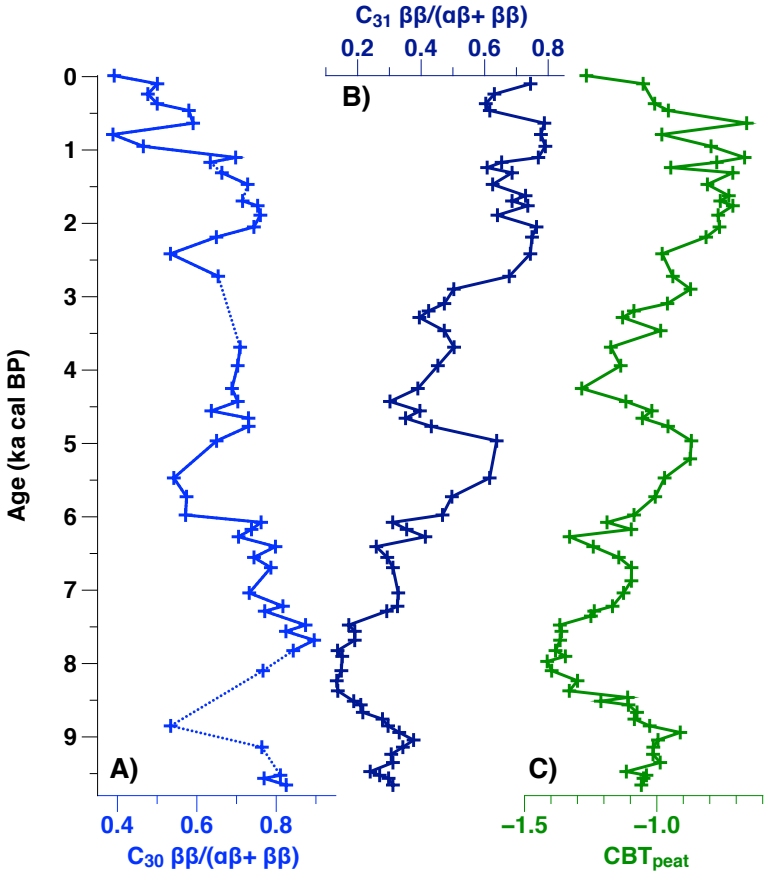

Figure 25: Downcore evolution of hopane- and GDGT- indices with time: C_{30} ββ/(αβ+ββ) (A), C_{31} ββ/(αβ+ββ) (B) and CBT_{peat} (C). The dotted line shows the gaps in the data and the isolated values compared to the other indices.

3.4. pH reconstructions

BrGDGT-based reconstructed pH values range from 4.5 to 6.5, while hopane-based reconstructed pH values range from 3.8 to 8.3 (Figure 26 E and F). From 9.7 ka cal BP until 9

ka cal BP, pH reconstructions record stable values around 4.8 and 5.5 for hopane-based and brGDGT-based reconstructions, respectively. Both pH reconstructions then decrease and present their lowest values between 8.4 and 7.4 ka cal BP. Values remain low until 6.2 ka cal BP. During the middle and late Holocene, pH globally increases with smaller scale variations visible in both pH records. In particular, both pH reconstructions show a constant decrease between 4.8 ka cal BP and 3.3 ka cal BP and more stable values after 3.3 ka cal BP. In contrast to the rest of the core, the most superficial samples show inverse trends for both pH reconstructions, with an increasing trend in the hopane-based pH and a decreasing trend in the GDGT-based pH (Figure 26 E and F).

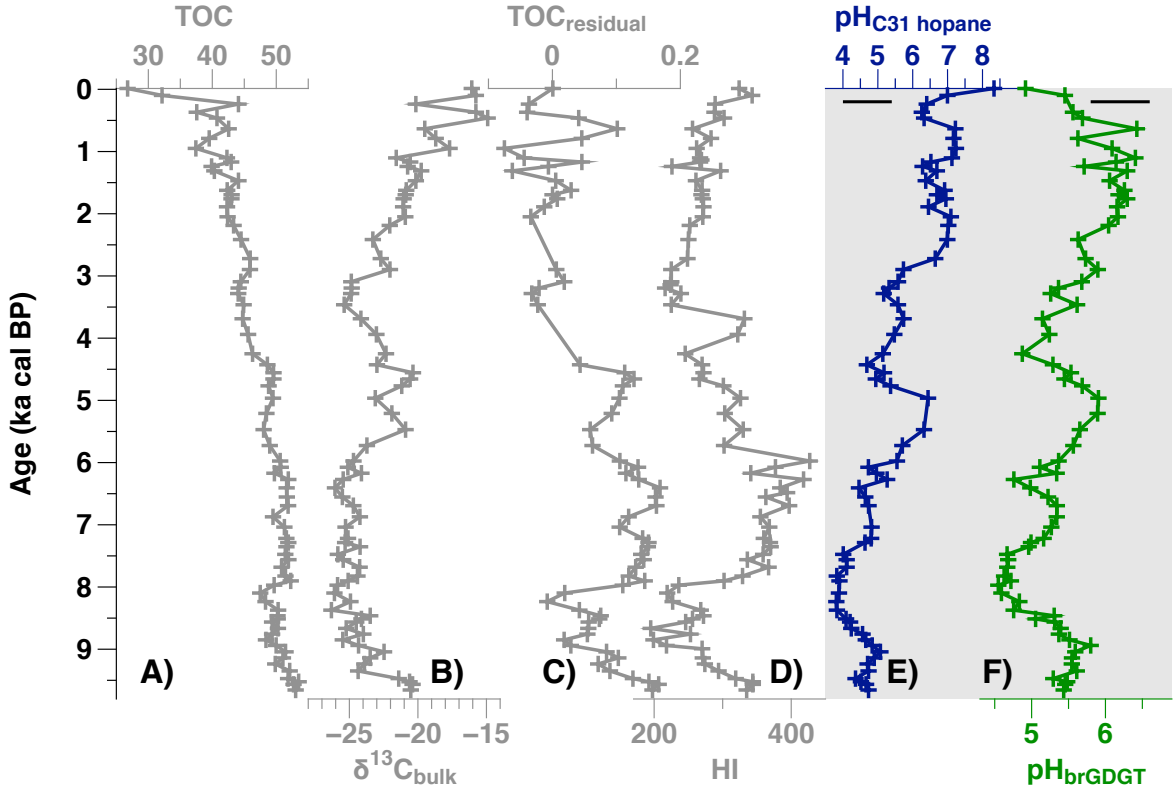

Figure 26: Downcore evolution of bulk organic data: TOC (A), $d^{13}C_{bulk}$ (B), $TOC_{residual}$ (C) and HI (D) (Schaaff et al., 2023) and pH reconstructions: C_{31} hopane-based pH (E), brGDGT-based pH (F). The RMSE associated with each pH calibration is indicated at the top of each panel.

4. Discussion

4.1. Constraints on the origin of hopanes

To explain the high abundance of C_{31} αβ isomer in peats (e.g., Quirk et al., 1984; Ries-Kautt and Albrecht, 1989; this study) as well as the correlation between the C31 ββ/(αβ+ββ) ratio and pH (Inglis et al., 2018), several hypotheses have been proposed and are illustrated in Figure 27. Using hopanes data from the NGaoundaba peat deposit as well as comparison with previously published data, this section reviews the pros and cons of each hypothesis.

The first hypothesis proposed to explain the high abundance of the "thermally mature" αβ hopane isomers in peats characterized by low pH values is related to an abiotic isomerization of the carbon skeleton at the C17 position of the ββ isomers catalyzed by the high acidity of the system (Figure 27 A) (Pancost et al., 2003). This hypothesis is consistent with the low abundance of the C_{31} αβ hopane in peat characterized by neutral pH (Dehmer, 1995; Inglis et al., 2018) but still lacks a clear demonstration, notably from laboratory experiments. Furthermore, several observations in the present study argue against such a direct acid-catalyzed isomerization of ββ hopanes. First, the opposite variations in the ββ/(αβ+ββ) ratios of C_{30} and C_{31} hopanes observed all along the core do not support a purely acid-catalyzed isomerization since C_{30} hopane and C_{31} homohopane should be affected similarly by such an abiotic process (Figure 25 A and B and supplementary material Figure S 4). Second, isomerizations by intramolecular rearrangement are associated with no or limited isotope effect (Hightower and Hall, 1967), which is consistent with the similar $\delta^{13}C$ values of C_{31} ββ and αβ hopanes during early diagenesis in oil shale (Sinninghe Damsté et al., 1995). At both the NGaoundaba peat deposit (Figure 24 C and D) and the Dajiuhu peatland (Huang et al., 2018, see supplementary material), the $\delta^{13}C$ values of C_{31} ββ and αβ hopanes present similar core profiles but differ by up to 5 to 10 ‰, arguing against a direct acid-catalyzed isomerization of hopanes sharing the same biological source organism(s).

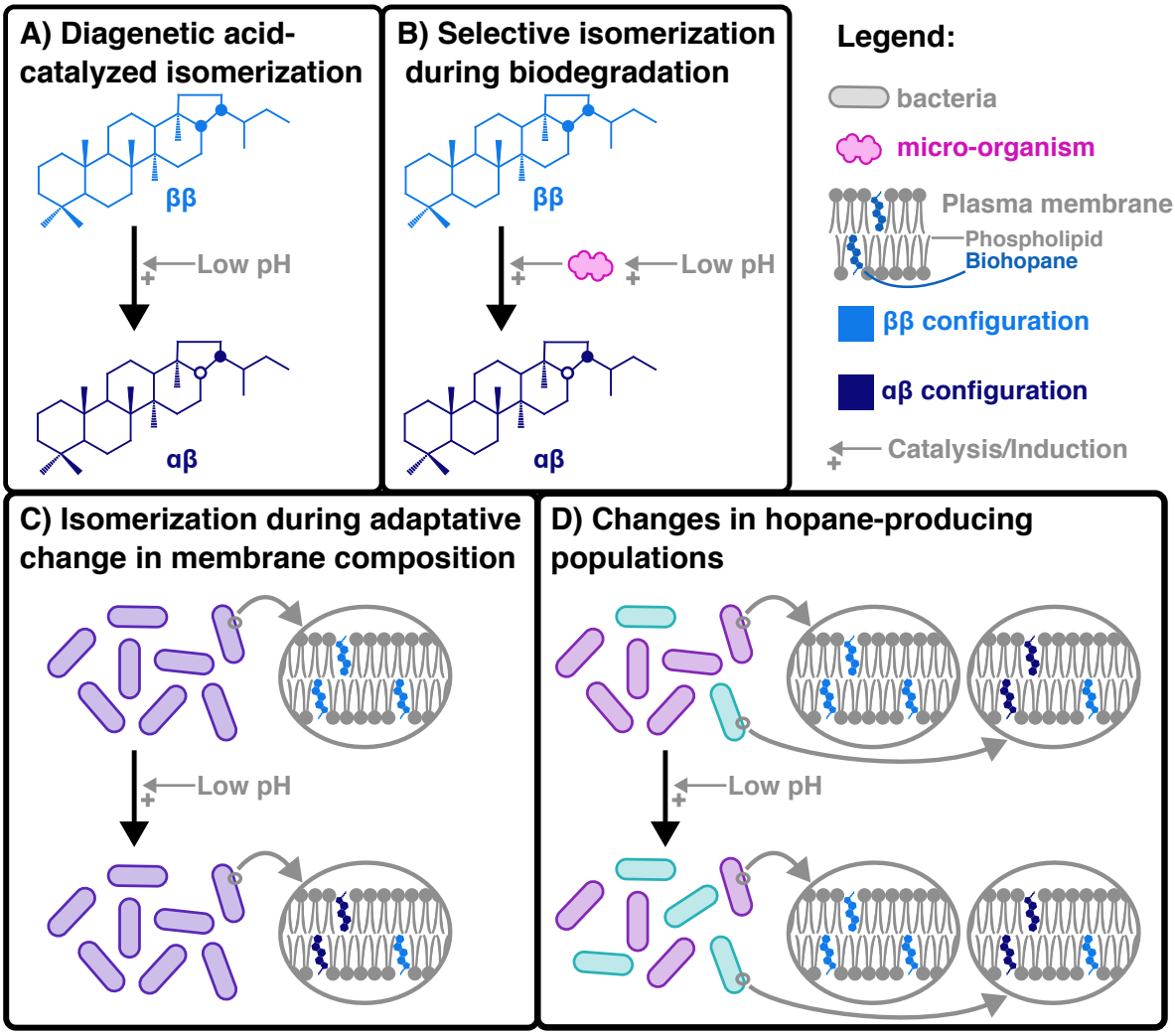

Figure 27: Different hypotheses are proposed to explain the high concentrations of the C_{31} αβ hopane in peats and the correlation between the C_{31} ββ/(αβ+ββ) ratio and pH. (A) The ββ configuration is the biologically produced configuration. The C_{31} ββ hopane is isomerized abiotically into the C_{31} αβ hopane catalyzed by the low pH of the peat. (B) The C_{31} ββ hopane is isomerized into the C_{31} αβ hopane as part of biodegradation by microorganisms. The development of the microorganisms involved in this degradation is likely pH-sensitive. (C) Both ββ and αβ configurations are biologically produced. Changes in membrane composition occur as an adaptation to changing pH. (D) Both ββ and αβ configurations are biologically produced and each species of bacteria has its own biohopane composition. Changes in the microbial community in response to pH variations are responsible for the observed distribution of ββ and αβ geohopanes. For simplification, bacterial membranes are represented here as a simple bilayer composed of phospholipids and biohopanes.

Such data rather support either a biological transformation of ββ hopanes into αβ isomers during early diagenesis (Figure 27 B) (Ries-Kautt and Albrecht, 1989), or a direct bacterial input of hopanes, having different isomeric configurations from bacteria (Figure 27 C or D). Indeed, it has been shown that some bacteria are capable of producing ββ, βα and αβ biohopanoids (Rosa-Putra et al., 2001) or biohopanoids epimers at C-22 (Peiseler and Rohmer, 1992). On the other hand, bacteria are able to alter their membrane composition in response to changes in environmental parameters, enabling them to maintain acceptable membrane fluidity and cell activity (Figure 27 C) (e.g., Russell and Fukunaga, 1990; Vinçon-Laugier et al., 2017). Changes in microbial community structure as well as membrane lipid composition are used to

explain the observed changes in MBT and CBT indices and in temperature and pH calibrations based on brGDGTs (e.g., Weijers et al., 2007b; Huguet et al., 2014; De Jonge et al., 2021; Naafs et al., 2021; Halamka et al., 2023). A similar adaptation may exist in biohopanoid-producing bacteria, with greater production of the more stable αβ-isomers under more acidic conditions (Figure 27 C). However, as far as we know, the impact of pH variations on the biohopanoid composition of bacterial membranes is not known. Thus far, no bacteria producing hopanes, whatever their configurations at C-17 and C-21 are, have been identified, and functionalized biohopanoids with the αβ configuration have only been reported in Frankia spp (Rosa-Putra et al., 2001). Further studies showing the occurrence of αβ hopanoids, and in particular hopanes, in living organisms are clearly needed.

Carbon isotopic data of microbial-derived biomarkers provide unique information about the origin of these compounds (e.g., Schouten et al., 2000a; Pancost et al., 2003; Schwartz-Narbonne et al., 2023). Overall, the range of $\delta^{13}C$ values of C_{31} ββ and αβ hopanes in the NGaoundaba peat deposit (Figure 24 C and D) is consistent with values reported in other studies (e.g., Pancost et al., 2003; Xie et al., 2004; McClymont et al., 2008; Huang et al., 2018; Inglis et al., 2019). The $\delta^{13}C$ values of C_{31} ββ and αβ hopanes follow the same variation as the $\delta^{13}C_{bulk}$, in line with previous studies suggesting a heterotrophic origin for these compounds without a major input from methanotrophic bacteria (Pancost et al., 2003; Inglis et al., 2019). The $\delta^{13}C$ values of C_{31} αβ hopane are nearly identical to those from the C_{bulk} at the bottom of the core and from 8.1 to 6.0 ka cal BP but present a positive shift compared to the $\delta^{13}C_{bulk}$ from 9.3 to 8.2 ka cal BP and around 4.8 ka cal BP. As suggested by Pancost and Damsté (2003), this shift towards more enriched values may suggest preferential bacterial consumption of labile ^{13}C-enriched carbon. However, C_{31} ββ hopane appears more depleted in ^{13}C than the C_{31} αβ isomer (Figure 24 D). Consumption of refractory ^{12}C-enriched carbon or depleted carbon sources such as methane by the producer(s) of the ββ isomer cannot be excluded. Data from the Dajiuhu peatland (Huang et al., 2018, see supplementary material) also show more depleted $\delta^{13}C$ values for C_{31} ββ hopane compared with those from C_{31} αβR hopane. The difference between the $\delta^{13}C$ values of C_{31} ββ and αβ hopanes thus supports distinct producers of these hopanes that use different carbon sources (Figure 27 D). Similarly, a source decoupling between C_{30} and C_{31} hopanes, as proposed by Inglis et al. (2019), may explain the opposite variations observed for the two hopane ratios at the NGaoundaba peat deposit.

The differences between the carbon isotopic values of the two isomers might also be explained by heavy isotope effects in enzyme-catalyzed reactions (Heipieper et al., 2004; O'Leary, 1980), such as those involved during biodegradation during early diagenesis (Figure 27 B). In enzyme-catalyzed reactions, the magnitude of the isotope effect depends on the structure of the transitional state related to the change in bonding to the isotopic atom

(O'Leary, 1980). Each scenario (B), (C) and (D) is not exclusive, and a combination of several of these scenarios is possible.

4.2. Biomarker-based pH reconstructions

4.2.1. Comparison between hopane- and brGDGT-based pH reconstructions

Using the brGDGT and hopane molecular data, we reconstruct two pH records using previously published empirical calibrations (Naafs et al., 2017b; Inglis et al., 2018). The two calibrations are respectively based on the C_{31} hopane ββ/(αβ+ββ) ratio and on the brGDGT CBT_{peat} ratio. These two ratios are a priori independent as they are based on two distinct classes of molecules known so far to be produced by at least somewhat different populations of bacteria.

A statistically significant positive correlation between the two pH reconstructions (r^2= 0.678, n=66, p-value<<0.01) is observed for the NGaoundaba peat record (Figure 28), with only one outlier data point corresponding to the uppermost sample (at 10 cm). The latter can be attributed to different production or degradation depths between hopanes and brGDGTs. Consistent with this hypothesis, either one or both of the hopane isomers are absent from several surface peat sediments (See supplementary material in Inglis et al., 2018). In the NGaoundaba peat record, the C_{31} αβ hopanes are absent in the topmost sample, leading to a ββ/(αβ+ββ) ratio equal to 1. Consequently, a maximum pH value is obtained with the calibration from Inglis et al. (2018). Similarly, brGDGTs also show strong variations in the more recent samples, with the topmost sample having the lowest concentrations for all brGDGTs studied.

The correlation between the two pH proxies suggests a similar response of these two independent proxies to environmental changes and thus supports their use for paleo-pH reconstructions despite different absolute values. The range of pH values is larger for hopane-based pH than for brGDGT-based pH (Figure 26 E, F and Figure 28), in line with results from the Schöningen lignite deposit (Inglis et al., 2018).

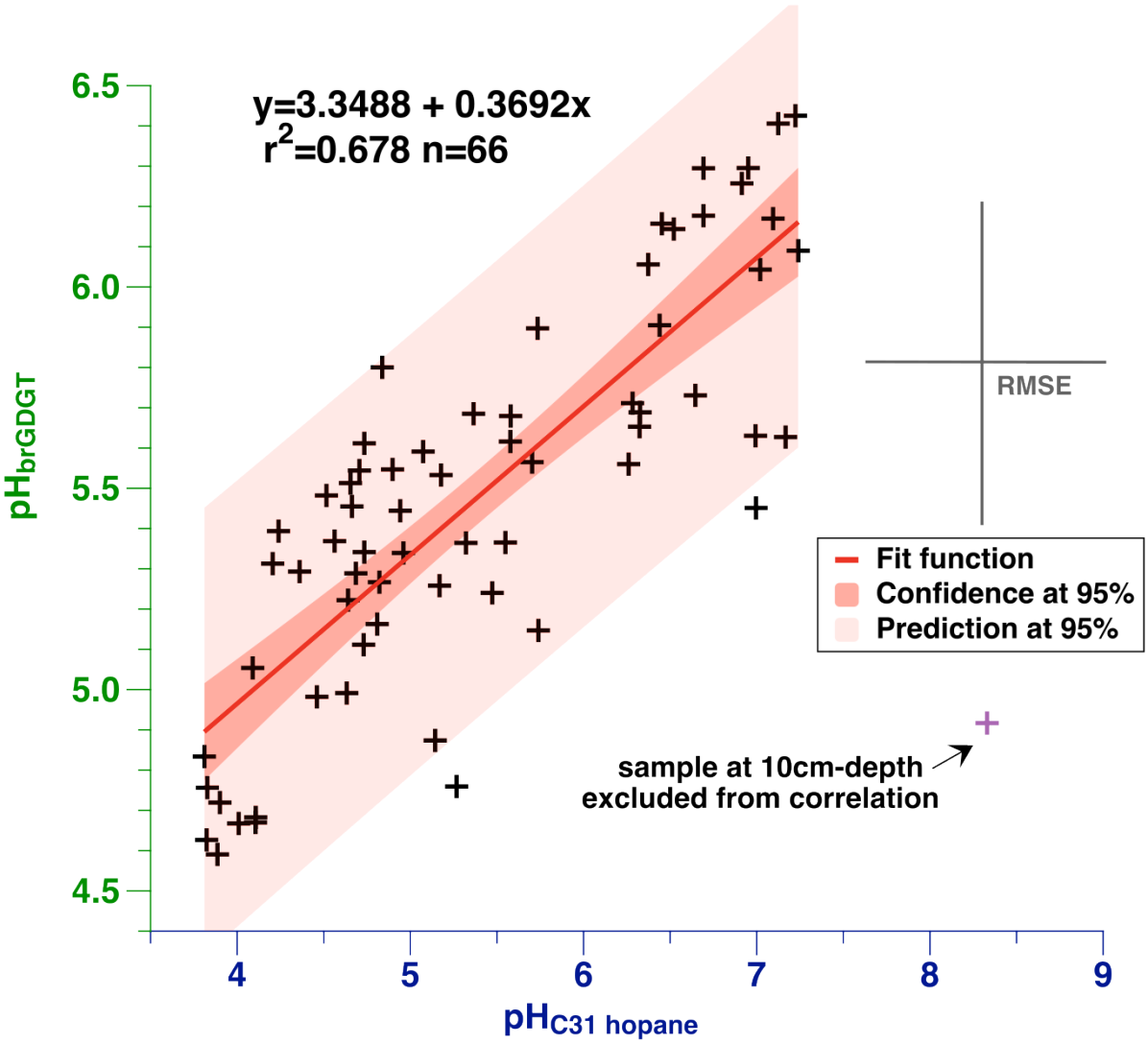

Figure 28: Correlation between C_{31} hopane- and brGDGT-reconstructed pH. The uppermost sample (10cm-depth) has been excluded from the correlation. The RMSE associated with each pH calibration is represented in light grey on the right.

4.2.2. Bias in absolute pH values due to existing calibration datasets

Unlike temperature, which can be estimated using climatic models, the pH values used in empirical calibrations must be measured directly in situ. Such data are lacking for some sites in the global peat database, resulting in a restricted pH calibration database (51 sites for pH out of the 96 used for temperature) (Figure 29 - Green cross) (Naafs et al., 2017b). Several studies have pointed out the lack of studies based on organic compounds in tropical peatlands and its impact on our understanding of brGDGT distributions and temperature/pH empirical calibrations (Weijers et al., 2011; Naafs et al., 2017b). Among low latitude sites, African sites are particularly scarce in previous calibrations, with only 1 site out of 51 for the brGDGT pH calibration and none out of 94 for the hopane pH calibration (Naafs et al., 2017b; Inglis et al.,

2018). This poor representation of low latitude peat deposits may significantly bias the global empirical calibrations as the specificities of these low-latitude records, such as precipitation regime (amount and seasonality), vegetation types, and temperature variations are not taken into account. Vegetation types influence peat microbial activity in both temperate and tropical peatlands (e.g., Fisk et al., 2003; Andersen et al., 2013; Nick T Girkin et al., 2020). For both hopane and brGDGT pH calibrations, vegetation diversity is well represented among the sampled peats (Naafs et al., 2017b; Inglis et al., 2018), meaning that biases associated with vegetation differences (Liang et al., 2019) are likely included in calibration errors. However, in the hopane-based pH calibration proposed by Inglis et al. (2018), 63 data points out of 94 come from four Chinese peats (Figure 29 - Blue Circles). The over-representation of the four sites located in a restricted geographical area may bias the global pH calibration and could partly explain the larger range of pH values reconstructed using hopanes compared to pH reconstruction based on brGDGTs (see Huang *et al.* (2015) for details on the environmental and climatic characteristics of these four sites).

The pH measurement is associated with a non-negligible uncertainty that is accounted for in both calibrations using Deming regressions (Naafs et al., 2017b; Inglis et al., 2018). The pH calibration from Naafs et al. (2017b) takes into account the potential difference between shallow and deep brGDGT distributions. The authors demonstrated that the overall brGDGT distribution is not significantly different between the upper 15 cm (acrotelm, likely oxic) and the peat sediment underneath (catotelm, likely anoxic). However, particularly in high-latitude peatlands, several sites do show strong differences in brGDGT distribution between both layers, likely associated with the seasonal bias of brGDGT production (Naafs et al., 2017b). To address this problem, Naafs et al. (2017b) retained all data from the upper 1 m without differentiating the acrotelm and the catotelm, and averaged all samples for each peatland, except for high latitude peats, where the top 20 cm were excluded. The same problem may be encountered with hopanes. While some studies show strong variations in hopane distributions (Huang et al., 2015) and concentrations (Farrimond and Flanagan, 1996; He et al., 2015) within the first meter of peat deposits, a rapid isomerization is suggested in several studies (Inglis et al., 2018; Quirk et al., 1984). The use of both surface and averaged samples from the upper first meter could therefore bias the calibrations and explain the differences between the ranges of pH values obtained from hopane and brGDGT calibrations.

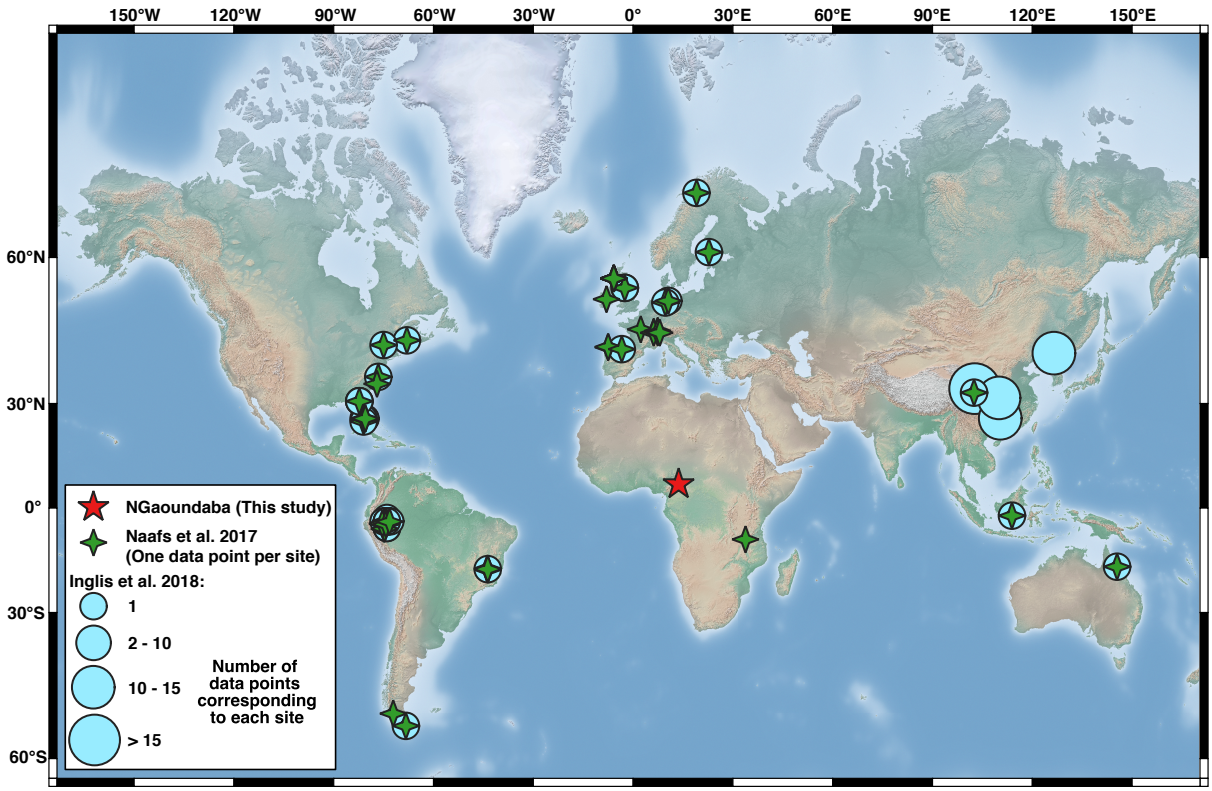

Figure 29: Map with the location of all peats used in the studies from Naafs et al. (2017b) (green cross) and Inglis et al. (2018) (blue circles) for pH calibrations. The size of the blue circles is proportional to the number of data points for each site. The location of the NGaoundaba peat deposit is indicated by the red star.

4.3. Local bias affecting pH reconstructions

4.3.1. Influence of microbial activity in lower peat layers

The microbial community structure has been shown to vary significantly over the first meter of peat, due to significant changes in peat properties and environmental variables such as pH, redox conditions, moisture content, or nutrient availability (e.g., Williams and Crawford, 1983; Ausec et al., 2009; Jackson et al., 2009; Andersen et al., 2013; Too et al., 2018; Nick T Girkin et al., 2020). The upper oxic layer (acrotelm) has a relatively high decomposition rate of organic matter compared to the lower anoxic layer (catotelm) (Clymo, 1984). The upper oxic layer is dominated by aerobic decomposition mediated by fungal and/or bacterial populations (Winsborough and Basiliko, 2010; Tripathi et al., 2016). Microbial diversity and activity are highest at the surface (Jackson et al., 2009; Too et al., 2018), but high relative abundance of certain phyla such as *Acidobacteria* has been reported in deeper layers (i.e., around 45cm-depth) (Too et al., 2018) and microbial activity has also been reported in deep peat at 2m depth (Kluber et al., 2020). As *Acidobacteria* are potential producers of both hopanes (Welander et al., 2010) and brGDGTs (Sinninghe Damsté et al., 2014, 2011), the potential influence of the presence of this phylum in the lower peat layer on pH reconstructions should

be considered. Lipid production in the lower layers may cause an offset between the molecular signal and the age of the bulk peat sediment. The latter may be older than the compounds analyzed and interpreted in terms of pH. To test this hypothesis, we artificially added an offset in one pH reconstruction and recalculated the correlation between the two pH reconstructions. Specifically, $pH_{C31\ hopane}$ at time t_n was compared to the pH_{brGDGT} at time t_{n+1} with n the sample number increasing with depth, and vice versa. Adding an offset did not improve the correlation, suggesting that there is no offset between the two pH reconstructions (see supplementary material, Figure S 5 A and B). Another possibility to identify an offset is to compare the pH reconstructions with other non-microbial proxies. Major climate transitions affect both vegetation and microbial communities. In the NGaoundaba peat record, the end of the African Humid Period (AHP) is well marked in bulk organic parameters (HI, $TOC_{residual}$ and $\delta^{13}C_{bulk}$; Schaaff et al. (2023)) around 5.8 and 5.7 ka cal BP (Figure 26 B, C and D, Schaaff et al., (2023)). A transition from low pH values during the AHP to higher pH values during the middle and late Holocene as well as changes in hopane and brGDGT concentrations are recorded between 6.0 and 5.8 ka cal BP (Figure 26 E and F). A limited impact of the difference in response time to climate change between the microbial community and vegetation is expected (e.g., Webb, 1986; Hughen et al., 2004; Waldrop and Firestone, 2006). Thus, an offset of less than 0.3 ka cal BP may occur at the NGaoundaba peat deposit between the age model and the variations recorded in the microbially-based proxies. The pH signal may also be an integrated signal of compounds produced in a centimetric or even decametric depth range. Weijers et al. (2011) showed an absence of correspondence between CBT-based pH values and in situ measured pore water pH, further suggesting that the brGDGT signal is more likely to represent a preserved 'fossil' biosignature than an in situ production in deep peat.

Caution is needed, however, when interpreting results from the upper part of the peat deposits. Analyses of short recent sequences can lead to misinterpretations, corresponding to recent changes in microbial community structure rather than a paleoclimatic signal.

4.3.2. A seasonal bias for pH?

Seasonality is a significant bias in brGDGT temperature reconstructions in various settings, likely resulting from adaptation of bacterial membranes to environmental changes or changes in the microbial community structure (e.g., Sun et al., 2011; Loomis et al., 2014; Cao et al., 2018; Miller et al., 2018). In a temperate lake, Loomis et al. (2014) showed large variations in brGDGT concentrations, fluxes, and fractional abundances over the annual cycle within the water column, and temperature reconstructions based on brGDGTs seemed biased toward the mixing season. Taking into account the seasonality of brGDGT production can improve the

brGDGT calibrations of both temperature and pH in lakes (Raberg et al., 2021). Since seasonal changes in microbial activity and microbial community structure have been reported in peats (e.g., Wynn-Williams, 1982; Bergman et al., 2000; Andersen et al., 2013), this may also affect paleo-pH reconstructions.

While temperature seasonality is of major concern in high-latitude and temperate records, tropical regions have narrower temperature variations throughout the year, making them less affected by temperature seasonality bias (Loomis et al., 2012; Pérez-Angel et al., 2020). However, as aforementioned, pH values can be affected by precipitation. Due to the strong seasonal variations in precipitation occurring in the tropics, this could affect the microbial community structure and activity, and in turn, pH reconstructions can be severely biased. Determining how seasonal climate and environmental changes will affect pH reconstructions in peat is beyond the scope of this study, but further studies are undoubtedly needed. Differences in sensitivity to seasonal variation between brGDGT producers and hopane producers may explain, in part, the observed difference in the range of reconstructed pH values (Figure 26 E and F and Figure 28).

4.4. A multi-causal interpretation of pH reconstructions

Changes in reconstructed pH have been proposed to reflect past changes in precipitation, with increased precipitation leading to a dilution effect and an increase in pH (Pancost et al., 2003; Inglis et al., 2018). The minimum reconstructed pH values for the NGaoundaba peat deposit, between 8.4 and 6.2 ka cal BP, coincide with a period of increased precipitation in agreement with the timing of the African Humid Period (Figure 26 B, C and D, Schaaff et al., (2023) – chapter 3) and are therefore not consistent with a potential dilution effect. Consistently, higher brGDGT-reconstructed pH values were recorded in a “dry” site compared to a “wet” site from the Frasne peatland (Jura Mountains, France), suggesting an influence of peat moisture level or oxygen availability on brGDGT distribution (Huguet et al., 2010).

A decrease in CBT-based pH (soil calibration) has been recorded in the Hongyuan peat (Central China), coinciding with an increase in precipitation and associated with an increase in humification index (Zheng et al., 2015). Zheng et al. (2015) proposed that increased precipitation and bog wetness increase humification and organic acid production, lowering the pH. Similar findings and interpretations are reported for the Shuizhuyang peat bog (Southeast China) (M. Wang et al., 2017). Hopane-based pH reconstruction from Dajiuhu peatland (Central China) shows the opposite trend, with a decrease in pH associated with a dry climate during the deglaciation (Zhang et al., 2020). The apparent inconsistency between the different paleo-pH records and associated interpretations may be the result of the influence of catchment lithology on pH. Indeed, while the Dajiuhu Basin is a closed karst basin

in the Shennongjia Mountains and is mainly composed of carbonates and dolomites (Zhang et al., 2022), the Hongyuan peat bog is located on the eastern edge of the Tibetan Plateau, whose lithology is dominated by quartz-rich sandstone as well as small occurrences of volcanic rocks (Large et al., 2009). The precise lithology of the Shuizhuyang catchment is unknown, but the site is located in the Cathaysia Block mainly composed of igneous rocks, particularly granitoids (Yu et al., 2012). The basement of the Adamawa Plateau around the NGaoundaba peat deposit is composed of granites and volcanic formations (Abba et al., 2023). It is thus likely that increased precipitation in the carbonate-dominated Dajiuhu catchment may increase alkaline inputs to the peatland through erosion, dissolution, and surface runoff, which may neutralize the organic acids produced by decomposition of organic matter and explain the differences observed between the evolution of pH at the Dajiuhu peatland and at the three other peat deposits. It is likely that paleo-pH reconstructions based on microbial compounds produced in-situ do not directly reflect precipitation changes, but rather changes in peat moisture level, reflecting the balance between precipitation and evapotranspiration and affected by surface runoff and changes in humification.

Additionally, changes in the peat-forming vegetation influence peat pH since some plants, such as *Sphagnum* mosses, directly contribute to peat acidification through cation exchange (Clymo, 1963). Major transitions previously observed in CBT-based pH reconstructions were attributed to major changes in vegetation, with the transition from sedge-dominated peat to Sphagnum-dominated peat associated with lower pH values during Sphagnum-dominated interval (Nichols et al., 2014; Weijers et al., 2011). Weijers et al. (2011) associated these changes with changes in the trophic status of the peat from a fen system to an ombrotrophic bog. As the catchment area of the NGaoundaba peat deposit is small and located in a maar crater with a slightly higher elevation than the surrounding area, this deposit has probably remained an ombrotrophic peat over the last 10 ka, fed primarily by rainfall water without a permanent water inlet. Despite the absence of Sphagnum mosses at NGaoundaba, pH variations based on brGDGTs and hopanes may coincide with major changes in local vegetation, as suggested by significant variations in $\delta^{13}C_{bulk}$ (Figure 26 D, E and F). The vegetation changes observed at the NGaoundaba peat deposit may coincide with changes in precipitation and associated changes such as water table depth and oxygenation level. Therefore, in the absence of *Sphagnum* mosses, simultaneous changes in vegetation and pH may only reflect a correlation between these two parameters without any causal effect.

In the current state of knowledge, the interpretation of past pH variations based on organic proxies remains complex, and pH variations cannot be attributed to a single cause. A good understanding of catchment characteristics (size, lithology, vegetation, and trophic status of

the peat) and evolution through time is fundamental before proposing any interpretation of paleo-pH records.

Conclusions and perspectives

Through the joint investigation of bacterial hopanes and brGDGTs in a sequence of African peat, our study validates the use of these families of molecules for the reconstruction of pH variations but also highlights their limitations and perspectives for improvement. The comparison of C_{30} and C_{31} ββ/(αβ+ββ) hopane ratios as well as the carbon isotopic composition of C_{31} ββ and αβ isomers demonstrate that the direct acid-catalyzed isomerization of ββ into αβ isomers is unlikely without biological mediation. Interpretation of peat-based paleoproxies using microbial biomarkers requires special attention to evaluate the possible influence of deep production of these biomarkers. The influence of deep peat hopane and brGDGT production appears to be limited at the NGaoundaba peat deposit since no downcore trend in hopane and brGDGT concentrations and abundances is observed and limited offset with proxies independent of microbial production has been found.

Future culturing and laboratory experiments should help confirming the potential occurrence of αβ hopanes in bacteria or other types of living (micro)organisms, or they potential formation during microbial adaptation to changing environment and/or biodegradation of organic matter. A good understanding of the evolution of the studied ecosystem is also needed to interpret pH paleo-record as several parameters influence the variation of pH and obscure the paleoclimatic and paleoenvironmental signals. Vegetation and precipitation changes certainly play an important role in pH variations in peat, but the catchment lithology also needs to be taken into account. More paleo-pH records from peat deposits with various climatic and environmental backgrounds are thus needed to better constrain the possible cause of the variation in pH reconstruction in peat deposits. Additionally, new sets of data will improve the pH calibrations based on hopane and brGDGT distributions and their potential as paleoenvironmental and paleoclimatic proxies.

Supplementary material:

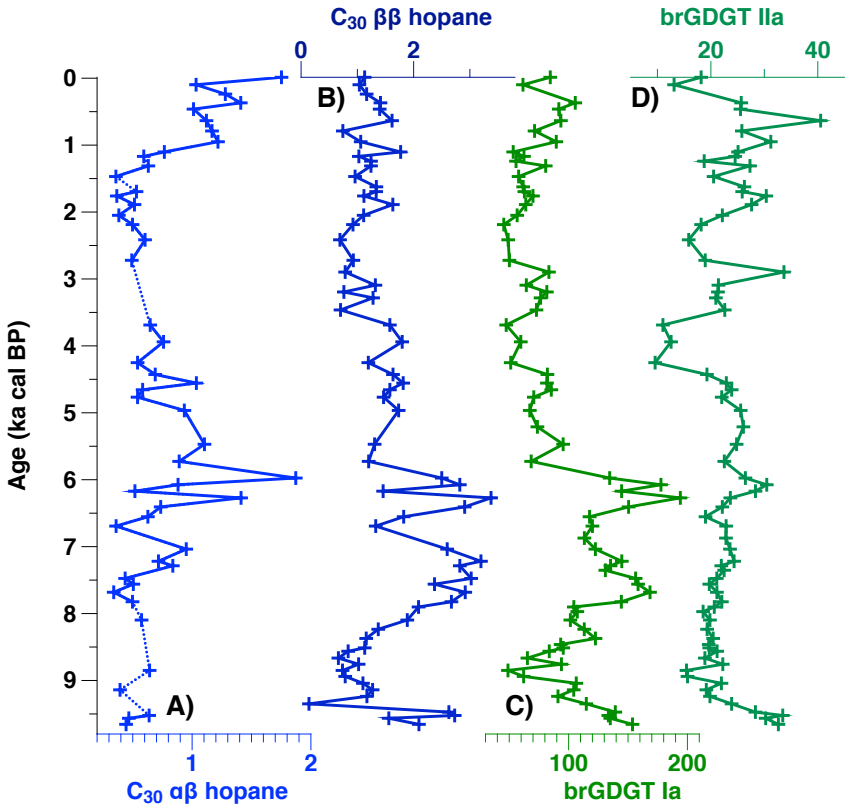

Figure S 2: Concentration in µg/g_{TOC} of the C_{30} αβ and ββ hopanes (A) and (B) and of the two most abundant brGDGTs (Ia and IIa, (C) and (D) respectively)

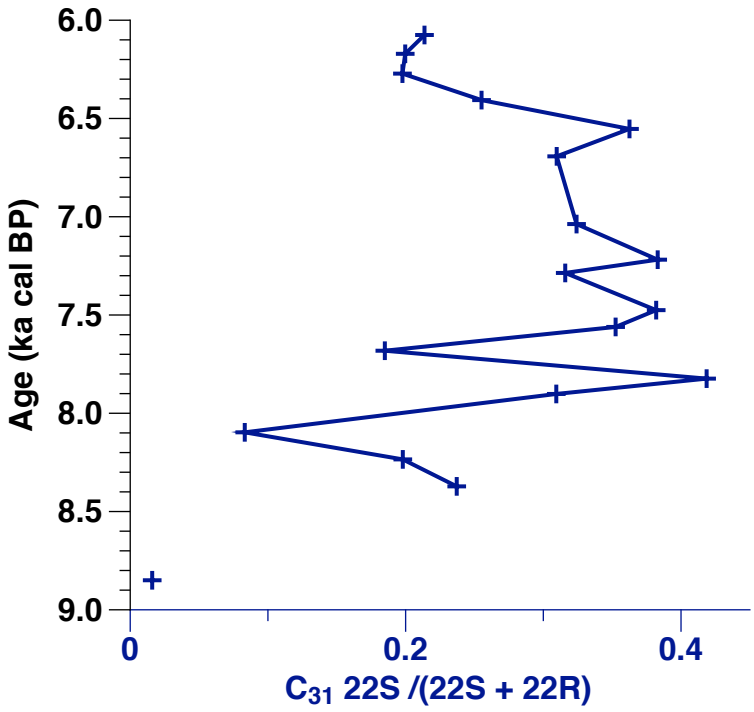

Figure S 3: C_{31} 22S/(22S + 22R) ratio developed by Mackenzie et al. (1980). The low or zero concentration of 22S isomer is responsible limited number of data points.

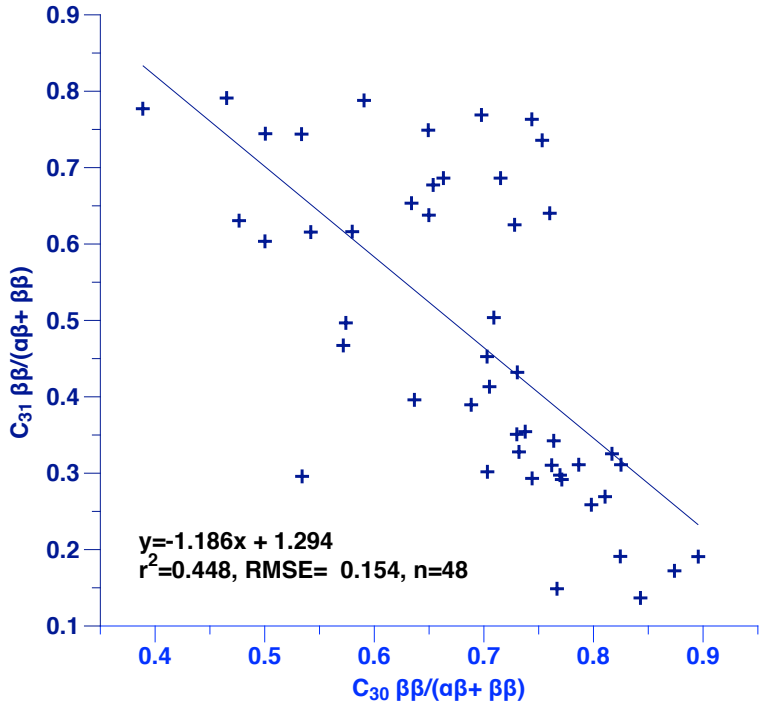

Figure S 4: Correlation between C_{30} ββ/(αβ+ββ) and C_{31} ββ/(αβ+ββ) hopane indices. The correlation is statistically significant (p-value is << 0.01).

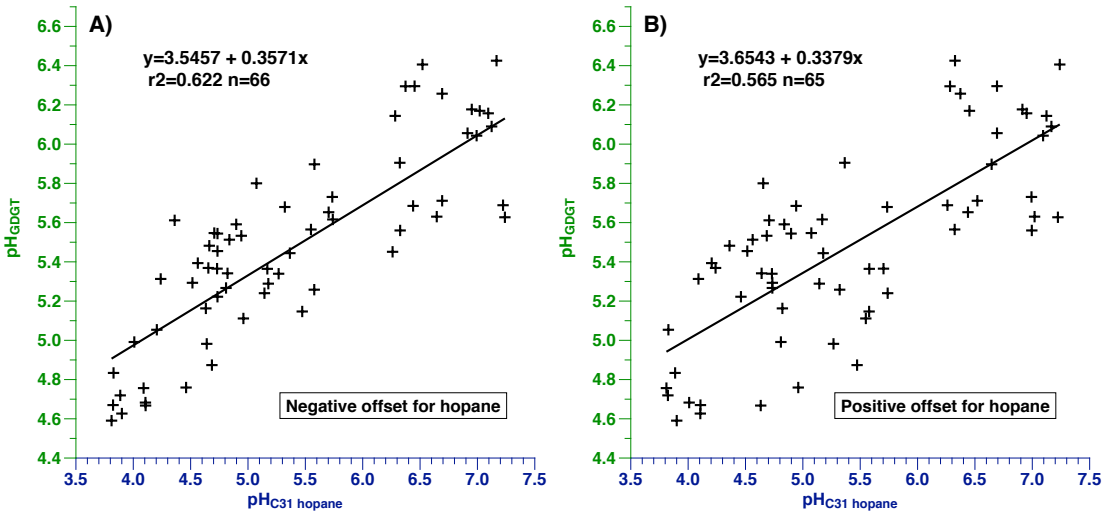

Figure S 5: Correlation between C_{31} hopane- and brGDGT-reconstructed pH. The uppermost pH value for C_{31} hopane-reconstruction is not taken into account. The negative offset for hopane (A) means that the $pH_{C31\ hopane}$ at time t_n is compared to the pH_{brGDGT} at time t_{n-1} and the positive offset for hopane (B) means that the $pH_{C31\ hopane}$ at time t_n is compared to the pH_{brGDGT} at time t_{n+1} with n the sample number increasing with increasing depth. Both correlations are statistically significant (p-value<<0.01)

Chapter 5: Paleoclimatic changes at the NGaoundaba peat deposit and specificity of tropical peat deposits

Abstract:

Based on a peat deposit from North East Cameroon, we analyzed lipid biomarkers (brGDGTs, n-alkanes) to reconstruct past changes in temperature and precipitation during the Holocene in tropical Africa. While temperature reconstruction and $\delta^{13}C_{wax}$ indicate a decrease in temperature and a switch to C_4-dominated vegetation around 5.8 ka cal BP marking the end of the African Humid Period (AHP), the δD_{wax} record shows a more progressive decrease in precipitation during the Holocene. The δD_{wax} record also highlights two 1-ka dry events between 8.9 and 7.9 ka cal BP and between 4.5 and 3.5 ka cal BP, respectively. Several brGDGT-based temperature calibrations were tested. The range of temperature variations for the Holocene is larger than the range predicted by climate models or measured in other records from West and Central Africa, potentially due to an impact of pH or moisture on peat-based temperature calibration. In addition, the range of δD_{wax} variations recorded at NGaoundaba is larger than the range observed in all other δD_{wax} records in West and Central Africa. Based on the comparison of peat-based records, we suggest that this large range is associated with a specificity of sedge-dominated peat deposits, where n-C_{31} alkanes input significantly change during the Holocene from plants from the catchment to a mix between sedges and grasses growing on the peat and plants from the catchment. The strong D-enrichment of the peat water during dry seasons may have further enriched the δD_{wax} signature during late Holocene, as sedges and grasses were a major source of n-C_{31} at this time.

Key words: African Humid Period, sedge-dominated peat, temperature and precipitation reconstructions

1. Introduction

Temperature and precipitation are key parameters for reconstructing past climatic conditions. Climate models often include these two key parameters (e.g., Randall et al., 2007; Rummukainen, 2010; Flato et al., 2014). The end of the African Humid Period and particularly the response of the African monsoon to changing insolation has been debated over several decades. While early climate models, taking only the atmosphere into account, are generally indicating a linear response of the African monsoon to changing orbital parameters (Prell and Kutzbach, 1987), including vegetation, land-surface or ocean surface feedbacks lead to more contrasted results (e.g., Kutzbach et al., 1996; Claussen et al., 1999; Renssen et al., 2006; Liu et al., 2007). In particular, models including vegetation feedbacks generally simulate a more abrupt termination (Claussen et al., 1999). Confronting climate model with paleoclimatic data has led to contrasting results with some records indicating gradual transitions (Kröpelin et al., 2008; Shanahan et al., 2015) while others present abrupt transitions (DeMenocal et al., 2000; Bristow et al., 2018). More than a debate on the African Humid Period, these discrepancies between data and model are questioning our understanding of tropical climates and our ability to reconstruct accurately past and future climatic conditions. This leads to constant improvement of climatic models (e.g., Jungandreas et al., 2021; Thompson et al., 2021) and additions of new study sites and proxies (e.g., Garcin et al., 2022; Lézine et al., 2023; Schaaff et al., 2023; Yacoub et al., 2023).

Sahara and Sahel regions were extensively studied with numerous climatic models focusing on these regions, but proxy data remain scarce and often discontinuous. At lower latitudes, some of these models suggest a drying during the African Humid Period while other indicate a more humid environment (Patricola and Cook, 2007; Dallmeyer et al., 2020). The complexity of the climate system in West and Central Africa further complicate interpretations of proxy data (e.g., Grist and Nicholson, 2001; Nicholson, 2009, 2018).

Numerous proxies have been developed to reconstruct past changes in precipitation and temperature over time, such as the hydrogen or nitrogen isotope composition of water in ice cores (e.g., Dansgaard, 1964; Kindler et al., 2014), pollen-based transfer functions (e.g., Mathewes and Heusser, 1981; Lu et al., 2011; Mauri et al., 2015), hydrogen isotopic compositions of leaf waxes, and GDGT-based temperature reconstructions in sediments (e.g., Eglinton and Eglinton, 2008; Loomis et al., 2012; Bird et al., 2020), etc. Proxies are constantly being revised and extended to new compounds, new sites, new types of records, etc (e.g., Jouzel et al., 1997; Henderson, 2002; Schlosser et al., 2008; Naafs et al., 2017a).

Lipids biomarkers comprise a wide range of compounds of biological origin that are abundant in sediments and have been used for paleoclimatic reconstructions. Long chain n-alkanes are derived from epicuticular leaf wax (Eglinton and Hamilton, 1967) and have been used to

reconstruct past changes in vegetation and precipitation using $\delta^{13}C_{n\text{-}alk}$ and $\delta D_{n\text{-}alk}$, respectively (Sachse et al., 2012; Diefendorf and Freimuth, 2017). Branched glycerol dialkyl glycerol tetraethers (brGDGTs) are membrane spanning lipids of bacterial origin (Weijers et al., 2006). The distribution of brGDGTs is influenced by environmental parameters such as temperature, pH, salinity, resulting from homeoviscous adaptation of bacterial membrane to environmental changes or changes in the composition of the bacterial community (e.g., Huguet et al., 2014; De Jonge et al., 2019; Martínez-Sosa et al., 2020; Halamka et al., 2023). Empirical calibrations of temperature and pH based on global database of present-day surface sediments have been proposed and are widely used for paleotemperature reconstructions (Loomis et al., 2012; Naafs et al., 2017b; e.g., Weijers et al., 2007b). To overcome the influence of sedimentological environment (marine, lacustrine, soil, peat) on the brGDGTs distribution, specific calibrations were developed for each environment (e.g., Weijers et al., 2007b; Naafs et al., 2017b; Martínez-Sosa et al., 2021).

Given the remarkable preservation of organic matter in peat deposits, peat records have great potential for paleoclimatic studies based on lipid biomarkers (Naafs et al., 2019 and references therein), particularly in tropical regions where records are scarce and often discontinuous. However, to date, only a few peat deposits from tropical Africa have been studied using lipid biomarkers (Coffinet et al., 2018; Garcin et al., 2022), and the specificities associated with interpretations of peat sediments in terms of paleoclimatic and paleoenvironmental changes are not yet well understood.

In West and Central Africa, the termination of the African Humid Period (AHP – de Menocal et al. (2000)) is still debated, as the timing and responses of proxies strongly differ. While several studies argue for an abrupt termination to the AHP resulting from a non-linear response to orbital parameters (e.g., DeMenocal et al., 2000; Collins et al., 2017), other studies indicate a time transgressive response to the end of the AHP (e.g., Amaral et al., 2013; Shanahan et al., 2015). The coexistence of the two conditions is not incompatible and may result from specific regional or local conditions (Tierney et al., 2017b). In addition to the AHP, short-term events punctuated late Holocene climate and are particularly visible in near equatorial pollen records, but their cause, climatic or anthropic, as well as their extension to present-day savannah zone is still debated (e.g., Salzmann and Hoelzmann, 2005; Garcin et al., 2018; Maley et al., 2018).

In this study, we present new temperature and precipitation records in central Africa over the last 10ka, based on a peatcore from the NGaoundaba peat deposit (Adamawa Plateau, northeast Cameroon). The site's small catchment area and transitional position between the Guineo-Congolian rainforest to the south and the Sudanian savannah to the north make it a highly promising site for recording climate changes during the Holocene. The main paleoclimatic characteristics of the NGaoundaba peat record are presented, highlighting the

site's high sensitivity to long- and short-term climatic changes. Several brGDGT temperature calibrations were tested and compared to investigate the potential factors influencing brGDGT-based temperature reconstructions. By comparing the NGaoundaba peat record with other δD records from tropical Africa, we show the specificity of sedge-based peat records in term of δD variations.

2. Material and methods

2.1. Sampling and ^{14}C dating

The NGaoundaba peat deposit is situated in a volcanic crater on the Adamawa Plateau in Northeast Cameroon (N7.135° E13.690°, 1175 m above sea level). The NGaoundaba peat deposit lies in the Soudano-Guinean shrubs savannas zone (Letouzey, 1958) and the in-situ growing vegetation is dominated by sedges (*Cyperus* sp). The current climate is characterized by two distinct seasons: a 6-month dry season from October to March and a 6-month rainy season from April to October. According to the CRU database, the mean annual air temperature (MAAT) is 22.19 °C and the mean annual precipitation (MAP) is 1482 mm (Harris et al., 2014).

Analyses are based on a 6-meter-long core (named NGBA19) collected in February 2019 using a Russian peat corer. The core is composed of dark brown peat without visible sandy or clayey zones. The core was sub-sampled at 2.5-cm intervals. Organic geochemical analyses were performed on 73 samples. The age model of the NGaoundaba peatcore is based on 30 radiocarbon dates carried out at the LMC14 Laboratory (Saclay, France). Details on the dating and calibration of the age model are given in Schaaff et al. (2023) (chapter 3).

2.2. Organic geochemical analyses

2.2.1. Sample preparation

All samples were freeze-dried, ground and homogenized. Lipid extraction was performed two times from 0.3g of each sample with 10mL of dichloromethane (DCM)/methanol (3:1, v/v) using a MARS 6 CEM microwave extraction system. Following each extraction, the supernatant was filtered through a sintered Teflon filter. Synthetic C_{46} GDGT was added to the combined extracts of each sample as an internal standard (Huguet et al., 2006). The total lipid extract was separated by column chromatography on silica gel into three fractions of increasing polarity. A hydrocarbon fraction containing n-alkanes was eluted first with 8mL of hexane. A second fraction was eluted with 5mL of hexane/DCM (1:1, v/v). The alcohols including brGDGTs were eluted in a third fraction with 10mL of DCM/methanol (1:1, v/v).

2.2.2. n-alkanes analyses

Copper curls activated with HCl were added to the hydrocarbon fractions to remove elemental sulfur. After a first GC-FID analysis (HP 6890A), GC-MS analyses (Agilent 6890N GC coupled to an Agilent 5975C MSD and Agilent 7890B GC coupled to an Agilent 5977B MSD) were performed for identification and quantification of the different compounds. Both GC-MS instruments provided comparable data. Integration of n-alkane peaks were performed using the m/z 71 ion chromatogram to limit the influence of coelution and compared with an external standard solution containing commercial pentacosane (n-C_{25}) for quantification. N-alkane abundances were calculated using all alkanes from n-C_{19} to n-C_{37}.

Prior to carbon and hydrogen isotopic measurements, the hydrocarbon fractions were separated into a saturated and an unsaturated fraction by column chromatography using silica gel impregnated with $AgNO_3$ (10 % wt). Saturated fractions containing n-alkanes were eluted with 3 to 4 mL of n-heptane. Unsaturated fractions were eluted with 3 to 4 mL of ethyl acetate. Carbon isotopic compositions were measured at the LGL-TPE (Université Claude Bernard Lyon 1) using an Agilent 7890B GC coupled to an Isoprime visION Isotope Ratio Mass Spectrometer via an Isoprime GC-5 combustion interface (Elementar). The GC-5 furnace was operated at 850 °C. An autotune and tests of stability and linearity of the signal were performed daily using the software ionOS. Stable carbon isotopic compositions (expressed as $\delta^{13}C$ values) were calibrated using a reference CO_2 gas reported to VPDB scale. Two Mix hydrocarbon B4 standards (A Schimmelmann, Indiana University) were measured every 4 to 5 samples and used to correct the $\delta^{13}C$ values. Samples were analyzed in duplicates. For δD measurements, the GC-5 pyrolysis furnace was operated at 1450°C. Daily autotune, H_3+ correction and test of stability were performed using the software ionOS. δD values were calibrated using the reference H_2 gas reported to VSMOW. Each week, the pyrolysis furnace was conditioned five times with 1µL hexane prior to any analysis and a series of 8 Mix B4 measurements was performed and used for data correction. In addition, one Mix B4 measurements was analyzed every 4 to 5 injections to assure the limited impact of drift. Samples were analyzed in duplicates.

2.2.3. brGDGT analyses

Fractions containing brGDGTs were filtered using 0.45 µm PTFE filters. BrGDGT analyses were performed using High Performance Liquid Chromatography Mass Spectrometry (HPLC-APCI-MS, Agilent 1200) at the LGL-TPE (ENS de Lyon). Separation was achieved on two silica columns in series (ACQUITY UPLC BEH HILIC, WATERS) following the procedure of Hopmans et al. (2016) slightly modified (i.e. using hexane/isopropanol (98.2:1.8, v/v)). Peaks

corresponding to brGDGTs were manually integrated and quantified using the peak area of C_{46}. The selected m/z values are 743.9, 1050.2, 1048.2, 1046.2, 1036.2, 1034.2, 1032.2, 1022.2, 1020.2 and 1018.2.

2.3. Soil- and peat-based brGDGT temperature calibrations

The methylation and cyclisation of branched tetraether ratios (MBT and CBT respectively) and brGDGT temperature calibrations based on soils and peats used in this study are presented in Table 4. In order to compare global and regional calibrations, we tested soil calibrations in addition to peat and peat & soil calibrations as local peat calibrations are not currently available. We tested the calibration from Coffinet et al. (2017) based on East African soil and the pan-tropical calibration from Pérez-Angel et al. (2020). We also applied the soil calibration from Naafs et al. (2017a), which excludes arid soils dominated by 6-methyl brGDGTs (characterized by $IR_{6me} > 5$). For the calibration from Dearing Crampton-Flood et al. (2020) and the calibration from Véquaud et al. (2022), two temperatures were calculated: T using the whole dataset and T0 using only sites with MAAT > 0°C.

Table 4: Indices and calibration formulas used for temperature reconstructions based on soils and peats brGDGTs distribution. The MBT' ratio has been slightly modified to take into account technical improvements since 2012 as proposed in De Jonge et al. (2014). All peat-based calibrations are global calibrations. Plot of MBT' and CBT are presented in the supplementary material of this chapter (Figure S 6)

Indice	Formula	Reference
MBT'	MBT' = (Ia + Ib + Ic)/(Ia + Ib + Ic + IIa + IIb + IIc + IIIa + IIa' + IIb' + IIc' + IIIa')	Peterse et al. (2012)
MBT'_{5Me}	MBT'_{5Me}= = (Ia + Ib + Ic)/(Ia + Ib + Ic + IIa + IIb + IIc + IIIa)	De Jonge et al. (2014)
CBT	CBT=-log[(Ib + IIb + IIb' + IIb'')/(Ia + IIa + IIa' + IIa'')]	Weijers et al. (2007b)
Calibrated on	**Formula**	**Reference**
Soil only (Global)	MAAT(°C) = -8.57 + 31.45*MBT'_{5Me} (n=222, r^2=0.66, RMSE=4.8)	De Jonge et al. (2014)
Soil only (Global)	MAAT'(°C) = -14.5 + 39.09*MBT'_{5Me} (n=177, r^2=0.76, RMSE=4.1) (only soil with IR_{6me}<0.5)	Naafs et al. (2017a)
Soil only (East Afr)	MAAT(°C) = 9.60– 8.76* CBT + 24.24*MBT' (n=176, r^2=0.77, RMSE=2.4)	Coffinet et al. (2017)
Soil only (Tropics)	MAAT(°C)= -11.76 + 38.13*MBT'_{5ME} (n=175, r^2=0.62, RMSE=3.5)	Pérez-Angel et al. (2020)

Peat only	$MAAT_{peat}$(°C) = -23.05 + 52.18*MBT'_{5Me} (n=96, r^2=0.76, RMSE=4.7)	Naafs et al. (2017b)
Peat + Soil	Bayesian statistics (BayMBT models) based on MBT'_{5Me}	Dearing-Crampton-Flood et al. (2020)
Peat + Soil	Machine learning algorithm (random forest algorithm) – multifactorial and non-parametric model	Véquaud et al. (2022)

2.4. Corrections on carbon and hydrogen isotopic values

2.4.1. Correction of Suess effect

Anthropogenic activities such as fossil fuel combustion lead to changes in atmospheric concentration and isotopic ratio of ^{13}C and ^{14}C, known as the Suess effect, which must be taken into account prior to interpretation (e.g., Keeling, 1979). This effect is significant since the 1860s (Francey et al., 1999) and is calculated as the difference between atmospheric $\delta^{13}C$ at the age of the sample and the value of pre-industrial atmospheric $\delta^{13}C$ (-6.4‰) measured using tree-ring samples (McCarroll and Loader, 2004), it can also be estimated using CO_2 extracted from ice core (Rubino et al., 2013).

2.4.2. Correction for vegetation

Changes in vegetation types and photosynthetic pathways can influence $\delta D_{n\text{-}alk}$ variations due to differences in hydrogen fractionation factors. To correct this effect, we applied the same procedure as in Garcin et al. (2018) using paired $\delta^{13}C_{n\text{-}C31}$ to correct $\delta D_{n\text{-}C31}$. The relative contribution of C_3 plant waxes (f_{C3}) to the sediment is assessed by using the linear binary mixing model as follow:

$$\delta^{13}C_{n-C31} = f_{C3}\delta^{13}C_{C3} + (1 - f_{C3})\delta^{13}C_{C4}$$

$$f_{C3} = \frac{\delta^{13}C_{n-C31} - \delta^{13}C_{C4}}{\delta^{13}C_{C3} - \delta^{13}C_{C4}}$$

The end-member values for C_3 plants ($\delta^{13}C_{C3}$=33.8‰) and C_4 plants ($\delta^{13}C_{C4}$=20.1‰) are taken from Garcin et al. (2014) and are based on an African plant dataset compiling several studies (Rommerskirchen et al., 2006; Vogts et al., 2009; Kristen et al., 2010; Garcin et al., 2014). These values are for n-C_{31} alkane, slight differences exist between long-chain n-alkanes (Garcin et al., 2014).

The influence of vegetation on $\delta D_{n\text{-}C31}$ can be associated to a difference in apparent fractionation ε between precipitation and n-alkane for C_3 plants (-129‰) on one hand and for C_4 plants (-145‰) on the other hand (Smith and Freeman, 2006; Feakins et al., 2016). Using previously calculated f_{C3}, we estimated the ε_{corr} of each sample as follows:

$$\varepsilon_{corr} = f_{C3}\varepsilon_{c3} + (1 - f_{C3})\varepsilon_{c4}$$

In a last step, we used ε_{corr} to correct $\delta D_{n\text{-}C31}$ and obtain $\delta D_{n\text{-}C31\text{-}corr}$:

$$\delta D_{n-C31-corr} = \left[\frac{\delta D_{n-C31} + 1000}{\left(\frac{\varepsilon_{corr}}{1000}\right) + 1}\right] - 1000$$

3. Results

3.1. brGDGTs

3.1.1. Relative abundance, concentration and MBT ratio

The most abundant brGDGT is brGDGT-Ia, which represent between 52.4 and 77.6 % of the brGDGT assemblages. The concentration of brGDGT-Ia range from 45.4 and 194.0 µg/g_{TOC} with a mean concentration of 96 µg/g_{TOC}. The relative abundance and concentration of brGDGTs decrease with increasing number of methylation (Ia to IIIa) and degree of methylation (Ia to Ic) (see chapter 4 for more details).

The MBT'$_{5Me}$ ratio ranges 0.7 to 0.9 (Figure 30). Before 5.8 ka cal BP, the MBT'$_{5me}$ presents higher values compared to late Holocene with a decrease centered at 8.7 ka cal BP. After 5.8 ka cal BP, two periods of increased MBT'$_{5Me}$ values is recorded around 4 ka cal BP and after 0.5 ka cal BP. The CBT_{peat} ratio is presented in chapter 4.

3.1.2. Temperature reconstructions

For all calibrations, the brGDGT-based temperature values range from 11.4 to 24.9°C (Figure 30 C and D). More specifically, for the calibration from Dearing Crampton-Flood et al. (2020) (T0 excluding sites with MAAT<0°C from the dataset), the brGDGT-based temperature values range from 17.3 to 23.5°C. All calibrations present similar variations with different amplitudes. Before 5.8 ka cal BP, brGDGT-based temperature is generally higher with a small decrease between 8.9 and 8.6 ka cal BP. The temperature is at its lowest level between 5.8 and 4.5 ka cal BP and between 3.5 ka cal BP and 0.5 ka cal BP. The temperature slightly increases at the

end of the record with values around 20.4°C for the calibration from Dearing Crampton-Flood et al. (2020).

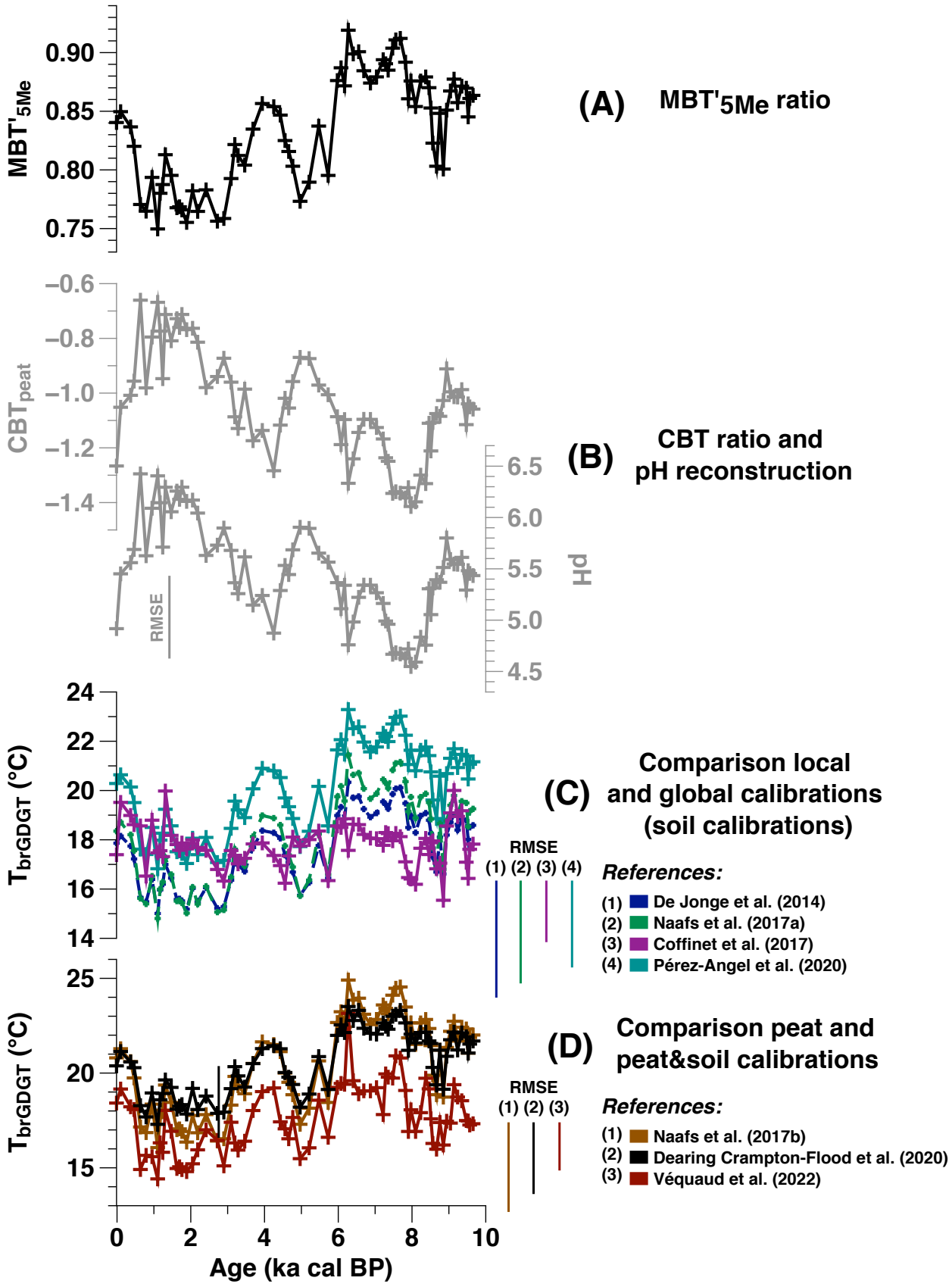

Figure 30: Methylation ratio (A), cyclisation ratio and pH reconstruction using the calibration from Naafs et al. (2017b) (see chapter 4) (B), comparison of temperature reconstructions based on global and local soil brGDGT calibrations (B) and comparison of temperature reconstruction based on global peat brGDGT calibrations (C). For the calibration from Dearing Crampton-Flood et al. (2020) and the calibration from Véquaud et al. (2022), we plot the temperature T0 using only the site where MAAT>0°C from the calibration dataset.

3.2. n-C_{31} alkane

3.2.1. Relative abundance and concentration

The n-C_{31} alkane represents between 11.0 and 30.0 % of the n-alkane assemblages with a mean value of 18.8 % (Figure 31). Low values are recorded before 3.5 ka cal BP with values generally below 20%. Minimum values occur around 8.2 ka cal BP and around 4 ka cal BP while maximum values occur around 3 ka cal BP. During late Holocene, n-C_{31} relative abundance presents intermediate values between 17.5 and 25.2 %. The n-C_{31} alkane concentration ranges between 8.1 and 57.1 µg/g_{TOC} with a mean value of 24.7 µg/g_{TOC} (Figure 31).

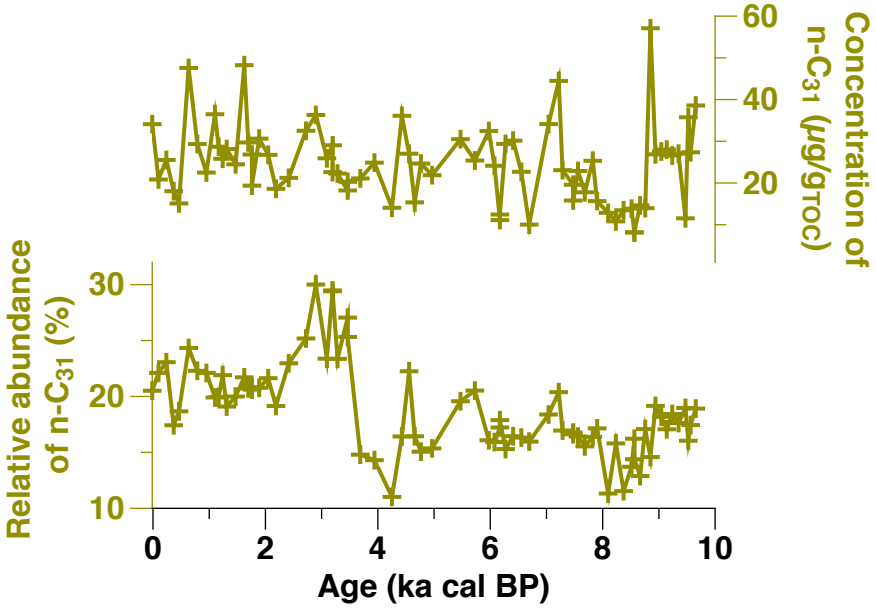

Figure 31: Downcore evolution of n-C_{31} alkane concentration (µg/g_{TOC}) and relative abundance (%). Relative abundance is calculated taking into account all n-alkanes from n-C_{19} to n-C_{37}.

3.2.2. Carbon isotopic composition

The $\delta^{13}C_{n\text{-}C31}$ values range from -32.0 to -22.9 ‰ with a mean value of -28.3 ‰ (Figure 33). The early Holocene from 9.7 to 9.4 ka cal BP is characterized by values between -24.6 and -23.9 ‰. The $\delta^{13}C_{n\text{-}C31}$ values then rapidly decrease. Low values around -30 ‰ are recorded from 9.4 to 5.5 ka cal BP except during a period of increase between 8.9 and 7.9 ka cal BP to values between -29.0 and -27.1 ‰. After 5.5 ka cal BP, the $\delta^{13}C_{n\text{-}C31}$ values are above -30 ‰ with short negative incursions around 4.6, 0.8 and after 0.5 ka cal BP.

3.2.3. Hydrogen isotopic composition

The $\delta D_{n\text{-}C31}$ values range from -90.1 to -2.7 ‰ with a mean value of -43.5 ‰ (Figure 33). Most depleted values are recorded between 7.4 and 5.8 ka cal BP. The $\delta D_{n\text{-}C31}$ values increase towards the end of the Holocene. Two 1-ka periods of less depleted values can be noted centered at 8.2 and 4 ka cal BP. The early Holocene is characterized by intermediate values around -50/-60 ‰ until 8.8 ka cal BP.

4. Discussion

4.1. Temperature reconstructions based on brGDGTs: calibration and temperature range of variation

4.1.1. Validity of the brGDGT data

The Figure 32 places the brGDGT data within the global calibration dataset for soil (Dearing Crampton-Flood et al., 2020) and peat (Naafs et al., 2017b).

The brGDGT are divided into three groups based on the number of methylations and are represented in a ternary plot (Figure 32). The brGDGT record from the NGaoundaba peat deposit shows high abundances of tetramethylated brGDGTs and low abundances of hexamethylated brGDGTs. The brGDGT distribution from the NGaoundaba peat deposit is consistent with both soil and peat calibration dataset (Figure 32). No outliers are present. Consequently, soil and peat calibration can be tested at the NGaoundaba peat deposit.

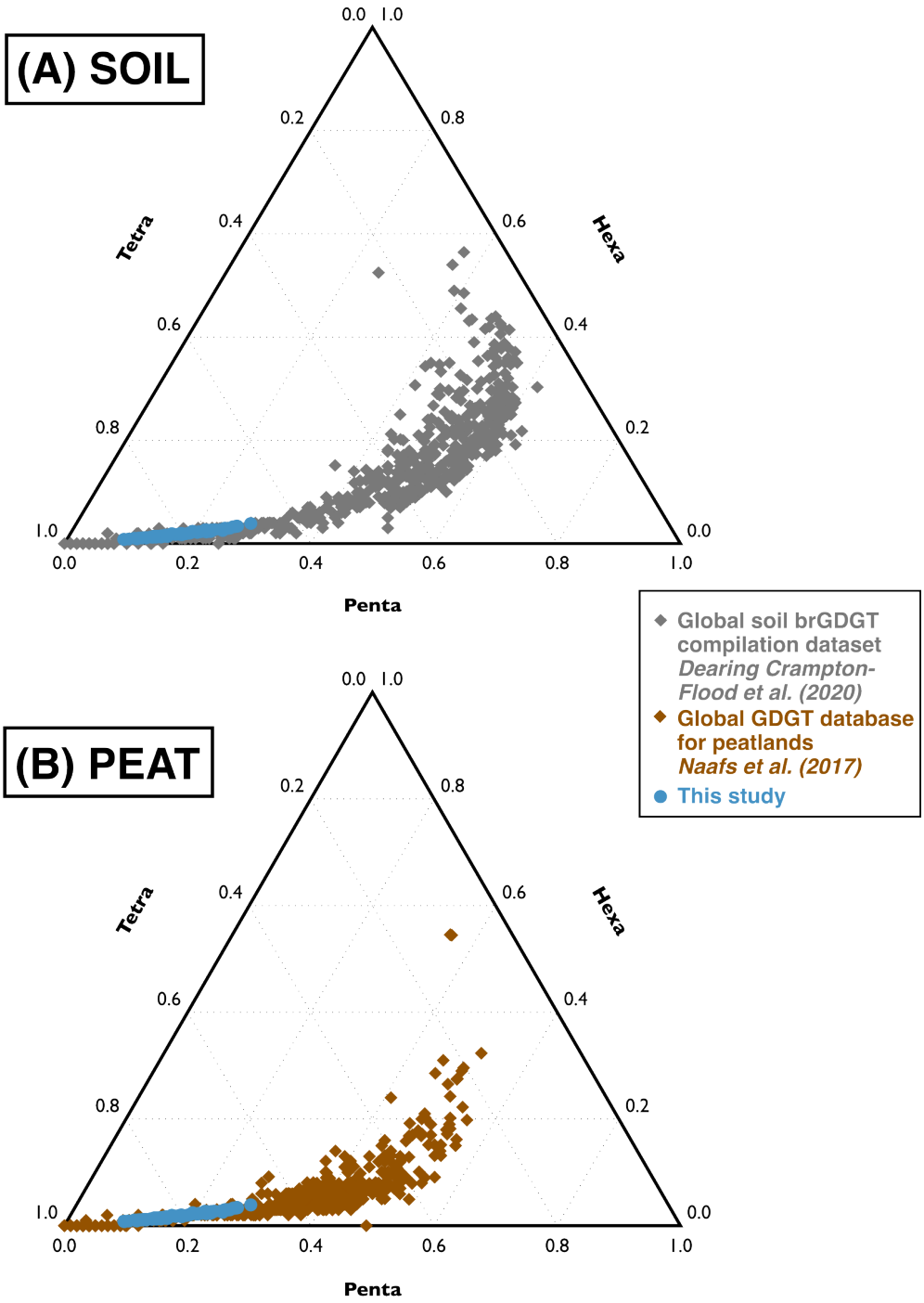

Figure 32: The brGDGT NGaoundaba peat record plotted with global soil (A) and peat (B) calibration dataset. The tetramethlylated brGDGTs are Ia, Ib, Ic, the pentamethylated are IIa, IIa', IIb, IIb', IIc and IIc' and the hexamethylated are IIIa, IIIa', IIIb, IIIb' and IIIc.

4.1.2. Do we need a tropical peat-based temperature calibration?

The brGDGT-based temperature variations during the Holocene range from 4.6 to 6.6 °C for the soil-based calibrations (Figure 30 C). The topmost temperature value (10-cm depth) of three out of four soil calibrations is consistent with the present-day MAAT of the NGaoundaba

peat deposit (22.2°C) when considering the RMSE of each calibration. The East-African calibration from Coffinet et al. (2017) may underestimate temperature as the topmost temperature value of the NGaoundaba peat deposit is below the MAAT even when considering the RMSE. The calibration dataset from Coffinet et al. (2017) is based on brGDGT distributions of several East African mountains and take into account many high altitude sites that may biased the result. As calibrations are based on soil sediments and not on peat sediments, the temperature reconstructions might be slightly biased by the difference in bacterial communities between soils and peats (Peterse et al., 2011). However, Dearing Crampton-Flood et al. (2020) demonstrate that soil and peat calibration datasets are not statistically different. The calibration from Coffinet et al. (2017) take into account i) the CBT ratio that is excluded from more recent calibration as it is influenced by pH variations (De Jonge et al., 2014) and ii) the MBT' ratio that doesn't separate the 5-methyl and the 6-methyl brGDGT isomers, the later also being influenced by pH variations (De Jonge et al., 2014; Ding et al., 2015; Xiao et al., 2015) and soil aridity (Dang et al., 2016). Strong pH variations in peat deposit may, therefore, biased this calibration. At the Kyambangunguru marsh, brGDGT-derived temperature in the peat is lower than local MAAT and between 4 and 6 °C lower than brGDGT-derived temperature in the surrounding soils when applying the same soil temperature calibration potentially associated with different bacterial communities (Coffinet, 2015). Despite a possible underestimation of temperature values, the calibration from Coffinet et al. (2017) presents the lowest range of temperature for the Holocene which is more consistent with models (Kaufman and Broadman, 2023) and other West and Central African temperature reconstructions (Schefuß et al., 2005; Weijers et al., 2007a) that suggest small temperature variation between the African Humid Period and the late Holocene. Peaks in the temperature reconstructions are present for the East-African calibration that are not coinciding with particular climatic event and seems unrealistic (Figure 30).

Some global soil calibrations saturate around 24-25°C (De Jonge et al., 2014; Naafs et al., 2017a) due to the scarcity of sites with high MAAT in the global calibrations and may not be appropriate to reconstruct temperature in tropical sites where past temperature may have exceed this threshold (Pérez-Angel et al., 2020). Bayesian and machine learning calibration methods enable to extend the upper limit of global calibration up to around 27°C for the calibrations from Dearing Crampton-Flood et al. (2020) and Véquaud et al. (2022) and development of tropical calibrations can also extend this limit up to 26.4°C for the calibration of Pérez-Angel et al. (2020). The higher temperature reconstructed using the pan-tropical calibration of Pérez-Angel et al. (2020) may be the result of this extended temperature threshold. Tropical peat-based calibrations could thus increase the accuracy of temperature reconstruction by extending the upper temperature limit and better taking into account the

specificity of tropical peat deposits in terms of vegetation or environmental conditions such as precipitation seasonality.

4.1.3. Global peat calibrations

The brGDGT-based temperature variations during the Holocene range from 5.6 to 8.8 °C for peat- and peat&soil-based calibrations (Figure 30 D). The range of temperature variation is larger than the temperature change during the Holocene predicted by models (Kaufman and Broadman, 2023) and reconstructed in other West and Central African sites (Schefuß et al., 2005; Weijers et al., 2007a). Several parameters can overprint the temperature signal and potentially affect the range of temperature variation.

Changes in the production of brGDGTs associated with temperature seasonality is responsible for large biases in brGDGT-reconstructed temperature in temperate region (Huguet et al., 2013), but its impact is proposed to be limited in tropical regions (Naafs et al., 2017b). However, calibrations can be biased by sites with high temperature seasonality especially sites with many days under 0°C (Naafs et al., 2017a). To address this problem, Dearing Crampton-Flood et al. (2020) and Véquaud et al. (2022) propose two calibrations using either the whole dataset (temperature noted T) or only the sites with MAAT > 0°C (temperature noted T0). For both calibrations, T0 values present a narrower range of variations more consistent with models and T values present a 'cold' bias likely due to the preferential production of brGDGTs during the summer season in soils that are frozen during winter (Figure S 7). The T and T0 temperature reconstructions from Véquaud et al. (2022) present a strong cold bias. The topmost value at 10-cm depth is below the MAAT of the NGaoundaba peat deposit even when considering the RMSE of each calibration. In particular, the T temperature calibration from Véquaud et al. (2022) ranges from 11.4 to 17.1 °C with an RMSE of 4.1°C. These temperatures are unrealistic for the region even when considering calibrations error (Figure S 7). In addition, the temperature reconstruction based the calibration from Véquaud et al. (2022) present a few short and abrupt temperature variations such as around 6.2 ka cal BP that do not seem to coincide with any particular climatic event (Figure 30 D). We suggest care in the application of this recent calibration, at least for tropical regions.

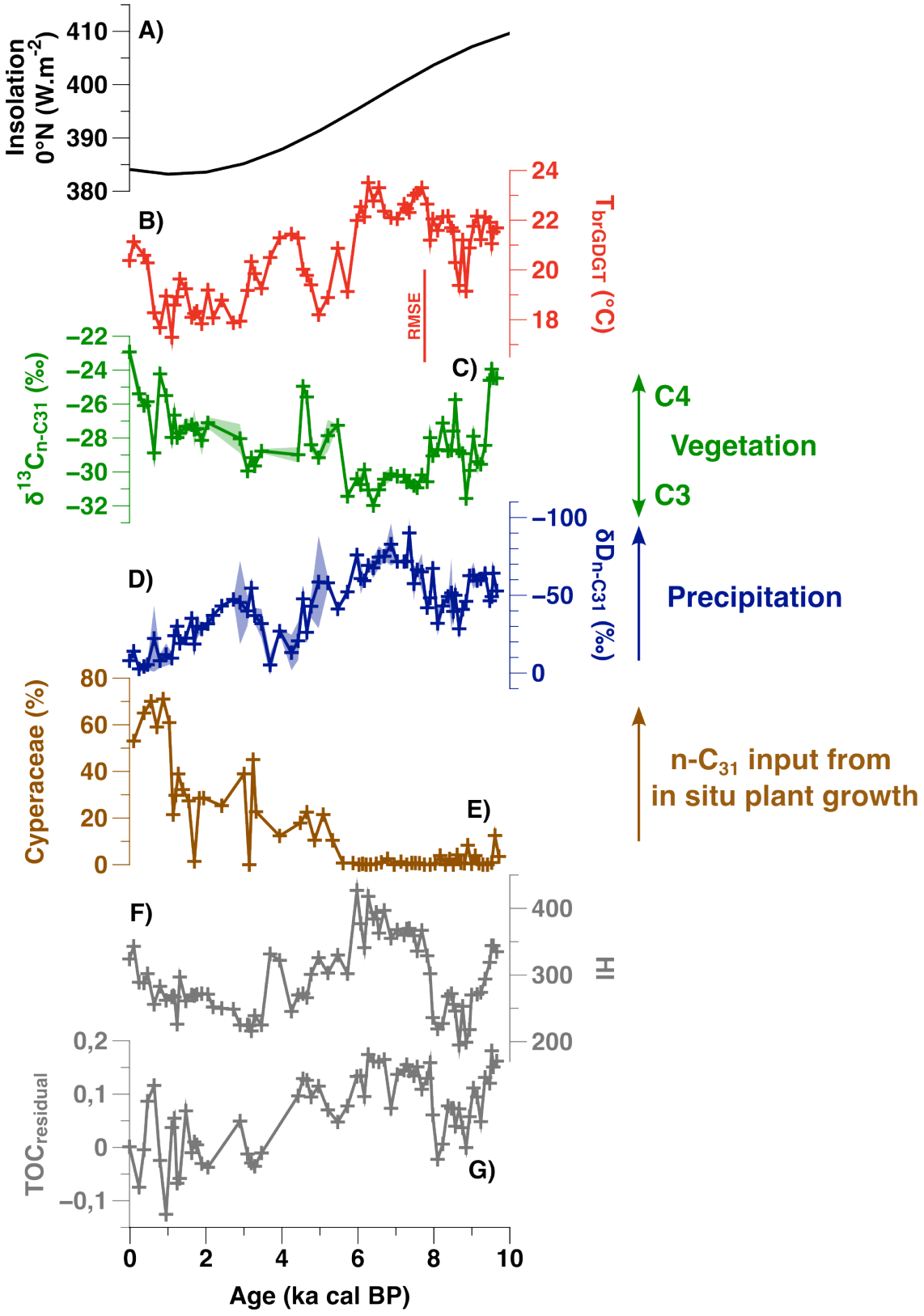

Figure 33: Insolation 0°N (W.m^{-2}) from Berger et al. (1981), brGDGT-based temperature reconstruction using the calibration from Dearing Crampton-Flood et al (2020) (T0) (B), $\delta^{13}C_{n\text{-}C31}$ corrected for Suess effect (C), $\delta D_{n\text{-}C31}$ corrected for vegetation change (reverse axis) (D), percentage of Cyperaceae pollens (among all pollen, excluding spores, cf chapter XX for the method of pollen analyses) (E), HI (F) and $TOC_{residual}$ (G) after Schaaff et al. (2023). The RMSE associated with brGDGT calibration is indicated on the graph. For n-alkane isotopic data, if not visible, uncertainties are smaller than the size of the data point.

Precipitation and moisture level might be responsible for part of the variation range (Rao et al., 2022). Based on soil warming experiments, pH variations are positively correlated to the brGDGTs used in the MBT'_{5Me} ratio and explain part of the variation in MBT'_{5Me} (De Jonge et al., 2021). At the NGaoundaba peat deposit, some temperature variations coincide with strong changes in brGDGT-reconstructed pH (Figure 30 B and D). It is likely that pH variations affect the range of temperature reconstructed at the NGaoundaba peat deposit. Changes in in situ-growing vegetation might affect the range of temperature reconstructed by affecting the bacterial community (Liang et al., 2019).

4.2. δD_{wax} records from NGaoundaba peat: how to explain such large variations?

The δD_{wax} record from the NGaoundaba peat deposit present a large range of variation compared to lake Barombi or lake Bosumtwi for example (Table 5). The δD_{wax} values are related to the hydrogen isotopic composition of precipitation (e.g., Niedermeyer et al., 2016), but it is hard to imagine such a large variation in δD_{precip} during the Holocene between sites that are not so far from each other. Therefore, the large range of δD_{wax} values recorded at the NGaoundaba peat deposit questions its validity and the possibility to use it as a paleoprecipitation proxy. Therefore, prior any paleoclimatic interpretation, we tried to understand the possible causes of this large range in δD_{wax} values. We conducted a compilation of existing δD_{wax} records in tropical Africa and compared the range of δD_{wax} variations among all these sites, then we focus on peat deposit and compared the NGaoundaba peat record with the other peat-based records in tropical Africa.

4.2.1. Compilation of existing δD_{wax} records in Africa

A compilation of the range of δD_{wax} values observed in δD_{wax} records from low and mid latitudes in Africa was carried out (Table 5 and Figure 34). This compilation regroups 15 records (2 peats, 8 lakes and 5 marine cores). The corrections applied to the raw δD_{wax} values were not the same in all the studies (vegetation, ice volume and sea level changes) and are summarized in Table 5. The δD_{wax} range is calculated over the same period as that covered by the NGaoundaba peat deposit, from 9.7 ka cal BP to present. The records from the lake Albert (Berke et al., 2014) and Kyambangunguru marsh (Coffinet et al., 2018) were excluded because they don't cover the whole 9.7 to 0 ka period.

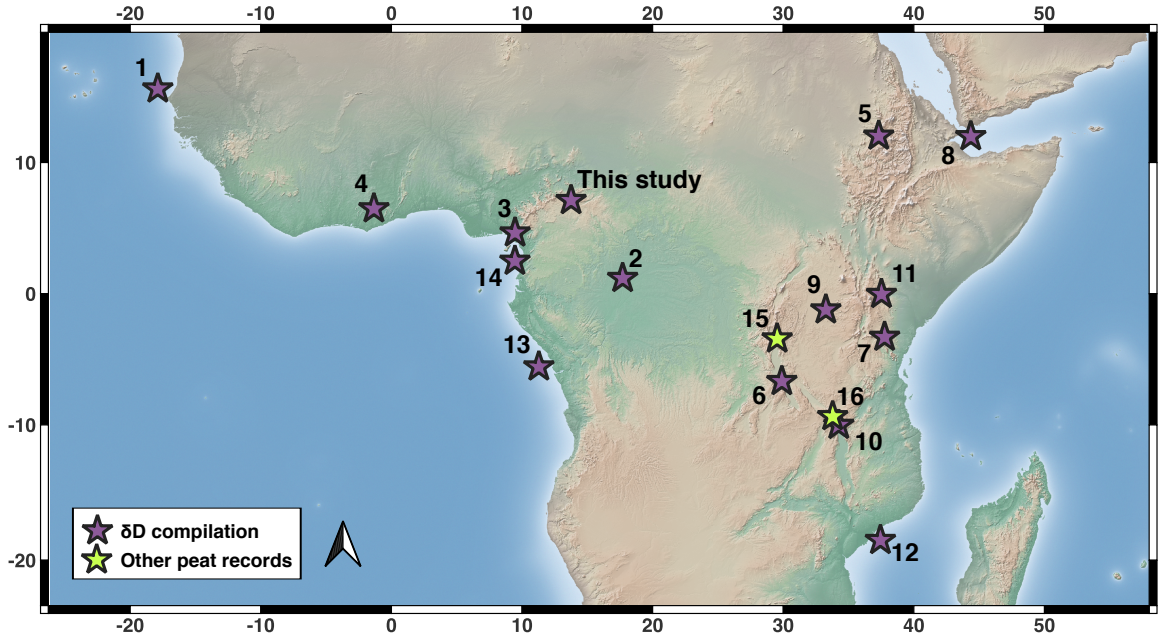

Figure 34: Position of the sites discussed in this section. The site numbers refer to the references associated with Table 5. The site 15 corresponds to the Kashiru peat (Aucour et al., 1996) and the site 16 to the Kyambangunguru marsh (Coffinet, 2015; Coffinet et al., 2018).

Table 5: Compilation of δD_{wax} range from African records. The δD range of modern precipitation is calculated using wateriso website version OIPC3.1 (https://wateriso.utah.edu/waterisotopes/pages/data_access/form_3_1.html).

Site	Ref	Type	Lat	Long	Alt (m)	Size (km^2)	Range δD_{wax}	Range δD_{precip}	Alk / Corr	Nb value
NGaoundaba	This study	P	7.13	13.69	1175	0.018	71.6/ 87.4	34	C_{31}/ C_{31}Veg	73
Off Senegal	1	M	15.50	-17.95	0		17.1	66	C_{31} Ice	14
Congo Peat	2	P	1.18	17.64	327		33.1	44	C_{29}	54
Barombi	3	L	4.66	9.40	334	5	34.8	27	C_{31} Veg	208
Bosumtwi	4	L	6.50	-1.41	150	49	31	21	C_{31} Veg	60
Tana	5	L	12	37.25	1830	3200	85	34	C_{28a} Ice	32
Tanganiika	6	L	-6.7	29.83	773	32600	45.1	21	C_{28ol} Iceveg	40
Challa	7	L	-3.32	37.7	880	4.2	28.1	21	C_{28a} Ice	79
Gulf Aden	8	M	11.96	44.3	0		26.8	41	C_{30a} Ice	39

Victoria	9	L	-1.23	33.20	1135	69000	33.5	31	C_{28a} Ice	17
Malawi	10	L	-10.02	34.19	474	29600	18.2	17	C_{28a} Ice	38
Rutundu	11	L	-0.04	37.46	3078	0.4	43.7	39	C_{29} Iceveg	24
Off Zambezi	12	M	-18.56	37.38	0		22.3	29	C_{31}	32
Off Congo Basin	13	M	-5.59	11.22	0		36	41	C_{29} Sealvl	71
Gulf Guinea	14	M	2.5	9.39	0		22.1	24	C_{29}	71

References:

1: Niedermeyer el al. (2010) *8: Tierney et deMenocal (2013)*

2: Garcin et al. (2022) *9: Berke et al. (2012)*

3: Garcin et al. (2018) *10: Konecky et al. (2011)*

4: Shanahan et al. (2015) *11: Garelick et al. (2021)*

5: Costa et al. (2014) *12: Schefuß et al. (2005)*

6: Tierney et al. (2011b) *13: Schefuß et al.*(2017)

7: Tierney et al. (Costa et al., 2014) *14: Collins et al. (2017)*

Abreviations:

Type: P: peat, L: lake, M: marine

Alk/corr: "a" refers to alkanoic acid, "ol" to alkanol

During the period under consideration, most records show amplitudes lower than those of the NGaoundaba record, with the lowest values generally recorded in marine records. Several African δD_{wax} records show significant amplitude of variations, especially at lake Tana (Costa et al., 2014) where the high range of δD_{wax} is attributed to changes in moisture sources leading to a decoupling of δD_{wax} from rainfall amount.

In an initial simplistic interpretation of the data set, a PCA analysis was conducted to search for similarities between the range of δD_{wax} and other parameters (Figure 35). As the δD_{precip} is influenced by the sources of moisture and by the distance from these sources, we tested the PCA analysis for the whole dataset and for West and Central African sites only. PCA analysis indicates similarity between elevation and the range of δD_{wax} observed in the data, while longitude, latitude, size of the catchment area (for lake and peat), or current range in δD_{precip} is not correlated with the range of δD_{wax}. Air masses get progressively depleted in heavy isotope when the altitude increase due to progressive condensation associated with decreasing temperature and atmospheric pressure (Dansgaard, 1964). In tropical Africa, altitude effect has been demonstrated several times (Gonfiantini et al., 2001; Zech et al., 2015;

Coffinet et al., 2017). Therefore, the altitude effect may be responsible for part of the range observed at NGaoundaba as this peat deposit is the highest δD_{wax} record available in West and Central Africa at the moment. However, this simple dataset cannot take into account the specificity of each site and the complexity of δD_{wax} and of its variations. For example, Lake Victoria and the NGaoundaba peat deposit are located at very similar altitudes and present a significant difference in the range of values covered by their δD_{wax} record (Table 5).

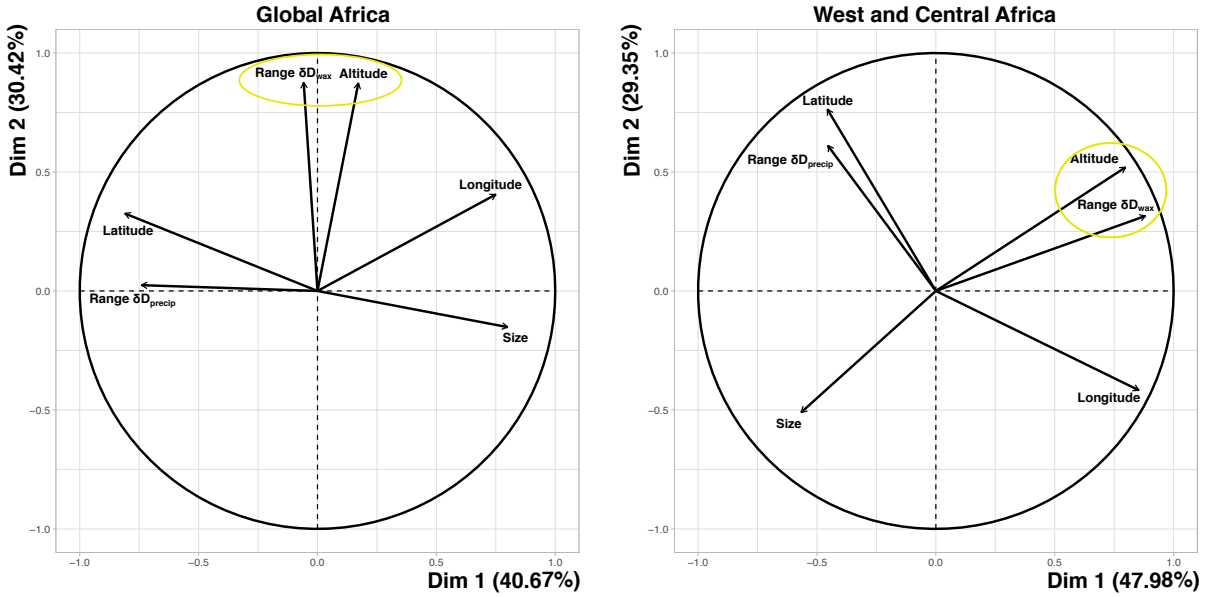

Figure 35: PCA analyses based on the data from table 5. The left panel includes all sites while the right panel only includes sites from West and Central Africa (1-4, 13, 14, NGaoundaba)

4.2.2. A focus on African tropical peat-based hydrogen isotopic records

As a global approach comparing the δD_{wax} records of tropical Africa did not allow us to explain the variations observed in the NGaoundaba peat bog, we decided to take to focus on peat deposits and to look for other tropical peat records. The following subsections briefly present the different sites and records we found.

4.2.2.1. The Kashiru peatland (Burundi)

The Kashiru peatland is a high-altitude peatbog (2240m asl) situated in Burundi (S3.45°, E29.53°) (Figure 34, site 15). The Kashiru peatbog covers an area of 0.5 km^2, for a catchment area of 4 km^2. The peatland has an outlet to a stream. A 40-ka core has been studied for pollen (Bonnefille and Riollet, 1988; Bonnefille et al., 1990), $\delta^{13}C_{bulk}$ (Aucour et al., 1994, 1999) and $\delta^{18}O_{cellulose}$ (Aucour et al., 1996). As for the NGaoundaba peatland, the Kashiru peatland is now dominated by sedges (Aucour et al., 1996).

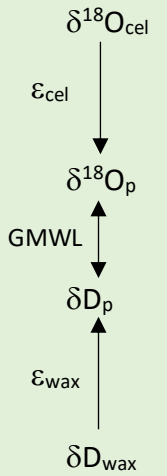

$$\varepsilon_{cel} = \left(\frac{1000 + \delta^{18}O_{cel}}{1000 + \delta^{18}O_P} - 1\right) * 1000$$

$$\Longrightarrow \delta^{18}O_{cel} = \left(\frac{\varepsilon_{cel}}{1000} + 1\right) * (1000 + \delta^{18}O_P) - 1000$$

$$\Longrightarrow \Delta\delta^{18}O_{cel} = \left(\frac{\varepsilon_{cel}}{1000} + 1\right)\Delta\delta^{18}O_P$$

$$\delta D_p = 8 * \delta^{18}O_p + 10 \Longrightarrow \Delta\delta D_p = 8 * \Delta\delta^{18}O_p$$

$$And\ \Delta\delta D_{wax} = \left(\frac{\varepsilon_{wax}}{1000} + 1\right)\Delta\delta D_P$$

$$So\ \Delta\delta D_{wax} = \frac{\left(\frac{\varepsilon_{wax}}{1000} + 1\right)}{\left(\frac{\varepsilon_{cel}}{1000} + 1\right)} * 8 * \Delta\delta^{18}O_{cel}$$

$$\boxed{\Longrightarrow \Delta\delta D_{wax} = \frac{1000 + \varepsilon_{wax}}{1000 + \varepsilon_{cel}} * 8 * \Delta\delta^{18}O_{cel}}$$

With: $\delta^{18}O_p$ and δD_p oxygen and hydrogen isotopic composition of precipitation
$\delta^{18}O_{cel}$ and δD_{wax} oxygen and hydrogen isotopic composition of cellulose and n-alkane, respectively
ε_{cel} the fractionation coefficient between precipitation and cellulose
ε_{wax} the fractionation coefficient between precipitation and n-alkane

Figure 36: Procedure used to convert a $\delta^{18}O_{cellulosis}$ range ($\Delta\delta^{18}O_{cellulose}$) to a δD_{wax} range ($\Delta\delta D_{wax}$). We use the Global Meteoric Water Line (GMWL) as defined by Craig (1961) to link $\delta^{18}O_p$ and δD_p values.

Based on Kashiru peatland (Burundi), Aucour et al. (1996) measured a range of $\delta^{18}O_{cellulose}$ of around 9 ‰ from 9.7 ka cal BP to present. Using the data in Aucour et al. (1996) and the following equations, we recalculated an apparent fractionation coefficient between precipitation and cellulose ε_{cel} of 42.5‰. The apparent fractionation coefficient between precipitation and n-alkanes is around -129‰ for C3 plants (Feakins et al., 2016) and -145‰ for C4 plants (Smith and Freeman, 2006); we thus choose a mean value of -135‰. Using the following procedure, we calculated a δD_{wax} range of 60‰ which is in the same order as the NGaoundaba range of δD_{wax}. We checked the method by applying the same procedure to the $\delta^{18}O_{cellulose}$ range of the Lake Victoria over the period 9.7-0 ka (Beuning et al., 1997, 2002). We found a range of 26.5‰ comparable to the δD range of 32‰ of the Lake Victoria (Berke et al., 2012).

4.2.2.2. The Kyambangunguru marsh (Tanzania)

The Kyambangunguru marsh is located in a maar crater of the Rungwe Volcanic Province in Tanzania (S9.37°, E33.78°, 660m a.s.l.) (Figure 34, site 16). The Kyambangunguru marsh is an

ombrotrophic bog, the water depth reaches less than 1m at the end of the rainy season and nearly dries out during the dry season. The basin does not have any outlet stream (Delalande et al., 2008). As for the NGaoundaba peatbog, the marsh itself and its catchment area are small (about 0.04 km^2 and 0.2 km^2, respectively). The marsh is dominated by sedges and the presence of floating and submerged macrophytes can be noted during the rainy season (Coffinet et al., 2018). A 4-ka core from the Kyambangunguru marsh has been studied for lipids biomarkers (Coffinet, 2015; Coffinet et al., 2018).

The range of δD_{wax} is between 36 and 76 ‰ for a period of 4-ka covering the end of the Holocene (Coffinet, 2015; Coffinet et al., 2018). This range is large compared to other nearby lakes (e.g., Tierney et al., 2008, 2010; Berke et al., 2012). Over the same period, the lake Malawi shows a range of 17 ‰ (Konecky et al., 2011) and the lake Challa shows a range of 19 ‰ (Tierney et al., 2011) for n-C_{28} n-alkanoic acid. During the same period, the range of δD_{wax} at the NGaoundaba peatbog is between 25 and 42 ‰ (with the same trends for similar chain length). Between 2.3 and 1.4 ka cal BP, the Cyperaceae percentage increases while the δD_{wax} decreases. This period is interpreted as a warm and relatively dry period. The simultaneous decrease in algae and aquatic plants suggests a fall in the water table (Coffinet et al., 2018).

4.2.2.3. The Congo basin swamp forest (Republic of the Congo)

The Congo Basin is a large river basin with a catchment area of 3.7 million km^2. Garcin et al. (2022) (Figure 34, site 2) collected three peatcores from a peat-filled interfluvial basin (N1.11°, E17.64°, 327 m above sea level). The peat vegetation is dominated by swamp forest. The range of δD_{wax} is 33 and 26 ‰ for C_{29} and C_{31} n-alkane, respectively. These ranges are close to those measured for West African lakes (Garcin et al., 2018; Shanahan et al., 2015).

4.2.3. n-alkanes hydrogen isotopic composition: toward a specificity of sedges-dominated peat deposit?

The high amplitude of δD_{wax} records could be due to the specificities of sedges-dominated peat deposits compared to lakes, marine sites and other types of peat deposits. While the Congo Basin is a peat swamp forest situated in a large river basin, the Kashiru peatland, the NGaoundaba peatland and the Kyambangunguru marsh are sedge-dominated peat deposits. In peat deposits, a significant part of the peat-forming material comes from in situ plant production such as sedges for mid- and high-altitude tropical peat deposits. High evaporation of water in peatlands and lakes can lead to enriched water through evaporation (Gat, 1996). In addition, transpiration in plant tissue further enriched the water used for organic

compound synthesis (Jacob and Sonntag, 1991; Wang and Yakir, 2000). This enrichment in deuterium is particularly important in closed basins such as the NGaoundaba or Kyambangunguru peatlands where evapotranspiration is the main factor of water loss in the system. On the Adamawa Plateau, Abba et al. (2023) analyzed isotopic composition of several lakes. Among them, the lake Tizong is the only closed basin and has the most enriched water. Lakes and peatlands in South West Tanzania have a Regional Evaporation Line that is strongly deviated from the Regional Meteoric Water Line, indicating water enrichment in each basin relative to precipitation water (Delalande et al., 2008). The use of this enriched water by plants leads to an enrichment of the δD_{wax} of these plants.

Floating and submerged macrophytes produce more mid-chain *n*-alkanes. The impact of these plants on the δD_{wax} records is likely to be visible on mid-chain than on long-chain homologues. Sedges cannot develop if the water table is constantly high. At NGaoundaba, the sedges begin to develop at the end of the AHP. During this period of lower precipitations, the development of sedges, using D-enriched water, leads to an increase in δD_{wax} which, in addition to the low amount of precipitation, induces a higher magnitude of δD_{wax} variation along the record (Figure 37). In the Congo basin, the forest cover has been permanent with arboreal fraction above 85% over the whole record (Garcin et al., 2022). The decline in some swamp forest taxa is not likely to have a profound impact the δD_{wax} signal as they don't represent a predominant part of the liter input.

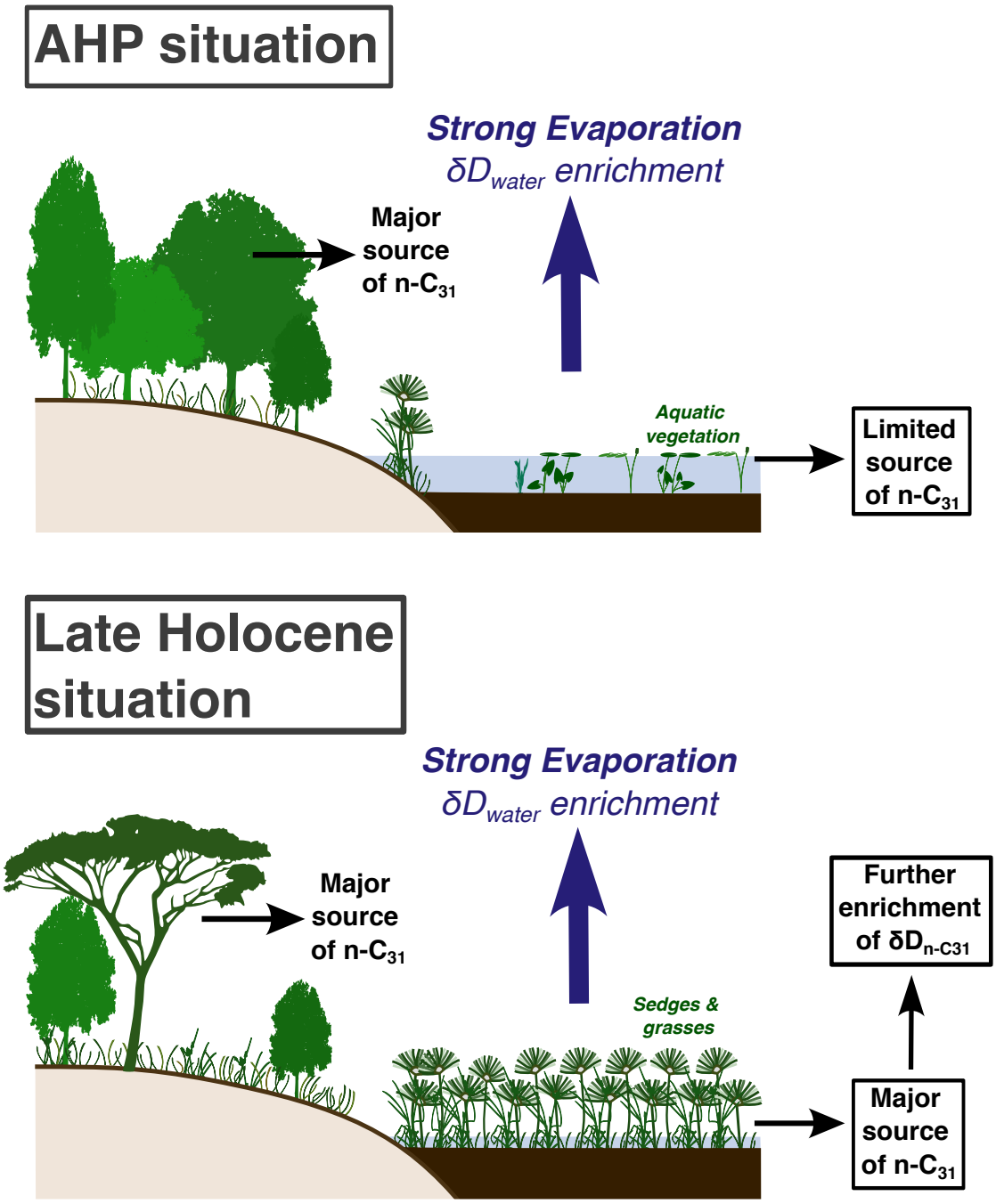

Figure 37: Specificity of sedge-dominated peat deposits. During late Holocene, the development of sedges and grasses increased the input of n-C_{31} alkanes from plants growing using peat water instead of direct precipitation. As evaporation has led to an isotopic enrichment of peat water, the $\delta D_{n\text{-}C31}$ has been enriched, amplifying the existing trend linked to reduced precipitation.

4.3. Paleoclimatic interpretation based on biomarkers

4.3.1. Long-term trend: a new record of the termination of the African Humid Period

Between 5.8 and 5.5 ka cal BP, biomarkers indicate high temperatures, C_3-dominated vegetation and high precipitation coinciding with the AHP (DeMenocal et al., 2000). The

predominance of C_3 plants likely indicate a more forested environment consistent with the maximum abundance of arboreal pollen recorded at lake MBalang (Vincens et al., 2010). After 5.8 ka cal BP, precipitation progressively decreased until present while the vegetation becomes more dominated by C_4 plants suggesting an opening of the environment consistent with the forest retreat recorded in pollen records from lake Mbalang (Vincens et al., 2010).
The end of the AHP has been widely discussed with controversies concerning the abruptness of its ending: some records and model suggesting a progressive termination of the AHP following the decrease in insolation (e.g., DeMenocal et al., 2000; Collins et al., 2017) while others indicate an abrupt termination with complex feedback effect on precipitation and potential regional or local effect (e.g., Tierney et al., 2017; Maley et al., 2018). Comparison of different proxies from the NGaoundaba peat record indicate that the response time seems to depend on the proxies. While precipitation seems to respond progressively to change in orbital forcing, vegetation and microbial community (as represented by the T_{brGDGT}) may respond abruptly to the end of the AHP. In the Sahara region, simulations show an abrupt shift of the vegetation and strong feedbacks between precipitation and vegetation cover (e.g., Claussen et al., 1999; Renssen et al., 2003).

4.3.2. Short dry events

The AHP is interrupted by a 1-ka dry event from around 8.9 to 7.8 ka cal BP associated with less depleted $\delta^{13}C_{n\text{-}C31}$ starting at around 8.8 ka cal BP suggesting an associated change in vegetation (Figure 33C). Change in brGDGT temperature is recorded only at the beginning of this period between 8.9 and 8.5 ka cal BP. Bulk proxies (HI and $TOC_{residual}$) present a strong decrease during the same period (Figure 33) suggesting either a change in the origin of organic matter or an increase in the decomposition of organic matter (Schaaff et al., 2023). A second dry event is recorded between 4.5 and 3.5 ka cal BP coinciding with an increase in brGDGT temperature (Figure 33B). These two events coincide with well-known dry climatic event frequently recorded in high and mid latitudes, the so-called 8.2 and 4.2 ka event (e.g., Rohling and Pälike, 2005; Ran and Chen, 2019; Bini et al., 2019) (see next chapter for more information on these two events). However, these two events are not recorded in the other δD records from West and Central Africa (e.g., Shanahan et al., 2015; Garcin et al., 2018, 2022) except the increase in the δD_{wax} record from Niedermeyer et al. (2010) around 8/7.8 ka cal BP. The pollen records from lake Tizong (Lebamba et al., 2016) and lake MBalang (Vincens et al., 2010) rather indicate forested phases between 3.9 and 3 ka cal BP and between 5.2 and 4.2 ka cal BP, respectively, which is not consistent with a dry phase around 4 ka cal BP. However, the lake Tizong presents an interval of reworked material (Nguetsop et al., 2013), suggesting that dating issues might be responsible for some discrepancies between records.

4.4. Climatic and environmental responses to the end of the AHP in West and Central Africa

In Western and Central Africa, rather abrupt decreases of lake levels are recorded at the end of the AHP (Gasse, 2000 and references therein). In close basin, lake level is a balance between water input from direct precipitation into the lake or from water run-off from the catchment and water output from outlet or evaporation-transpiration. Lake response to climatic changes is also influenced by basin geomorphology and hydrology, therefore the magnitude of the lake response is likely to be non-linear and may vary from one lake to another (Fritz, 2008). In addition, paleoshorelines and stratigraphic sections are a discontinuous record of lake level and might record preferential maximum and minimum lake level while intermediate states may have been erased by more recent event.

δD_{wax} records from West and Central Africa follow a general decreasing trend dictated by orbital forcing with less depleted values during the early Holocene compared to the late Holocene. Several records present positive and negative excursions away from this general trend, making it difficult to determine the global picture of the termination of the AHP. Dry or wet events can be observed and linked with well-known climatic events. For example, a dry event is recorded around the 8.2 ka event at the NGaoundaba peat deposit (this study) and in a marine core off Senegal (Niedermeyer et al., 2010). At lake Bosumtwi, less depleted δD_{wax} values are recorded around 8 to 6 ka cal BP (Shanahan et al., 2015) while other nearby records are presenting most depleted δD_{wax} values during the same period (Collins et al., 2017; Garcin et al., 2018; This study) and while the lake level of lake Bosumtwi is high (Shanahan et al., 2006). Shanahan et al. (2015) suggest a secondary time-transgressive rainfall maxima at lower latitude associated with seasonality change accompanying the southward retreat of the rainbelt. This later increase in precipitation coincides with forest regeneration around the same period at some sites (Vincens et al., 2010) and some models also suggest a rebound in vegetation with a similar timing (Liu et al., 2007). However, this rewetting period coincides with the “Ghost interval” defined by Garcin et al. (2022) suggesting a drying trend leading to highly decomposed peat in the Congo Basin. At the NGaoundaba peat deposit, it coincides with a dry event from 4.5 to 3.5 ka cal BP, independent from the AHP. Regional and local responses to climate changes may be responsible for the discrepancies between the different sites. It has been suggested that δD_{wax} estimates of precipitation may be overestimated as they don’t take into consideration the enrichment of precipitation due to evaporation (Thompson et al., 2021).

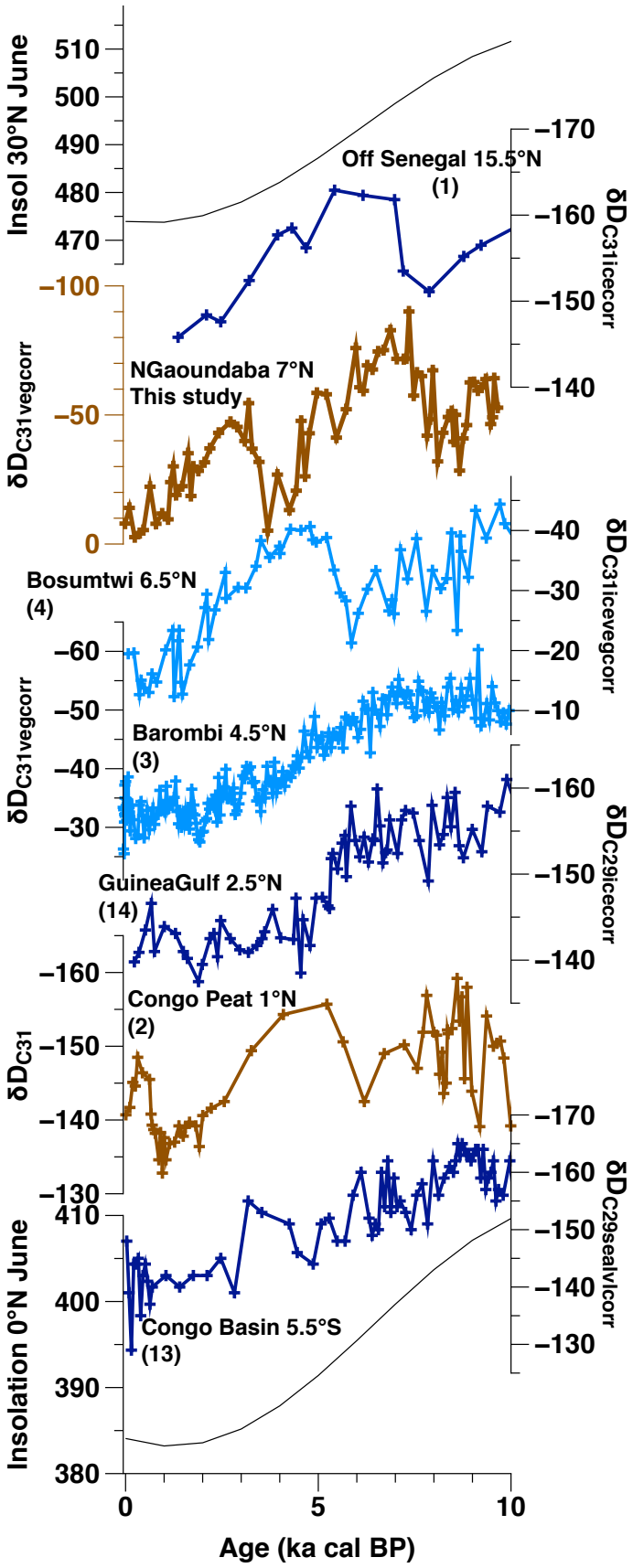

Figure 38 : Compilation of δD_{wax} records from West and Central Africa and insolation at 0° and 30° (W/m^{-2}) from Berger et al. (1981). The color refers to the type of the record (marine, lake or peat). The numbering refers to Table 5.

Are modeling data consistent with all these observations? First, Liu et al. (2007) suggests a gradual decrease in precipitation at the end of the AHP while the vegetation may have responded more abruptly. In their model, the change in precipitation is dominated by internal climate variability and a gradual response to orbital forcing while the vegetation responds nonlinearly to a precipitation threshold. Second, the nature of the response of precipitation to orbital changes may be regional. Renssen et al. (2006) suggest that the abrupt decrease of the precipitation may only be seen in Western Sahara and Sahel while other regions of Africa may record a more gradual response. In tropical and equatorial Africa, changes in vegetation do not induce a marked change in albedo and therefore change in albedo may not have been sufficient to amplify the reduction in precipitation (Renssen et al., 2006). Thus, a progressive decrease in precipitation in tropical and equatorial Africa doesn't preclude abrupt precipitation changes in the Sahara and Sahel regions.

Conclusions

The distribution of brGDGTs and of n-C_{31} alkane as well as the δD and $\delta^{13}C$ compositions of the latter were measured on a peat deposit from the Adamawa Plateau (North East Cameroon). brGDGT temperature and $\delta^{13}C_{n\text{-}C31}$ indicate a termination of the AHP around 5.8 ka cal BP consistent with a nearby pollen record (Vincens et al., 2010) while the $\delta D_{n\text{-}C31}$ gradually decreases. The NGaoundaba peat record also highlights two dry events from 8.9 to 7.9 ka cal BP and from 4.5 to 3.5 ka cal BP, marked by changes in vegetation and in microbial community.

Confronting the NGaoundaba peat record with existing studies indicate that care is needed when interpreting lipid biomarkers in peat deposits. Both brGDGT temperature and $\delta D_{n\text{-}C31}$ records present wider ranges of variation compared to other non-peat records. A wider range of temperature variation might be related to co-influencing factor in the empirical calibration such as pH or moisture changes. $\delta D_{n\text{-}C31}$ record is likely influenced by the growth of sedges and grasses directly on the peatlands. As these plants produce long chain n-alkanes, they may represent a significant input of n-C_{31} alkanes. We argue that strong evaporation of peat water leads to enriched peat water and therefore increases the range of hydrogen isotopic variations.

Supplementary figures:

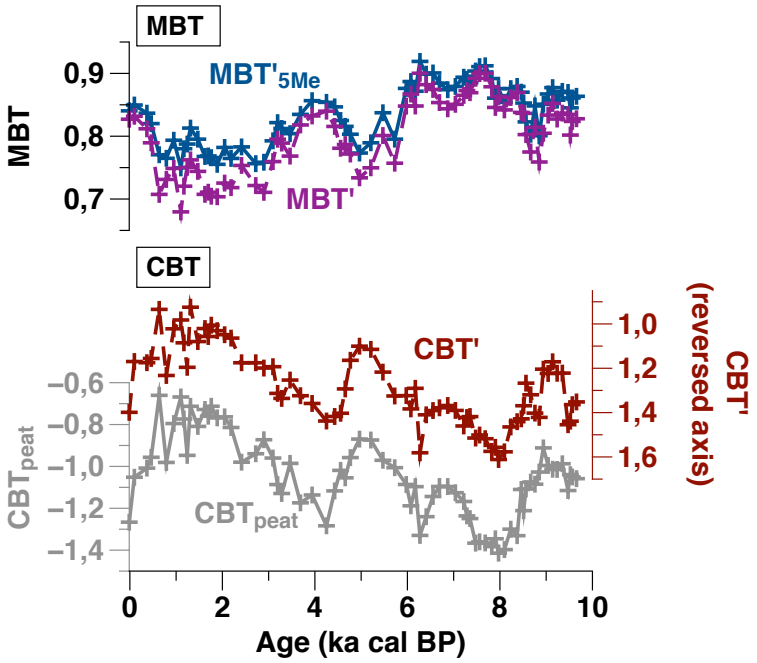

Figure S 6: Comparison of the MBT' and MBT'$_{5Me}$ ratios and of the CBT' and CBT$_{peat}$ ratios. The MBT' and MBT'$_{5Me}$ ratios present similar values and variations due to the small abundance of the 6-methyl brGDGTs. The small abundance of 6-methyl brGDGTs is consistent with the modern global peat dataset from Naafs et al. (2017b). The axis of the CBT' ratio is reversed to be able to compare the variations with the CBT$_{peat}$ ratios. Both CBT ratio present similar variations.

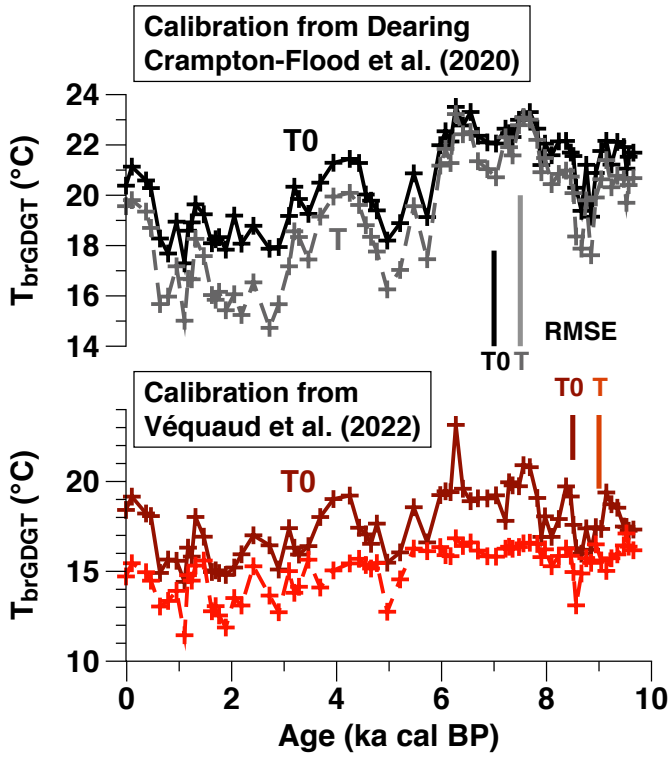

Figure S 7 : Comparison of T (whole dataset) and T0 (only sites with MAAT>0°C) calibrations for the peat & soil calibrations from Dearing Crampton-Flood et al. (2020) and Véquaud et al. (2022). As expected, temperature reconstructions show lower values for T calibrations than for T0 calibrations. The T temperature reconstruction from Véquaud et al. (2022) don't exceed 17.1 °C with an RMSE of 4.1°C, unrealistically too low for this site. We suggest care in the application of this calibration, especially for tropical sites.

Chapter 6: Short timescale events and seasonality change at NGaoundaba: from local environmental changes to global implications

Abstract:

Using a large panel of lipid biomarkers and pollen data, we present the environmental changes occurring in a tropical peat deposit (North East Cameroon) during two 1-ka dry events occurring around 8.2 and 4 ka cal BP. Each event has led to large and distinct changes in the local landscape affecting vegetation and microbial communities. A review of hydrological records of tropical Africa (δD_{wax} and lake level) indicates that these two events are widespread but unevenly recorded in the tropics suggesting important regional and local effects either amplifying or attenuating these changes. The records of these two events in tropical Africa generally indicate longer perturbations compared to higher latitudes. In addition, in several records such as the NGaoundaba peat record, changes pre-date the 8.2-ka event suggesting that this event occurs during a period of general climate degradation. These changes pre-date the drainage of North American lakes into the North Atlantic Ocean that is proposed as the main cause of the 8.2-ka event. These 1-ka events rise questions about the link between the changes observed in the tropics and those observed at high latitudes.

Key words: 1-ka event, long- and mid-chain alkanes, GDGTs, botryococcenes, evapotranspiration reconstruction

1. Introduction

The late Quaternary was punctuated by short climatic events on centennial to millennial timescales, such as the Younger Dryas (12.9-11.7 ka BP) (Alley, 2000; Rasmussen et al., 2006), the so-called 8.2 ka event (Johnsen et al., 1992; Dansgaard et al., 1993; Alley et al., 1997) or the Little Ice Age (approximately 0.4-0.1 ka BP) (Grove, 2012). Initially studied at high latitudes, most of these events have been reported worldwide, at all latitudes, including tropical Africa (Garcin et al., 2007; Russell and Johnson, 2007; Tierney et al., 2017). Changes in solar activity (Mauquoy et al., 2002; Rohling and Pälike, 2005), perturbations of oceanic circulation (Broecker et al., 1988; Barber et al., 1999), increased volcanic activity (Miller et al., 2012; Kobashi et al., 2017), etc. many causes are proposed to explain these events, which are likely to be multicausal (Rohling and Pälike, 2005; Renssen et al., 2015). These events are of particular interest as they have influenced many human civilizations (e.g., Sereno et al., 2008; Ran and Chen, 2019).

These climatic events have widespread effects on environments. The drying associated with the 8.2 ka event lead to immediate response from the vegetation in Europe (Tinner and Lotter, 2001). In tropical Africa, a sensitivity of forest environment has been suggested at lake Bambili (West Cameroon), as opening of the canopy started as early as 8.2 ka cal BP, long before the end of the African Humid Period (Lézine et al., 2013). This event also drove changes in aquatic environments affecting the productivity of lake ecosystems (Hede et al., 2010). Vegetation and environment are sensitive to changes in the amount of precipitation but also in the seasonality of precipitation (e.g., Magny et al., 2012; Dubois et al., 2014). Climate change affect both the magnitude, timing and duration of precipitation (Wang and Alo, 2012; Feng et al., 2013). Understanding changes in seasonality and its impact on environment is fundamental to prepare West and Central African countries to adapt and cope with the consequences of future climate change.

Paleoenvironmental changes can be reconstructed using a variety of lipid biomarkers derived from terrestrial or aquatic plants or microbial communities, providing insights into specific past climatic events. While long chain n-alkanes are mainly produced by terrestrial plants, a significant part of mid chain n-alkanes is derived from submerged and floating macrophytes (Ficken et al., 2000; Diefendorf and Freimuth, 2017). Carbon and hydrogen isotopic compositions of n-alkane are used to infer past changes in vegetation and precipitation, respectively (Sachse et al., 2012; Diefendorf and Freimuth, 2017). In addition, temperature reconstruction can be provided using branched glycerol diakyl glycerol tetraethers (brGDGTs) temperature calibrations (Naafs et al., 2017b; Peterse et al., 2012; e.g., Weijers et al., 2007b). Proxies that utilize brGDGTs are based on natural response of bacterial communities or

bacterial membranes to changes in environmental conditions (e.g., Huguet et al., 2013; Naafs et al., 2017b; Halamka et al., 2023).

A multiproxy analysis was conducted on a 10-ka records from the NGaoundaba peat deposit (North East Cameroon). Based on molecular analyses (relative abundance, concentration, carbon and hydrogen isotopic data), we reconstruct the past environmental changes occurring during two dry periods at the NGaoundaba peat deposit (8.9-7.9 ka cal BP and 4.5-3.5 ka cal BP). By comparing mid and long-chain n-alkane hydrogen isotopic compositions, we present a record of past changes in evapotranspiration at the NGaoundaba peat deposit during the Holocene and highlight changes in evapotranspiration (combined processes of evaporation of water in lake, soils, etc and of transpiration by plants) during the two dry events. The timing of the beginning of these events preceding those usually observed in high and intermediate latitude raises new questions concerning the origin of these two events and the interconnection between high and low latitudes climates.

2. State of the art: the 8.2 and 4.2 ka climatic events

2.1. Climatic changes around the 8.2 ka event

The 8.2 ka event is a cold event first reported in Greenland ice cores (Johnsen et al., 1992; Dansgaard et al., 1993; Alley et al., 1997). If this event is well documented in high and mid latitudes (Rohling and Pälike, 2005), its extent and cause(s) still remain debated. Its duration in high and mid latitudes is usually around 400 to 600 years with even shorter duration reported in some Greenland ice cores (Rohling and Pälike, 2005). A weakening of the thermohaline circulation (slowdown of the North Atlantic Deep Water (NADW)), due to the catastrophic drainage of glacial lakes of Agassiz and Ojibway (North Eastern Canada) at 8.5 ± 0.3 ka cal BP (Barber et al., 1999) bringing a massive meltwater flood to the North Atlantic, is the main hypothesis proposed to explain the 8.2 ka event (Barber et al., 1999; Clark et al., 2001; Renssen et al., 2001). This hypothesis is consistent with sharp climate changes recorded around 8.3 ka BP recorded in a speleothem from SW Ireland (McDermott et al., 2001). However, some records indicate climatic changes pre-dating this flood-related event (Rohling and Pälike, 2005) suggesting broader period of climate deterioration possibly associated with reduced solar activity (Bond et al., 2001; Rohling and Pälike, 2005).

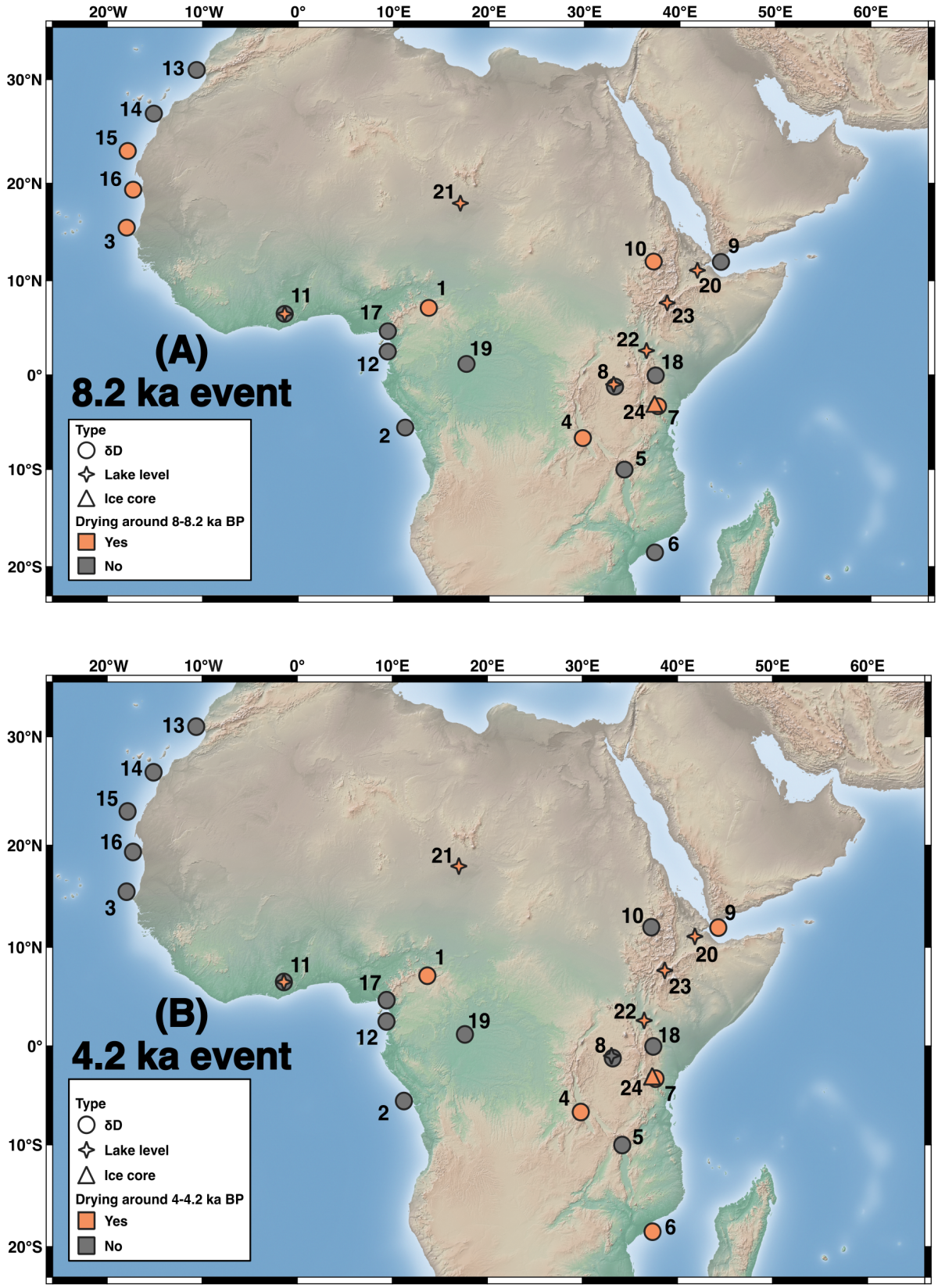

Figure 39: Hydrological changes in tropical Africa around the 8.2 ka and the 4.2 events recorded in δD_{wax} and lake level records. Sites in orange record a drying event around 8.2 ka or 4.2 ka while the sites in grey don't. For references, see table S 2 (supplementary material of this chapter)

In tropical and subtropical Africa, lake level drops are recorded between 8.5 and 7.8 ka BP (Gasse, 2000; Johnson et al., 2000; Forman et al., 2014; Shanahan et al., 2015 and references therein). δD_{wax} records from lake Tana (Ethiopia, East Africa) and from a marine core off the Senegal coast (15°N, Atlantic Ocean) show a δD_{wax} enrichment corresponding with the timing of the 8.2 ka event (Niedermeyer et al., 2010; Costa et al., 2014). In West Africa, no other δD_{wax} records suggest a decrease in precipitation around 8.2 ka cal BP. In East Africa, brief increases in n-alkane hydrogen isotopic composition are recorded in several lakes (e.g., Tierney et al., 2008; Costa et al., 2014). Intriguingly, while ^{14}C dating of exposed lacustrine sediment and sedimentological analysis of sediment core at lake Bosumtwi (Ghana) clearly indicates drops in lake level coinciding with the 8.2 event (Talbot and Delibrias, 1977; Talbot et al., 1984; Shanahan et al., 2006), the δD_{wax} record doesn't indicate decreased precipitation during these periods (Shanahan et al., 2015). As the water balance of lake Bosumtwi is mainly controlled by rainfall amount and evaporation (Turner et al., 1996), this may suggest that decrease in lake level was govern by increase in evaporation rather than decrease in precipitation. In the Kilimanjaro ice-core, increased aerosol concentrations around 8.3 ka BP suggest dry climatic conditions (Thompson et al., 2002). Tierney et al. (2017) proposed a pause in Green Sahara conditions around 8ka based on δD_{wax} between 19°N and 23°N and on archeological evidence from the Gobero site in Niger (Sereno et al., 2008).

2.2. Climatic changes around 4.2 ka

The 4.2 ka event has been reported as a dry and/or cool interval in many regions worldwide (e.g., Thompson et al., 2002; Booth et al., 2005; Drysdale et al., 2006; Berkelhammer et al., 2012). This event has strongly affected several major ancient civilizations (Ran and Chen, 2019). Several causes are proposed for this event such as a change in sea surface temperature regime linked to ENSO events (Moy et al., 2002), increase volcanic activity (e.g., Haflidason et al., 2000; Johnson et al., 2002) and/or dust emission (Thompson et al., 2002) likely associated with numerous feedback from albedo or vegetation changes (Marchant and Hooghiemstra, 2004). Concerning the influence of ENSO events, increase of El Nino events (Marchant and Hooghiemstra, 2004) or La Nina events (Booth et al., 2005) were both proposed to explain the observed climatic changes. Although suggested as another potential cause, a decrease in solar activity around 4 ka BP is not observed (Marchant and Hooghiemstra, 2004).

Lake level records around the 4.2 ka BP event are more ambiguous. As this period happens after the end of the AHP, several lake levels decrease around 4.2 ka but don't increase afterwards or present large uncertainty in the lake level fluctuations (Gasse, 2000; Johnson et al., 2000; Forman et al., 2014; Shanahan et al., 2015 and references therein). Except for the

NGaoundaba peat record (chapter 5), the 4.2 ka BP event is not recorded in the hydrogen isotopic composition of n-alkanes from other West and Central African sites. In East Africa, δD_{wax} record from lake Challa show less depleted values between 4.3 and 3.7 ka cal BP (Tierney et al., 2011) and brief peaks are recorded in δD_{wax} records from lake Tanganiika and from the Gulf of Aden (Tierney et al., 2010; Tierney and deMenocal, 2013). Thompson et al. (2002) highlight an increase in dust emission around 4 ka BP in the Kilimanjaro ice-core.

3. Material and methods

3.1. Sampling and ^{14}C dating

The NGaoundaba peat deposit is situated in a volcanic crater on the Adamawa Plateau in Northeast Cameroon (N7.135° E13.690°, 1175 m above sea level). The NGaoundaba peat deposit lies in the Soudano-Guinean shrubs savannas zone (Letouzey, 1958) and the in-situ growing vegetation is dominated by sedges (*Cyperus* spp). The current climate is characterized by two distinct seasons: a 5-month dry season from November to March and a 7-month rainy season from April to October. According to the CRU database, the mean annual air temperature (MAAT) is 22.2 °C and the mean annual precipitation (MAP) is 1482 mm (Harris et al., 2014).

Analyses are based on a 6-meter-long core (named NGBA19) collected in February 2019 using a Russian peat corer. The core is composed of dark brown peat without visible sandy or clayey zones. The core was then sub-sampled at 2.5-cm intervals. The age model of the NGaoundaba peatcore is based on 30 radiocarbon dates carried out at the LMC14 Laboratory (Saclay, France). Details on the dating and calibration of the age model are given in Schaaff et al. (2023).

3.2. Organic geochemical analyses

3.2.1. Sample preparation

Organic geochemical analyses were performed on 73 samples. All samples were freeze-dried, ground and homogenized. Extraction was performed two times for 0.3g of each sample with 10mL of dichloromethane (DCM)/methanol (3:1, v/v) using a MARS 6 CEM microwave extraction system. Following each extraction, the supernatant was filtered through a sintered Teflon filter. Synthetic C_{46} GDGT was added to the combined extracts of each sample as an internal standard (Huguet et al., 2006). The total lipid extract was separated by column chromatography on silica gel into three fractions. The hydrocarbon fraction containing hopanes was eluted first with 8mL of hexane. A second fraction was eluted with 5mL of

hexane/DCM (1:1, v/v). BrGDGTs were eluted in a third fraction with 10mL of DCM/methanol (1:1, v/v).

3.2.2. Analyses of the hydrocarbon fraction

Copper curls activated with HCl were added to the hydrocarbon fractions to remove elemental sulfur. After a first GC-FID analysis (HP 6890A), GC-MS analyses (Agilent 6890N GC coupled to an Agilent 5975C MSD and Agilent 7890B GC coupled to an Agilent 5977B MSD) were performed for identification and quantification of the different compounds. Both GC-MS instruments provided comparable data. Integration of n-alkane peaks were performed using the m/z 71 ion chromatogram to limit the influence of coelution and compared with an external standard solution containing pentacosane for quantification. n-alkane abundances were calculated using all alkanes from n-C_{19} to n-C_{37}. Botryococcenes are in the hydrocarbon fractions. They were partially identified based on their mass spectral characteristics (fragmentation and Kovats retention index) and on previous literature data (see chapter 8 for more detail about botryococcenes).

Prior to carbon and hydrogen isotopic measurements, the hydrocarbon fractions were separated into a saturated and an unsaturated fraction by column chromatography using silica gel impregnated with $AgNO_3$ (10 % wt). Saturated fractions containing n-alkanes were eluted with 3 to 4 mL of n-heptane. Unsaturated fractions were eluted with 3 to 4 mL of ethyl acetate. Carbon isotopic compositions were measured at the LGL-TPE (Université Claude Bernard Lyon 1) using an Agilent 7890B GC coupled to an Isoprime visION Isotope Ratio Mass Spectrometer via an Isoprime GC-5 combustion interface (Elementar). The GC-5 furnace was operated at 850 °C. An autotune and tests of stability and linearity of the signal were performed daily using the software ionOS. Stable carbon isotopic compositions (expressed as $\delta^{13}C$ values) were calibrated using a reference CO_2 gas reported to VPDB scale. Two Mix hydrocarbon B4 standards (A Schimmelmann, Indiana University) were measured every 4 to 5 samples and used to correct the $\delta^{13}C$ values. Samples were analyzed in duplicates. For δD measurements, the GC-5 pyrolysis furnace was operated at 1450°C. Daily autotune, H_3+ correction and test of stability were performed using the software ionOS. δD values were calibrated using reference H_2 gas reported to VSMOW scale. Each week, the pyrolysis furnace was conditioned five times with 1µL hexane prior to any analysis and a series of 8 Mix B4 measurements was performed and used for data correction. In addition, one Mix B4 measurements was analyzed every 4 to 5 injections to assure the limited impact of drift. Samples were analyzed in duplicates.

3.2.3. N-alkane ratios

The carbon preference index (CPI), which describe the relative abundance of C-odd vs C-even *n*-alkanes, was calculated for C_{25} to C_{35} homologues using the revised equation from Marzi et al. (1993):

$$CPI = \frac{(C_{25} + C_{27} + C_{29} + C_{31} + C_{33}) + (C_{27} + C_{29} + C_{31} + C_{33} + C_{35})}{2 * (C_{26} + C_{28} + C_{30} + C_{32} + C_{34})}$$

The average chain length (ACL) describes the dominant chain-length of a fixed range of odd numbered *n*-alkanes. The considered range of n-alkanes is usually C_{27} to C_{31} (Poynter and Eglinton, 1990) but shorter (e.g. C_{23}, C_{25}) and longer chain (e.g. C_{33}) *n*-alkanes can also be included (Poynter et al., 1989). As C_{33} n-alkane is an important component of long chain n-alkane assemblage, we chose the following equation for ACL calculation:

$$ACL_{27-33} = \frac{(27 * C_{27} + 29 * C_{29} + 31 * C_{31} + 33 * C_{33})}{(C_{27} + C_{29} + C_{31} + C_{33})}$$

The P_{aq} ratio was calculated using the equation from Ficken et al. (2000) based on lacustrine vegetation.

$$P_{aq} = \frac{(C_{23} + C_{25})}{(C_{23} + C_{25} + C_{29} + C_{31})}$$

Originally developed as a proxy for the contribution of submerged versus emerged macrophytes, the P_{aq} ratio has been reinterpreted in Sphagnum peat as a proxy for the contribution of Sphagnum species compared to other peat-forming plants (Nichols et al., 2006). Given the absence of Sphagnum species in the NGaoundaba peat, this reinterpretation of the P_{aq} ratio is not valid for this peat deposit**.**

3.3. Pollen analyses

Pollen analyses were performed by C. Kiahtipes (University of South Florida) who write the following paragraph presenting the method for pollen analyses. For this thesis work, only part pollen record will be used to compare with lipid biomarker data, but no extensive analyses of the pollen result will be provided.

Subsamples were shipped to the IASCE paleoecology laboratory at the University of South Florida. Samples were weighed and their volume was estimated using displacement. Two tablets of Lycopodium sp. spores were added to each sample (Batch #100320201) and

dissolved with 10% Hydrochloric acid (HCl). Samples were centrifugated-decanted-rinsed until pH neutral, then fine materials were isolated using gravity separation and screening through 250µm sieves. Because these samples were organic with little mineral content, we omitted treatment with Hydrofluoric acid. The organic fraction was digested through a 10-minute hot bath in a 10% Potassium Hydroxide solution at 80°C. Samples were then centrifuged, the solution was decanted, and a small (~0.5 ml) volume of concentrated (27%) HCl was added to the samples. Samples were centrifugated-decanted-rinsed until pH neutral and the supernatant comes clean. Samples were rinsed into 99% Glacial Acetic Acid, centrifugated-decanted, and then were treated using the Acetolysis reaction series. Acetolysis is triggered by the addition of a 9:1 solution of Acetic Anhydride and Sulfuric Acid, each at stock concentrations (99.5% and 48% respectively). Samples were left in a 90°C hot bath for 6 minutes, centrifugated-decanted, rinsed in Glacial Acetic Acid, and then centrifugated-decanted-rinsed until pH neutral. Microbotanical fossils were recovered from the remaining residue using density separation in a solution of 5% HCl and Zinc Bromide at a specific gravity of 2.3 g/ml. At this density, we were able to retrieve both pollen and phytoliths from the samples. This material was retrieved from the density separation in ethanol and then transferred into glycerine and stored in glass vials. Sample residues prepared in the laboratory were mounted on microscope slides and analyzed using a binocular microscope at 400x and 1000x magnification. Each slide was surveyed in linear transects and all fossil pollen and Lycopodium sp. spores encountered were counted.

4. Data processing: Reconstructing past changes in evapotranspiration using mid-chain and long-chain n-alkane isotopic data

4.1. Precipitation vs evapotranspiration balance at the NGaoundaba peat deposit

We tried to estimate the precipitation/evaporation balance by comparing mid- and long-chain n-alkanes hydrogen isotopic signals. Long-chain n-alkanes (C_{27} to C_{35}) mainly derived from terrestrial plants while mid-chain n-alkanes (C_{23} and C_{25}) have substantial input from aquatic and submerged plants in addition to terrestrial plants (Figure 40) (e.g., Barnes and Barnes, 1978; Cranwell, 1984; Ficken et al., 2000). At the NGaoundaba peat deposit, since the end of the African Humid Period, the pollen record indicates a progressive increase of Cyperaceae pollen suggesting a progressive colonization of the peat surface by Cyperaceae (see chapter 5, figure 33). Cyperaceae present a dominance of long-chain n-alkanes and were classified as emergent/sub-aerial plants (Ficken et al., 2000). The term “aquatic plants” will be used to refer to submerged and floating plants such as Nymphaea sp. or Potamogeton sp. that are dominated by mid-chain n-alkanes (Ficken et al., 2000) and will not include Cyperaceae.

The water balance of the NGaoundaba peatbog, an ombrotrophic peat, is controlled mainly by the balance between precipitation and evapotranspiration. Strong evaporative signal can be recorded in tropical lakes (Delalande et al., 2008; Abba et al., 2023) and the hydrogen isotopic signature of the NGaoundaba peat water might be affected by a strong evaporative enrichment. In humid temperate regions where evapotranspiration is limited, aquatic n-alkanes are usually not affected by evapotranspiration while terrestrial n-alkanes can present enriched values due to evapotranspiration (Sachse et al., 2004). In tropical monsoonal regions, we hypothesized that the evapotranspiration signal is likely to be more limited in plants growing on the catchment compared to plants growing directly on the peat as leaf production of terrestrial plants is emphasized during the early rainy season (van Schaik et al., 1993) when precipitation largely exceed evapotranspiration while aquatic plants will have sufficient water resource during the whole year. Therefore, the seasonality of the production of n-alkanes might be different between the plant growing on the peat and those growing on the catchment.

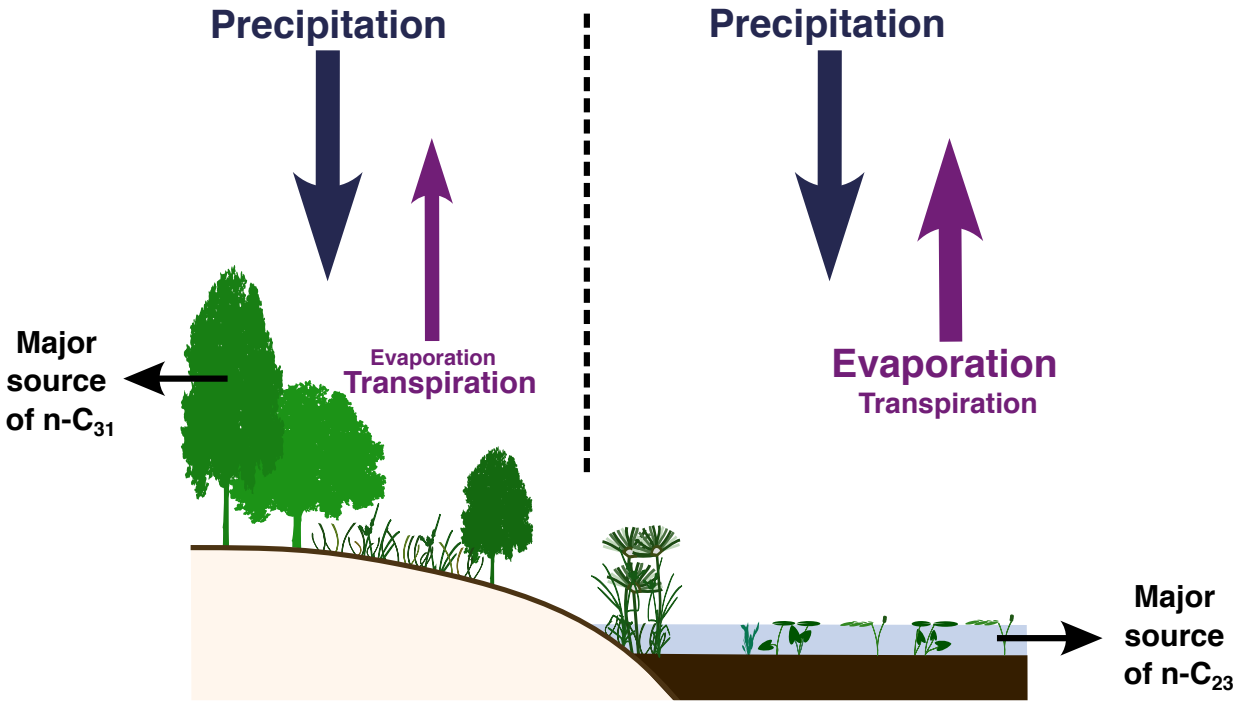

Figure 40: Starting hypothesis of the evapotranspiration balance between aquatic and terrestrial environments at the NGaoundaba peat deposit. Terrestrial plants and emerged macrophytes such as Cyperaceae mostly produce long-chain n-alkanes while submerged and floating plants mostly produce mid-chain n-alkanes. The differences in evapotranspiration between terrestrial and aquatic environment are both spatial and temporal with a difference in the seasonality of leaf wax production between terrestrial and aquatic plants.

The hydrogen isotopic signal of n-alkanes is influenced by the isotopic signature of the water used for leaf wax synthesis, reflecting the isotopic signature of the precipitation water more or less affected by evapotranspiration, and by the fractionation coefficient of the plant. The

difference between the fractionation coefficient of aquatic and terrestrial plants will affect the hydrogen isotopic signature of n-C_{23} alkane while the n-C_{31} alkane will only be affected by the C_3/C_4 plants balance. Prior comparing the hydrogen isotopic signature of n-C_{23} and n-C_{31} alkanes, each δD records was corrected for potential vegetation change. For n-C_{31}, we applied the same procedure as described in chapter 5 section 2.4. For n-C_{23}, the detailed procedure is described in the following subsections.

4.2. Estimating the input of aquatic n-alkanes to n-$C_{23\ alkane}$ using a multisource mixing model

By compiling n-alkane distributions of modern terrestrial and aquatic plants, Gao et al. (2011) performed a cluster analysis to group plants with similar chain-length distributions of n-alkanes. Among the five plant groups revealed by the cluster analysis, group 5 only contains aquatic plants (floating, submerged or emergent) allowing to calculate the input of aquatic plants to the sedimentary n-alkanes using a multi-source mixing model. For each sample, the program developed by Gao et al. (2011) calculates the fraction estimates of each plant group using a "least-square" method (Figure 41 A and B). Then, the input of aquatic plants (group 5) to n-C_{23} alkanes f_{aq} can be calculated using the average n-alkane distribution pattern of each group (Figure 41 C).

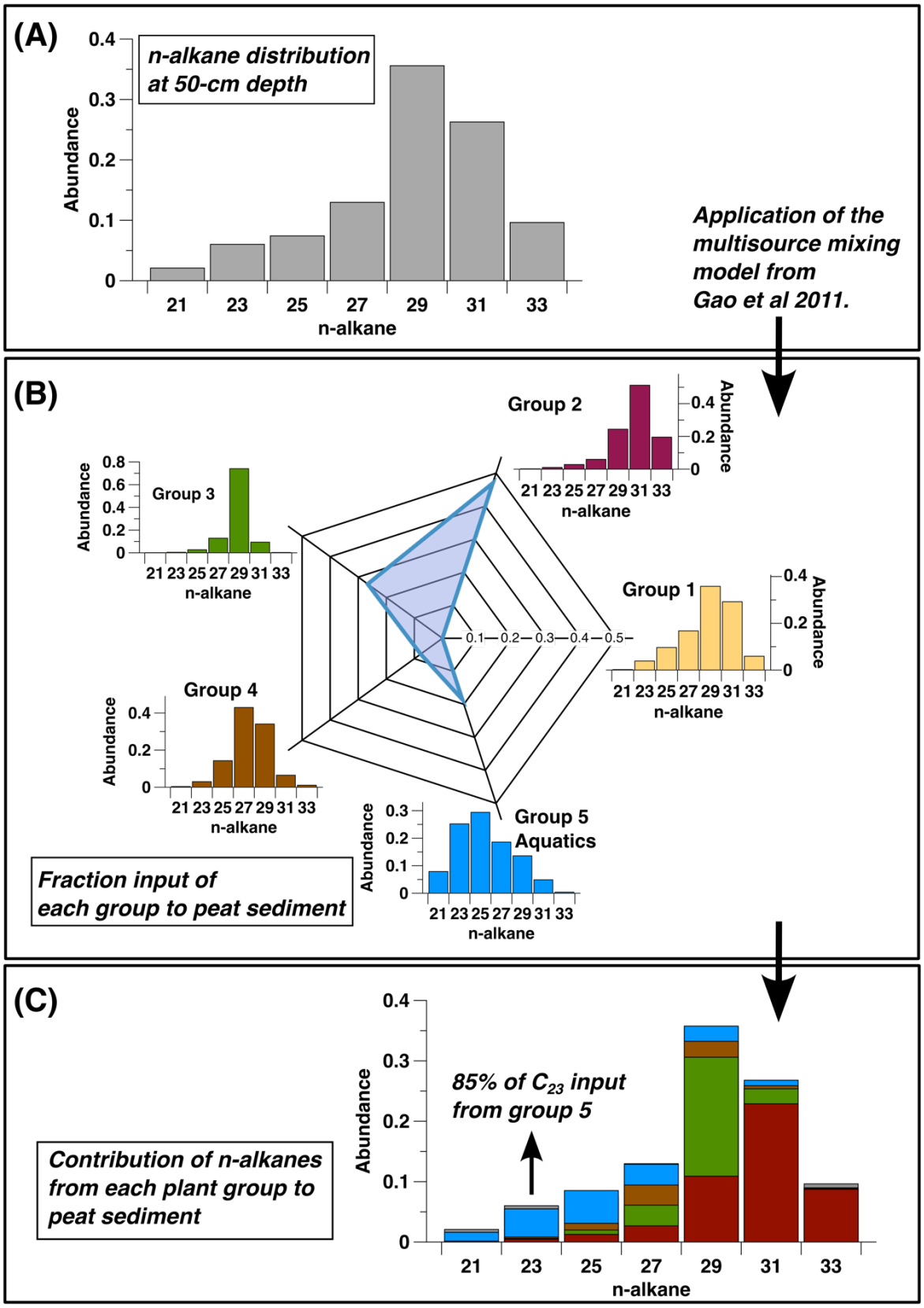

Figure 41: Application of the multi-source mixing model developed by Gao et al. (2011) to estimate the input of aquatic plants to n-C_{23} alkanes f_{aq}. The figure is based on the sample at 50 cm-depth from the NGaoundaba peat deposit (A). We applied the multisource mixing model to determine the fraction input of the different plant groups (B). The n-alkane distributions of each plant group are based on the data from Gao et al. (2011). Finally, we estimate the n-C_{23} input from aquatic plants (group 5) in the sample (C).

4.3. Fractionation coefficient of aquatic and terrestrial plants

A few studies reported the hydrogen isotopic fractionation coefficient between water and n-alkanes for aquatic plants (ε_{aq}): -158 ‰ for samples of the genus Zostera (Sessions et al., 1999), -135±17 ‰ for freshwater plants, -155±34 ‰ for seaweeds (Chikaraishi and Naraoka, 2003), and an average of -162 ‰ for diverse algae and submerged plants (Liu and Liu, 2019). Similar fractionation coefficients are reported for submerged plants and algae (Liu and Liu, 2019). We chose a mean fractionation coefficient ε_{aq} of -155‰ for aquatic plants.

We use the ε_{corr} calculated for n-C_{31} (see chapter 5, section 2.4) as the fractionation coefficient for terrestrial plants. Thus, the fractionation coefficient of terrestrial plants is variable along the core. A correction using a fixed fractionation coefficient for terrestrial plants was also tested (see supplementary material of this chapter - Figure S 9 and Figure S 10) and did not significantly change the results.

Therefore, the corrected apparent coefficient fractionation $\varepsilon_{corrC23}$ applied to n-C_{23} hydrogen isotopic values can be written as follows:

$$\varepsilon_{corrC23} = f_{aq}\varepsilon_{aq} + (1 - f_{aq})\varepsilon_{corr}$$

Last, the following equation was used to correct the $\delta D_{n\text{-}C23}$ values:

$$\delta D_{n-C23-corr} = \left[\frac{\delta D_{n-C23} + 1000}{\left(\frac{\varepsilon_{corrC23}}{1000}\right) + 1}\right] - 1000$$

Once corrected for vegetation influence, we calculated the difference between the δD records of n-C_{23} and n-C_{31} alkanes, noted $\Delta\delta D_{23\text{-}31}$ as follows:

$$\Delta\delta D_{23-31} = \delta D_{n-C23-corr} - \delta D_{n-C31-corr}$$

5. Results

5.1. n-alkanes relative abundance, distribution and concentration

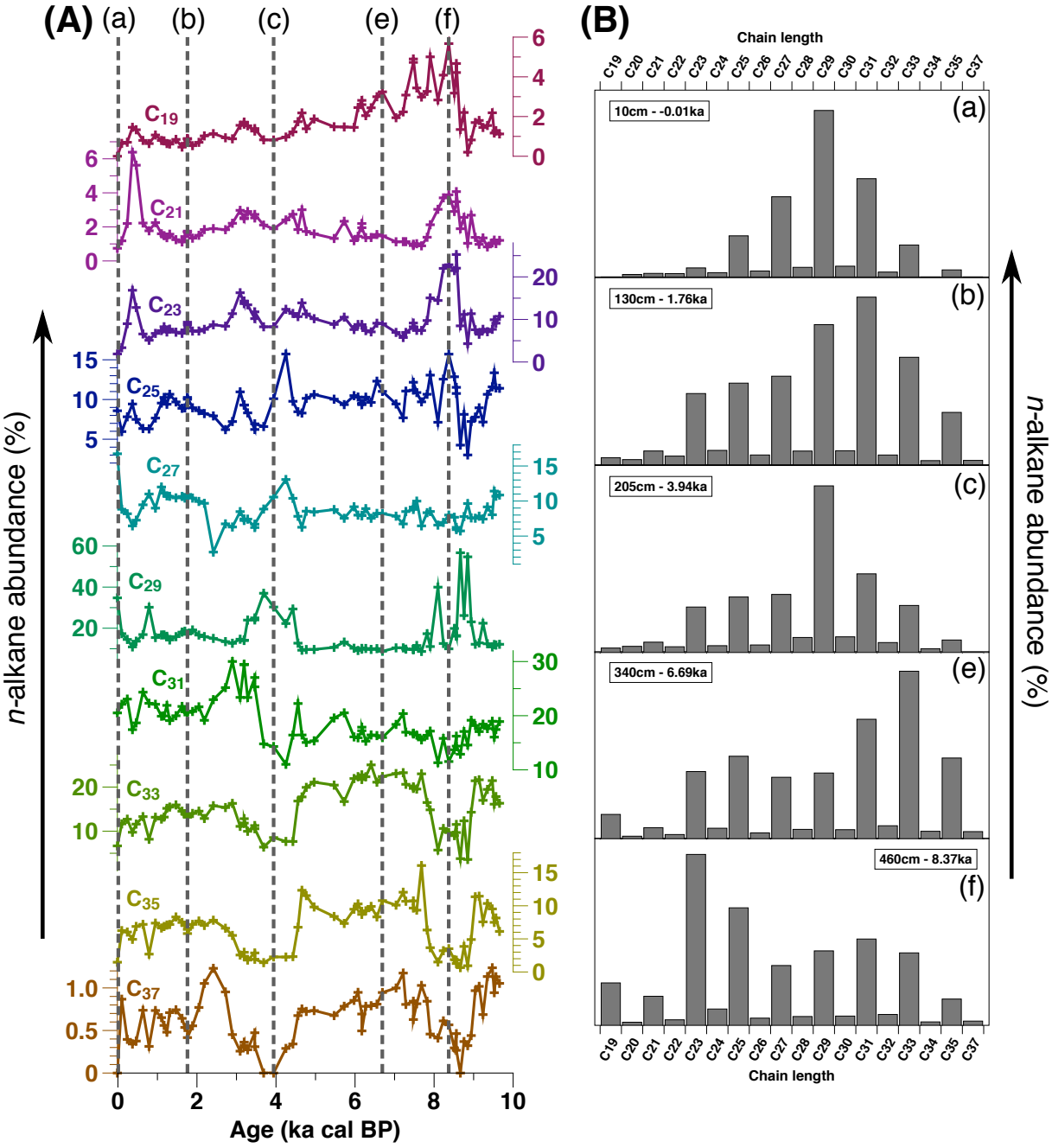

Figure 42: Variation of n-alkane abundances with depth (A) and distribution pattern at five contrasted depth/age (B, a to f). n-alkane C_{36} was not detected and is therefore not included in the figure. The five contrasted ages (a to f) are indicated on panel A by a vertical dotted line.

The topmost sample is marked by a unimodal distribution pattern with a predominance of n-C_{29} alkanes (Figure 42 B.a). The upper part of the core, corresponding to ages between 3.2 ka cal BP and present, presents a similar distribution pattern but is dominated by n-C_{31} alkane with high contributions of n-C_{23} and n-C_{25} alkane (Figure 42 A.b).

Among long-chain n-alkanes, n-C_{33}, n-C_{35}, and n-C_{37} present similar trends with high abundance until 4.5 ka cal BP, except between 8.9 and 8.0 ka cal BP (Figure 42 A). This similarity between n-C_{33}, n-C_{35} and n-C_{37} homologues is also visible in the PCA analyses of the

odd-numbered n-alkanes (Figure 43 B). Between 9.7 and 8.9 ka cal BP and between 7.9 and 5.8 ka cal BP, the typical n-alkanes distribution pattern is characterized by a high abundance of n-C_{31}, n-C_{33}, and n-C_{35} alkanes, with a non-negligible amount of mid-chain n-C_{23} and n-C_{25} alkanes still representing around 10% of the assemblage each (Figure 42 B.e). A particular period can be noted from 8.6 to 8.2 ka cal BP with a bimodal distribution pattern associated with the predominance of mid-chain alkanes (n-C_{23} and n-C_{25}) (Figure 42 B.f). The n-C_{29} alkane presents the highest amplitude of variations among n-alkanes, representing 8.7 to 56.7% of the assemblage. The n-alkane distributions between 8.9 and 8.6 ka cal BP as well as between 4.5 and 3.2 ka cal BP are strongly dominated by n-C_{29} alkane (Figure 42 B.c).

Total n-alkanes concentration ranges from 50.1 to 391.5 µg/g_{TOC} with a mean value of 133.0 µg/g_{TOC}. Trends are similar to those observed for n-alkane relative abundances (Figure 43).

5.2. Ratios based on n-alkanes

CPI values range from 4.1 to 45 with an average value of 10.9 (Figure 43 C.b), in the range of the CPI values of fresh plant material (4-40 in plants with different photosynthetic metabolism types (C3, C4, CAM) (Collister et al., 1994), and 1.6 to 50 for equatorial east African plants (Griepentrog et al., 2019)). There is no clear correlation with depth. The topmost sample presents a higher CPI, likely resulting from less degraded plant material (Lehtonen and Ketola, 1993; Killops and Killops, 2013). Two periods of increase in CPI values can be noted, from 2.8 to 3.5 ka cal BP, and a second period centered at 8.7 ka cal BP. The CPI increase around 8.7 ka cal BP may be an integration bias associated with the very high concentration of n-C_{29} in these two samples, leading to difficulties in integrating small peaks in GC analyses, i.e., peaks of even-numbered n-alkanes.

The $ACL_{27\text{-}33}$ ranges from 29.1 to 31.1 with a mean value of 30.4 (Figure 43 C.c). Two periods of lower ACL values can be noted around 8.7 ka cal BP and from 4.5 to 3.5 ka cal BP. In addition, the topmost sample also presents a lower ACL value.

For the NGaoundaba peat deposit, P_{aq} ranges from 0.1 to 0.6 with an average value of 0.4 (Figure 43 C.d). A sharp decrease in P_{aq} driven by an extremely abundant n-C_{29} in two samples, followed by a sharp increase in $P_{aq,}$, can still be noted between 8.9 and 8.2 ka cal BP (Figure 43 C.d). This period presents a change in the distribution of long- and mid-chain n-alkanes with higher abundances of mid chain n-alkanes (C_{23} and C_{25}) and of n-alkane C_{29} compared to previous and following periods (Figure 42).

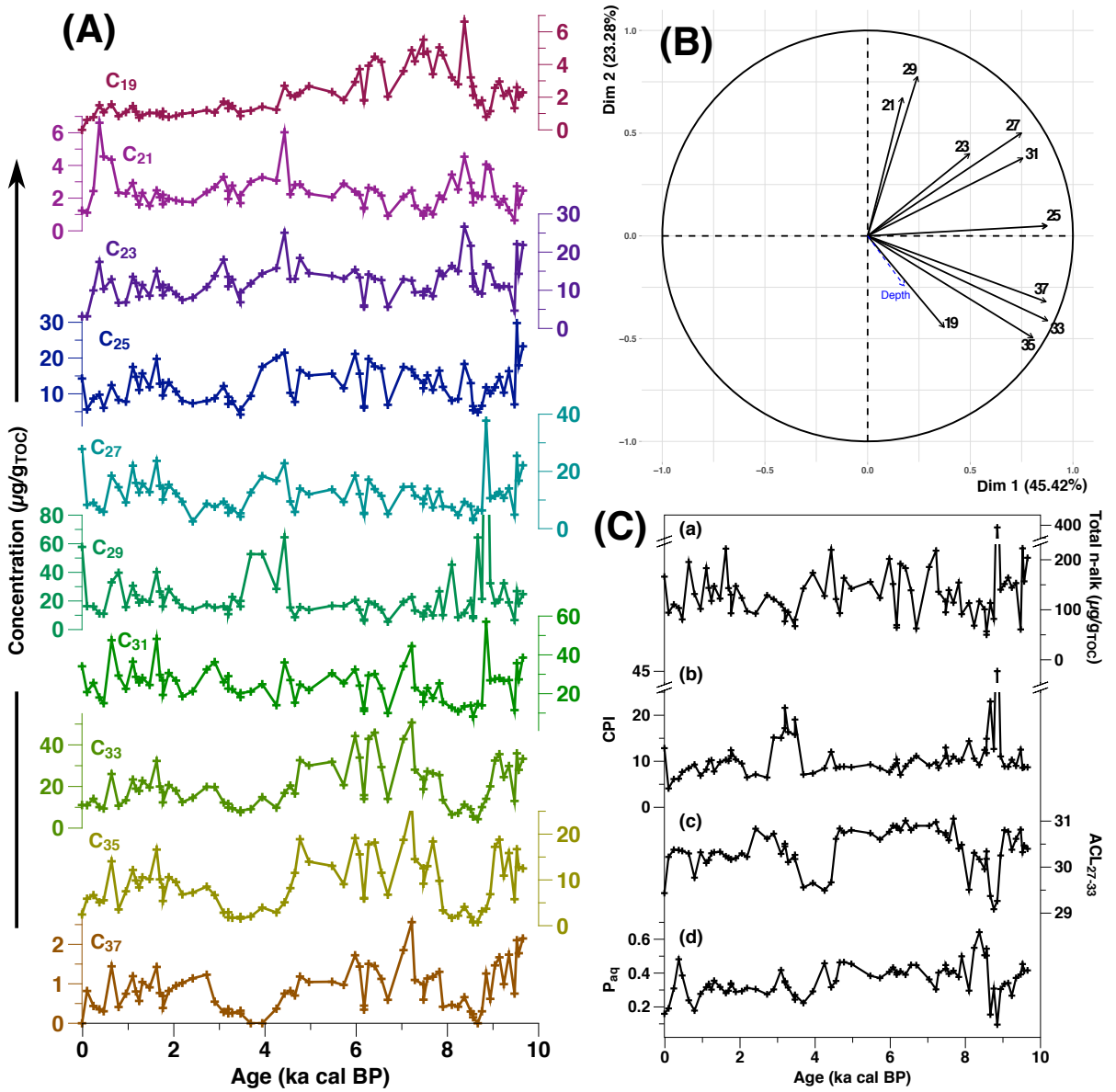

Figure 43: (A) Concentration of odd-numbered n-alkanes, (B) PCA of odd-numbered n-alkanes concentration and (C) total concentration of n-alkanes as well as n-alkane-based ratios. The n-C_{29} concentration of one value has been cut out of concentration graph for readability reason, this value worth 214 µg/gTOC.

The aquatic input values reconstructed based on the multi-source mixing model from Gao et al. (2011) follow the same trend as the P_{aq} ratio with a similar average value of 0.39 but a larger range of variation from 0.05 to 0.75 (Figure 44). As P_{aq} and the input of aquatic plants are both based on n-alkane distributions, a correlation between the two ratios was expected (Figure 44). The input of aquatic plants to n-C_{23} alkane ranges from 0.53 to 0.99 with a mean value of 0.93 (Figure 44). Except the two most recent samples and a sample at 8.8 ka cal BP, all values are above 0.84.

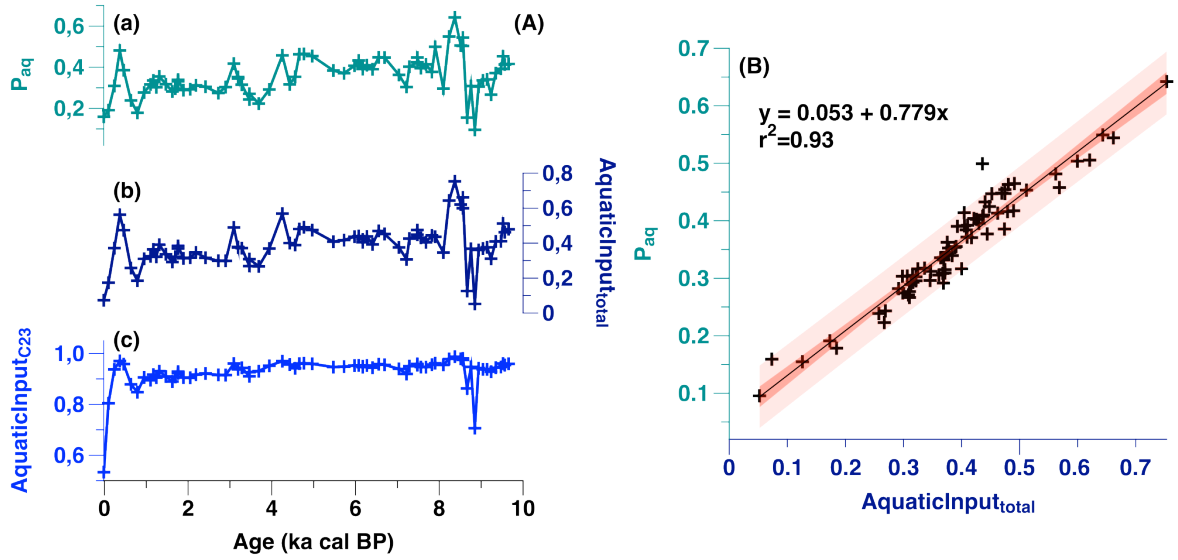

Figure 44: Estimating aquatic input in the NGaoundaba peat deposit. P_{aq} ratio (A.a), total aquatic input (A.b) and aquatic input for the n-C_{23} alkane (A.c) based on the procedure from Gao et al. (2011) and correlation between the P_{aq} ratio and the total aquatic input (B).

5.3. n-alkane carbon and hydrogen isotopic compositions and $\Delta\delta D_{23\text{-}31}$ record

The carbon and hydrogen isotopic values of n-C_{31} alkane are presented in Chapter 5. $\delta^{13}C_{n\text{-}C23}$ values range from -28.57 to -18.16‰ with a mean value of -24.1 ‰ (Figure 45 E). Showing values around the mean value during the early Holocene, $\delta^{13}C_{n\text{-}C23}$ values start increasing around 8.9 ka cal BP, reaching values around -18 to -20 ‰ until 8 ka cal BP. $\delta^{13}C_{n\text{-}C23}$ values then decrease rapidly, reaching -28 ‰ at 7.6 ka cal BP. Low values are then recorded until 5.8 ka cal BP and from 2.1 to 0.5 ka cal BP.

$\delta D_{n\text{-}C23}$ values corrected for aquatic and terrestrial vegetation change increased roughly during the Holocene, from its minimum of -57.7‰ at 9.7 ka cal BP to its maximum of 29.8 ‰ at 0.9 ka cal BP (Figure 45 F). A short-term $\delta D_{n\text{-}C23}$ depletion is recorded, centered at 8.2 ka cal BP, and particularly enriched values are recorded around 3.7 ka cal BP.

Values of $\Delta\delta D_{23\text{-}31}$ range from -23‰ to 63.4‰ with an average value of 26.4‰. Values are minimal between 8.8 and 8 ka cal BP, with most values below 10‰. High values are recorded between 7.9 and 5.8 ka cal BP and around 2.8 ka cal BP.

A discussion of the choice of the n-alkane used for establishing the $\Delta\delta D$ record is presented in supplementary material from this chapter.

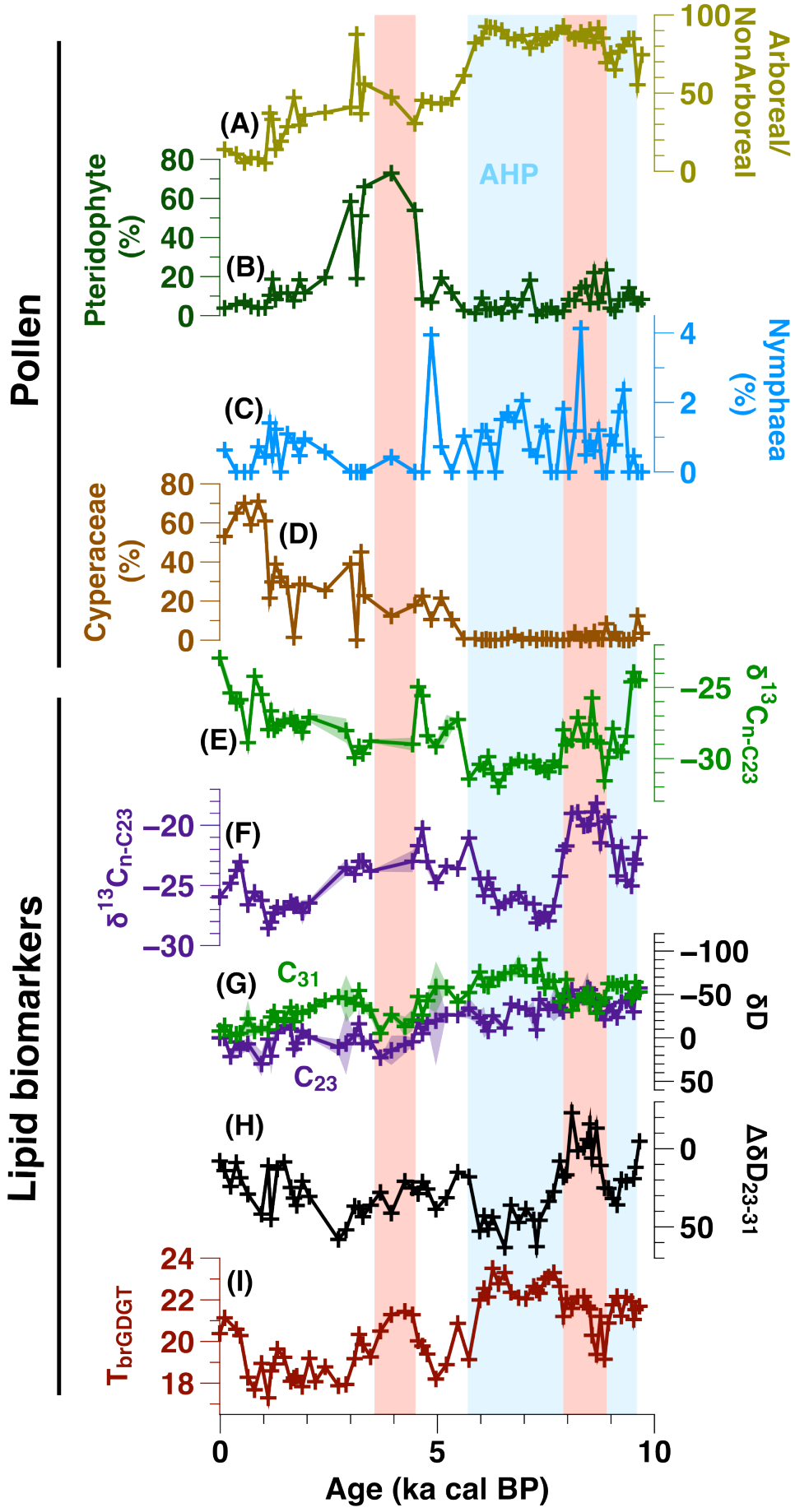
Pollen
Lipid biomarkers
(A)
(B)
(C)
(D)
(E)
(F)
(G)
(H)
(I)
AHP
Arboreal/
NonArboreal
100
50
0
Pteridophyte
(%)
80
60
40
20
0
Nymphaea
(%)
4
2
0
Cyperaceae
(%)
80
60
40
20
0
δ13Cn-C23
−25
−30
δ13Cn-C23
−20
−25
−30
C31
C23
δD
−100
−50
0
50
ΔδD23-31
0
50
TbrGDGT
24
22
20
18
0
5
10
Age (ka cal BP)

Figure 45: Lipid biomarkers data (E to I) and pollen data of the NGaoundaba peat deposit (A to D). (A) Percentage of arboreal pollen relative to non-arboreal pollen, (B) percentage of Pteridophytes spores (ferns) calculated as a percent of fern spores + pollens, (C) percentage of Nymphaea sp. pollen calculated as a percent of grasses/tree/shrubs (excluding wetlands plants such as Cyperaceae, Typha, etc.) and (D) percentage of Cyperaceae calculated as a percent of all pollen. (E) and (F) carbon isotopic composition of n-C_{31} and n-C_{23} alkanes, respectively, (G) hydrogen isotopic composition of n-C_{31} and n-C_{23} alkanes corrected for vegetation changes, (H) $\Delta\delta D_{23\text{-}31}$ and (I) temperature based on brGDGTs (°C)

5.4. Botryococcenes

Botryococcenes are unsaturated isoprenoid hydrocarbons produced by the colonial microalga *Botryococcus braunii* (Metzger et al., 1985b, 1988). Different structures of botryococcenes are observed in some parts of the studied peat core. Botryococcenes *b* are present until 5.4 ka cal BP with very variable concentrations during the early Holocene (Figure 46). Very low concentration of botryococcenes *b* is detected between 9.4 and 7.9 ka cal BP. On the contrary, the concentration of botryococcenes *a* increases between 8.7 and 8.0 ka cal BP reaching maximum value at 8.2 ka cal BP (Figure 46). Low concentration of botryococcenes *a* is observed during middle and late Holocene except a slight increase observed between 4.3 and 3.5 ka cal BP.

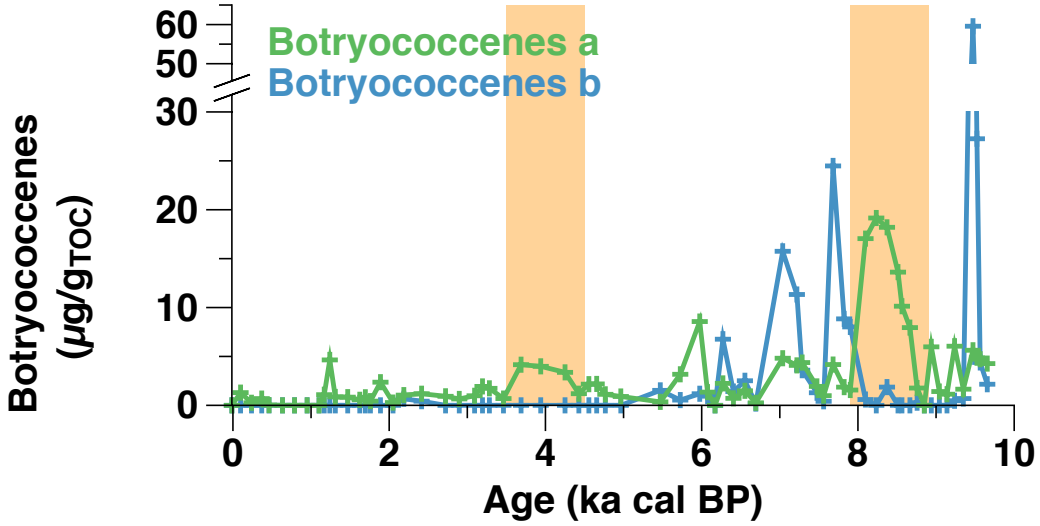

Figure 46: Variation in the concentration of two botryococcenes at the Ngaoundaba peat deposit. The two short dry events are highlighted in orange.

5.5. Preliminary pollen data

The percentage of arboreal pollen vs non-arboreal pollen present two distinct periods (Figure 45 A). From the bottom of the core to 5.8 ka cal BP, arboreal pollens represent more than 50 % of the pollen assemblage. The values then drop to values around 30% during middle Holocene and the last 1 ka is characterized by values below 15%. The Pteridophyte spores are low during

most of the Holocene except between 4.5 and 3 ka cal BP where they became more abundant than pollen (Figure 45 B). *Nymphaea* sp. pollen are reported in most samples but in low abundance during all the Holocene except between 4.7 and 3 ka cal BP and during the last ka when they are not reported at all (Figure 45 C). Cyperaceae pollen start to increase after 5.5 ka cal BP. The last 1 ka is characterized by more than 50% of Cyperaceae pollen in the pollen assemblage (Figure 45 D).

6. Discussion

6.1. Estimation of the evapotranspiration changes: methods validity and limits

As demonstrated in chapter 5, sedge-based peat deposits are likely to be impacted by the strong input of sedges and grasses growing in-situ. Based on the pollen data, the input of sedges and grasses growing in-situ seems limited until around 5 ka cal BP while aquatic plants (such as Nymphaea sp.) seem to be present in most samples especially until the end of the AHP around 5.6 ka cal BP. Despite these important changes in vegetation input, little changes were observed in the macroscopic aspect of the sediment during coring. The seasonality reconstruction is only applicable when the input of long chain n-alkanes from the vegetation growing in-situ is limited. When this condition is not satisfied, $\delta D_{n\text{-}C31}$ and $\delta D_{n\text{-}C23}$ values should converge to similar values. Therefore, the convergence of both δD_{wax} records during late Holocene likely reflects the increasing influence of in situ-growing sedges and Poaceae rather than a decrease in seasonality (Figure 45).

Correcting a signal is a balance between improving signal quality and adding new sources of error and bias. As plants fractionation coefficient influences the δD_{wax} signal, it was necessary to try to correct this influence. However, many hypotheses and approximations have been made as constraints on the fractionation coefficient of aquatic plants from the site and more generally from tropical areas are lacking. The $\Delta\delta D_{23\text{-}31}$ record based on uncorrected and corrected δD_{wax} present similar trends suggesting that the signal is not “overcorrected” (see supplementary Figure S 9). Given the complexity of the system and the limited data available for n-alkanes in aquatic plants, it is likely that the signal remains “undercorrected” and part of the signal may be due to vegetation changes.

Leaf waxes are synthesized soon after leaf formation. In temperate regions, a spring bias has been recorded in leaf growth and wax production, suggesting that a similar bias could exist in δD_{wax} records (Tipple et al., 2013). In tropical ecosystems, leaf production is mainly controlled by water availability, solar irradiance and herbivore pressure (Wright and van Schaik, 1994; Wright, 1996). An increased leaf production has been demonstrated at the end of the dry season/beginning of the rainy season (van Schaik et al., 1993; Malhi et al., 2014). The seasonality of leaf production is accentuated in regions with a marked dry season (Reich,

1995). Leaf waxes hydrogen isotopic record might thus be slightly biased toward the end of the dry season (Ponton et al., 2014). As plant growing in-situ are not subjected to the same environmental stresses, the seasonality of leaf production might be different. As the hydrogen isotopic composition of the peat water and of the precipitation water do not follow the same evolution along the year, a difference in plant growth seasonality between submerged and floating plants, on one hand, and terrestrial plants, on the other hand, likely affects the paleoenvironmental reconstruction based on plant waxes.

6.2. Changes in evapotranspiration balance at NGaoundaba during the Holocene

The $\Delta\delta D_{23\text{-}31}$ record shows values mostly above zero all along the core, meaning that $\delta D_{n\text{-}C23}$ values are enriched compared to $\delta D_{n\text{-}C31}$ values in most samples. This suggests that most of the time, the water used by peat plants has undergone greater evaporation than the water used by the terrestrial vegetation. Most positive values of $\Delta\delta D_{23\text{-}31}$ are recorded between 7.7 and 5.8 ka cal BP, suggesting high evaporation of peat water at this time and/or limited evapotranspiration for terrestrial plants. These results are surprising as terrestrial vegetation generally present a stronger evaporation signal compared to the aquatic vegetation, at least in temperate region (Sachse et al. 2004). The seasonality of precipitation associated with the uneven seasonality of plant growth and n-alkane production between aquatic and terrestrial plants may explain the result observed here. Basically, evaporation requires energy supply providing heat of vaporization and transport mechanism to remove the vapor (Penman, 1956). A high $\Delta\delta D_{23\text{-}31}$ may be favored by an increase in temperature, consistent with the brGDGT-based temperature increase recorded during the same interval. However, modeled data indicate a limited increase in temperature and part of the brGDGT-based temperature increase at NGaoundaba may be related to changes in other parameters (moisture level, pH, …) (see chapter 5). Intensification of the monsoon system during the AHP may have strengthened the Harmattan wind during the dry season, favoring evaporation. However, records of dust emission indicate a decrease in dust emission during the AHP (DeMenocal et al., 2000; McGee et al., 2013; Ehrmann et al., 2017). This decrease is mostly associated with the increase vegetation cover but there is no evidence of increased wind intensity during this period (McGee et al., 2013; Egerer et al., 2016). In addition, during the rainy season, high precipitation favored vegetation growth and leaf production, while high ambient relative humidity limited transpiration by terrestrial plants. During the dry season, vegetation growth of terrestrial plants is limited due to water limitation, while aquatic plants may continue to grow during the dry season and therefore produce n-alkanes with a strong evaporated signal as peat water evaporates.

From 8.9 to 8 ka cal BP, $\delta D_{n\text{-}C31}$ values get more enriched suggesting a decrease in precipitation. However, the $\delta D_{n\text{-}C23}$ get slightly more depleted during the same period. As $\delta D_{n\text{-}C23}$ values seems strongly impacted by evaporation, we propose a significant decrease in peat water evaporation at the time compensating the decrease in precipitation. In addition, $\delta^{13}C_{n\text{-}C23}$ record shifts to less depleted values around -18 to -20‰ (Figure 45) indicating change in the vegetation input. A shift to C4 vegetation cannot explain the amplitude of the $\delta^{13}C_{n\text{-}C23}$. First, a large proportion of the n-C_{23} alkanes comes from aquatic plants (Figure 44) which are C_3 plants (Anton Hough and Wetzel, 1977; Chikaraishi and Naraoka, 2003). Second, a shift to C_4 vegetation is recorded in $\delta^{13}C_{n\text{-}C31}$ values but with a much more limited amplitude (Figure 45). We suggest a significant input of (micro)algal n-C_{23} as (1) algae can present enriched carbon isotopic signature compared to terrestrial plants (Chikaraishi and Naraoka, 2003; Meyers, 2003) and several studies report a possible input of n-C_{23} by algae and microalgae (Volkman et al., 1998; Liu and Liu, 2019) and (2) an increase in some botryococcenes (Figure 46), biomarkers produced by unicellular green algae, is reported during the same period suggesting environmental conditions favoring algal development. In addition, an increase in n-C_{19} alkane abundance, an n-alkane reported in microalgae (Weete, 1976; Volkman et al., 1998), is recorded consistent with microalgal development during this period (Figure 42). A different fractionation coefficient and the low transpiration of these microalgae may be responsible for part of the signal.

6.3. A dry event during a humid phase: the 8.9-7.9 ka cal BP event

The distribution of n-alkanes changes dramatically between 8.9-7.9 ka cal BP suggesting important changes in vegetation. N-alkanes are not specific enough to precisely reconstruct vegetation changes, but significant changes in n-alkanes distribution can still provide reliable information on vegetation groups (e.g., Nott et al., 2000; Vogts et al., 2012). Notably the high concentration of n-C_{35} and noticeable presence of n-C_{37} homologues remain enigmatic as these n-alkanes are generally not abundant in plants, although they have been reported in some conifers and in C_4 graminoids (Bush and McInerney, 2013; Diefendorf and Freimuth, 2017). Conifers are barely reported in the pollen records from the NGaoundaba peat deposit (C.Kiahtipes, personal communication, ongoing analyses) and carbon isotopic data indicate a C_3 predominance during the AHP (Figure 45). Nevertheless, the strong decrease in n-C_{33}, n-C_{35} and n-C_{37} concentrations and relative abundances between 8.9 and 7.9 ka cal BP suggest significant vegetation changes even if the arboreal vs non arboreal pollen ratio stays stable during this period (Figure 43A).

Surprisingly, the arboreal vs non-arboreal pollen record doesn't indicate a drop during this period suggesting a resilience of vegetation to climatic changes. Still, a detailed analysis of pollen data indicates modification of pollen assemblages including a slight increase in ferns and in sedges (Figure 45).

The increase in $\delta^{13}C_{n\text{-}C23}$ values between 8.9 and 7.9 ka cal BP may record past microalgal blooming as the increase in productivity can lead to dissolved CO_2 limitation and the use of ^{13}C-enriched dissolved HCO_3^-, enriching the carbon isotopic signature of these (micro)algae (Keely and Sandquist, 1992; Meyers, 2003). This is consistent with the increase in concentration of some botryococcenes recorded between 8.7 and 8 ka cal BP, a biomarker produced by the unicellular green algae *Botryococcus braunii* (Metzger et al., 1985a, 1985b). As algal blooms are triggered by excess nutrients, particularly phosphorus and nitrogen, either from the catchment (Paerl et al., 2011; Janssen et al., 2019) or from more distant sources (Goudie and Middleton, 2001), climatic changes during this period likely triggered changes in the nutrient status of the peat at this time. Several hypotheses can be proposed:

- Reduce precipitation led to vegetation degradation and increase runoff from the catchment area during precipitation. A similar hypothesis has been proposed to explain the increase productivity during the 8.2 ka event in a lake from Denmark (Hede et al., 2010). However, pollen data don't indicate a marked drop in arboreal vs non-arboreal pollen at that time (Figure 45 A). Drier condition may also have enhanced the frequency of natural fires favoring runoff during precipitation.
- Increase nutrient input brought by Harmattan winds. Interestingly, this period coincides in a "pause" in Green Sahara conditions (Tierney et al., 2017) reported in lake level records (Gasse, 2000), hydrogen isotopic record (Niedermeyer et al., 2010) and temporary abandonment of archeological sites (Sereno et al., 2008). As vegetation cover reduce dust emission (Kim et al., 2017), vegetation degradation may have favored dust emission from the Sahara. This period coincide with an increase in Saharan dust supply in North African (Zielhofer et al., 2017). However, this increase in dust emission is not recorded everywhere (McGee et al., 2013).
- Increase storminess. Bloom of *Botryococcus braunii* in the Darwin River Reservoir has been associated with an episode of extreme cyclone (Wake and Hillen, 1980). Increase in storms may have resulted in vegetation degradation and nutrient input from catchment runoff.

Modern threatening of aquatic ecosystems associated with increased frequency of algal blooming have been linked with rising temperature (Paerl and Huisman, 2008). However, the decrease in brGDGT-based reconstructed temperature is not inconsistent with increase algal blooming as some phytoplankton species such as diatoms (that may produce mid-chain n-

alkanes) and green algae (some of them producing botryococcenes) grow better at lower temperature compared to cyanobacteria (Reynolds, 2006; Paerl and Huisman, 2008).

Estimating water level between 8.9 and 7.9 ka cal BP is complicated as $\delta D_{n\text{-}C31}$ values indicate less precipitation but $\Delta\delta D_{23\text{-}31}$ suggests lower evaporation. Water depth controls the light condition at the bottom of the lake/peat, and deeper water level may restrict vegetation growth and promote phytoplankton development (Scheffer and van Nes, 2007). But, shallower water table conditions may cause partial desiccation and damage the vegetation favoring phytoplankton when the water level increases again (Blindow et al., 1993). The changes observed in the botryococcenes assemblages may reflect changes in seasonality with lower evaporation allowing the persistence of standing water even during the dry season and the development of microalgeae.

In addition to changes in terrestrial and aquatic vegetations, the 8.9-7.9 ka event might have affected the microbial communities living in surface peat sediments. Variations in the distribution and abundance of bacterial-derived brGDGTs and hopanes can provide some insight into the changes occurring in the bacterial community during this period. Low concentrations of some brGDGTs and of $\alpha\beta$ and $\beta\beta$ C_{31} hopanes are recorded until 8.5 ka cal BP (see chapter 4). The concentration of these compounds then increases coinciding with a drop in the $\delta^{13}C$ values of $\alpha\beta$ C_{31} hopanes (chapter 4). The concentration of $\alpha\beta$ C_{31} hopanes starts decreasing at 8 ka cal BP until 7.3 ka cal BP, suggesting that the consequences of this drying event on microbial community have expend long after its event. Hopane-based and brGDGT-based pH reconstructions indicate a slow decrease of pH starting around 8.9 ka cal BP until 8.5 ka cal BP, and pH values remain low until 7.3 ka cal BP. It seems that the 1-ka period can be further subdivided in two sub-periods with a switch around 8.5-8.4 ka cal BP (see chapter 4 Figure 26).

6.4. A dry event during a dry phase: the 4.5-3.5 ka cal BP event

Both n-C_{23} and n-C_{31} δD records follow the same trend from 4.5 to 3.5 ka cal BP, suggesting a change in precipitation amount rather than a marked change in evapotranspiration. The *Nymphaea* sp pollen are close to zero during this period suggesting limited development of submerged and floating macrophytes. Therefore, the evapotranspiration proxy $\Delta\delta D_{23\text{-}31}$ cannot be used during this period.

Pollen analyses indicate a strong increase in fern spores (Ptéridophytes) between 4.5 and 3 ka cal BP (Figure 45 B). Low ACL values of n-alkanes recorded between 4.5 and 3.5 ka cal BP likely resulted from vegetation changes. More specifically, n-C_{27} and n-C_{29} concentrations and relative abundances significantly increase during this period. Low ACL values are reported in

two fern species from the Dajiuhu peat deposit (Huang et al., 2011; Zhao et al., 2018) with a predominance of n-C_{27} and n-C_{29} alkanes. The strong development of ferns during this period might explain the decrease observed in ACL values and the dominance of n-C_{27} and n-C_{29} alkanes. However, n-alkanes production by ferns seems to be small compared to other type of plants (Zhao et al., 2018) and an ACL value around 30 has also been reported for one fern specimen from Japan (Chikaraishi and Naraoka, 2003). No or limited increase in short and mid-chain n-alkane proportions (n-C_{19} to n-$_{25}$) is reported during this period suggesting limited development of microalgae and aquatic plants. As during the previous dry event, the n-C_{35} and n-C_{37} alkanes concentrations strongly decrease during this interval. A slight increase in botryococcenes is recorded but is not accompanied by an increase is recorded in the mid- and short-chain n-alkanes. As for the 8.9-7.9 ka dry event, limited change is observed in the arboreal vs non arboreal pollen ratio (Figure 45 A) suggested limited change in the regional vegetation.

The gap in the age model during this period may suggest a period of lower sediment deposition or higher sediment degradation. The increase in Hydrogen Index (HI) appears inconsistent with higher sediment degradation but change in organic matter sources such as an input of microalgal biomass can have influenced the HI of the peat (see chapter 4, Figure 26). An increase in CPI values is recorded from the end of this interval and it is difficult to say whether it is linked to this event or not (Figure 43). We suggest that the dry phase between 4.5 and 3.5 ka cal BP led to a shallowing of the water table and likely to peat exposure during at least part of the year.

6.5. Hydrological changes around the 8.2 and 4.2 ka BP events in tropical Africa

6.5.1. The 8.9-7.9 ka BP event

In the Cariaco basin, a reduction of the northward migration of the ITCZ in summer and enhanced intensities of trade winds in winter have been demonstrated between 8.4 and 7.75 and 8.25 and 8.1 ka ca BP, respectively (Hughen et al., 1996; Haug et al., 2001). A similar pattern in tropical Africa could explain the change in precipitation recorded at the NGaoundaba peat deposit and at other sites. The observed environmental changes at the NGaoundaba peat deposit can also be achieved by increasing interannual climatic variability such as an increase in ENSO events that could have destabilize vegetation, but such change may not explain the decrease in δD_{wax}. If high and low latitudes 8.2 ka event are related, the drainage of lake Agassiz and lake Ojibway into the North Atlantic cannot explain the whole dry period as increase dryness is reported long before the meltwater discharge. At NGaoundaba, the decrease in precipitation starts more than 500 hundred years before the drainage of the two Canadian lakes. The drainage of the lakes may have strengthened the existing climate

deterioration and coincides with maximum dryness at NGaoundaba. Fleitmann et al. (2008) suggest a widespread cooling event around 9.2 ka cal BP, well recorded in Greenland and Northern Europe (Von Grafenstein et al., 1999; Vinther et al., 2006) and in the Asian monsoon domain (Dykoski et al., 2005; Fleitmann et al., 2007). This event seems to have been really short (100-200 yr) but may be related to a smaller drainage of Canadian lakes (Teller and Leverington, 2004; Fleitmann et al., 2008). Interestingly, several small drainage of the lake Agassiz are reported prior to the final drainage (Teller and Leverington, 2004). The succession of freshwater water drainage could have periodically weakened the Atlantic oceanic circulation affecting low latitude climates on a long term. Decrease in solar insolation has also been suggested as an cause for climate degradation around 8.5-8.2 ka cal BP (Muscheler et al., 2004). However, the duration of the anomalies in solar insolation are shorter than the duration of the dry event at the NGaoundaba peat deposit.

6.5.2. The 4.5-3.5 ka BP event

In the tropics, changes in ENSO were suggested as a major climate forcing behind the 4.2 ka event as anomalies in tropical SSTs with enhanced El Nino activity has been proposed (e.g., Marchant and Hooghiemstra, 2004; Toth and Aronson, 2019). In the Mediterranean region, the 4.2 ka BP event has been related with changes in seasonality with drier winter conditions (Bini et al., 2019). Renssen et al. (2022) demonstrate that the 4.2ka event was best modeled using an experiment including desertification in North Africa and SST anomalies in tropical equatorial Pacific and Atlantic.

This event also coincides with dry conditions associated with crisis of the rainforest in Central Africa (e.g., Vincens et al., 1998; Bostoen et al., 2015; Desjardins et al., 2013). The cause of these crises have been debated with possible influence of climate and human expansion (e.g., Garcin et al., 2018; Giresse et al., 2020). The preliminary pollen results from the NGaoundaba pollen records do not support a major changes in the regional vegetation cover and the forest recovery describe by Vincens et al. (2010) during the same period was not observed at the NGaoundaba peat deposit (Figure 45 A). Rainforests and wooded/shrub savannas might have responded differently to the changes in climatic conditions. Environmental changes are reported at the NGaoundaba peat deposit, particularly through the development of fern that are reported in the pollen record during this period (Figure 45 B).

Conclusions and perspectives

Based on a 10-ka peat records, we reconstructed significant environmental changes during two 1-ka dry events from 8.9 to 7.9 and from 4.5 to 3.5 ka cal BP, respectively. These periods

probably led to a degradation of the vegetation at the NGaoundaba peat deposit. The pause in AHP conditions between 8.9 and 7.9 ka cal BP was marked by strong increase in algal blooms competing with the aquatic vegetation dominating the aquatic environment at that time, leading to a significant eutrophication of the ecosystem. The dry event after the end of the AHP (4.5 to 3.5 ka cal BP) was marked by less pronounced algal blooms and a colonization of the catchment area by ferns. The decrease in precipitation could even have led to peat exposure that would explain the strong decrease in sedimentation rate during this period.

These two dry events are widely reported in tropical Africa. However, the poor resolution and the dating discrepancies of the records limit their comparison of existing records. The extension of these two events seems to be generally larger than the extension reported in the high and mid latitudes reaching 1-ka such as at the NGaoundaba peat deposit. For the 8.9-7.9 ka event, this suggests that other causes than the lakes Agassiz and Ojibway drainage to the North Atlantic are involved and that this event occurs during a period of climatic degradation in the tropics. For now, the study focuses on precipitation and paleohydrological records, but these two events are also recorded in temperature and vegetation reconstructions at the NGaoundaba peat deposit and a comparison with other temperature and pollen records from tropical Africa is needed to complete the story presented here.

Supplementary material:

A) Statistical grouping of n-alkanes

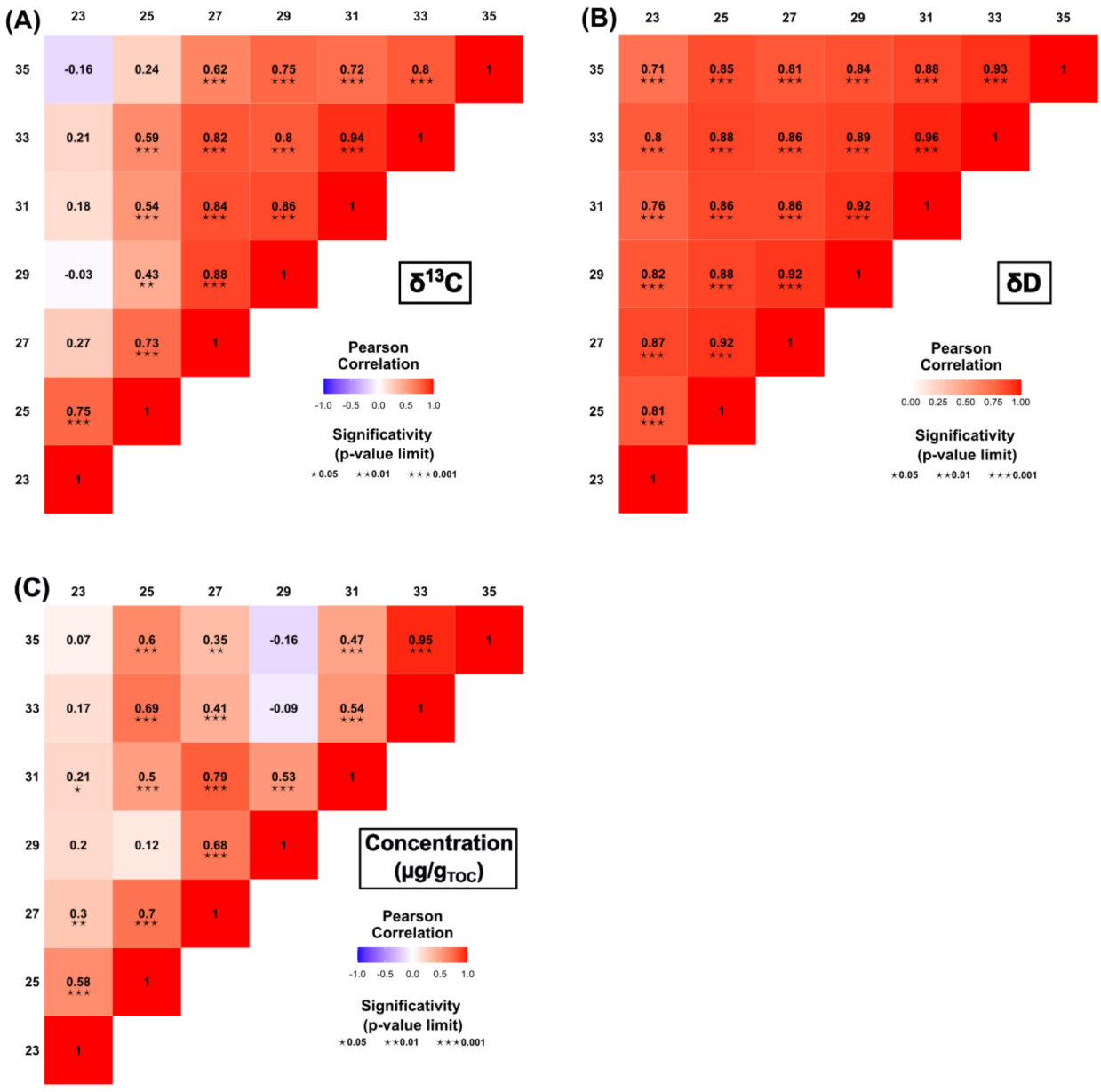

Figure S 8: Heatmap based on n-alkanes $\delta^{13}C$ (A), δD (B) and concentration (C). The color represents the Pearson correlation coefficient, and the significance of the correlation is indicated for each cell

We performed statistical analyses (heat maps) on n-alkanes concentrations and carbon and hydrogen isotopic compositions. Values can be comprised between -1 and 1 and a higher Pearson correlation for a pair of n-alkanes indicate a stronger relationship between the two compounds. For concentrations, the strongest correlation is between n-C_{33} and n-C_{35} alkanes suggesting similar sources for these two n-alkanes. The n-C_{23} present a significant correlation with n-C_{25} but no correlation with long-chain n-alkanes suggesting different sources and

consistent with the interpretation made in this Chapter. The significant but low Pearson coefficients for many pair of n-alkanes is consistent with mixed sources of n-alkanes and the low specificity of these compounds.

There is a good correlation between the different $\delta D_{n\text{-}alk}$ signals, all value being above 0.71 and all correlation being significant. Based on an environmental soil transect in Cameroon, Schwab et al. (2015) showed a correlation between δD_{sw} (sw = soil water) and $\delta D_{n\text{-}alk}$ from n-C_{27} to n-C_{31} n-alkanes supporting their use as a proxy for reconstructing precipitation variation while the δD from n-C_{33} n-alkane didn't present any correlation with δD_{sw} likely due to a more mixed contribution from both C_3 and C_4 plants hiding the precipitation signal. At the NGaoundaba peat deposit, statistical analyses don't support the exclusion of n-C_{33} alkane as n-C_{33} is strongly correlated with n-C_{31} alkane for $\delta^{13}C$ and δD. We suggest that for the NGaoundaba peat deposit, all δD record a paleohydrological signal.

B) Test for the evapotranspiration ratio

The Figure S 9 presents different combinations of n-alkanes tested for the evapotranspiration ratio. The trend observed for the different tests are similar but the range of variation of the $\Delta\delta D_{23\text{-}31}$ depends on the choice of the n-alkane and of the correction. We didn't choose the n-C_{33} alkane in the end as some samples present a coelution. All combination tested presented negative values between 8.9 and 7.9 ka cal BP and positive values during the AHP. We compare the reconstruction with the pH reconstruction presented in chapter 4. The pH variation present similar variations compared to the $\Delta\delta D_{23\text{-}31}$ and both could change in evapotranspiration. However, significant differences are observed between the pH records and the $\Delta\delta D_{23\text{-}31}$ particularly during middle and late Holocene possibly associated with the increase influence of sedges on the evapotranspiration ratio.

The $\Delta\delta D_{23\text{-}31}$ values calculated using a fixed fractionation coefficient for the terrestrial endmember of the vegetation correction of n-C_{23} alkane present nearly identical values as the $\Delta\delta D_{23\text{-}31}$ values calculated using a variable fractionation coefficient for the terrestrial endmember Figure S 10.

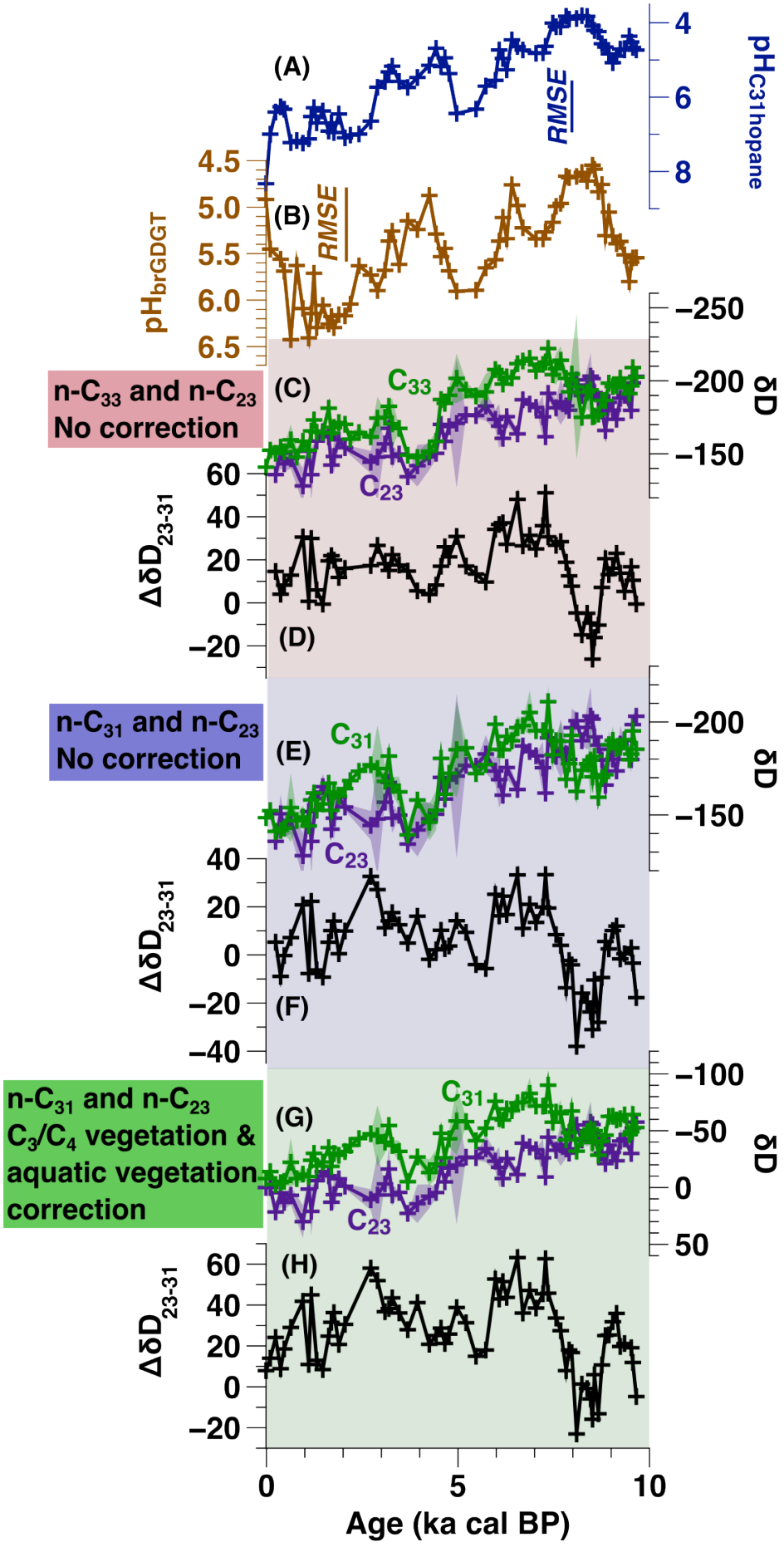
(A)
RMSE
4
6
8
pHc31hopane
(B)
RMSE
4.5
5.0
5.5
6.0
6.5
pHbrGDGT
n-C33 and n-C23
No correction
(C)
C33
C23
−250
−200
−150
δD
60
40
20
0
−20
ΔδD23-31
(D)
n-C31 and n-C23
No correction
(E)
C31
C23
−200
−150
δD
40
20
0
−20
−40
ΔδD23-31
(F)
n-C31 and n-C23
C3/C4 vegetation &
aquatic vegetation
correction
(G)
C31
C23
−100
−50
0
50
δD
60
40
20
0
−20
ΔδD23-31
(H)
0
5
10
Age (ka cal BP)

Figure S 9: Influence of n-alkane chain-length and vegetation correction on the evapotranspiration ratio at the NGaoundaba peat deposit. The evapotranspiration ratios are compared with the pH reconstruction based on hopane (A) and brGDGT (B) (see chapter 4 for more details). We calculated the evapotranspiration ratio based on n-C_{33} alkane instead of n-C_{31} alkane without vegetation correction (C and D), based on n-C_{31} alkane without vegetation correction (E and F) and based on n-C_{31} alkane with the vegetation correction presented in section 4.3 of this chapter (G and H). Briefly for G and H, the hydrogen isotopic composition of n-C_{31} alkane is corrected for C_3/C_4 change and the hydrogen isotopic composition of n-C_{23} alkane is corrected for the influence of aquatic vegetation.

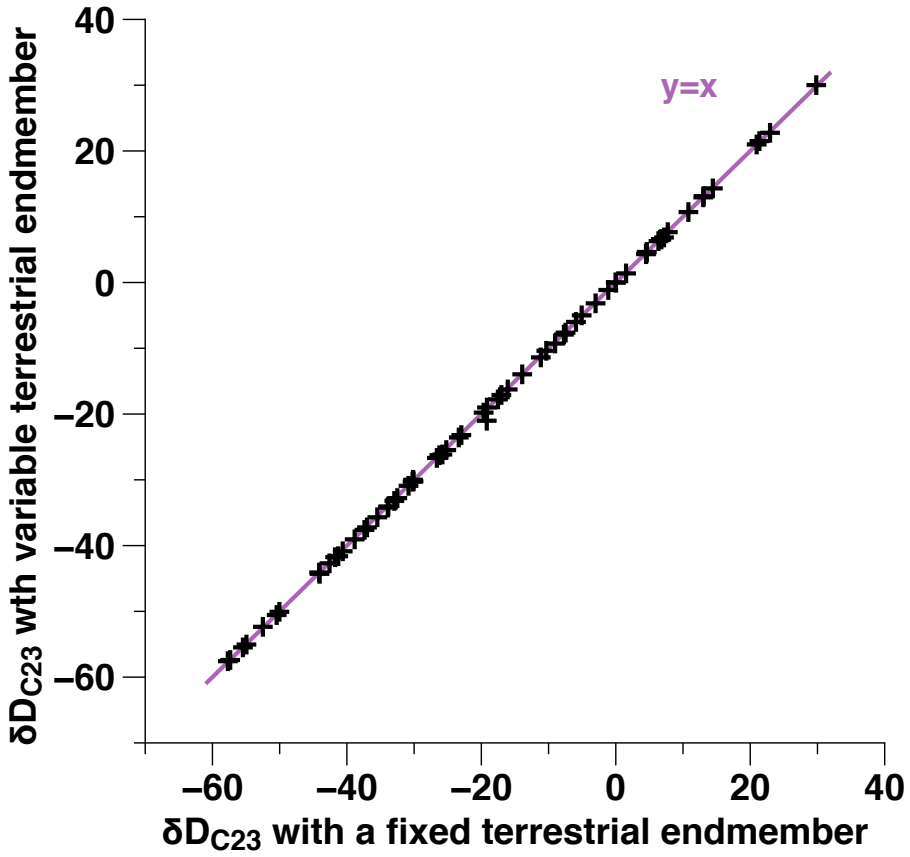

Figure S 10: Comparison between the δD_{C23} values calculated with a fixed fractionation coefficient for terrestrial plant and with a variable terrestrial fractionation coefficient. The fixed fractionation coefficient is the mean fractionation coefficient calculated for the n-C_{31} alkane (see chapter 5). A 1:1 function is trace on the graph.

C) References for the 8 and 4 ka events

Table S 2: Site presented in section 2 of this chapter and in Figure 39. Site are ordered by type of analysis and then by chronological order. The confidence is based on comment in the original articles or when the interpretation is based on only one or two sample.

Site	N°	Reference	Lat	Lon	Altitude (m)	Analyse	Type	8 ka	4 ka	Confidence 8ka / 4ka
Ngaoundaba	1	This study	7.13	13.69	1175	δD_{wax}	Peat	y	y	Ok / Ok
Congo Basin	2	Schefuß et al. (2005)	-5.59	11.22	0	δD_{wax}	Marine	n	n	Ok / Ok
Off Senegal	3	Niedermeyer et al. (2010)	15.51	-17.96	0	δD_{wax}	Marine	y	n	Ok / Ok
Tanganiika	4	Tierney et al. (2010)	-6.7	29.83	773	δD_{wax}	Lake	y	y	Ok / ?
Malawi	5	Konecky et al. (2011)	-10.02	34.19	474	δD_{wax}	Lake	n	n	Ok / Ok
Off Zambezi	6	Schefuß et al. (2011)	-18.56	37.38	0	δD_{wax}	Marine	n	y	Ok / Ok
Challa	7	Tierney et al. (2011b)	-3.32	37.7	880	δD_{wax}	Lake	y	y	Ok / Ok
Victoria	8	Berke et al. (2012)	-1.23	33.2	1135	δD_{wax}	Lake	n	n	Ok / Ok
Gulf Aden	9	Tierney and deMenocal (2013)	11.96	44.3	0	δD_{wax}	Marine	n	y	? / ?
Tana	10	Costa et al. (2014)	12	37.25	3200	δD_{wax}	Lake	y	n	Ok / Ok
Bosumtwi	11	Shanahan et al. (2015)	6.50	-1.41	150	δD_{wax}	Lake	n	n	Ok / Ok
Guinea Gulf	12	Collins et al. (2017)	2.5	9.39	0	δD_{wax}	Marine	n	n	? / ?
Atlantique - GC27	13	Tierney et al. (2017b)	30.88	-10.63	0	δD_{wax}	Marine	n	n	Ok / Ok
Atlantique - GC237	14	Tierney et al. (2017b)	26.82	-15.12	0	δD_{wax}	Marine	n	n	Ok / Ok
Atlantique - GC49	15	Tierney et al. (2017b)	23.21	-17.85	0	δD_{wax}	Marine	y	n	Ok / Ok
Atlantique - GC68	16	Tierney et al. (2017b)	19.36	-17.28	0	δD_{wax}	Marine	y	n	Ok / Ok
Barombi	17	Garcin et al. (2018)	4.66	9.40	334	δD_{wax}	Lake	n	n	Ok / Ok
Rutundu	18	Garelick et al. (2021)	-0.04	37.46	3078	δD_{wax}	Lake	n	n	Ok / Ok
Congo Peat	19	Garcin et al. (2022)	1.18	17.64	327	δD_{wax}	Peat	n	n	Ok / Ok
Abhe	20	Gasse (1977)	11.08	41.83	240	Lake level	Lake	y	y	Ok / Ok

Bosumtwi	11	Talbot and Delibrias (1977) Talbot et al. (1984) Shanahan et al. (2006)	6.50	-1.41	100	Lake level	Lake	y	y	Ok / Ok
Bahl-el-ghazal	21	Servant and Servant-Vildary (1980) in Gasse (2000)	18	17	176	Lake level	Lake	y	y	Ok / Ok
Turkana	22	Owen et al. (1982) Brown and Fuller (2008) Garcin et al. (2012a) Forman et al. (2014)	2.6	36.5	450	Lake level	Lake	y	y	Ok / Ok
Ziway-Shala	23	Gillespie et al. (1983)	7.67	38.67	1597	Lake level	Lake	y	y	? / ?
Victoria	8	Johnson et al. (2000)	-1.00	33.06	1133	Lake level	Lake	y	n	Ok / Ok
Kilimanjaro	24	Thompson et al. (2002)	-3.07	37.35	5893	Dust	Ice core	y	y	Ok / Ok

Chapter 7: Methane cycling during the Holocene at the NGaoundaba peat deposit

Abstract:
Based on a tropical peat record covering the last 10 ka, we present a record of methanotrophy and methanogenesis during the Holocene based on microbial lipid biomarkers. The carbon isotopic composition of β-C_{27} hopane indicates an increase in methanotrophy during the middle and late Holocene. By comparing with other paleoclimatic records presented in previous chapters (chapters 3 to 6), we conclude that methanotrophs are favored during periods of prevailing dry conditions, either after the end of the African Humid Period (AHP) or during 1-ka dry events. We propose that dry periods favor aerobic conditions, increasing the efficiency of methane oxidation. Isoprenoid glycerol dialkyl glycerol tetraethers (isoGDGTs) are used to infer past changes in methanogenic activity, and we discuss potential biases associated with the deep production of these compounds on the paleoclimatic signal. We find a general good agreement between proxies unaffected by deep-peat production (such as n-alkane derived from terrestrial plants) and microbial proxies investigated at the NGaoundaba peat deposit.

Key words: Methane cycling, tropical peat, archaeal and bacterial lipid biomarkers

1. Introduction

Since 1750, the atmospheric concentration of the greenhouse gas methane (CH_4) has increased by over 150 % largely as a result of human activities (Masson-Delmotte et al., 2021). Methane is already the second contributor to 2010-2019 warming just after CO_2 (Masson-Delmotte et al., 2021). Methane emissions can come from both natural (freshwater wetlands, …) and anthropogenic (fossil fuel, livestock, …) sources. Freshwater wetlands account for more than a quarter of total present-day CH_4 emissions (Masson-Delmotte et al., 2021) and their response to future climate warming is unclear as they could either amplify or reduce the impact of climate changes (e.g., Strack et al., 2004; Amesbury et al., 2019; Loisel et al., 2021; Morris, 2021). Paleoclimatic records report significant variations of CH_4 emissions during the Holocene (e.g., Blunier et al., 1995; Kaplan et al., 2006) and beyond (e.g., Brook et al., 2000; Petrenko et al., 2017). Peatlands from both high and low latitudes have been suggested as major drivers of these CH_4 emissions (Korhola et al., 2010; Singarayer et al., 2011) but response of peatlands to climatic changes are complex and require further investigation (Frolking and Roulet, 2007; Zheng et al., 2014).

Complex climatically driven biogeochemical processes impact the amount of CH_4 wetlands can produce and release. The influence of temperature, change in precipitation regime, or variations in the availability of nutrient (Dean et al., 2018) on these processes are still poorly understood and require more constraints. A great opportunity to evaluate these biogeochemical feedbacks over longer timescales is provided by the use of some lipid biomarkers that have been suggested as potential tracers of methanogenesis or methanotrophy (Naafs et al., 2019 and references therein). Isoprenoid glycerol dialkyl glycerol tetraethers (isoGDGTs) are membrane-spanning lipids produced by archaea including methanogenic archaea (Schouten et al., 2007; Weijers et al., 2009; Schouten et al., 2013). IsoGDGTs preserved in the geological record have been used to infer past changes in methanogenesis in various settings (Zhang et al., 2011; Inglis et al., 2015; Zheng et al., 2015). However, most methanogen have an anaerobic metabolism (Thauer, 1998) and the production of lipids from methanogens thriving in anoxic sediments/soils may obscure the paleoclimatic signal (Huguet et al., 2010). In addition, isoGDGTs can have multiple microbial sources with different metabolic pathways, which further complicates paleoreconstructions based on isoGDGTs distribution (Schouten et al., 2013). Hopanoids are pentacyclic triterpenoids derived from bacteria that are generally preserved as hydrocarbons (i.e., geohopanoids) in sediments and are particularly abundant in peat sediments (e.g., Quirk et al., 1984; Ries-Kautt and Albrecht, 1989; Inglis et al., 2018). A wide diversity of hopanes can be detected in peat sediments, with different carbon numbers and isomerizations (e.g., Quirk et al., 1984; Inglis et al., 2018). Recent analyses of hopane distribution suggest that these

compounds can be used as a proxy for pH in peat (Inglis et al., 2018). Furthermore, the carbon isotopic composition of hopanes records the microbial ecology and changes in metabolic pathways of the bacterial community (Inglis et al., 2019).

Methane of biological origin presents strongly depleted carbon isotopic signatures, from around -50 to -60 ‰ when formed from fermentation of methylated substrate and down to -110 ‰ when produced by the hydrogenotrophic pathway (Whiticar, 1999). Therefore, the carbon isotopic compositions of lipid biomarkers has been used as marker of past methanogenesis or past methanotrophy (e.g., Hinrichs, 2002; Wooller et al., 2012; Elvert et al., 2016). Hopanes and hopenes have been proposed as biomarkers of past methanotrophic activity in peats (e.g., Pancost et al., 2003; Zheng et al., 2014; Elvert et al., 2016; Inglis et al., 2019), the depleted $\delta^{13}C$ of C_{27} to C_{30} hopanes suggest methanogenic activity in the bacterial community (Inglis et al., 2019).

We report a 10-ka record of methanotrophic and methanogenic activity in a tropical peat deposit. The study is based on a 10-m core from the NGaoundaba peat deposit (North-East Cameroon). We report the distribution and concentration of isoGDGTs and of β-C_{27} and $\beta\beta$-C_{29} hopanes. C_{30} and C_{31} hopanes were previously investigated in chapter 4 and will not be presented again in this chapter. The carbon isotopic composition of β-C_{27} hopane is used to infer past changes in methanotrophic activity while isoGDGT ratios are used to estimate past changes in methanogenesis. We also discuss the limitations associated with these proxies.

2. Methods

2.1. Sample preparation

The 6-meter core from the NGaoundaba peat deposit was subsampled at 2.5-cm intervals. A total of 73 samples was used for this study. Sample preparation follow the same procedure as in chapter 4 to 6. Briefly, lipid biomarkers were extracted using a MARS 6 CEM microwave extraction system with 10mL of dichloromethane (DCM)/methanol (3:1, v/v) repeated two times. The total lipid extract was separated into three fractions with 8mL hexane, 5mL hexane/DCM (1:1, v/v) and 10 mL DCM/methanol (1:1, v/v), respectively. The hopanes were eluted in the first fraction while the isoGDGTs were eluted in the last fraction.

2.2. Hopane identification and analyses

The analysis of hopanes is detailed in chapter 4. Briefly, GC-MS analyses (Agilent 6890N GC coupled to an Agilent 5975C MSD and Agilent 7890B GC coupled to an Agilent 5977B MSD) were performed for identification and quantification of hopanes. Hopanes were identified based on their retention time and mass spectrum by comparison with previously published

literature (Figure 47) (Naafs et al., 2019 and reference therein). Prior to carbon isotopic measurements, the fractions containing hopanes were separated into saturated and unsaturated fractions. Carbon isotopic measurements were performed on an Agilent Agilent 7890B GC coupled to an Isoprime visION Isotope Ratio Mass Spectrometer via an Isoprime GC-5 combustion interface operated at 850°C (Elementar). Stable carbon isotopic compositions (expressed as $\delta^{13}C$ values) were calibrated using a reference CO_2 gas reported to VPDB scale. Samples were analyzed in duplicates when the quantity of samples allowed it.

Since the ββ-C_{29} hopane might coelutes with another unidentified compound in some samples, its concentration and carbon isotopic composition of the ββ-C_{29} hopane are presented in the result section but the discussion mainly focuses on the β-C_{27} hopane.

As suggested by Inglis et al. (2019), we compare the difference between the carbon isotopic composition of β-C_{27} hopane and n-C_{31} alkane expressed as $\Delta^{13}C_{hop\text{-}alk}$ as well as the difference between the carbon isotopic composition of β-C_{27} hopane and bulk organic matter expressed as $\Delta^{13}C_{hop\text{-}bulk}$:

$$\Delta^{13}C_{hop-alk} = \delta^{13}C_{hop} - \delta^{13}C_{n-C31\ alk}$$

$$\Delta^{13}C_{hop-bulk} = \delta^{13}C_{hop} - \delta^{13}C_{bulk}$$

2.3. IsoGDGT analyses

The fractions containing GDGTs were filtered using 0.45 µm PTFE filters. GDGT analyses were performed using High Performance Liquid Chromatography Mass Spectrometer (HPLC-APCI-MS, Agilent 1200). Separation was achieved on two silica columns in series (ACQUITY UPLC BEH HILIC, WATERS) following the procedure of Hopmans et al. (2016), slightly modified using hexane/isopropanol (98.2:1.8). The different GDGTs were manually integrated and quantified using the peak area of the different m/z values (1303.6, 1300.5, 1298.5, 1296.5, 1294.5, 1292.5 for GDGT-0 to GDGT-4 and Crenarchaeol, respectively (Figure 47)) and of the of C_{46}. Internal standard (m/z 743.9).

Several ratios based on isoGDGT were tested. The ratio GDGT-0/Crenarchaeol was calculated as proposed by Blaga et al. (2009). The fractional abundance of GDGT-0 relative to other regular isoGDGTs (GDGT-0, GDGT-1, GDGT-2, GDGT-3, GDGT-4) was calculated as in Zheng et al. (2015). Finally, we tested the %GDGT-0 proposed by Inglis et al. (2015) and calculated as follows:

$$\%GDGT-0 = \left(\frac{[GDGT-0]}{[GDGT-0]+[Crenarcheol]}\right) * 100$$

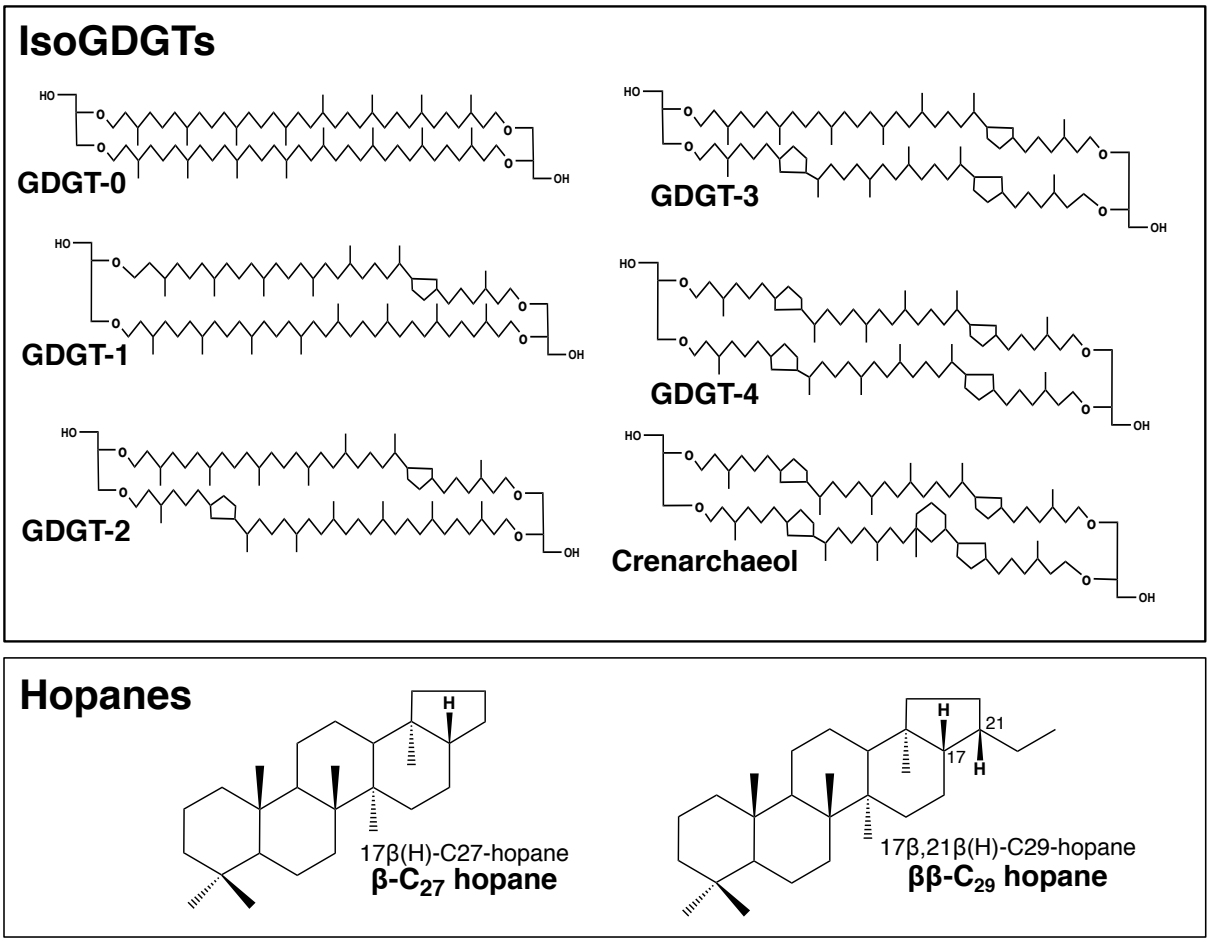

Figure 47: Structure of isoGDGTs and hopanes discussed in this chapter

3. Results

3.1. C_{27}-C_{30} hopanes

3.1.1. Concentrations

The β-C_{27} hopane concentration ranges from 1.4 to 8.2 µg/g_{TOC} with a mean concentration of 3.9 µg/g_{TOC} (Figure 48 A). ββ-C_{29} hopane concentration ranges from 1.0 to 7.6 µg/g_{TOC} with a mean concentration of 4.0 µg/g_{TOC} (Figure 48 B). Small amounts of βα-C_{29} hopane are recorded with concentrations below 2.0 µg/g_{TOC}. β-C_{27} and ββ-C_{29} hopanes present similar variations with the highest concentrations between 6.4 and 4.9 ka cal BP, and the lowest concentrations between 9.4 and 8.2 ka cal BP and between 2.9 and 2.0 ka cal BP. Between 9.7 and 9.4 ka cal BP, the concentration of ββ-C_{29} hopane is high while the concentration of β-C_{27} hopane is low. Short-term variations in concentration are recorded for both hopanes particularly during the late Holocene.

3.1.2. Carbon isotopic composition

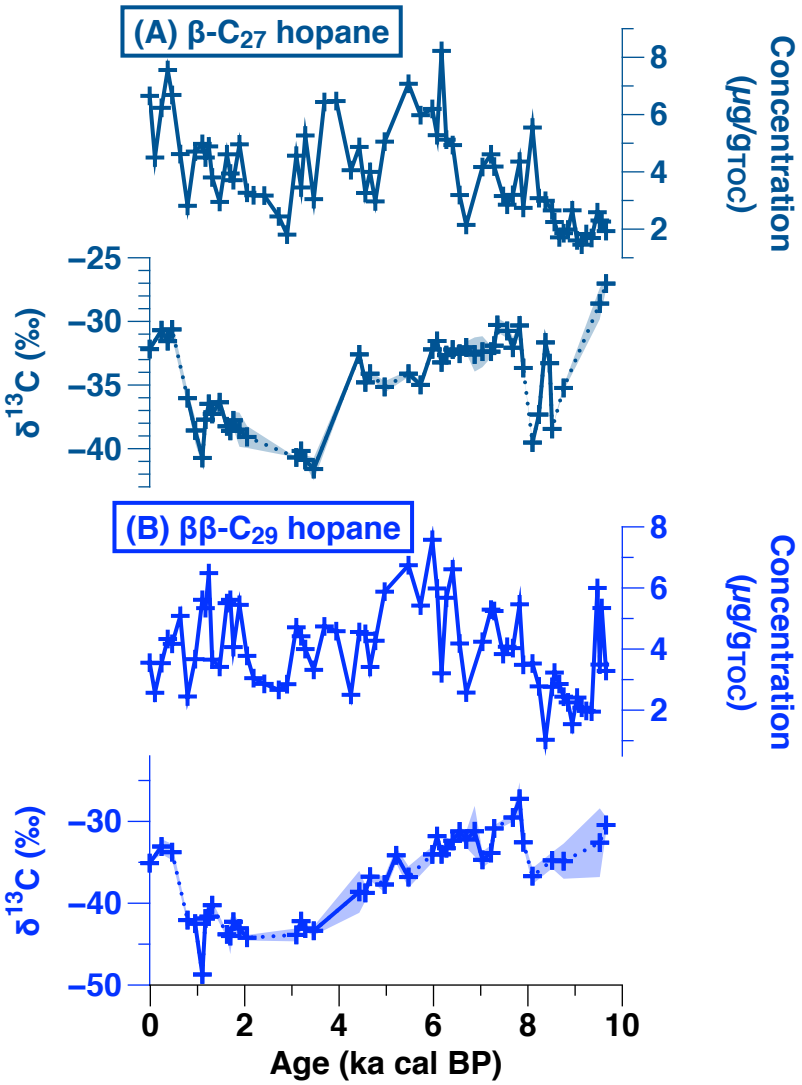

Figure 48: Concentration and carbon isotopic signature of β-C_{27} (A) and ββ-C_{29} (B) hopanes. For carbon isotopic measurements, the uncertainty measurements for the $\delta^{13}C$ are plotted on the figure; when it was not possible to analyze the sample in duplicate, we plotted the mean uncertainty. Dotted lines show the gaps in the data.

The $\delta^{13}C$ values of β-C_{27} and ββ-C_{29} hopanes were measured for 50 and 43 samples out of 73, respectively. The low concentrations of hopanes observed between 9.4 and 8.2 ka cal BP and between 2.9 and 2.0 ka cal BP prevented compound specific carbon isotopic measurements during these two periods. The $\delta^{13}C$ values of β-C_{27} hopane range from -41.6 to -27.0 ‰ with a mean value of -34.6 ± 0.4‰ (± min: 0, max: 1.3 ‰) (Figure 48 A). Around 9.5 ka cal BP, the $\delta^{13}C_{\beta\text{-}C27}$ presents enriched values around -28‰ compared to the mean value. The $\delta^{13}C_{\beta\text{-}C27}$ values are depleted between 8.8 and 8 ka cal BP except around 8.4 ka cal BP with values below -35‰. Between 7.9 and 4.4 ka cal, BP $\delta^{13}C_{\beta\text{-}C27}$ values range from -35.1 to -30.3‰. The $\delta^{13}C_{\beta\text{-}C27}$ values decrease to their lowest values around -41.6‰ at 3.5 ka cal BP and values remain below -36‰ until 0.8 ka cal BP. Late Holocene is characterized by more enriched $\delta^{13}C_{\beta\text{-}C27}$ values around -31‰.

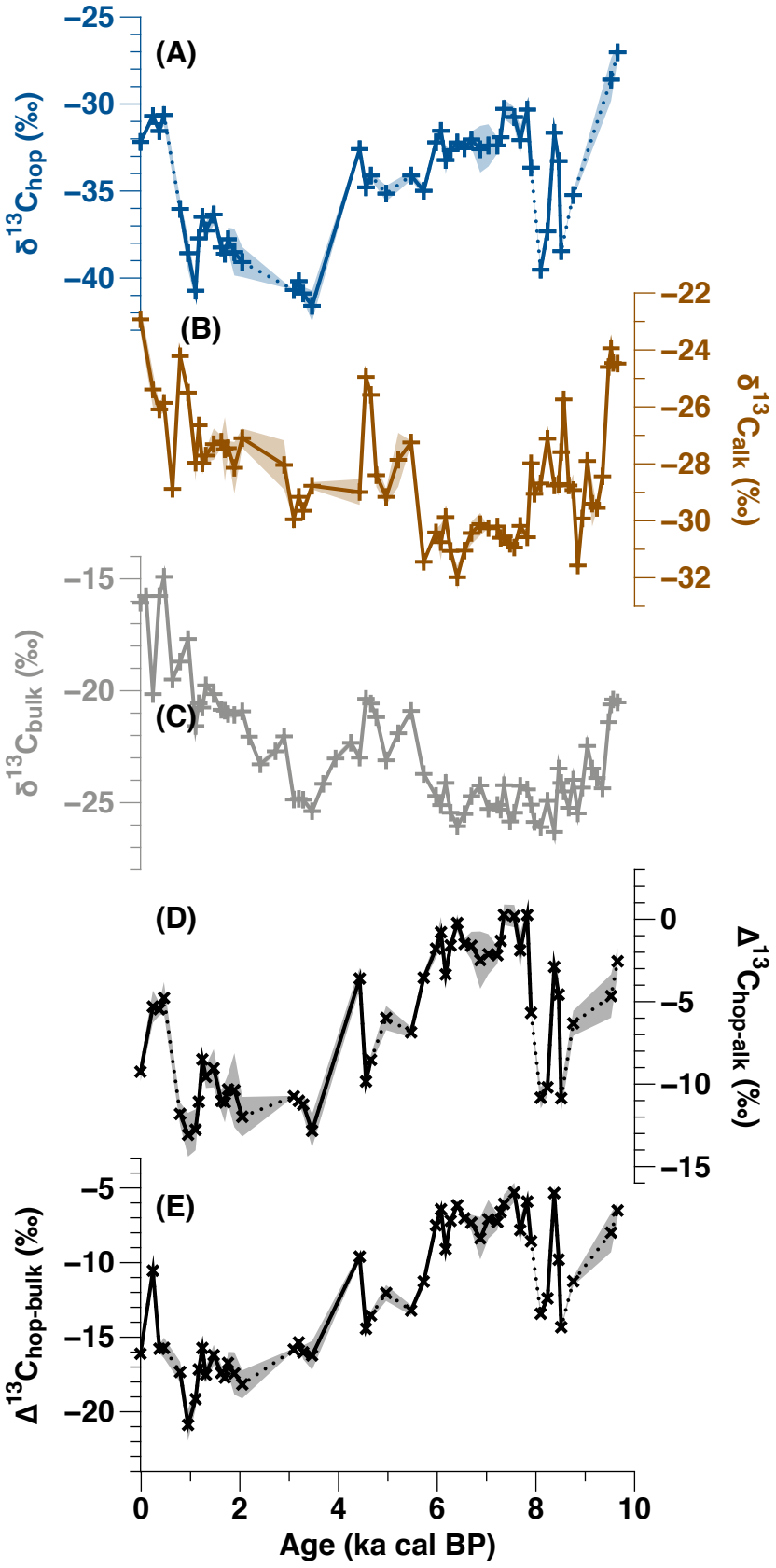

Figure 49: Carbon isotopic compositions of β-C_{27} hopane (A), n-C_{31} alkane (chapter 5) (B) and bulk organic matter (Schaaff et al., 2023) (chapter 3) (C), and $\Delta^{13}C_{hop\text{-}alk}$ (D) and $\Delta^{13}C_{hop\text{-}bulk}$ (E) calculated as proposed by Inglis et al. (2019). The dotted line indicates the gaps in the data.

The $\delta^{13}C$ values of $\beta\beta$-C_{29} hopane range from -48.7 to -27.2‰ with a mean value of -36.9 ± 1.0‰ (± min: 0, max: 4.2 ‰) (Figure 48 B). The $\delta^{13}C_{\beta\beta\text{-}C29}$ values show variations similar but smoother than those of the β-C_{27} hopane. Early Holocene is characterized by enriched $\delta^{13}C_{\beta\beta\text{-}C29}$ values above -37‰. The $\delta^{13}C_{\beta\beta\text{-}C29}$ values decrease during mid Holocene to values below -40‰ until 0.8 ka cal BP. The last 1 ka is characterized by more enriched $\delta^{13}C_{\beta\beta\text{-}C29}$ values around -31‰.

3.1.3. $\Delta^{13}C_{hop\text{-}bulk}$ and $\Delta^{13}C_{hop\text{-}alk}$

The $\Delta^{13}C_{hop\text{-}alk}$ ranges from -13.0 to 0.3 ‰ and the $\Delta^{13}C_{hop\text{-}bulk}$ ranges from -20.9 to -5.3 ‰ (Figure 49 D and E). Both indices present similar variations as the $\delta^{13}C$ of the β-C_{27} hopane (Figure 49 A). The $\Delta^{13}C_{hop\text{-}bulk}$ and $\Delta^{13}C_{hop\text{-}alk}$ values are higher between 9.7 and 5.8 ka cal BP than during more recent periods, except between 8.8 and 7.9 ka cal BP where they show much lower values. Contrary to the $\delta^{13}C_{hop}$ values (Figure 49 A), the $\Delta^{13}C_{hop\text{-}bulk}$ and $\Delta^{13}C_{hop\text{-}alk}$ values present a progressive decrease starting at 5.8 ka cal BP. The lowest values of $\Delta^{13}C_{hop\text{-}bulk}$ and $\Delta^{13}C_{hop\text{-}alk}$ are recorded between 3.5 and 0.8 ka cal BP and an increase is recorded around 0.3 ka cal BP.

3.2. IsoGDGTs

3.2.1. Relative abundance and concentration

GDGT-0 is the most abundant GDGT with a relative abundance comprised between 73.6 % and 92.7 % and an average value of 85.3 % (Figure 50 A). Its abundance drops significantly (<80%) between 7.9 and 5.8 ka cal BP and after 0.4 ka cal BP. The other regular isoGDGTs never present an individual abundance higher than 7 % but all show a higher contribution to the GDGT pool before 5.8 ka cal BP, particularly between 7.9 and 5.8 ka cal BP. The high proportion of Crenarchaeol and GDGT-4 associated with the low proportion of GDGT-0 in the most superficial samples (above 15 cm- depth) likely indicate the present-day transition between oxic and anoxic zones.

In term of concentration, GDGT-0 is the most dominant GDGT with concentration comprised between 5.6 and 49.5 $\mu g/g_{TOC}$ and a mean concentration of 24.4 $\mu g/g_{TOC}$ (Figure 50 B). The concentration of GDGT-0 presents a slightly decrease during the Holocene while the other regular isoGDGTs present globally low concentrations but with a a significant increase in concentration between 7.9 and 5.8 ka cal BP. In the 2 or 3 most recent/superficial samples,

the concentration of GDGT-0 to GDGT-3 decrease while the concentrations of GDGT-4 and Crenarchaeol slightly increase.

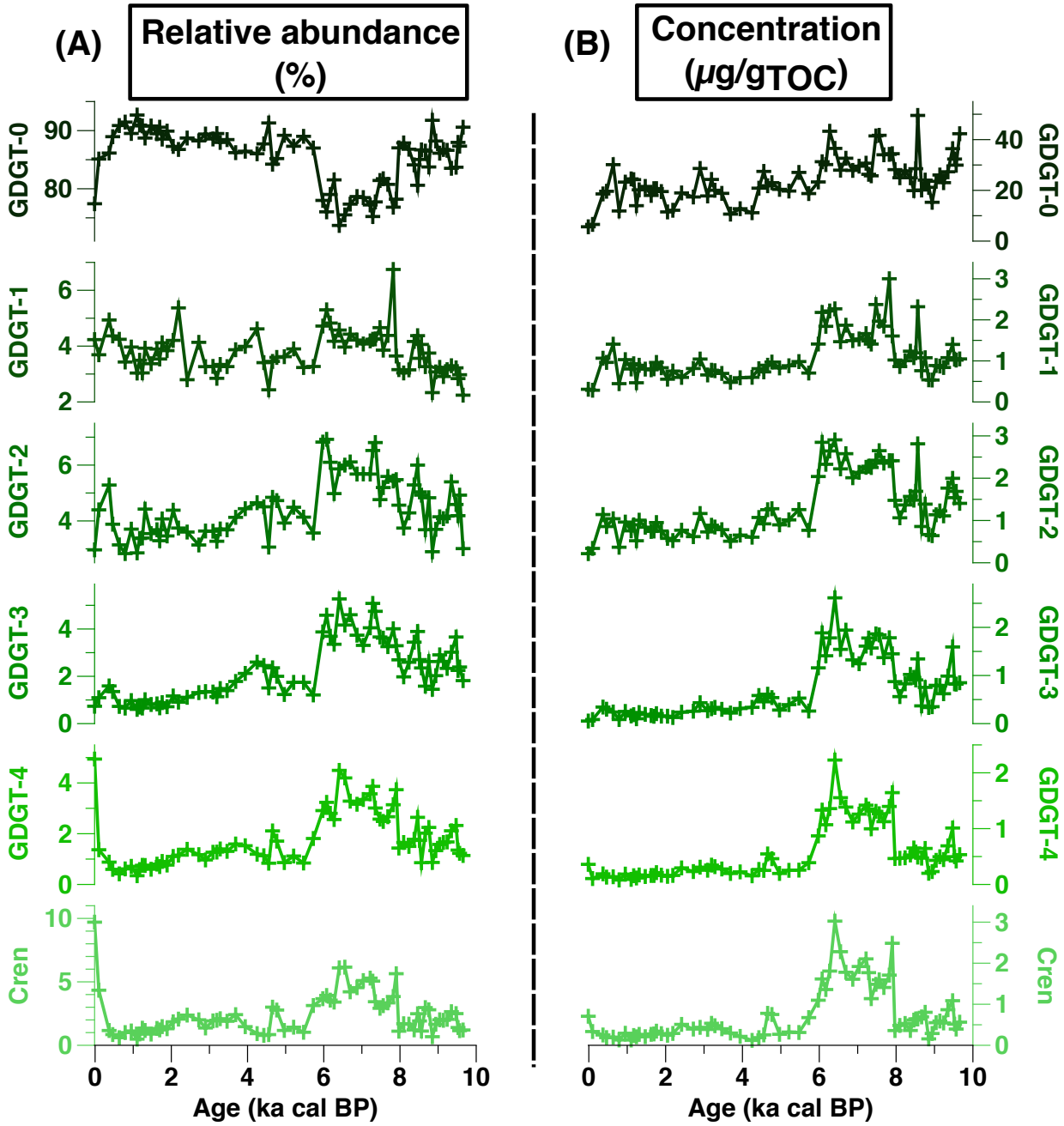

Figure 50: Relative abundance (A) and concentration (B) of isoGDGTs (GDGT-0 to GDGT-4 and Crenarchaeol)

3.2.2. IsoGDGTs ratio

Several ratios based on isoGDGT-0 were tested, we present the %GDGT-0 ratio proposed by Inglis et al. (2015) (Figure 51 G). Other ratios were tested and are presented in Figure S 11 at the end of this chapter (supplementary material).
The %GDGT-0 ratio ranges from 88.9 to 99.5% with a mean value of 97.2% (Figure 51 G). The values are above 97% during most of the Holocene. A period of decrease in %GDGT-0 ratio is recorded between 7.9 and 5.7 ka cal BP. %GDGT-0 is lower in the two most superficial samples (Figure 51 G).

4. Discussion

4.1. Past methanotrophic activity enhanced during drier periods

The lowest $\delta^{13}C_{\beta\text{-}C27}$ values are observed during the late Holocene, after the end of the AHP, and with the 8.9-7.9 dry event (chapter 5 & 6), suggesting an increased methanotrophic activity during drier periods at the NGaoundaba peat deposit (Figure 51). The low $\Delta^{13}C_{hop\text{-}alk}$ and $\Delta^{13}C_{hop\text{-}bulk}$ during the same periods confirms that these changes are not associated only with vegetation changes and modification of the carbon isotopic composition of the organic matter used by decomposers (Inglis et al., 2019). The decrease in peat water level during this period may have enhanced the development of the aerobic bacterial community including methanotrophic bacteria. These results are similar to those of Zheng et al. (2014) and Huang et al. (2018) who reported a high methanotrophic activity during the dry mid Holocene period at the Hongyuan and Dajuihu peat deposits, respectively. Zheng et al. (2014) further suggested an enhancement of methane oxidation efficiency associated with sedges development and root-facilitated transport of O_2 into the peat. Several studies indicate increasing methanotrophic activity with increased water level and temperature (Kip et al., 2010; Larmola et al., 2010), but these studies are based on the symbiotic relationship between *Sphagnum* mosses and methanotrophic bacteria (Basiliko et al., 2004; Raghoebarsing et al., 2005) and the conclusions are likely not applicable to sedges-dominated peat deposits where *Sphagnum* mosses are absent. While methanotrophs alone seam less efficient in limiting the methane flux from peat than methanotrophs associated with *Sphagnum* (van Winden et al., 2012), sedges produces an environment favorable for methanotrophy through aerating the rhizosphere (Rupp et al., 2019) and could counterbalance this effect. In tropical peatlands, however dominated by swamp forest and not sedge, root oxygen significantly mitigates peat surface methane emissions (Nicholas T. Girkin et al., 2020). Lamit et al. (2021) demonstrates a strong effect of the water table on the microbial community of the upper 20cm of peat. Higher CH_4 fluxes were measured in tropical peats from Panama with water table located above the peat surface likely resulting from anoxic conditions enhancing methanogenesis and limiting

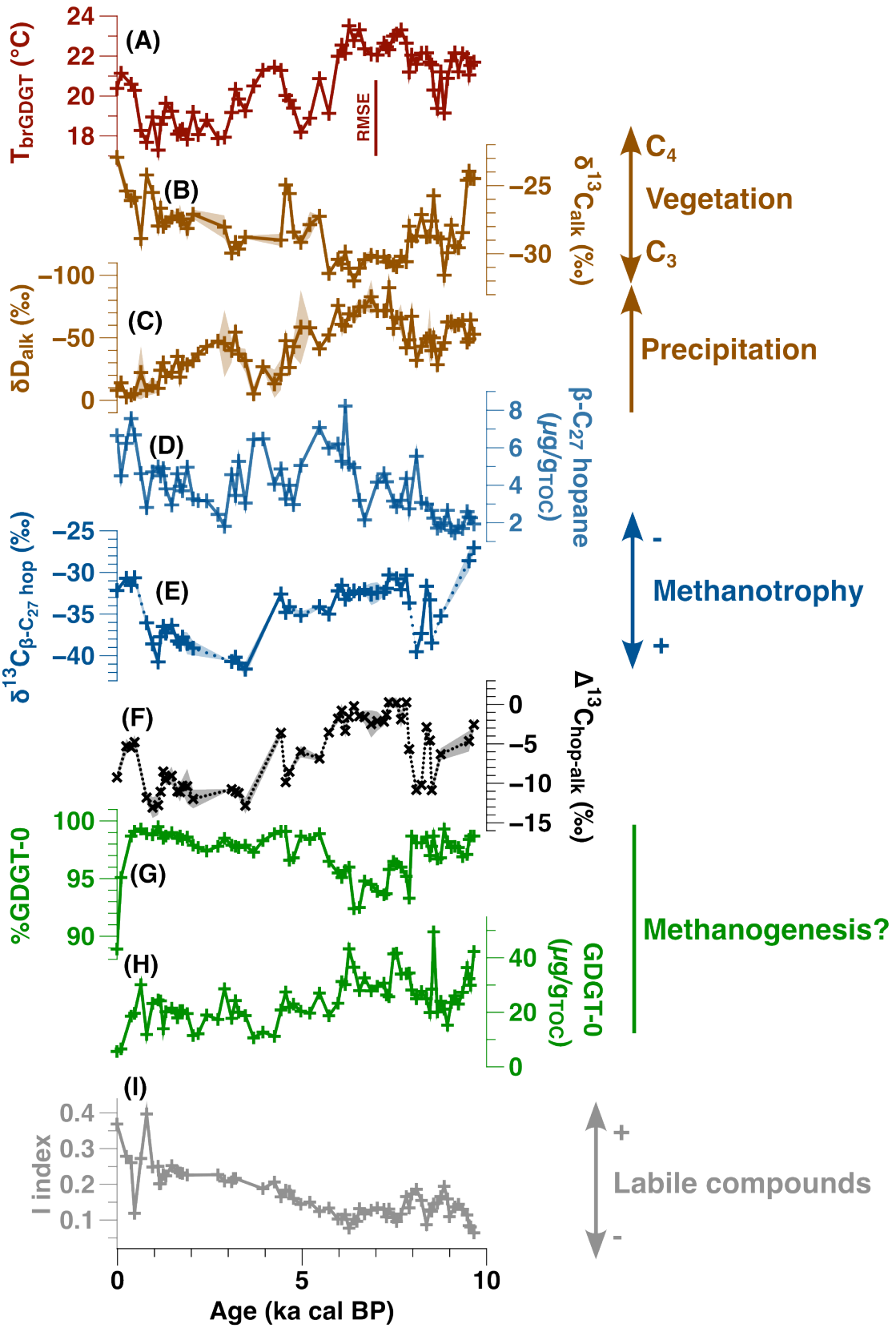

Figure 51: Comparison of methanotrophy and methanogenesis proxies with other paleoclimatic and paleoenvironmental proxies at the NGaoundaba peat deposit. (A) temperature based on brGDGTs reconstructed using the T0 calibration from Dearing Crampton-Flood et al. (2020), (B) and (C) carbon and hydrogen isotopic composition of n-C_{31} n-alkanes. Hydrogen

isotopic composition are corrected for C_3/C_4 vegetation changes as presented in chapter 5. (D) Concentration ($\mu g/g_{TOC}$) and (E) carbon isotopic composition of β-C_{27} hopanes, (F) $\Delta^{13}C_{hop\text{-}alk}$, (G) %GDGT-0 calculated as proposed by Inglis et al. (2015) and concentration of GDGT-0 ($\mu g/g_{TOC}$) and (I) I-index, bulk organic data presented in chapter 3.

methanotrophy (Hoyos-Santillan et al., 2019). Thus, drier conditions at the NGaoundaba peat deposit likely enhanced oxic conditions, favoring aerobic methanotrophs and enhancing methane oxidation efficiency.

4.2. Reconstructing methanogenesis in peat sediment

The main problem with reconstructing past methanogenic activity in peat deposit is that methanogenesis is an anaerobic process that can, in theory, happens at any depth in the peat sediment. Therefore, the signal reconstructed using lipid biomarkers might not only be a paleo-signal but also a present-day signal from the living microbial community. In tropical peatlands, CH_4 production has been reported at least down to 80 cm (Inubushi et al., 1998; Melling et al., 2005) but other studies suggest a dominance of subsurface CH_4 production above 30 cm (Wright et al., 2011). For the moment, in the tropics, metagenomic analyses usually focuses on the top 50 cm of peat deposits and particularly on peat swamp forest and some studies report methanogens while others don't (e.g., Jackson et al., 2009; Kanokratana et al., 2011; Too et al., 2018). Wright et al. (2011) suggested that greater peat lability in surface peat may enhance surface methane production compared to deep peat. In particular, Cyperus sites are characterized by high microbial content and enzyme activity in the surface peat, likely leading to nutrient and substrate limitation in deep peat (Wright et al., 2011). The NGaoundaba peat deposit is also dominated by Cyperus and may, therefore, experience a similar pattern of gas production. The I-index values, which reflects the lability of the organic matter, suggests that sediment older than 6 ka cal BP (>3m deep) presents a low content of labile organic matter, precluding methane production at depth (Schaaff et al., 2023). In addition, there is no clear relationship between the concentration of hopanes or isoGDGTs and depth or age. Therefore, methane production in the deep horizons of the NGaoundaba peat deposit is probably limited and the lipid biomarkers investigated probably record a paleo-signal. Biomarkers may still record an integrated signal of methanogenesis other several meters of peat above 3 m depth. Whether the deep production significantly biased the paleo-signal or not remain questionable.

Methanogenic archaea mostly synthesize GDGT-0 and only small amount of other isoGDGTs (Koga et al., 1993; Weijers et al., 2006; Blaga et al., 2009). Thus, GDGT-0 likely derived primarily from methanogens in peat sediment (Weijers et al., 2006). Blewett et al. (2022) presented $\delta^{13}C$ values of isoGDGTs in peat sediment and further confirmed that the methanogens are

major contributors of the GDGT-0 pool while isoGDGT-1 to -3 have a distinct origin. At the NGaoundaba peat deposit, the distinct variation in the relative abundance of GDGT-0 compared to other isoGDGTs (Figure 50) is consistent with previous findings.

The increase peat water level during the African Humid Period likely favored anoxic conditions and could have promote the development of methanogens (Figure 52). This pattern was previously observed in the Hongyuan peat deposit in the study based on the concentration of archeaol (Zheng et al., 2014). However, at the NGaoundaba peat deposit, the %GDGT-0 decreases during the African Humid Period, but this decrease is mainly driven by the increase in Crenarchaeol. The isoGDGT-1 to -4 also increase during this period but are not taken into account in the calculation of the %GDGT-0 ratio. We suggest that the decrease in %GDGT-0 indicates a decreased proportion of methanogens in the archaeal community but do not necessarily imply a decrease in the methanogenesis itself. The slightly decreasing concentration of GDGT-0 (Figure 51) might suggest a slight decrease of methanogenesis during the Holocene or a slight influence of deep isoGDGT-production with a progressive accumulation of GDGT-0 (Figure 52).

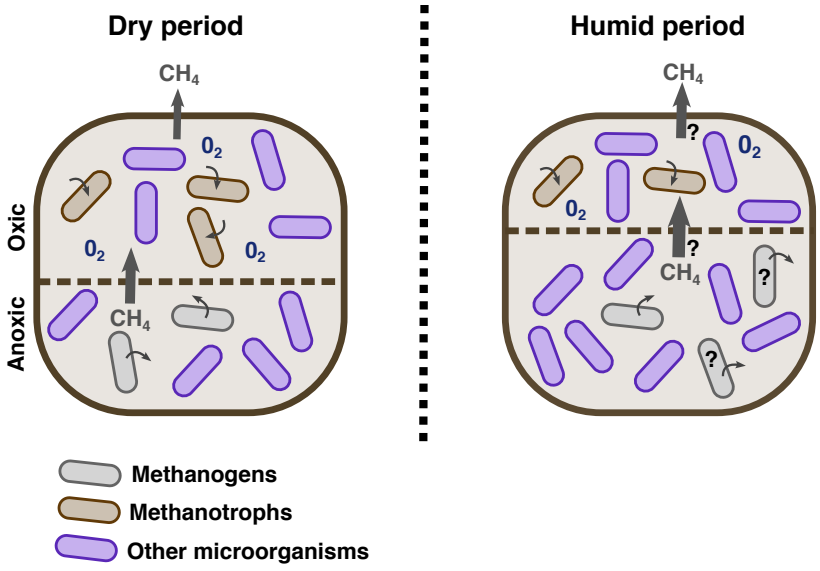

Figure 52: Simplified representation of methane cycle during dry and humid periods at the NGaoundaba peat deposit reconstructed based on hopanes and GDGT-0.

Conclusions and perspectives

Based on microbially-derived biomarkers, we reconstruct the evolution of methane cycling in a tropical peat deposit. In higher latitude peat deposits, temperature has been suggested as an important driver of methane production and consumption with increasing temperature enhancing both methanogenesis and methanotrophy (Elvert et al., 2016). At the NGaoundaba peat deposit, higher brGDGT-reconstructed temperatures are recorded during the African

Humid Period but coincide with a low methane oxidation efficiency. We suggest that in monsoon-driven regions, rainfall amount and peat hydrologic conditions are more important drivers of the methane cycle than increasing temperature.

The increase in methane oxidation efficiency leads to a better recycling of methane produced by the methanogens and may be related to a decrease in methane emission as less methane reaches the surface of the peat and is release in the atmosphere.

In monsoon driven region, methanotrophy is likely enhanced by dry conditions as testified by depleted carbon isotopic composition of $<C_{30}$ hopanes. We demonstrate that the proportions of methanogens in the archaeal community was minimal during the most humid period. The present isoGDGT data were inconclusive to determine a period of increase methanogenesis as the most humid period seems to have enhanced the global archaeal community, obscuring the specific biosignatures of methanogens.

The possible production of archaeal isoGDGT in deep peat layers has to be taken into consideration. However, the absence of a clear correlation between isoGDGT concentration and depth, the low I-index ratio in deep peat layers and the good correspondence of isoGDGT variations with other paleoclimatic proxies (temperature based on brGDGT, precipitation based on n-C_{31} alkane) unaffected by this bias suggest that the influence of deep production might be limited at the NGaoundaba peat deposit, especially below 3m depth.

Methanotrophic and methanogenic microbial communities present complex responses to changes in climatic conditions (Peltoniemi et al., 2016) that are difficult to precisely decipher only based on lipid biomarkers. Further analyses of microbial activity and microbial communities in peat and particularly in deep peat (below 2m) coupled to biomarker analyses are needed to better constraint the signal from lipid biomarkers and their potential as paleoclimatic proxy.

Supplementary material:

A) Comparison of the different GDGT-0 based methanogenesis proxies

We compare three different ratios based on isoGDGTs that have been proposed as proxies for methanogenesis in various settings.

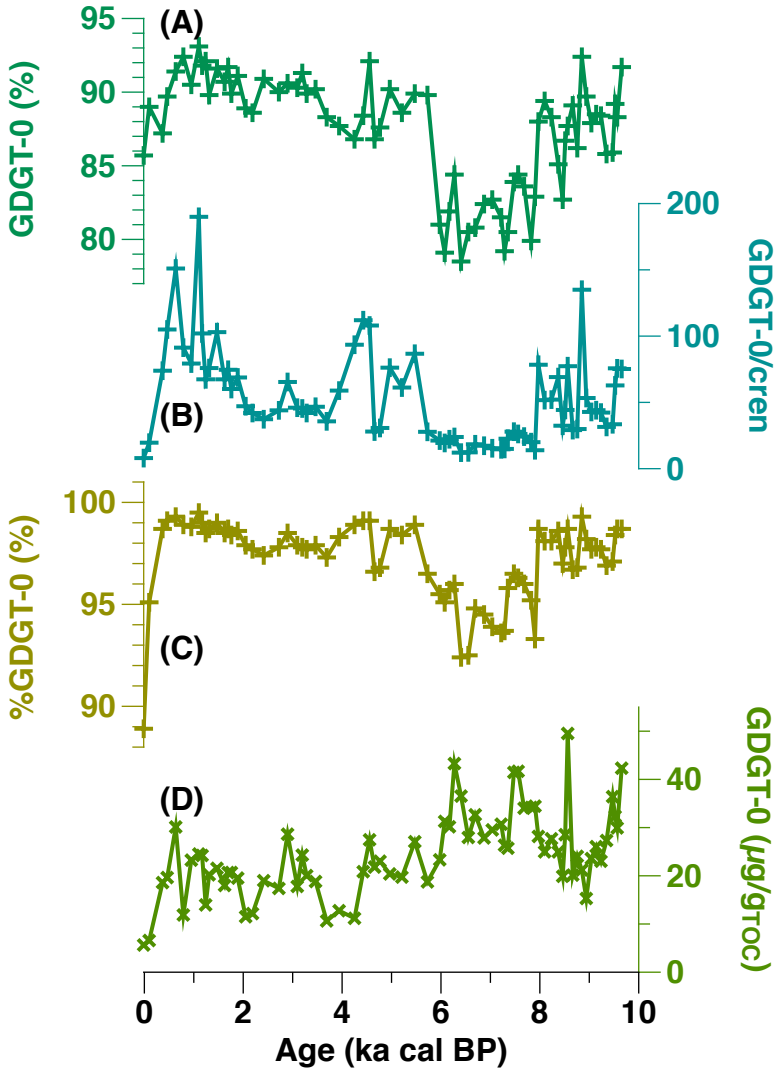

Figure S 11: Comparison of the different ratio proposed to reconstruct past methanogenesis. (A) Relative abundance of GDGT-0 calculated as proposed by Zheng et al. (2015) taking into account the GDGT-0 to the GDGT-4 but not the Crenarchaeol, (B) GDGT-0/Crenarchaeol ratio as proposed by Blaga et al. (2009) and (C) %GDGT-0 calculated as proposed by Inglis et al. (2015) taking into account only the GDGT-0 and the Crenarchaeol. GDGT-0/Crenarchaeol and %GDGT-0 were developed for lake and marine environment, respectively and, to our knowledge, were not tested for peat sediment. We consider the Crenarchaeol with its main isomer.

The abundance of GDGT-0 calculated as proposed by Zheng et al. (2015) and the %GDGT-0 calculated as proposed by Inglis et al. (2015) present similar variation with high values except between 7.9 and 5.7 ka cal BP and in the 2 most superficial samples (Figure S 11 A and B). The GDGT-0/Cren ratio proposed by Blaga et al. (2009) also present low values between 7.9 and 5.7 ka cal BP and in the two most superficial samples but the contrast with the post AHP period is less important. In addition, peaks are observed during late Holocene are not recorded in the two other proxies. An increase in GDGT-0/Cren ratio is recorded during the two first dry event deposit between 8.9 and 7.9 ka cal BP and after the end of the AHP between 5.5 and 4 ka cal BP. A slight increase is also recorded during the same periods in the %GDGT-0 (Figure S 11 B and C). This could indicate an increase of methanogenesis during these periods but is not supported by the changes observed in the concentration of GDGT-0 (Figure S 11 D).

Chapter 8: Exploring understudied lipid biomarkers: insight into botryococcenes, des-A-triterpenoids and 5-*n*-alkylresorcinols records from the NGaoundaba peat deposit

Abstract:
This section revisits some of the research avenues that are currently being investigated but could not be completed within the thesis work schedule. This chapter presents some preliminary results concerning families of compounds that are not frequently investigated for now. We present the distribution and concentration of these compounds in peat sediments, and we complement the results with analyses of fresh plant samples. The aim is to formulate hypotheses concerning the origin of these compounds in the NGaoundaba peat deposit and their potential for paleoclimate and paleoenvironmental investigation in tropical peatlands. This chapter is divided into three independent parts, each focusing on one family of compounds.

Keywords: Botryococcenes, des-A-triterpenoids, 5-*n*-alkylresorcinols

Part 1: Botryococcenes

1. Introduction

Botryococcenes are hydrocarbon compounds produced by several strains of the unicellular colonial green alga *Botryococcus braunii* race B (Metzger et al., 1985a, 1985b, 1988). They are found in the sediments of freshwater lakes and wetlands (e.g., Huang et al., 1999; Gao et al., 2007; de Mesmay et al., 2008; Atahan et al., 2015). A wide diversity of botryococcenes has been described, and their variations in sediments appear to reflect complex physiological and/or physicochemical variations (Fuhrmann et al., 2003; Smittenberg et al., 2005; Grossi et al., 2012). A succession of botryoccocenes with different structures (acyclic, monocyclic, and bicyclic) has been recorded at Lake Masoko, suggesting blooms of distinct strains of *Botryococcus braunii* with distinct physiological preferences (Grossi et al., 2012). The carbon isotopic composition of botryococcenes can exhibit contrasting values from -6.2 to -35.4 ‰ in Lake Huguang (South China), which have been suggested to reflect changes in the carbon source (CO_2 to dissolved bicarbonate) (Fuhrmann et al., 2003) and more globally to environmental conditions (nutrient availability, pH, etc.) (Huang et al., 1999; Atahan et al., 2015).

We present preliminary work on botryococcenes from the NGaoundaba peat deposit. Using mass spectra and the Kovats retention Index, we propose a tentative identification of the four most abundant botryococcenes by comparing them with previously published literature (Huang et al., 1999; Gao et al., 2007; de Mesmay et al., 2008) but their precise structure still need to be confirmed. Using PCA analyses, we present statistical clustering of botryococcenes detected at the NGaoundaba peat deposit. The abundance and concentration of botryococcenes are compared to the other paleoclimatic and paleoenvironmental proxies, interpreted in terms of variation of the microalgal community and supported by the carbon isotopic composition of botryococcenes.

2. Methods

We followed the same method as presented in previous chapters 4 and 5. Botryococcenes were studied in 73 samples. Briefly, lipid biomarkers were extracted using a MARS 6 CEM microwave extraction system. The extraction was performed twice with 10 mL of dichloromethane (DCM)/methanol (3:1, v/v) each time. The resulting total lipid extract was separated into three fractions. The botryococcenes were eluted in the first fraction (hydrocarbon fraction) with 8 mL of hexane. Identification and quantification were performed using GC-MS analyses (Agilent 6890N GC coupled to an Agilent 5975C MSD and Agilent 7890B

GC coupled to an Agilent 5977B MSD). Semi-quantification was performed using the TIC by comparison with an external standard solution containing cholestane.

Botryococcenes were partially identified based on their mass spectral characteristics (fragmentation and Kovats retention index) and on previous literature data (Huang et al., 1999; Gao et al., 2007). Kovats retention index (RI) (Kovats, 1958) was calculated using the following formula with R the GC retention time, x the compound of interest, n and n+1 the chain length of the nearest n-alkane eluting before and after x, respectively, and :

$$RI = 100 * \frac{(R_x - R_n)}{(R_{n+1} - R_n)} + 100 * n$$

For carbon isotopic measurements, the hydrocarbon fraction was further separated into "saturated" and "unsaturated" fractions using column chromatography with $AgNO_3$-impregnated silica gel following the procedure presented in chapter 4. While the n-alkane eluted in the "saturated" fraction, the botryococcenes eluted in the "unsaturated" fraction. We only analyzed one "unsaturated" fraction (375cm-depth – 7.3 ka cal BP). Carbon isotopic measurements follow the same method as presented in chapter 4 and 5.

3. Results and discussion

3.1. Tentative identification

A total of 8 botryococcenes were detected (Figure 53). Some of them are present in very low amount and/or in only a few samples. We focus our attention on the 4 major botryococcenes (a,b, e, g). Botryococcenes a and b were already presented and interpreted in chapter 6.

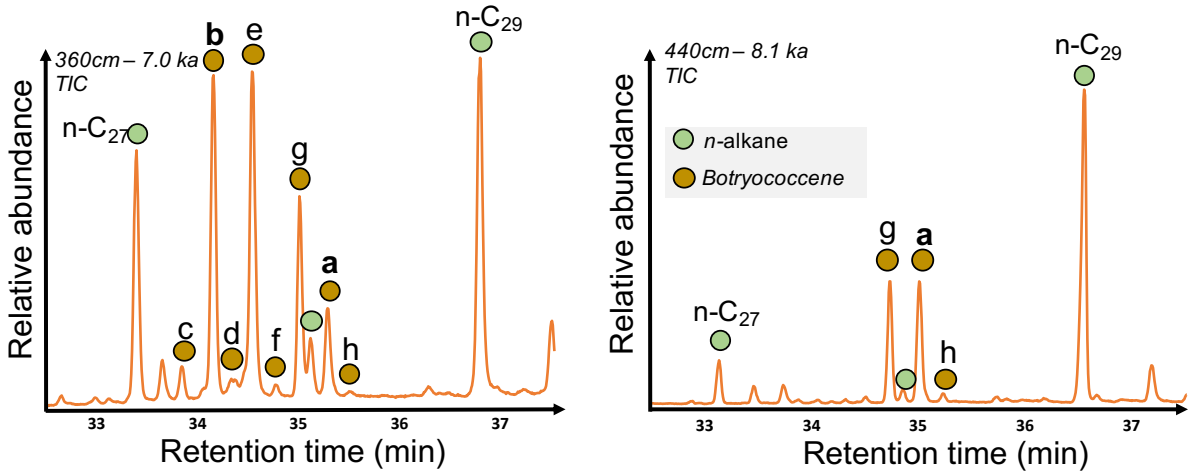

Figure 53: GC-MS partial chromatograms of the hydrocarbon fractions of two samples with contrasting botryococcenes assemblages at 360cm-depth (left panel) and 440cm-depth (right panel) depth. The ages of the samples are given in ka cal BP.

Compound *a* presents a molecular ion (M^+) of 466 ($C_{34}H_{58}$) and a Kovats retention index of 2810 (Figure 54). The Kovats retention index and the diagnostic ions in mass spectrum are

really close to the compound n°25 describe by Gao et al. (2007). This compound presents 4 double bounds and 2 ring (Gao et al., 2007). Compound g presents a molecular ion (M^+) of 470 ($C_{34}H_{62}$) and a Kovats retention index of 2794 (Figure 54). The Kovats retention index and the diagnostic ions in mass spectrum are really close to the compound n°24 describe by Gao et al. (2007). This compound presents 3 double bounds and 1 ring (Gao et al., 2007).

Compound b presents a molecular ion (M^+) of 452 ($C_{34}H_{58} – C_{33:6}$) and a Kovats retention index of 2744 (Figure 54). This compound presents all the diagnostic ions present in the compound 5 from Huang et al. (1999) but the Kovats retention index is different (RI=2731). Similarly, compounds e presents a molecular ion (M^+) of 456 ($C_{34}H_{60} – C_{33:4}$) (Figure 54) and diagnostic ions are consistent with the compound 3 described in Huang et al. (1999) and identified as the Sacredicene (Huang et al., 1995) but the Kovats retention index is larger (RI=2766) than the Kovats retention index given in the study from Huang et al. (1999) (RI=2739). The identification of these two botryococcenes still needs to be confirmed.

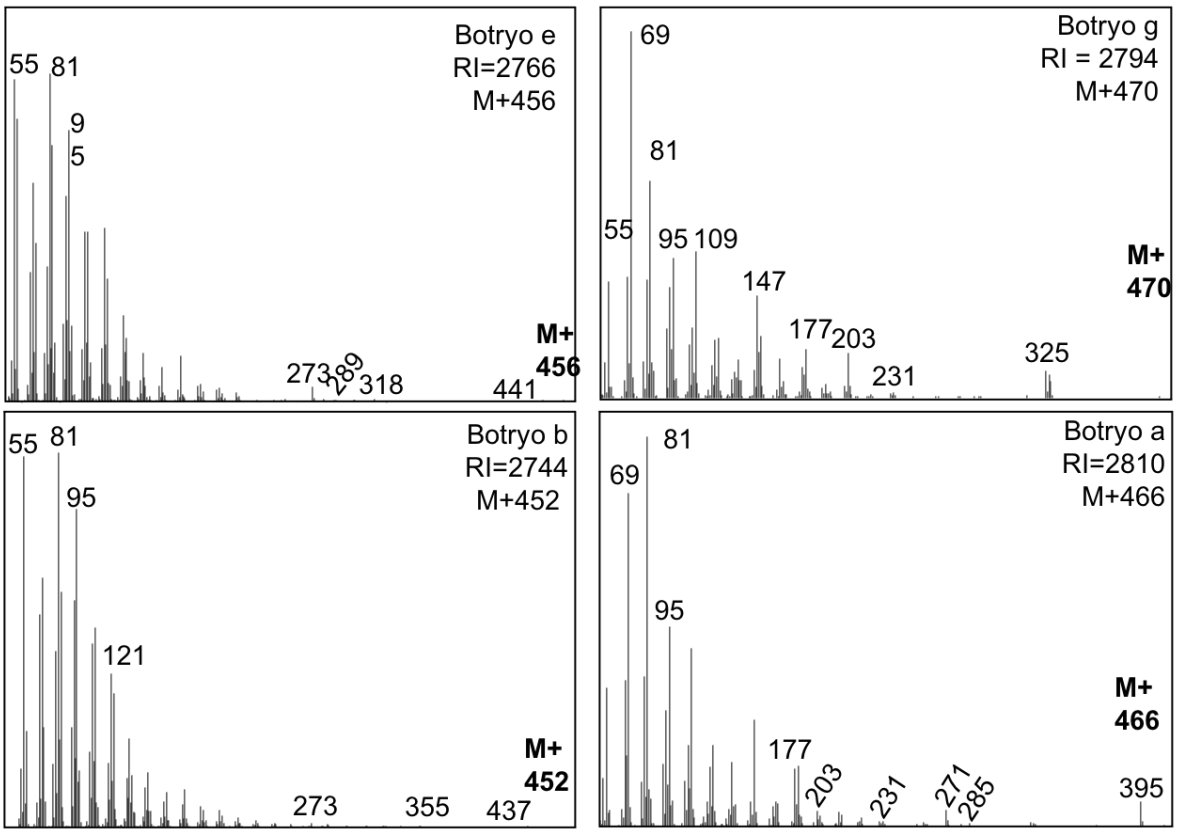

Figure 54: Mass spectrum of the four most abundant botryococcenes. The molecular ion (M^+) usually presents a really low intensity but was detectable in some of the samples. We indicate the Kovat retention index for each compound.

3.2. Variation of botryococcenes in the Ngaoundaba peat deposition

Botryococcenes present high variations in their concentrations. Botryococcene a and g ranges from 0 to 21.7 and 19.1 µg/g_{TOC}, respectively, with a mean concentration of 4.9 and 3.1 µg/g_{TOC}, respectively (Figure 55). The concentration of botryococcenes a and g globally decrease during the Holocene with lowest concentrations recorded during the last 1ka. Highest concentrations are recorded during early Holocene and between 8.5 and 7.9 ka cal BP. Botryococcenes b and e are mostly present between 9.7 and 9.2 ka cal BP and between 8 and 5 ka cal BP corresponding to the African Humid Period (Figure 55) (see chapter 5).

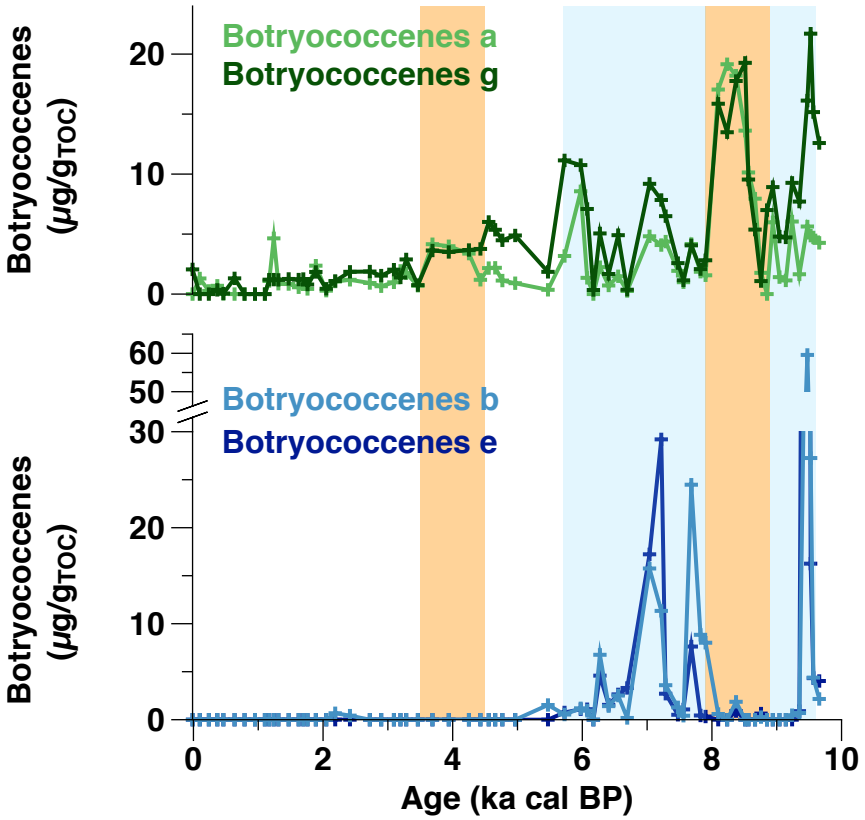

Figure 55: Concentration of the four most abundant botryococcenes (µg/g_{TOC})

We perform PCA analyses taking into account all botryococcenes detected in the NGaoundaba peat deposit to try to find grouping between the different compounds (Figure 56). Botryococcenes can be divided into two cluster of compounds. The grouping observed on figure 55 is confirmed by the PCA analyses with compounds a and g forming one cluster with compounds h and f and compounds e and b forming the second cluster with compounds c and d (Figure 56). This clustering is consistent with the carbon isotopic composition of botryococcenes (Table 6). Grossi et al. (2012) show a succession of botryococcenes structure (acyclic, monocyclic and bicyclic) in the sediment from lake Masoko. Based on the tentative identification of botryococcene, the clustering doesn't seem to depend on the structure of the

compounds (acyclic, monocyclic and bicyclic) at the NGaoundaba peat deposit. Compound a and g, forming a cluster together, are bicyclic and monocyclic botryococcenes, respectively. The clustering mostly regroups compounds with similar carbon numbers (C_{33} vs C_{34}). The close carbon isotopic composition of the compound a and g and compound b and e, respectively, suggest similar sources. However, wild strain of *Botryococcus braunii* race b seems to produce various botryococcenes with various chain length (Metzger et al., 1985a, 1988).

The paleoclimatic interpretation were presented in chapter 6. Briefly, botryococcenes were interpreted as algal blooms and changes in the distribution of botryococcenes, particularly during the dry event between 8.9 and 7.9 ka cal BP, suggest changes in the environmental conditions (nutrient input, water level, …).

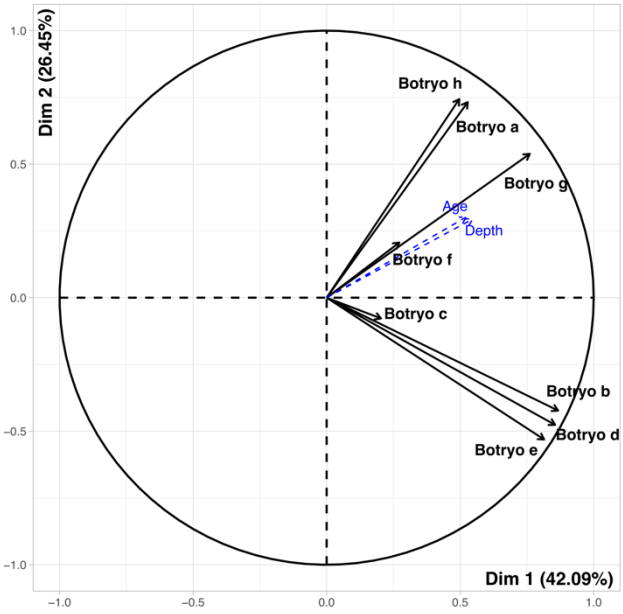

Figure 56: PCA analysis based on botryococcene concentrations (µg/g_{TOC}). See Figure 53 and Figure 54for the labelling. Age and depth are given as complementary variable.

Table 6: The four most abundant botryococcenes.

N°	Kovats	M+	Formula	$\delta^{13}C_{botryo}$	Reference
b	2744	452	$C_{33}H_{56}$	-27.0 ± 2.0 ‰	N°5? from Huang et al. (1999)
e	2766	456	$C_{33}H_{60}$	-25.9 ± 2.1 ‰	N°3? from Huang et al. (1999)
g	2794	470	$C_{34}H_{62}$	-13.9 ± 0.5 ‰	N°24 from Gao et al. (2007)
a	2810	466	$C_{34}H_{58}$	-17.57 ± 0.6 ‰	N°25 from Gao et al. (2007)

Conclusions and perspectives

We present a 10-ka record of botryococcenes variation from the NGaoundaba peat deposit. Botryococcenes can be divided into two clusters with really distinct variations during the Holocene. These two clusters seem to group compounds with the same carbon number and the similar carbon isotopic composition within each cluster further suggest similar sources or that the botryococcenes were produced under similar environmental conditions.
In order to precise the identification of major botryococcenes, we also performed hydrogenation on 3 samples with contrasted distribution on lipid biomarkers. This technique hydrogenates all the double bounds in a compound. The comparison of the hydrogenated and of the non-hydrogenated chromatograms allow to have access to the number of unsaturation in the compound and some information on their position by looking at the mass fragmentation. The interpretation of the results of these analyses is not completed yet but will help to confirm the identification of the botryococcenes presented here.

Part 2: Des-A-triterpenoids

1. Introduction

Des-A-triterpenoids are triterpenoids derivatives commonly found in various geological and sedimentological settings (e.g., Trendel et al., 1989; Stout, 1992; ten Haven et al., 1992; Huang et al., 2008). They are proposed to be diagenetic products of pentacyclic triterpenoids from higher plants (Trendel et al., 1989), produced either by photochemistry (Corbet et al., 1980) or by anaerobic microbial processes (Lohmann et al., 1990). In sediments, des-A-triterpenoids have been used to infer past changes in paleoenvironment (Jacob et al., 2007; Regnery et al., 2013; van Bree et al., 2016). However, it has also been suggested that des-A-triterpenoids record reflects diagenetic (anoxic) conditions rather than any paleoclimatic signal (Huang et al., 2008). Zheng et al. (2010) suggest that des-A-triterpenoids are strongly impacted by both vegetation changes and microbial activities. Based on the carbon isotopic signature of des-A-lupane, usually the most abundant des-A-triterpenoids in sediment, van Bree et al. (2016) suggested that this compound derives from C_3 plants and can be used as a direct proxy of C_3 plant $\delta^{13}C$ values.
We here report a preliminary work on des-A-triterpenoids presence and distribution at the NGaoundaba peat deposit. A total of 8 des-A-triterpenoids were detected, some of which could not be structurally characterized. Based on the qualitative and quantitative distributions of the most abundant des-A-triterpenoids, on their carbon isotopic composition, on PCA analyses and on the comparison with other paleoclimatic and paleoenvironmental proxies, we

gained more insight into the origin and the potential paleoclimatic and paleoenvironmental significance of these compounds.

2. Methods

We followed the same method as presented in previous chapters 4 to 7. Des-A-triterpenoids were studied in 73 samples. Briefly, lipid biomarkers were extracted using a MARS 6 CEM microwave extraction system. The extraction was performed twice with 10 mL of dichloromethane (DCM)/methanol (3:1, v/v) each time. The resulting total lipid extract was separated into three fractions. The des-A-triterpenoids were eluted in the first fraction (hydrocarbon fraction) with 8 mL of hexane. Identification and quantification were performed using GC-MS analyses (Agilent 6890N GC coupled to an Agilent 5975C MSD and Agilent 7890B GC coupled to an Agilent 5977B MSD). Semi-quantification was performed using the TIC by comparison with an external standard solution containing cholestane.

Following GC-MS analyses, des-A-triterpenoids were partially or precisely identified based on their mass spectral characteristics and on previous literature data (Table 7). Note that some mass spectrums of des-A-triterpenoids are really similar to each other and some tentative identifications also rely on comparison of retention time between the NGaoundaba peat deposit and published literature. Kovats retention index (RI) (Kovats, 1958) was calculated using the following formula with R the GC retention time, x the compound of interest, n and n+1 the chain length of the nearest n-alkane eluting before and after x, respectively, and :

$$RI = 100 * \frac{(R_x - R_n)}{(R_{n+1} - R_n)} + 100 * n$$

Carbon isotopic measurements follow the same method as presented in chapter 4 and 5.

3. Results and discussion

3.1. Tentative identification of des-A-triterpenoids

Des-A-triterpenoids, eluting between n-C_{23} and n-C_{26} alkane, were detected in 41 out of 73 samples (Figure 57). A total of 8 triterpenoids with molecular ions (M+) of 326, 328 or 330 were detected. Table 7 and Figure 58 summarize the mass spectra and putative identifications of these compounds. The compound with a molecular weight at m/z 330 presents present a characteristic fragment $[M-43]^+$ corresponding to the loss of an isopropyl group (Jacob et al., 2007) and was identified as des-A-lupane. Compound (a) to (d) and (g) are mono-unsaturated des-A-triterpenes (M+328). Compounds (a), (b) and (c) were tentatively identified as des-A-olean-13(18)-ene, des-A-olean-12-ene and des-A-urs-13(18)-ene, respectively, based on the comparison with previous literature data (See Table 7 and Figure 58 for mass spectrum, key

fragments and references). Compound (d) has the same $[M-43]^+$ characteristic fragment as des-A-lupane and could be a des-A-lupene. Logan and Eglinton (1994) and Huang et al. (2008) reported compound (g), but this compound was not structurally characterized. It most likely has an ursane or oleanane skeleton. Two di-unsaturated des-A-triterpenes (M+ 326) were found but remain unidentified; compound (h) seems to correspond to the compound VIII with a lupane skeleton reported by Mille et al. (2006).

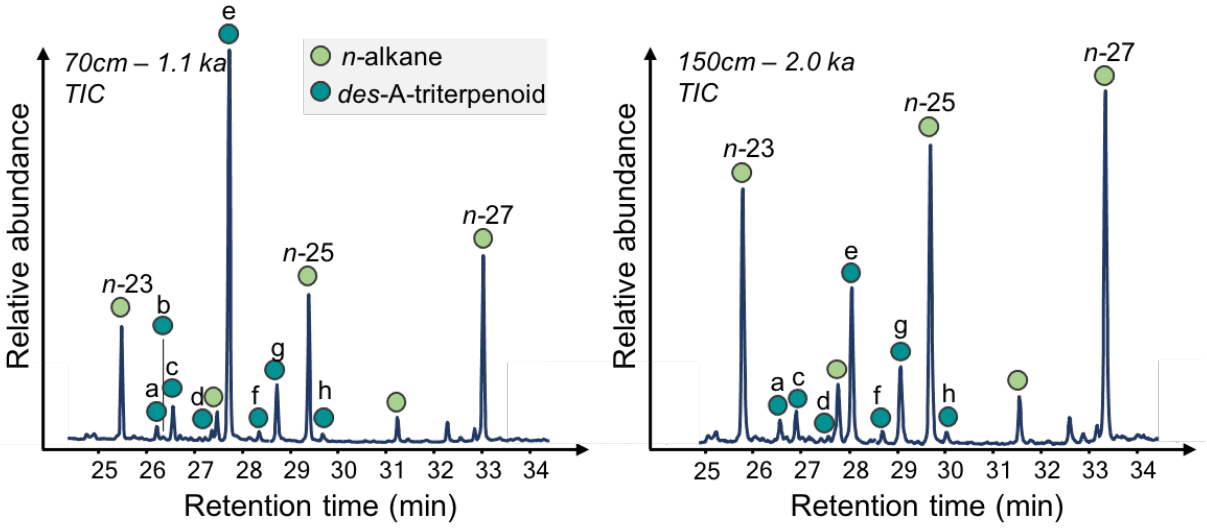

Figure 57: GC-MS partial chromatograms of the hydrocarbon fractions of two samples with contrasting des-A-triterpenoid distributions at 70cm-depth (left panel) and 150cm-depth (right panel) depth. The ages of the samples are given in ka cal BP

Table 7: List of des-A-triterpenoids reported in the NGaoundaba peat deposit, including molecular ions, key fragments and potential identification.

Peak No.	Kovat index	M+	Key ions (in order of decreasing abundance)	Formula	(Tentative) identification	Ref
a	2336	328	313, 189, 205, 328, 203, 218, 233, 175, 161, 248	$C_{24}H_{40}$	*des*-A-olean-13(18)-ene	A, D, F
b	2343	328	203, 218, 155, 313, 189, 328, 175, 295, 161	$C_{24}H_{40}$	*des*-A-olean-12-ene	A, D
c	2353	328	177, 313, 189, 175, 328, 149, 161, 204, 218	$C_{24}H_{40}$	*des*-A-urs-13(18)-ene	D
d	2395	328	136, 149, 205, 328, 163, 177, 191	$C_{24}H_{40}$	-	-
e	2413	330	149, 163, 191, 330, 177, 287, 206, 315	$C_{24}H_{42}$	*des*-A-lupane	B, D, E, F
f	2446	326	136, 189, 147, 203, 326, 161, 175, 230, 292, 311	$C_{24}H_{38}$	-	-
g	2465	328	217, 328, 189, 149, 175, 245, 204, 259, 161, 313	$C_{24}H_{40}$	-	A*, E*, F*
h	2516	326	326, 189, 175, 271, 161, 203, 230	$C_{24}H_{38}$	-	C

A: Logan and Eglinton (1994) B: Woodhouse et al. (1992) C : Mille et al. (2006) D: Jacob et al. (2007) E: Huang et al. (2008) F: Zheng el al. (2010)

* compound detected but not precisely characterized

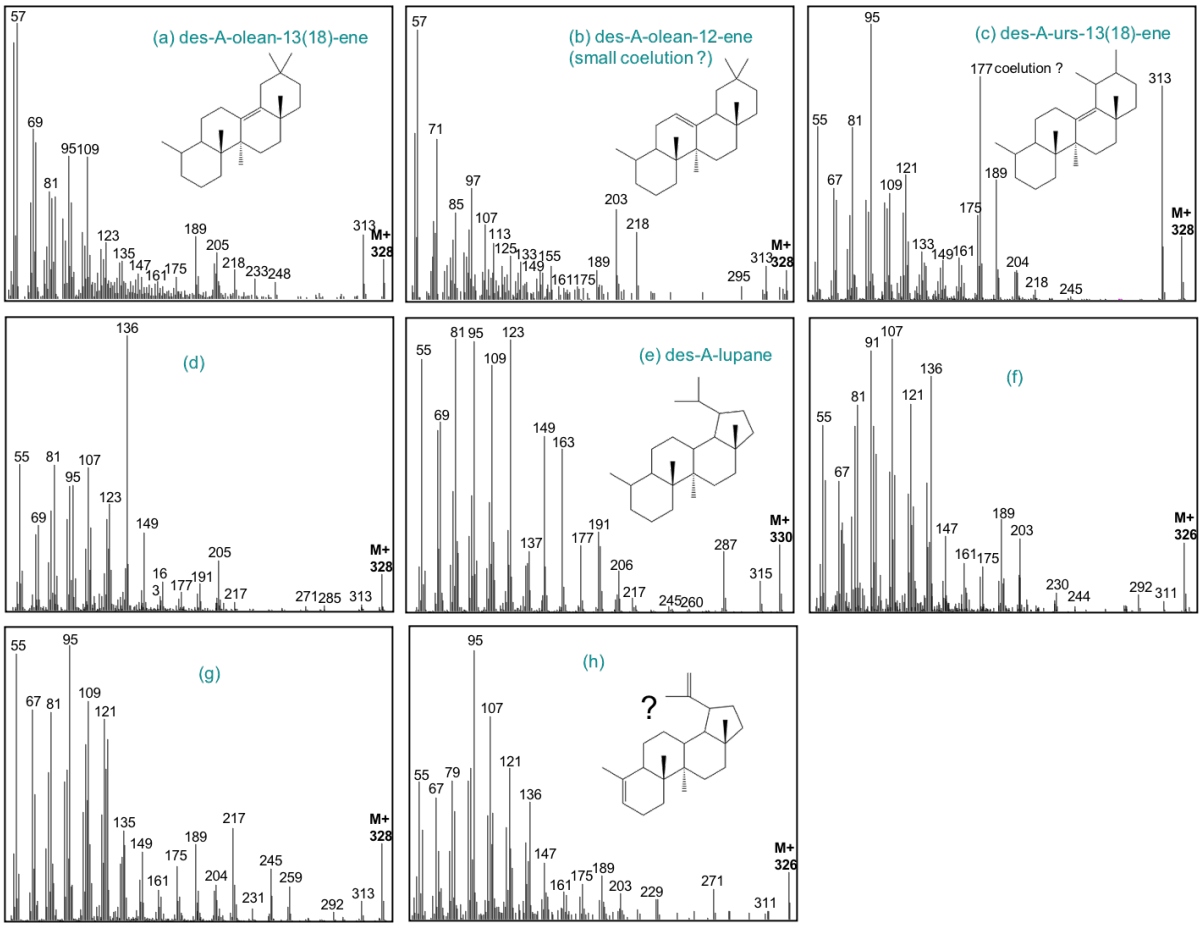

Figure 58: Mass spectra of des-A-triterpenoids and (tentative) identifications and structures.

3.2. Origin of des-A-triterpenoids

Des-A-lupane is the most abundant des-A-triterpenoids in the NGaoundaba peat record (Figure 59). It is frequently reported as the most abundant des-A-triterpenoids in lake and peat sediment (e.g., Jacob et al., 2007; Regnery et al., 2013; van Bree et al., 2016). It has sometimes been related with a distinct source compared to other des-A-triterpenoids (e.g., Jacob et al., 2007; Regnery et al., 2013). A PCA analysis shows that all des-A-triterpenoids from the NGaoundaba peat deposit are tightly related, with the first dimension of the PCA accounting for about 80 % of the variability (Figure 60). There is no evidence of significantly distinct sources of precursors of des-A-triterpenoids at the NGaoundaba peat deposit. The absence of des-A-triterpenoids above 40 cm-depth (< 0.6 ka cal BP) could imply either an absence of des-A-triterpenoids precursors before 0.6 ka ago or that the des-A-triterpenoids diagenesis is still incomplete above 40 cm-depth. He et al. (2022) suggests that des-A-triterpenoids might derived from submerged macrophytes in Lake Wuliangsu (China) and could represent a new proxy for submerged macrophytes. However, at the NGaoundaba,

there is no des-A-triterpenoids during the AHP when input from submerged macrophytes were significant (see chapter 6).

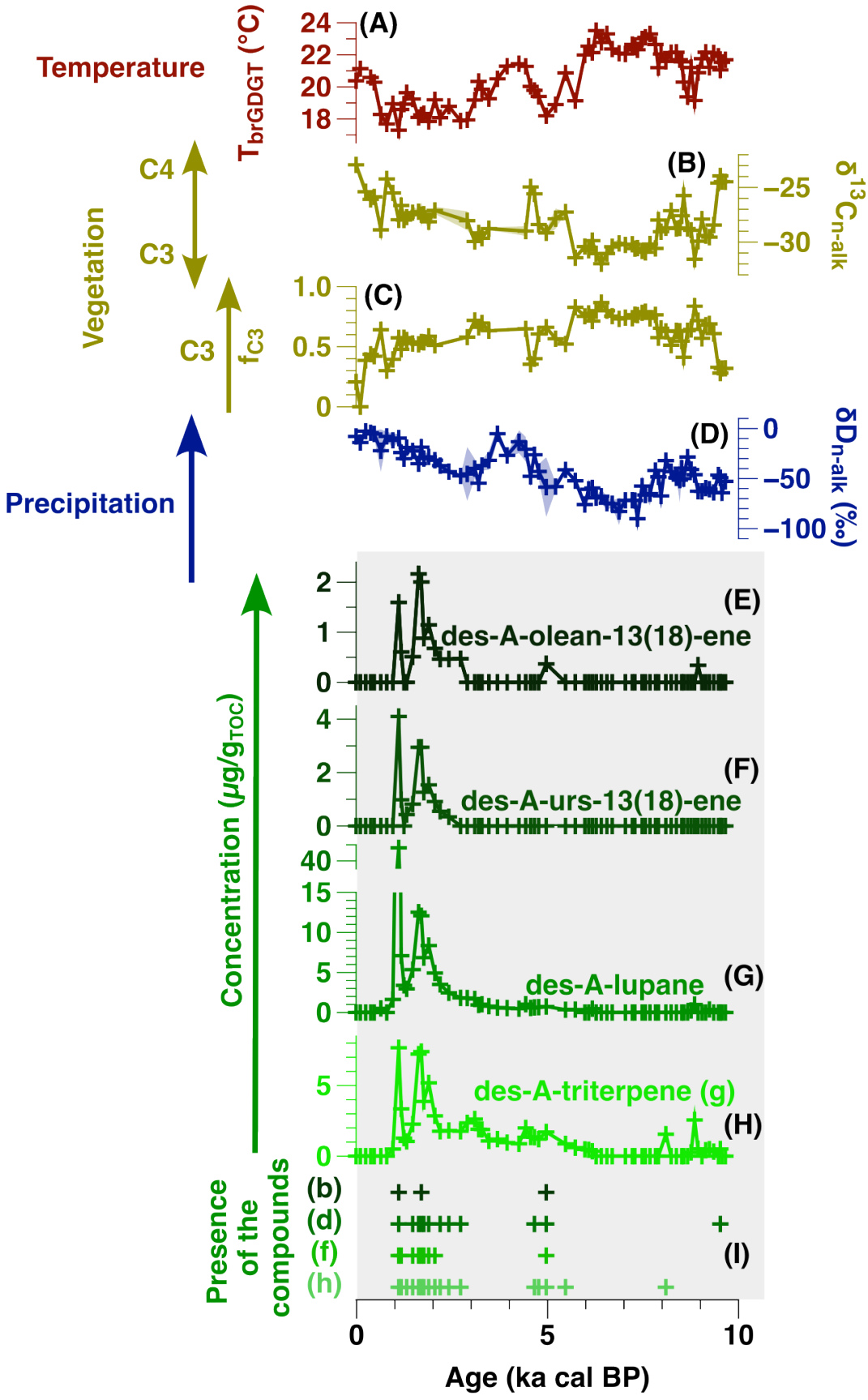

Figure 59: Concentrations of the four most abundant des-A-triterpenoids (µg/g_{TOC}) (E to H) and presence of the four less abundant des-A-triterpenoids (I). Temperature based on brGDGTs (A), carbon isotopic and fractional abundance of C_3 plants based on the carbon isotopic composition of n-C_{31} alkane (B and C) and hydrogen isotopic composition of n-C_{31} alkane and corrected for C_3/C_4 vegetation changes as presented in chapter 5.

The two most abundant des-A-triterpenoids start increasing around 6.2 ka cal BP slight before the end of the AHP recorded in T_{brGDGT} and $\delta^{13}C_{n\text{-}alk}$ suggesting that the source of these compound might be only present since the end of the AHP (Figure 59).

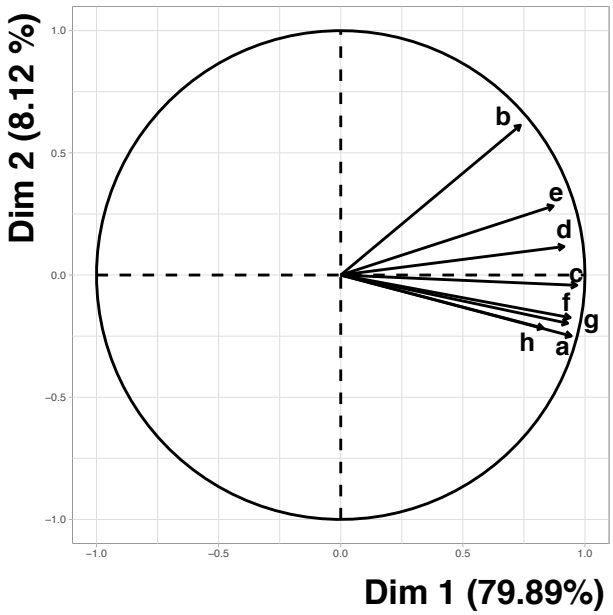

Figure 60: PCA analysis based on des-A-triterpenoids concentrations. See Figure 58 and Table 7 for the labelling.

Carbon isotopic values of des-A-lupane were obtained for 11 samples out of the 73 samples. The range of values is -27.6 to -30.0 ‰, with a mean value of -28.5 ‰. The carbon isotopic signature indicates that des-A-lupane is primarily derived from C_3, which is consistent with previously published results (Regnery et al., 2013; van Bree et al., 2016). According to Van Bree et al. (2016), the carbon isotopic composition of des-A-lupane could be used as a proxy for the stable carbon isotopic composition of local C_3 plants. In the present case, the des-A-lupane concentrations do not correlate with the fraction of C_3 plants (f_{C3}) reconstructed based on the carbon isotopic composition of n-C_{31} alkane (Figure 59). It is possible that des-A-lupane derives exclusively from C_3 plants but that its ^{13}C composition is not indicative of the entire C_3 vegetation carbon isotopic signature due to i) small but significant differences among the carbon isotopic compositions of C_3 plants (e.g., Kohn, 2010; Garcin et al., 2014) and ii) not all C_3 plants produce the biological precursor of des-A-lupane.

Conclusions and perspectives

We present a new record of des-A-triterpenoids from a tropical peat deposit during the Holocene. All des-A-triterpenoids present at the NGaoudaba peat deposit present similar trend and are highly correlated with each other which suggest similar sources for all des-A-triterpenoids at the NGaoundaba peat deposit. Sources are dominated by C_3 plants that where probably not present during the AHP period. Further analyses are needed to better constrain the des-A-triterpenoid signal, in particular a comparison with pollen data.
The link between des-A-triterpenoids and paleoclimate remains uncertain as there is no clear link between the des-A-triterpenoids relative abundance and concentration and the main paleoclimatic records (T_{brGDGT}, carbon and hydrogen isotopic composition of n-C_{31} alkane).

Part 3: 5-n-alkylresorcinol

1. Introduction

Changes in vegetation can have a strong impact on molecular proxies used for paleoclimatic and paleoenvironmental reconstructions. This is especially the case for proxies based on microbial lipids such as brGDGT used to reconstruct pH and temperature (Weijers et al., 2011; Nichols et al., 2014; Liang et al., 2019) (see chapter 4 and 5). The hydrogen isotopic composition of leaf plant n-alkanes, used for reconstructing past precipitation, is influenced by the photosynthetic pathway (C_3, C_4, or CAM) of n-alkane-producing plants (Garcin et al., 2012b; Wang et al., 2013) and $\delta D_{n\text{-}alk}$ values are often corrected for the impact of vegetation (see chapter 5 and 6). Both the vegetation growing on the catchment and on the peat itself contribute to the vegetation deposited in the peat. Each of these vegetation sources can record slightly different environmental conditions. For example, vegetation growing in-situ has access to peat water, which may have a different isotopic signature compared to precipitation water as strong evapotranspiration during the dry season might enriched the hydrogen isotopic composition of peat water (see chapter 5). Consequently, vegetation growing on the peatland can affect the hydrogen isotopic signature of n-alkane, especially in sedge-dominated peat deposits where the in-situ-growing plants (ie the sedges) produce the same n-alkane chain length as the nearby terrestrial plants (Chapter 5).
Alkylresorcinols (or 5-*n*-alkylresorcinols) are 3,5-dihydroxy-phenolic lipids that have been reported in many plants such as cereals (rye, wheat, barley) (Ross et al., 2003 and references therein) and Proteaceae (Gadea et al., 2022) but also in certain fruits (mango, ginkgo) (Żarnowska et al., 2000; Knödler et al., 2009), bacteria (Reusch and Sadoff, 1979; Kozubek et

al., 1996; Blokker et al., 2001), and algae (Zarnowski et al., 2000). Several biological functions of alkylresorcinols have been proposed in plants, such as antimicrobial and antifungal properties or antioxidant activity (Zarnowski et al., 1999; Kozubek and Tyman, 1999; Zabolotneva et al., 2022).

High abundances of 5-*n*-alkylresorcinols have been reported in peat sediments (Avsejs et al., 2002; Xie et al., 2004; McClymont et al., 2008; Ortiz et al., 2010). Based on a strong positive correlation between the concentration total 5-*n*-alkylresorcinols and sedge macrofossil abundance, Avsejs et al. (2002) suggested that 5-*n*-alkylresorcinols could be used as a proxy for sedges in peat deposits. The 5-*n*-alkylresorcinols being predominant in sedges while sterols dominate other type of plants such as Sphagnum, the 5-*n*-alkylresorcinols/sterols ratio was proposed to reflect past changes in peat vegetation and the transition from Sphagnum-dominated to sedge-dominated peatland (Xie et al., 2004; Ortiz et al., 2010).

Until now, to our knowledge, no published study has presented 5-*n*-alkylresorcinols in tropical peat deposits, where the use of these biomarkers as a proxy for sedges must be confirmed, due to differences in plant species between the two types of peats. The distribution of 5-*n*-alkylresorcinols was investigated in peat sediments and in fresh plant samples from the NGaoundaba peat deposit (North East Cameroon). Nowadays, the vegetation in this peat ecosystem is dominated by Cyperaceae (*Cyperus* sp.), but Poaceae also grow directly on the peat.

2. Methods

2.1. Analyses of sediment

For this study, 9 samples were extracted and separated for this study following a procedure identical to that in Chapter 4 and 5. The third lipid fraction obtained during separation of the TLE was further separated (without previous filtration) into three fractions by column chromatography on silica gel (3.5-4 g). The fraction containing n-alkanols and most of the 5-n-alkylrecorsinols was eluted with 40 mL of heptane/etyl acetate (EA) (85:15, v/v). A second fraction containing n-alkanoic acids was eluted with 20 mL of hept/EA (1:1, v/v) and 20 mL of EA. A third fraction was eluted with 40 mL of DCM/MeOH (1:1, v/v). The extraction/separation procedure is summarized in Figure 61. Prior to GC analyses, fractions containing 5-n-alkylrecorsinols were silylated prior to GCMS analyses using 100 µL BSTFA and 200 µL pyridine for 50 min at 60°C. After a first GC-FID analysis, GC-MS analyses were performed for identification and quantification using TIC and mass fragmentograms at m/z 268.

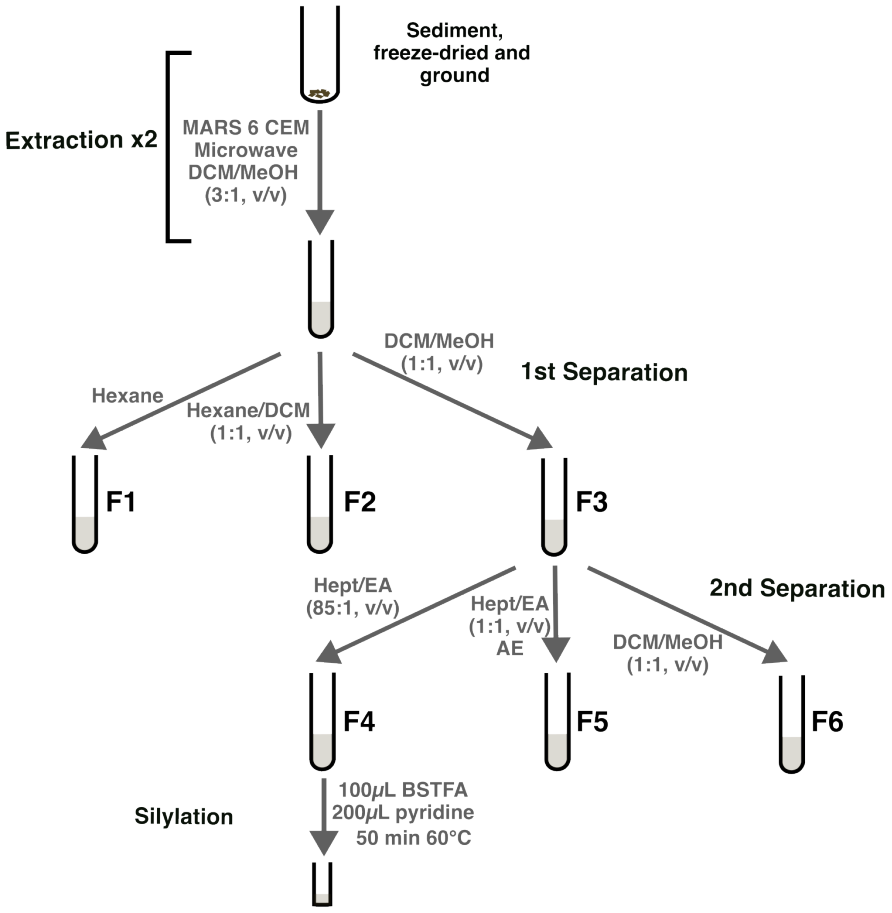

Figure 61: The extraction and separation protocols used for the preparation of sediment samples for 5-n-alkylrecorsinol analyses.

2.2. Analyses of fresh plants

Seventeen fresh plant samples were collected from the NGaoundaba peat deposit at the end of the rainy season in November 2022 (P. Deschamps). Samples were taken directly from the peat deposit and from the surrounding area (Figure 62). The plants were tentatively identified using the website *africanplantdatabase.ch* and with the assistance of C. Kiahtipes. To determine the photosynthetic pathway of each plant sample (C_3 or C_4), organic bulk composition analyses were measured using an elemental analyzer (EA-IRMS) following the same procedure as in Schaaff et al. (2023) (chapter 3). For bulk analyses, each plant sample was analyzed in triplicate. Nine of these fresh samples were selected for biomarker analyses focusing on Poaceae, Cyperaceae and a few other species due to limited time left before the end of this thesis work.

The plant samples were freeze-dried and ground. The extraction, separation, and silylation methods for fresh plant samples are detailed in Table 8 and Figure 63. For 4 samples from the

Poaceae and Cyperaceae families, we also performed saponification and acid hydrolysis following the procedure detailed in Figure 63.

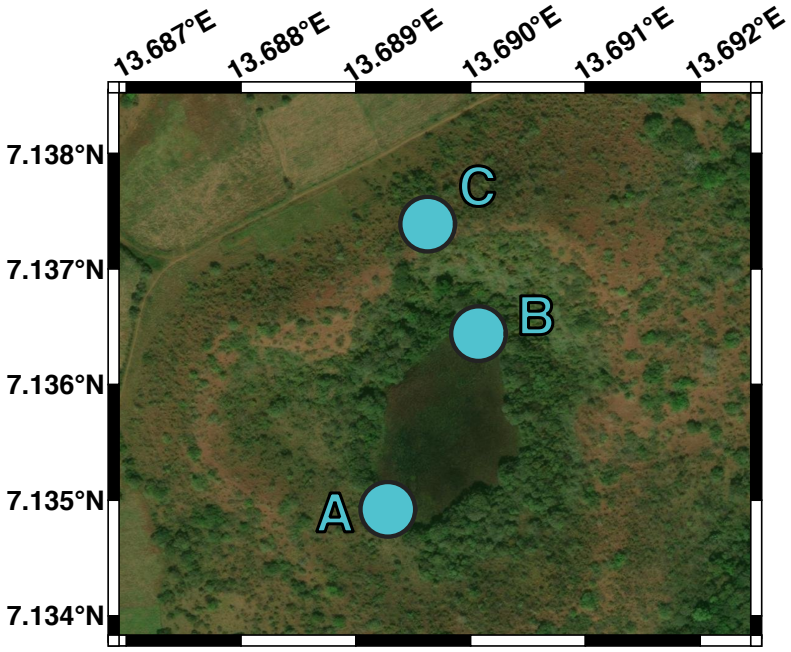

Figure 62: Position of the sampling site of the vegetation samples.

*Table 8: Summary of plant samples analyzed in this study. The protocol numbers correspond to the procedures detailed in Figure 63. Samples 6 and 14 belong to the same genus and were analyzed to check the consistency of the lipid biomarker assemblages in two specimens of the same species. Samples 2 and 3 may belong to the same species. The C_3/C_4 status of each plant sample is based on bulk carbon isotopic composition. Samples marked with an asterisk * were analyzed (extraction/separation) in duplicate. ** tentative identifications that will need to be confirmed. ***The family has not been precisely determined, but this plant sample is neither a Poaceae nor a Cyperaceae.*

n°	Family	Genus /Specie**	$\delta^{13}C_{bulk}$	C_3/C_4	Location	Protocol		
						(1)	(2)	(3)
2	Poaceae	?	-27.1±0.4	C_3	A (Inside)	X	X	X
3	Poaceae	?	-26.8±0.1	C_3	A (Inside)	X	X	X
5	Poaceae	Hyparrhenia?	-10.3±0.4	C_4	A (Inside)	X*	X	X
6	Cyperaceae	Cyperus	-8.4±0.3	C_4	A (Inside)	X*	X	X
7	Fabaceae	Piliostigma	-29.8±0.7	C_3	A (Side)	X		
8	? ***	?	-27.9±0.2	C_3	A (Side)	X		
10	Euphorbiaceae	Alchornea?	-27.7±0.1	C_3	A (Side)	X		
14	Cyperaceae	Cyperus	-9.5±0.6	C_4	B	X		
17	Combretaceae	Terminalia?	-27.6±0.2	C_3	C	X		

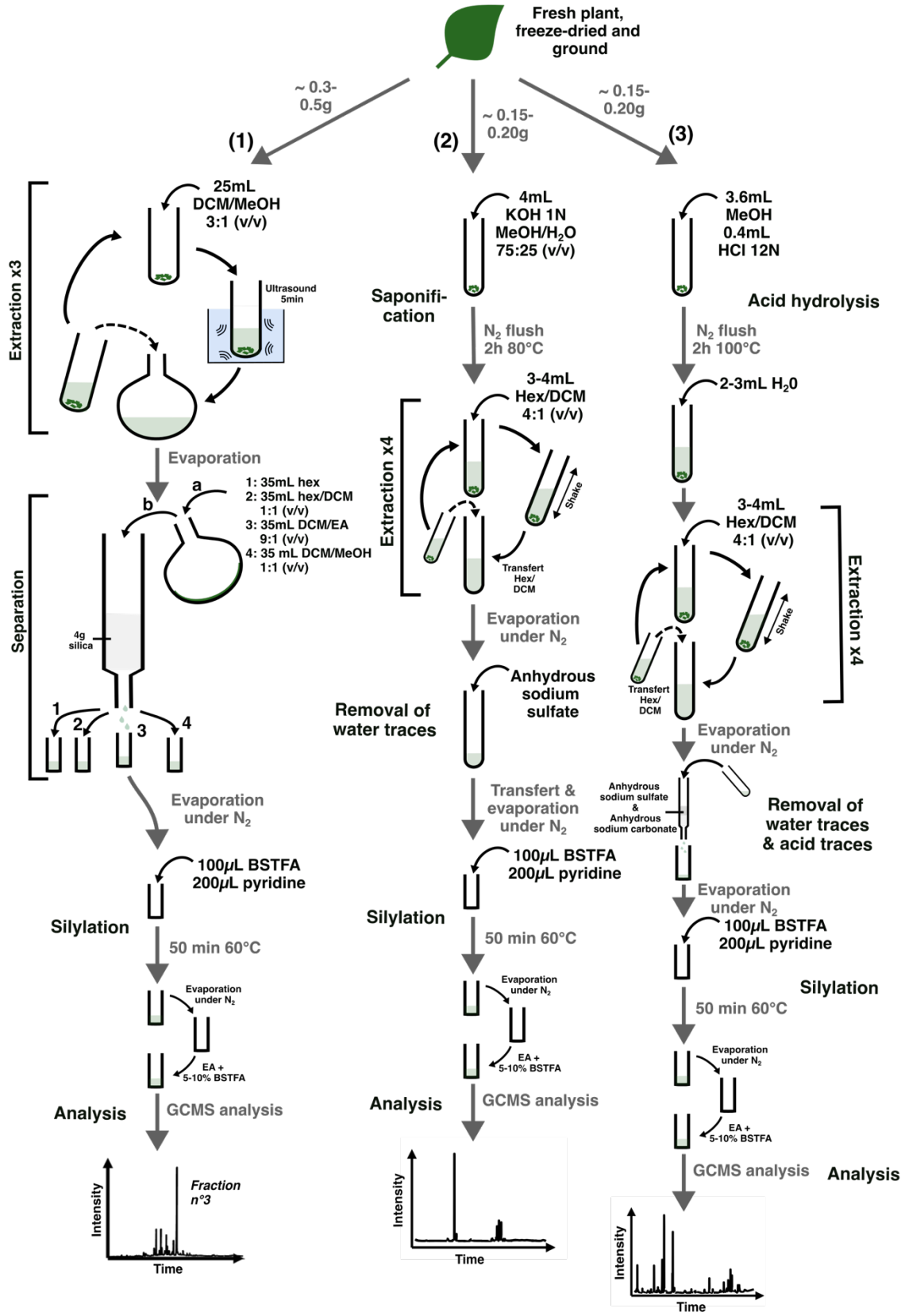

Figure 63: Protocol applied to fresh plant samples. All plant samples were analyzed using the "classic" extraction/separation method (1). Saponification (2) and acid hydrolysis (3) were further performed on sedges and grasses growing directly on the peat.

2.3. Ratio based on 5-*n*-alkylresorcinols

We calculated an average chain length for 5-*n*-alkylresorcinols ACL_r using the following equation similar to the equation classically used for n-alkanes:

$$ACL_r = \frac{(17 * C_{17} + 19 * C_{19} + 21 * C_{21} + 23 * C_{23} + 25 * C_{25} + 27 * C_{27} + 29 * C_{29} + 31 * C_{31})}{(C_{17} + C_{19} + C_{21} + C_{23} + C_{25} + C_{27} + C_{29} + C_{31})}$$

3. Results and discussion

3.1. Identification and distribution of 5-n-alkylresorcinols

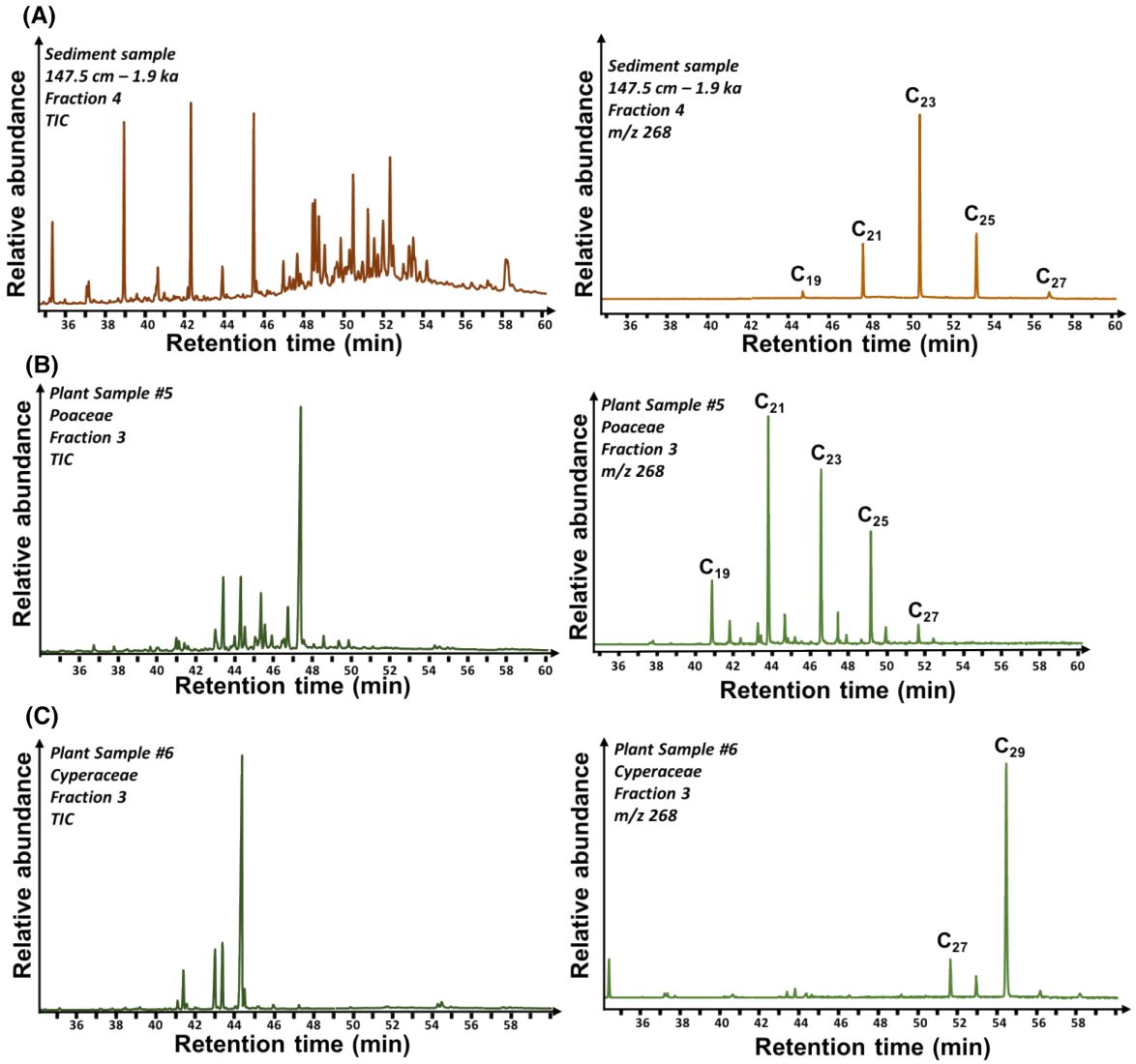

Figure 64: Chromatograms (TIC and m/z 268) of a sediment sample (147.5 cm-depth – 1.9ka) (A) and of two fresh plant samples containing 5-n-alkylresorcinols (B and C).

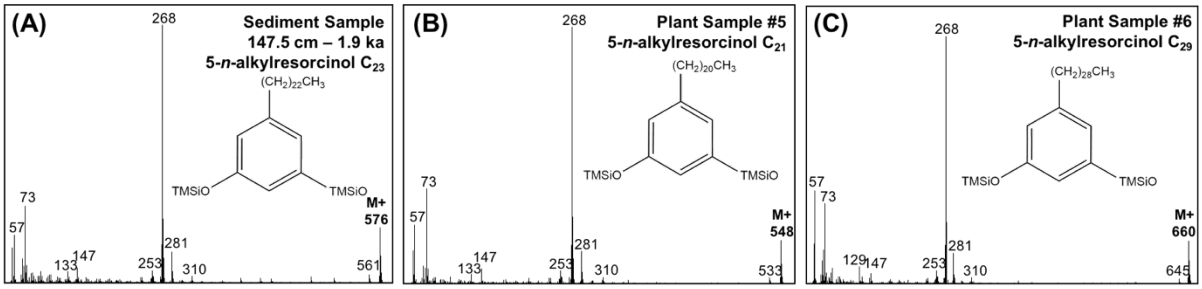

Figure 65: Mass spectrum of the dominant 5-n-alkylresorcinol in one sediment samples (A) and two plant samples (B and C).

A series of 5-*n*-alkylresorcinols was identified in all peat sediment samples and in 5 of the 9 fresh plant samples. 5-*n*-alkylresorcinols show a characteristic fragment ion at m/z 268 (base peak) and additional characteristic fragment ions at m/z 310 and 281 (Avsejs et al., 2002) (Figure 65). In peat sediments, 5-*n*-alkylresorcinols range from C_{17} to C_{31}, with a predominance of odd-numbered chain length (Figure 64 A and Table 9). All sediment samples show a unimodal distribution, maximizing at C_{23}. For now, we focused on the F4 fractions, but small amounts of 5 n-alkylresorcinols were also detected in some of the F5 fractions. However, when both F4 and F5 fractions were analyzed (sample at 147cm depth, see Table 9), the distribution of 5-*n*-alkylresorcinols was similar in F4 fractions alone and in combined F4+F5 fractions. We plan to analyze the other F5 fractions to improve the quantification of 5-*n*-alkylresorcinols.

*Table 9: Relative abundance of 5-n-alkylresorcinols in sediment samples in fraction F4 *Calculation taking into account both F4 and F5 fractions. All other sediment sample need to be reanalyzed to take into account the 5-n-alkylresorcinols in fraction F5.*

Depth (cm)	Age (ka cal BP)	Relative abundance of 5-n-alkylresorcinol (%)								ACL_r
		C17	C19	C21	C23	C25	C27	C29	C31	
17	0.16	0	8.6	25.0	30.9	25.1	10.3	0	0	23.1
70	1.1	0.9	5.5	26.1	49.8	17.7	0	0	0	22.6
147	1.9	0	2.6	15.4	54.2	23.3	2.8	1.0	0.8	23.3
*147**	*1.9*	*0*	*2.7*	*17.7*	*55.7*	*21.3*	*1.6*	*0.5*	*0.5*	*23.1*
262	5.5	1.2	7.9	18.8	55.7	14.6	1.8	0	0	22.6
327	6.5	0	2.6	15.3	51.5	23.8	3.3	2.3	1.3	23.4
360	7.0	0	6.2	19.2	50.1	19.9	2.4	1.4	0.7	23.0
462	8.4	0	3.6	24.2	36.7	24.1	3.5	3.9	4.0	23.5
507	8.8	0	4.6	21.8	43.7	14.9	5.3	5.3	4.4	23.6
570	9.4	0	10.3	27.3	29.1	27.8	2.6	1.3	1.6	22.9

All fresh plant samples containing 5-*n*-alkylresorcinols were sedges (Cyperaceae) and Poaceae. 5-*n*-alkylresorcinols were not detected in any other plant families tested. When present, 5-*n*-alkylresorcinols showed a unimodal distribution dominated by C_{17} or C_{21} for Poaceae species and by C_{29} for the two Cyperus specimens (Figure 64 B and C and Table 10). No 5-*n*-alkylresorcinols were detected in saponified or acid-hydrolyzed samples, suggesting that the 5-*n*-alkylresorcinols are free and minor lipids and that i) the high amounts alcools released by saponification obscured the detection of alkylresorcinols and ii) alkylresorcinols are degraded during acid hydrolysis.

*Table 10: Relative abundance of 5-n-alkylresorcinols in plant samples. For sample 5 and 6, uncertainty measurements are based on the duplicate extraction/separation/analyses of same plant (2*standard deviation/Ö2).*

N°	Family	Relative abundance of 5-n-alkylresorcinol (%)								ACL_r
		C17	C19	C21	C23	C25	C27	C29	C31	
2	Poaceae	0	26 .4	73.6	0	0	0	0	0	20.5
3	Poaceae	8.9	76.7	14.4	0	0	0	0	0	19.1
5	Poaceae	0.2	15.8	41.1	25.4	14.9	2.6	0	0	21.9
		±0.3	±9.4	±6.7	±8.0	±6.7	±1.0			±0.7
6	Cyperaceae	0	0	0	0	0	15.0	85.0	0	28.7
							±8.2	±8.2		±0.2
7	Fabaceae	*-- No 5-n-alkylresorcinol detected --*								/
8	?	*-- No 5-n-alkylresorcinol detected --*								/
10	Euphorbiaceae	*-- No 5-n-alkylresorcinol detected --*								/
14	Cyperaceae	0	0	0	0	0	17.1	82.9	0	28.7
17	Combretaceae	*-- No 5-n-alkylresorcinol detected --*								/

3.2. Distinct distribution of alkylresorcinols between peat soil and plant families

The distribution of 5-*n*-alkylresorcinols in peat sediments strongly differ from that of 5-*n*-alkylresorcinols in fresh plants, but striking differences were also observed between Poaceae and sedges. Several hypotheses can be made to explain such discrepancies:

- The 5-*n*-alkylresorcinols present in peat soil are a mixture of Poaceae and sedge-derived 5-*n*-alkylresorcinols. This seems rather unlikely based on the distinct distributions observed in soils and the two families of fresh plants
- The 5-*n*-alkylresorcinols present in peat soil mainly correspond to an unidentified plant contribution dominated by the C_{23} homologue that may not be present anymore at NGaoundaba.

- The production of 5-*n*-alkylresorcinols by plants can vary over time and/or within different specimens of the same species (the 5-*n*-alkylresorcinol assemblages of the two *Cyperus* sp. specimens are, however, quite similar).

3.3. 5-n-alkylresorcinols in peat: a biomarker not specific for sedges

At the NGaoundaba peat, 5-*n*-alkylresorcinols are not restricted to sedges but are also found in Poaceae. Numerous studies have reported 5-*n*-alkylresorcinols in cereal species (Ross et al., 2003; Ross, 2012), which are generally dominated by the C_{19} or C_{21} homologues (Ross et al., 2003; Liu et al., 2018). 5-*n*-alkylresorcinols have not been found in rice, maize, sorghum, or millet (Ross et al., 2003) and thus cannot be used to track human settlement and agricultural development in the region (Neumann, 2018; Champion et al., 2021). However, caution is needed when using 5-*n*-alkylresorcinols as a biomarker for sedges in peat. Because no Poaceae were reported among the plants sampled in the Bolton Fell Moss peatland (UK) by Avsejs et al. (2002), the abundance of 5-*n*-alkylresorcinols could indeed represent the sedge contribution. Poaceae, on the other hand, are common plants in ecosystems, and a large contribution from the watershed cannot be ruled out. Further research on the origin of 5-*n*-alkylresorcinols in peat sediments could be conducted using wild Poaceae species from temperate and tropical habitats.

The abundance of 5-*n*-alkylresorcinols in the NGaoundaba peat deposit may indicate an increase in Poaceae and Cyperaceae inputs and a vegetated peat surface. Furthermore, the distinct ACL_r of alkylresorcinols of Poaceae and Cyperus could be used to differentiate the two plant groups. The *Carex* sp. analyzed by Avsejs et al. . (2002), another Cyperaceae genus, have lower ACL_r values than the *Cyperus* sp. from the NGaoundaba peat deposit ranging from 21.4 to 24.4 but the ACL_r of *Carex* sp. is still higher than the ACL_r of Poaceae.

Conclusions and perspectives

Preliminary investigations of fresh plants from the NGaoundaba peat deposit show that 5-*n*-alkylresorcinols are not limited to sedges (Cyperus spp.), as some Poaceae species also produce these compounds. However, sedges and Poaceae appear to have distinct distributions of 5-*n*-alkylresorcinols. The ACL_r of 5-*n*-alkylresorcinols may thus be used to distinguish the sources of the 5-*n*-alkylresorcinols and to trace the variation in sedge and Poaceae input. However, the distribution of 5-*n*-alkylresorcinols in the sediment doesn't coincide with the ACL_r of the sedge and of the Poaceae. More research is needed to constrain the variation of 5-*n*-alkylresorcinols in NGaoundaba peat deposit and test this hypothesis. The presence of 5-*n*-alkylresorcinols contained in the fractions F5 must be considered. In addition, the lipid biomarker data in the sediment will be compared to pollen data to see if a relationship exists between the abundance of 5-*n*-alkylresorcinol and the abundance of some

species in the pollen record. Furthermore, proper identification of the fresh plants analyzed is required.

Lastly, the present data will be compared to the 5-n-alkylresorcinol data from the Kyambangunguru peat deposit (East Africa), another sedge-dominated tropical peat deposit examined by L. Rouyer & A. Huguet (Sorbonne University), to see if common trends can be drawn for comparable peat sites.

General conclusion and perspectives

This thesis presents a new high-resolution paleoclimatic and paleoenvironmental record from tropical Africa covering the last 10ka. We focus on a tropical peat deposit: a continental archive still understudied. Using bulk organic data and lipid biomarkers analyses, we redraw the paleoclimatic and paleoenvironmental history of the NGaoundaba peat deposit (Northeastern Cameroon) over the past 10ka. In addition, we present new records for understudied lipid biomarkers such as hopanes, des-A-triterpenoids or botryococceccenes to highlight their potential in paleoclimatic and paleoenvironmental studies.

Starting with bulk organic data, we demonstrate that it is possible to remove the decomposition signal to highlight the paleoclimatic and paleoenvironmental signals in bulk organic data. This method can be useful for identifying key paleoclimatic and paleoenvironmental variations in a new record and for adapting the sampling strategy for subsequent analyses such as lipid biomarker analyses or pollen analyses.

Focusing on microbial biomarkers, we present new data on the distribution and concentration of hopanes, brGDGTs, and isoGDGTs. Based on the NGaoundaba peat record, we evaluate the use of these compounds to reconstruct past pH variations and the methane cycle. By using the carbon isotopic composition of hopanes, we were able to better understand the origin of these compounds. This work highlights several perspectives for future studies on microbial biomarkers in peat:

- The sources of these compounds need to be better understood. Interpretations based on these compounds are currently limited by the poor understanding of their sources, in surface but also in deep peat. Several prospects can be noted:
    - Coupled analyses of lipid biomarkers (both core lipid and intact polar lipid) and the microbial community in surface peat could improve our understanding of these biomarkers.
    - Estimation of deep-peat production of microbial compounds and of its potential influence on paleoclimatic and paleoenvironmental interpretations. Most studies to date focus on the upper 50 cm of peat and rarely down to 2m, with contrasting results. As a huge diversity of peat deposits exist with various hydrological conditions, forming vegetation, temperature, etc., it's important

to better characterize the influence of these factors on the microbial community to be able to compare the different peat-based records.

- Paleoclimatic and paleoenvironmental interpretations based on pH are currently limited because we still don't understand what can cause pH variations on a large timescale and even what is recorded by pH reconstructions: are they "true" pH values or simply a proxy tracing a paleoclimatic signal without representing "true" pH variations? By comparing currently available pH records based on hopanes or brGDGTs, this work highlights the multiple causes of pH variations in peat: catchment lithology, vegetation changes, precipitation-evapotranspiration balance, etc.

We also present new records of understudied lipid biomarkers such as des-A-triterpenoids and 5-*n*-alkylresorcinols. Biomarkers are abundant in peat and could represent promising new proxies if their origin, diagenetic pathway, and paleoenvironmental significance were better constrained.

A multiproxy approach using a large panel of lipid biomarkers, pollen data, bulk organic data, etc. can provide helpful information to reconstruct the responses of various environments to climate change. As peatland can be an important source or sink of greenhouse gases, understanding the response of peatland to climatic change is crucial. Evaluate the climatic parameters influencing the decomposition of organic matter, methane and carbon cycling in peat on a large timescale, which can only be achieved by modeling or paleoclimatic studies. In addition, the NGaoundaba peat deposit as well as most lakes and water resources are essential for the subsistence of local populations and are frequently hotspot of biodiversity. The response of these environments to climatic changes can have significant consequences for human populations: eutrophication, non potability or rarefaction of the water resources that paleoenvironmental and paleoecological studies can help to anticipate.

Using a multiproxy approach, we were able to reconstruct precise paleoenvironmental and paleoecological changes in the vegetation and microbial community of the NGaoundaba peat deposit over the last 10 ka. We highlight several major paleoclimatic and paleoenvironmental changes during the last 10 ka:

- We present a new record of the termination of the AHP in West and Central Africa. The $\delta D_{n\text{-}alk}$ record indicates a progressive termination of the African Humid Period, with values decreasing during most of the Holocene starting after 7.4 ka cal BP and consistent with the insolation forcing during this period. The vegetation and microbial-based proxies present an abrupt change around 5.7-5.8 ka cal BP at the NGaoundaba peat deposit, suggesting a threshold for ecosystems to climatic changes.

- Two 1-ka events were recorded between 8.9 and 7.9 ka cal BP and between 4.5 and 3.5 ka cal BP. These events roughly coincide with two well-knowns paleoclimatic events frequently recorded in high latitudes (the 8.2 and 4.2 ka events). However, in high latitudes, these events are usually much shorter, starting after the beginning of the events recorded at the NGaoundaba peat deposit. A review of these events in tropical Africa (for now focusing on paleohydrological records) indicates that they are frequently recorded in tropical Africa and that their duration is often longer than in high latitudes. This work raised many questions:
    - Are these events in the tropics linked to the events in high latitudes? They could occur during a period of global climatic deterioration, and the tropics and high latitudes respond differently.
    - Particularly for the 8.2 ka event, if climate changes start in the tropics before those in high latitude, could changes in tropical climate have influenced the high latitude climate?
    - Many records from tropical Africa have low temporal resolution or uncontinuous sedimentation. In addition, the timing of the 4.5-3.5 ka event, close to the end of the AHP, makes it difficult to discern in paleoclimatic records.

  We highlight significant changes between 8.9 end 7.9 ka cal BP with a shift in the production of botryococcenes and an increase in short- and mid-chain n-alkanes, which we interpret as frequent algal blooms during a period of low water level.

We also highlight the specificities of this type of peat deposit compared with other sites studied until now for $\delta D_{n\text{-}alk}$ analyses in tropical Africa due to the increasing contribution of long-chain n-alkanes from sedges and grasses growing directly on the peat during the Holocene.

References

Abba, S., Hamelin, B., Michelot, J.-L., Garcin, Y., Deschamps, P., 2023. Water budget of tropical volcanic lakes in center-north Cameroon: Reconciling the stable isotope and chloride mass balance. Hydrol. Process. 37, e14923. https://doi.org/10.1002/hyp.14923

Abernethy, K., Maisels, F., White, L.J.T., 2016. Environmental Issues in Central Africa. Annu. Rev. Environ. Resour. 41, 1–33. https://doi.org/10.1146/annurev-environ-110615-085415

Adkins, J., deMenocal, P., Eshel, G., 2006. The "African humid period" and the record of marine upwelling from excess 230Th in Ocean Drilling Program Hole 658C. Paleoceanography 21. https://doi.org/10.1029/2005PA001200

Ågren, G.I., Bosatta, E., Balesdent, J., 1996. Isotope discrimination during decomposition of organic matter: a theoretical analysis. Soil Sci. Soc. Am. J. 60, 1121–1126.

Alley, R.B., 2000. The Younger Dryas cold interval as viewed from central Greenland. Quat. Sci. Rev. 19, 213–226. https://doi.org/10.1016/S0277-3791(99)00062-1

Alley, R.B., Mayewski, P.A., Sowers, T., Stuiver, M., Taylor, K.C., Clark, P.U., 1997. Holocene climatic instability: A prominent, widespread event 8200 yr ago. Geology 25, 483–486. https://doi.org/10.1130/0091-7613(1997)025<0483:HCIAPW>2.3.CO;2

Amaral, P., Vincens, A., Guiot, J., Buchet, G., Deschamps, P., Doumnang, J.-C., Sylvestre, F., 2013. Palynological evidence for gradual vegetation and climate changes during the African Humid Period termination at 13 N from a Mega-Lake Chad sedimentary sequence. Clim. Past 9, 223–241.

Amesbury, M.J., Gallego-Sala, A., Loisel, J., 2019. Peatlands as prolific carbon sinks. Nat. Geosci. 12, 880–881. https://doi.org/10.1038/s41561-019-0455-y

Amorim, H.C., Hurtarte, L.C., Souza, I.F., Zinn, Y.L., 2022. C: N ratios of bulk soils and particle-size fractions: Global trends and major drivers. Geoderma 425, 116026.

Andersen, R., Chapman, S.J., Artz, R.R.E., 2013. Microbial communities in natural and disturbed peatlands: A review. Soil Biol. Biochem. 57, 979–994. https://doi.org/10.1016/j.soilbio.2012.10.003

Andriesse, J.P., 1988. Nature and management of tropical peat soils. Food & Agriculture Org.

Anton Hough, R., Wetzel, R.G., 1977. Photosynthetic pathways of some aquatic plants. Aquat. Bot. 3, 297–313. https://doi.org/10.1016/0304-3770(77)90035-3

Atahan, P., Heijnis, H., Dodson, J., Grice, K., Le Métayer, P., Taffs, K., Hembrow, S., Woltering, M., Zawadzki, A., 2015. Pollen, biomarker and stable isotope evidence of late Quaternary environmental change at Lake McKenzie, southeast Queensland. J. Paleolimnol. 53, 139–156. https://doi.org/10.1007/s10933-014-9813-3

Aucour, A.-M., Bonnefille, R., Hillaire-Marcel, C., 1999. Sources and accumulation rates of organic carbon in an equatorial peat bog (Burundi, East Africa) during the Holocene: carbon isotope constraints. Palaeogeogr. Palaeoclimatol. Palaeoecol. 150, 179–189.

Aucour, A.-M., Hillaire-Marcel, C., Bonnefille, R., 1996. Oxygen isotopes in cellulose from modern and quaternary intertropical peatbogs: implications for palaeohydrology. Chem. Geol. 129, 341–359.

Aucour, A.-M., Hillaire-Marcel, C., Bonnefille, R., 1994. Late Quaternary Biomass Changes from 13C Measurements in a Highland Peatbog from Equatorial Africa (Burundi).

Quat. Res. 41, 225–233. https://doi.org/10.1006/qres.1994.1024
Ausec, L., Kraigher, B., Mandic-Mulec, I., 2009. Differences in the activity and bacterial community structure of drained grassland and forest peat soils. Soil Biol. Biochem. 41, 1874–1881. https://doi.org/10.1016/j.soilbio.2009.06.010
Autio, J., Hicks, S., 2004. Annual variations in pollen deposition and meteorological conditions on the fell Aakenustunturi in northern Finland: Potential for using fossil pollen as a climate proxy. Grana 43, 31–47. https://doi.org/10.1080/00173130310017409
Avsejs, L.A., Nott, C.J., Xie, S., Maddy, D., Chambers, F.M., Evershed, R.P., 2002. 5-n-Alkylresorcinols as biomarkers of sedges in an ombrotrophic peat section. Org. Geochem. 33, 861–867. https://doi.org/10.1016/S0146-6380(02)00046-3
Baker, A., Routh, J., Blaauw, M., Roychoudhury, A., 2014. Geochemical records of palaeoenvironmental controls on peat forming processes in the Mfabeni peatland, Kwazulu Natal, South Africa since the Late Pleistocene. Palaeogeogr. Palaeoclimatol. Palaeoecol. 395, 95–106.
Barber, D.C., Dyke, A., Hillaire-Marcel, C., Jennings, A.E., Andrews, J.T., Kerwin, M.W., Bilodeau, G., McNeely, R., Southon, J., Morehead, M.D., Gagnon, J.-M., 1999. Forcing of the cold event of 8,200 years ago by catastrophic drainage of Laurentide lakes. Nature 400, 344–348. https://doi.org/10.1038/22504
Barnes, M.A., Barnes, W.C., 1978. Organic Compounds in Lake Sediments, in: Lerman, A. (Ed.), Lakes: Chemistry, Geology, Physics. Springer New York, New York, NY, pp. 127–152. https://doi.org/10.1007/978-1-4757-1152-3_5
Barré, P., Plante, A.F., Cécillon, L., Lutfalla, S., Baudin, F., Bernard, S., Christensen, B.T., Eglin, T., Fernandez, J.M., Houot, S., Kätterer, T., Le Guillou, C., Macdonald, A., van Oort, F., Chenu, C., 2016. The energetic and chemical signatures of persistent soil organic matter. Biogeochemistry 130, 1–12.
Basiliko, N., Knowles, R., Moore, T.R., 2004. Roles of moss species and habitat in methane consumption potential in a northern peatland. Wetlands 24, 178–185. https://doi.org/10.1672/0277-5212(2004)024[0178:ROMSAH]2.0.CO;2
Bayon, G., Dennielou, B., Etoubleau, J., Ponzevera, E., Toucanne, S., Bermell, S., 2012. Intensifying Weathering and Land Use in Iron Age Central Africa. Science 335, 1219–1222. https://doi.org/10.1126/science.1215400
Bayon, G., Schefuß, E., Dupont, L., Borges, A.V., Dennielou, B., Lambert, T., Mollenhauer, G., Monin, L., Ponzevera, E., Skonieczny, C., André, L., 2019. The roles of climate and human land-use in the late Holocene rainforest crisis of Central Africa. Earth Planet. Sci. Lett. 505, 30–41.
Beck, H.E., Zimmermann, N.E., McVicar, T.R., Vergopolan, N., Berg, A., Wood, E.F., 2018. Present and future Köppen-Geiger climate classification maps at 1-km resolution. Sci. Data 5, 180214. https://doi.org/10.1038/sdata.2018.214
Behar, F., Beaumont, V., De B. Penteado, H.L., 2001. Rock-Eval 6 technology: performances and developments. Oil Gas Sci. Technol. 56, 111–134.
Behling, H., Safford, H.D., 2010. Late-glacial and Holocene vegetation, climate and fire dynamics in the Serra dos Órgãos, Rio de Janeiro State, southeastern Brazil. Glob. Change Biol. 16, 1661–1671.
Belyea, L.R., Malmer, N., 2004. Carbon sequestration in peatland: patterns and mechanisms of response to climate change. Glob. Change Biol. 10, 1043–1052.
Bender, M.M., 1971. Variations in the 13C/12C ratios of plants in relation to the pathway of

photosynthetic carbon dioxide fixation. Phytochemistry 10, 1239–1244. https://doi.org/10.1016/S0031-9422(00)84324-1
Benner, R., Fogel, M.L., Sprague, E.K., Hodson, R.E., 1987. Depletion of ^{13}C in lignin and its implications for stable carbon isotope studies. Nature 329, 708–710.
Berger, A., Guiot, J., Kukla, G., Pestiaux, P., 1981. Long-term variations of monthly insolation as related to climatic changes. Geol. Rundsch. 70, 748–758.
Berger, A.L., 1977. Support for the astronomical theory of climatic change. Nature 269, 44–45.
Bergman, I., Klarqvist, M., Nilsson, M., 2000. Seasonal variation in rates of methane production from peat of various botanical origins: effects of temperature and substrate quality. FEMS Microbiol. Ecol. 33, 181–189. https://doi.org/10.1111/j.1574-6941.2000.tb00740.x
Berke, M.A., Johnson, T.C., Werne, J.P., Grice, K., Schouten, S., Sinninghe Damsté, J.S., 2012. Molecular records of climate variability and vegetation response since the Late Pleistocene in the Lake Victoria basin, East Africa. Quat. Sci. Rev. 55, 59–74. https://doi.org/10.1016/j.quascirev.2012.08.014
Berke, M.A., Johnson, T.C., Werne, J.P., Livingstone, D.A., Grice, K., Schouten, S., Damsté, J.S.S., 2014. Characterization of the last deglacial transition in tropical East Africa: Insights from Lake Albert. Palaeogeogr. Palaeoclimatol. Palaeoecol. 409, 1–8. https://doi.org/10.1016/j.palaeo.2014.04.014
Berkelhammer, M., Sinha, A., Stott, L., Cheng, H., Pausata, F.S.R., Yoshimura, K., 2012. An Abrupt Shift in the Indian Monsoon 4000 Years Ago, in: Climates, Landscapes, and Civilizations, Geophysical Monograph Series. pp. 75–88. https://doi.org/10.1029/2012GM001207
Berner, R.A., 2020. Early diagenesis. Princeton University Press.
Beuning, K.R.M., Kelts, K., Ito, E., Johnson, T.C., 1997. Paleohydrology of Lake Victoria, East Africa, inferred from 18O/16O ratios in sediment cellulose. Geology 25, 1083–1086. https://doi.org/10.1130/0091-7613(1997)025<1083:POLVEA>2.3.CO;2
Beuning, K.R.M., Kelts, K., Russell, J., Wolfe, B.B., 2002. Reassessment of Lake Victoria–Upper Nile River paleohydrology from oxygen isotope records of lake-sediment cellulose. Geology 30, 559–562. https://doi.org/10.1130/0091-7613(2002)030<0559:ROLVUN>2.0.CO;2
Biester, H., Knorr, K.-H., Schellekens, J., Basler, A., Hermanns, Y.-M., 2014. Comparison of different methods to determine the degree of peat decomposition in peat bogs. Biogeosciences 11, 2691–2707.
Bini, M., Zanchetta, G., Perşoiu, A., Cartier, R., Català, A., Cacho, I., Dean, J.R., Di Rita, F., Drysdale, R.N., Finnè, M., Isola, I., Jalali, B., Lirer, F., Magri, D., Masi, A., Marks, L., Mercuri, A.M., Peyron, O., Sadori, L., Sicre, M.-A., Welc, F., Zielhofer, C., Brisset, E., 2019. The 4.2 ka BP Event in the Mediterranean region: an overview. Clim Past 15, 555–577. https://doi.org/10.5194/cp-15-555-2019
Bird, M.I., Haig, J., Hadeen, X., Rivera-Araya, M., Wurster, C.M., Zwart, C., 2020. Stable isotope proxy records in tropical terrestrial environments. Palaeogeogr. Palaeoclimatol. Palaeoecol. 538, 109445. https://doi.org/10.1016/j.palaeo.2019.109445
Blaauw, M., Christen, J.A., 2011. Flexible paleoclimate age-depth models using an autoregressive gamma process. Bayesian Anal. 6, 457–474.
Blaga, C.I., Reichart, G.-J., Heiri, O., Sinninghe Damsté, J.S., 2009. Tetraether membrane lipid

distributions in water-column particulate matter and sediments: a study of 47 European lakes along a north–south transect. J. Paleolimnol. 41, 523–540. https://doi.org/10.1007/s10933-008-9242-2
Blewett, J., Elling, F.J., Naafs, B.D.A., Kattein, L., Evans, T.W., Lauretano, V., Gallego-Sala, A.V., Pancost, R.D., Pearson, A., 2022. Metabolic and ecological controls on the stable carbon isotopic composition of archaeal (isoGDGT and BDGT) and bacterial (brGDGT) lipids in wetlands and lignites. Geochim. Cosmochim. Acta 320, 1–25. https://doi.org/10.1016/j.gca.2021.12.023
Blindow, I., Andersson, G., Hargeby, A., Johansson, S., 1993. Long-term pattern of alternative stable states in two shallow eutrophic lakes. Freshw. Biol. 30, 159–167. https://doi.org/10.1111/j.1365-2427.1993.tb00796.x
Blokker, P., van Bergen, P., Pancost, R., Collinson, M.E., de Leeuw, J.W., Sinninghe Damste, J.S., 2001. The chemical structure of Gloeocapsomorpha prisca microfossils: implications for their origin. Geochim. Cosmochim. Acta 65, 885–900. https://doi.org/10.1016/S0016-7037(00)00582-2
Blunier, T., Chappellaz, J., Schwander, J., Stauffer, B., Raynaud, D., 1995. Variations in atmospheric methane concentration during the Holocene epoch. Nature 374, 46–49. https://doi.org/10.1038/374046a0
Bond, G., Kromer, B., Beer, J., Muscheler, R., Evans, M.N., Showers, W., Hoffmann, S., Lotti-Bond, R., Hajdas, I., Bonani, G., 2001. Persistent Solar Influence on North Atlantic Climate During the Holocene. Science 294, 2130–2136. https://doi.org/10.1126/science.1065680
Bonnefille, R., Chalié, F., 2000. Pollen-inferred precipitation time-series from equatorial mountains, Africa, the last 40 kyr BP. Paleomonsoon Var. Terr. Environ. Change 26, 25–50. https://doi.org/10.1016/S0921-8181(00)00032-1
Bonnefille, R., Riollet, G., 1988. The Kashiru Pollen Sequence (Burundi) Palaeoclimatic Implications for the Last 40,000 yr B.P. in Tropical Africa. Quat. Res. 30, 19–35. https://doi.org/10.1016/0033-5894(88)90085-3
Bonnefille, R., Riollet, G., Buchet, G., Icole, M., Lafont, R., Arnold, M., Jolly, D., 1995. Glacialanterglacial record from intertropical Africa, high resolution pollen and carbon data at Rusaka, Burundi. Quat. Sci. Rev. 14, 917–936.
Bonnefille, R., Roeland, J.C., Guiot, J., 1990. Temperature and rainfall estimates for the past 40,000 years in equatorial Africa. Nature 346, 347–349. https://doi.org/10.1038/346347a0
Booth, R.K., Jackson, S.T., Forman, S.L., Kutzbach, J.E., Bettis, E.A., Kreigs, J., Wright, D.K., 2005. A severe centennial-scale drought in midcontinental North America 4200 years ago and apparent global linkages. The Holocene 15, 321–328. https://doi.org/10.1191/0959683605hl825ft
Booth, R.K., Jackson, S.T., Gray, C.E., 2004. Paleoecology and high-resolution paleohydrology of a kettle peatland in upper Michigan. Quat. Res. 61, 1–13.
Bostoen, K., Clist, B., Doumenge, C., Grollemund, R., Hombert, J.-M., Muluwa, J.K., Maley, J., 2015. Middle to late Holocene Paleoclimatic change and the early Bantu expansion in the rain forests of Western Central Africa. Curr. Anthropol. 56, 354–384.
Bouchette, F., Schuster, M., Ghienne, J.-F., Denamiel, C., Roquin, C., Moussa, A., Marsaleix, P., Duringer, P., 2010. Hydrodynamics in Holocene Lake Mega-Chad. Quat. Res. 73, 226–236. https://doi.org/10.1016/j.yqres.2009.10.010
Bowen, G.J., 2008. Spatial analysis of the intra-annual variation of precipitation isotope

ratios and its climatological corollaries. J. Geophys. Res. Atmospheres 113. https://doi.org/10.1029/2007JD009295
Bray, E.E., Evans, E.D., 1961. Distribution of n-paraffins as a clue to recognition of source beds. Geochim. Cosmochim. Acta 22, 2–15. https://doi.org/10.1016/0016-7037(61)90069-2
Bremond, L., Alexandre, A., Peyron, O., Guiot, J., 2005. Grass water stress estimated from phytoliths in West Africa. J. Biogeogr. 32, 311–327. https://doi.org/10.1111/j.1365-2699.2004.01162.x
Brierley, C., Manning, K., Maslin, M., 2018. Pastoralism may have delayed the end of the green Sahara. Nat. Commun. 9, 4018. https://doi.org/10.1038/s41467-018-06321-y
Bristow, C.S., Holmes, J.A., Mattey, D., Salzmann, U., Sloane, H.J., 2018. A late Holocene palaeoenvironmental 'snapshot' of the Angamma Delta, Lake Megachad at the end of the African Humid Period. Arch. Hum. Environ. Their Interact. – Pap. Honour Profr. C Neil Roberts Profr. Henry F Lamb 202, 182–196. https://doi.org/10.1016/j.quascirev.2018.04.025
Brocks, J.J., Logan, G.A., Buick, R., Summons, R.E., 1999. Archean Molecular Fossils and the Early Rise of Eukaryotes. Science 285, 1033–1036. https://doi.org/10.1126/science.285.5430.1033
Broecker, W.S., Andree, M., Wolfli, W., Oeschger, H., Bonani, G., Kennett, J., Peteet, D., 1988. The chronology of the last Deglaciation: Implications to the cause of the Younger Dryas Event. Paleoceanography 3, 1–19. https://doi.org/10.1029/PA003i001p00001
Brook, E.J., Harder, S., Severinghaus, J., Steig, E.J., Sucher, C.M., 2000. On the origin and timing of rapid changes in atmospheric methane during the Last Glacial Period. Glob. Biogeochem. Cycles 14, 559–572. https://doi.org/10.1029/1999GB001182
Brooks, S.J., Birks, H.J.B., 2001. Chironomid-inferred air temperatures from Lateglacial and Holocene sites in north-west Europe: progress and problems. Eur. Quat. Biostratigraphy 20, 1723–1741. https://doi.org/10.1016/S0277-3791(01)00038-5
Brown, F.H., Fuller, C.R., 2008. Stratigraphy and tephra of the Kibish Formation, southwestern Ethiopia. Paleoanthropology Kibish Form. South. Ethiop. 55, 366–403. https://doi.org/10.1016/j.jhevol.2008.05.009
Brubaker, K.L., Entekhabi, D., Eagleson, P.S., 1993. Estimation of Continental Precipitation Recycling. J. Clim. 6, 1077–1089. https://doi.org/10.1175/1520-0442(1993)006<1077:EOCPR>2.0.CO;2
Bush, R.T., McInerney, F.A., 2013. Leaf wax n-alkane distributions in and across modern plants: Implications for paleoecology and chemotaxonomy. Geochim. Cosmochim. Acta 117, 161–179. https://doi.org/10.1016/j.gca.2013.04.016
Cao, M., Rueda, G., Rivas-Ruiz, P., Trapote, M.C., Henriksen, M., Vegas-Vilarrúbia, T., Rosell-Melé, A., 2018. Branched GDGT variability in sediments and soils from catchments with marked temperature seasonality. Org. Geochem. 122, 98–114. https://doi.org/10.1016/j.orggeochem.2018.05.007
Castañeda, I.S., Schouten, S., 2011. A review of molecular organic proxies for examining modern and ancient lacustrine environments. Quat. Sci. Rev. 30, 2851–2891. https://doi.org/10.1016/j.quascirev.2011.07.009
Cerling, T.E., Harris, J.M., 1999. Carbon isotope fractionation between diet and bioapatite in ungulate mammals and implications for ecological and paleoecological studies. Oecologia 120, 347–363. https://doi.org/10.1007/s004420050868

Chambers, F.M., Beilman, D.W., Yu, Z., 2011. Methods for determining peat humification and for quantifying peat bulk density, organic matter and carbon content for palaeostudies of climate and peatland carbon dynamics. Mires Peat 7, 1–10.
Champion, L., Gestrich, N., MacDonald, K., Nieblas-Ramirez, L., Fuller, D.Q., 2021. Pearl millet and iron in the West African Sahel: Archaeobotanical investigation at Tongo Maaré Diabal, Mali. J. Archaeol. Sci. Rep. 39, 103110. https://doi.org/10.1016/j.jasrep.2021.103110
Chen, Y., Zheng, F., Yang, H., Yang, W., Wu, R., Liu, X., Liang, H., Chen, H., Pei, H., Zhang, C., Pancost, R.D., Zeng, Z., 2022. The production of diverse brGDGTs by an Acidobacterium providing a physiological basis for paleoclimate proxies. Geochim. Cosmochim. Acta 337, 155–165. https://doi.org/10.1016/j.gca.2022.08.033
Chikaraishi, Y., Naraoka, H., 2003. Compound-specific δD–δ13C analyses of n-alkanes extracted from terrestrial and aquatic plants. Phytochemistry 63, 361–371. https://doi.org/10.1016/S0031-9422(02)00749-5
Chikaraishi, Y., Naraoka, H., Poulson, S.R., 2004. Hydrogen and carbon isotopic fractionations of lipid biosynthesis among terrestrial (C3, C4 and CAM) and aquatic plants. Phytochemistry 65, 1369–1381. https://doi.org/10.1016/j.phytochem.2004.03.036
Chimner, R.A., Ewel, K.C., 2005. A tropical freshwater wetland: II. Production, decomposition, and peat formation. Wetl. Ecol. Manag. 13, 671–684.
Clark, P.U., Marshall, S.J., Clarke, G.K.C., Hostetler, S.W., Licciardi, J.M., Teller, J.T., 2001. Freshwater Forcing of Abrupt Climate Change During the Last Glaciation. Science 293, 283–287. https://doi.org/10.1126/science.1062517
Claussen, M., Dallmeyer, A., Bader, J., 2017. Theory and Modeling of the African Humid Period and the Green Sahara. https://doi.org/10.1093/acrefore/9780190228620.013.532
Claussen, M., Kubatzki, C., Brovkin, V., Ganopolski, A., Hoelzmann, P., Pachur, H.-J., 1999. Simulation of an abrupt change in Saharan vegetation in the Mid-Holocene. Geophys. Res. Lett. 26, 2037–2040. https://doi.org/10.1029/1999GL900494
Clist, B., Bostoen, K., de Maret, P., Eggert, M.K.H., Höhn, A., Mbida Mindzié, C., Neumann, K., Seidensticker, D., 2018. Did human activity really trigger the late Holocene rainforest crisis in Central Africa? Proc. Natl. Acad. Sci. 115, E4733–E4734. https://doi.org/10.1073/pnas.1805247115
Clymo, R.S., 1984. The limits to peat bog growth. Philos. Trans. R. Soc. Lond. B Biol. Sci. 303, 605–654.
Clymo, R.S., 1963. Ion Exchange in Sphagnum and its Relation to Bog Ecology. Ann. Bot. 27, 309–324. https://doi.org/10.1093/oxfordjournals.aob.a083847
Clymo, R.S., Turunen, J., Tolonen, K., 1998. Carbon accumulation in peatland. Oikos 368–388.
Coffinet, S., 2015. Validation and application of lipid biomarkers to reconstruct past environmental changes in East Africa. Paris 6.
Coffinet, S., Huguet, A., Bergonzini, L., Pedentchouk, N., Williamson, D., Anquetil, C., Gałka, M., Kołaczek, P., Karpińska-Kołaczek, M., Majule, A., Laggoun-Défarge, F., Wagner, T., Derenne, S., 2018. Impact of climate change on the ecology of the Kyambangunguru crater marsh in southwestern Tanzania during the Late Holocene. Quat. Sci. Rev. 196, 100–117. https://doi.org/10.1016/j.quascirev.2018.07.038
Coffinet, S., Huguet, A., Pedentchouk, N., Bergonzini, L., Omuombo, C., Williamson, D., Anquetil, C., Jones, M., Majule, A., Wagner, T., Derenne, S., 2017. Evaluation of branched GDGTs and leaf wax n-alkane δ2H as (paleo) environmental proxies in East

Africa. Geochim. Cosmochim. Acta 198, 182–193. https://doi.org/10.1016/j.gca.2016.11.020
Collins, J.A., Prange, M., Caley, T., Gimeno, L., Beckmann, B., Mulitza, S., Skonieczny, C., Roche, D., Schefuß, E., 2017. Rapid termination of the African Humid Period triggered by northern high-latitude cooling. Nat. Commun. 8, 1372. https://doi.org/10.1038/s41467-017-01454-y
Collins, M., 2000. The El Niño–Southern Oscillation in the Second Hadley Centre Coupled Model and Its Response to Greenhouse Warming. J. Clim. 13, 1299–1312. https://doi.org/10.1175/1520-0442(2000)013<1299:TENOSO>2.0.CO;2
Collister, J.W., Rieley, G., Stern, B., Eglinton, G., Fry, B., 1994. Compound-specific δ 13C analyses of leaf lipids from plants with differing carbon dioxide metabolisms. Org. Geochem. 21, 619–627. https://doi.org/10.1016/0146-6380(94)90008-6
Cooper, H.V., Vane, C.H., Evers, S., Aplin, P., Girkin, N.T., Sjögersten, S., 2019. From peat swamp forest to oil palm plantations: The stability of tropical peatland carbon. Geoderma 342, 109–117.
Corbet, B., Albrecht, P., Ourisson, G., 1980. Photochemical or photomimetic fossil triterpenoids in sediments and petroleum. J. Am. Chem. Soc. 102, 1171–1173.
Costa, K., Russell, J., Konecky, B., Lamb, H., 2014. Isotopic reconstruction of the African Humid Period and Congo Air Boundary migration at Lake Tana, Ethiopia. Quat. Sci. Rev. 83, 58–67. https://doi.org/10.1016/j.quascirev.2013.10.031
Cranwell, P.A., 1984. Lipid geochemistry of sediments from Upton Broad, a small productive lake. Org. Geochem. 7, 25–37.
Dallmeyer, A., Claussen, M., Lorenz, S.J., Shanahan, T., 2020. The end of the African humid period as seen by a transient comprehensive Earth system model simulation of the last 8000 years. Clim Past 16, 117–140. https://doi.org/10.5194/cp-16-117-2020
Dang, X., Yang, H., Naafs, B.D.A., Pancost, R.D., Xie, S., 2016. Evidence of moisture control on the methylation of branched glycerol dialkyl glycerol tetraethers in semi-arid and arid soils. Geochim. Cosmochim. Acta 189, 24–36. https://doi.org/10.1016/j.gca.2016.06.004
Dansgaard, W., 1964. Stable isotopes in precipitation. Tellus 16, 436–468. https://doi.org/10.3402/tellusa.v16i4.8993
Dansgaard, W., Johnsen, S.J., Clausen, H.B., Dahl-Jensen, D., Gundestrup, N.S., Hammer, C.U., Hvidberg, C.S., Steffensen, J.P., Sveinbjörnsdottir, A.E., Jouzel, J., Bond, G., 1993. Evidence for general instability of past climate from a 250-kyr ice-core record. Nature 364, 218–220. https://doi.org/10.1038/364218a0
Dargie, G.C., 2015. Quantifying and understanding the tropical peatlands of the central Congo basin (PhD Thesis). University of Leeds.
Davis, B.A.S., Brewer, S., Stevenson, A.C., Guiot, J., 2003. The temperature of Europe during the Holocene reconstructed from pollen data. Quat. Sci. Rev. 22, 1701–1716. https://doi.org/10.1016/S0277-3791(03)00173-2
De Jonge, C., Hopmans, E.C., Stadnitskaia, A., Rijpstra, W.I.C., Hofland, R., Tegelaar, E., Sinninghe Damsté, J.S., 2013. Identification of novel penta- and hexamethylated branched glycerol dialkyl glycerol tetraethers in peat using HPLC–MS2, GC–MS and GC–SMB-MS. Org. Geochem. 54, 78–82. https://doi.org/10.1016/j.orggeochem.2012.10.004
De Jonge, C., Hopmans, E.C., Zell, C.I., Kim, J.-H., Schouten, S., Sinninghe Damsté, J.S., 2014. Occurrence and abundance of 6-methyl branched glycerol dialkyl glycerol tetraethers

in soils: Implications for palaeoclimate reconstruction. Geochim. Cosmochim. Acta 141, 97–112. https://doi.org/10.1016/j.gca.2014.06.013
De Jonge, C., Kuramae, E.E., Radujković, D., Weedon, J.T., Janssens, I.A., Peterse, F., 2021. The influence of soil chemistry on branched tetraether lipids in mid- and high latitude soils: Implications for brGDGT- based paleothermometry. Geochim. Cosmochim. Acta 310, 95–112. https://doi.org/10.1016/j.gca.2021.06.037
De Jonge, C., Radujković, D., Sigurdsson, B.D., Weedon, J.T., Janssens, I., Peterse, F., 2019. Lipid biomarker temperature proxy responds to abrupt shift in the bacterial community composition in geothermally heated soils. Org. Geochem. 137, 103897. https://doi.org/10.1016/j.orggeochem.2019.07.006
de Mesmay, R., Metzger, P., Grossi, V., Derenne, S., 2008. Mono- and dicyclic unsaturated triterpenoid hydrocarbons in sediments from Lake Masoko (Tanzania) widely extend the botryococcene family. Org. Geochem. 39, 879–893. https://doi.org/10.1016/j.orggeochem.2008.01.024
de Rosa, M., de Rosa, S., Gambacorta, A., Minale, L., Bu'lock, J.D., 1977. Chemical structure of the ether lipids of thermophilic acidophilic bacteria of the Caldariella group. Phytochemistry 16, 1961–1965. https://doi.org/10.1016/0031-9422(77)80105-2
Dean, J.F., Middelburg, J.J., Röckmann, T., Aerts, R., Blauw, L.G., Egger, M., Jetten, M.S.M., de Jong, A.E.E., Meisel, O.H., Rasigraf, O., Slomp, C.P., in't Zandt, M.H., Dolman, A.J., 2018. Methane Feedbacks to the Global Climate System in a Warmer World. Rev. Geophys. 56, 207–250. https://doi.org/10.1002/2017RG000559
Dearing Crampton-Flood, E., Tierney, J.E., Peterse, F., Kirkels, F.M.S.A., Sinninghe Damsté, J.S., 2020. BayMBT: A Bayesian calibration model for branched glycerol dialkyl glycerol tetraethers in soils and peats. Geochim. Cosmochim. Acta 268, 142–159. https://doi.org/10.1016/j.gca.2019.09.043
Dehmer, J., 1995. Petrological and organic geochemical investigation of recent peats with known environments of deposition. Int. J. Coal Geol. 28, 111–138. https://doi.org/10.1016/0166-5162(95)00016-X
Delalande, M., Bergonzini, L., Massault, M., 2008. Mbaka lakes isotopic (18O and 2H) and water balances: discussion on the used atmospheric moisture compositions. Isotopes Environ. Health Stud. 44, 71–82. https://doi.org/10.1080/10256010801887414
DeMenocal, P., Ortiz, J., Guilderson, T., Adkins, J., Sarnthein, M., Baker, L., Yarusinsky, M., 2000. Abrupt onset and termination of the African Humid Period: rapid climate responses to gradual insolation forcing. Quat. Sci. Rev. 19, 347–361.
Demenou, B.B., Piñeiro, R., Hardy, O.J., 2016. Origin and history of the Dahomey Gap separating West and Central African rain forests: insights from the phylogeography of the legume tree Distemonanthus benthamianus. J. Biogeogr. 43, 1020–1031. https://doi.org/10.1111/jbi.12688
Depreux, B., Lefèvre, D., Berger, J.-F., Segaoui, F., Boudad, L., El Harradji, A., Degeai, J.-P., Limondin-Lozouet, N., 2021. Alluvial records of the African Humid Period from the NW African highlands (Moulouya basin, NE Morocco). Quat. Sci. Rev. 255, 106807. https://doi.org/10.1016/j.quascirev.2021.106807
Desjardins, T., Turcq, B., Nguetnkam, J.-P., Achoundong, G., Mandeng-Yogo, M., Cetin, F., Lézine, A.-M., 2013. δ13C variation of soil organic matter as an indicator of vegetation change during the Holocene in central Cameroon. Comptes Rendus Geosci. 345, 266–271.
Diefendorf, A.F., Freimuth, E.J., 2017. Extracting the most from terrestrial plant-derived n-

alkyl lipids and their carbon isotopes from the sedimentary record: A review. Org. Geochem. 103, 1–21.
Ding, S., Xu, Y., Wang, Y., He, Y., Hou, J., Chen, L., He, J.-S., 2015. Distribution of branched glycerol dialkyl glycerol tetraethers in surface soils of the Qinghai–Tibetan Plateau: implications of brGDGTs-based proxies in cold and dry regions. Biogeosciences 12, 3141–3151. https://doi.org/10.5194/bg-12-3141-2015
Disnar, J.-R., Guillet, B., Kéravis, D., Di-Giovanni, C., Sebag, D., 2003. Soil organic matter (SOM) characterization by Rock-Eval pyrolysis: scope and limitations. Org. Geochem. 34, 327–343.
Dodla, S.K., Wang, J.J., DeLaune, R.D., 2012. Characterization of labile organic carbon in coastal wetland soils of the Mississippi River deltaic plain: relationships to carbon functionalities. Sci. Total Environ. 435, 151–158.
Drake, N.A., Blench, R.M., Armitage, S.J., Bristow, C.S., White, K.H., 2011. Ancient watercourses and biogeography of the Sahara explain the peopling of the desert. Proc. Natl. Acad. Sci. 108, 458–462. https://doi.org/10.1073/pnas.1012231108
Drollinger, S., Kuzyakov, Y., Glatzel, S., 2019. Effects of peat decomposition on ^{13}C and ^{15}N depth profiles of Alpine bogs. Catena 178, 1–10.
Drysdale, R., Zanchetta, G., Hellstrom, J., Maas, R., Fallick, A., Pickett, M., Cartwright, I., Piccini, L., 2006. Late Holocene drought responsible for the collapse of Old World civilizations is recorded in an Italian cave flowstone. Geology 34, 101–104. https://doi.org/10.1130/G22103.1
Dubois, N., Oppo, D.W., Galy, V.V., Mohtadi, M., van der Kaars, S., Tierney, J.E., Rosenthal, Y., Eglinton, T.I., Lückge, A., Linsley, B.K., 2014. Indonesian vegetation response to changes in rainfall seasonality over the past 25,000 years. Nat. Geosci. 7, 513–517. https://doi.org/10.1038/ngeo2182
Dumoulin, J., Comby-Zerbino, C., Delqué-Količ, E., Moreau, C., Caffy, I., Hain, S., Perron, M., Thellier, B., Setti, V., Berthier, B., Beck, L., 2017. Status report on sample preparation protocols developed at the LMC14 Laboratory, Saclay, France: from sample collection to 14C AMS measurement. Radiocarbon 59, 713–726.
Dunne, J., Evershed, R.P., Salque, M., Cramp, L., Bruni, S., Ryan, K., Biagetti, S., di Lernia, S., 2012. First dairying in green Saharan Africa in the fifth millennium bc. Nature 486, 390–394. https://doi.org/10.1038/nature11186
Dykoski, C.A., Edwards, R.L., Cheng, H., Yuan, D., Cai, Y., Zhang, M., Lin, Y., Qing, J., An, Z., Revenaugh, J., 2005. A high-resolution, absolute-dated Holocene and deglacial Asian monsoon record from Dongge Cave, China. Earth Planet. Sci. Lett. 233, 71–86. https://doi.org/10.1016/j.epsl.2005.01.036
Egerer, S., Claussen, M., Reick, C., Stanelle, T., 2016. The link between marine sediment records and changes in Holocene Saharan landscape: simulating the dust cycle. Clim Past 12, 1009–1027. https://doi.org/10.5194/cp-12-1009-2016
Eglinton, G., Hamilton, R.J., 1967. Leaf Epicuticular Waxes. Science 156, 1322–1335. https://doi.org/10.1126/science.156.3780.1322
Eglinton, T.I., Eglinton, G., 2008. Molecular proxies for paleoclimatology. Earth Planet. Sci. Lett. 275, 1–16. https://doi.org/10.1016/j.epsl.2008.07.012
Ehrmann, W., Schmiedl, G., Beuscher, S., Krüger, S., 2017. Intensity of African Humid Periods Estimated from Saharan Dust Fluxes. PLOS ONE 12, e0170989. https://doi.org/10.1371/journal.pone.0170989
Elvert, M., Pohlman, J.W., Becker, K.W., Gaglioti, B., Hinrichs, K.-U., Wooller, M.J., 2016.

Methane turnover and environmental change from Holocene lipid biomarker records in a thermokarst lake in Arctic Alaska. The Holocene 26, 1766–1777. https://doi.org/10.1177/0959683616645942
Ensminger, A., Van Dorsselaer, A., Spyckerelle, C., Albrecht, P., Ourisson, G., 1974. Pentacyclic triterpenes of the hopane type as ubiquitous geochemical markers: origin and significance. Adv. Org. Geochem. 1973 245–260.
Evans, M.G., Burt, T.P., Holden, J., Adamson, J.K., 1999. Runoff generation and water table fluctuations in blanket peat: evidence from UK data spanning the dry summer of 1995. J. Hydrol. 221, 141–160.
Farquhar, G.D., Ehleringer, J.R., Hubick, K.T., 1989. Carbon Isotope Discrimination and Photosynthesis. Annu. Rev. Plant Physiol. Plant Mol. Biol. 40, 503–537. https://doi.org/10.1146/annurev.pp.40.060189.002443
Farrimond, P., Bevan, J.C., Bishop, A.N., 1996. Hopanoid hydrocarbon maturation by an igneous intrusion. Org. Geochem. 25, 149–164. https://doi.org/10.1016/S0146-6380(96)00128-3
Farrimond, P., Flanagan, R.L., 1996. Lipid stratigraphy of a Flandrian peat bed (Northumberland, UK): comparison with the pollen record. The Holocene 6, 69–74.
Farrimond, P., Love, G.D., Bishop, A.N., Innes, H.E., Watson, D.F., Snape, C.E., 2003. Evidence for the rapid incorporation of hopanoids into kerogen. Geochim. Cosmochim. Acta 67, 1383–1394. https://doi.org/10.1016/S0016-7037(02)01287-5
Feakins, S.J., Bentley, L.P., Salinas, N., Shenkin, A., Blonder, B., Goldsmith, G.R., Ponton, C., Arvin, L.J., Wu, M.S., Peters, T., West, A.J., Martin, R.E., Enquist, B.J., Asner, G.P., Malhi, Y., 2016. Plant leaf wax biomarkers capture gradients in hydrogen isotopes of precipitation from the Andes and Amazon. Geochim. Cosmochim. Acta 182, 155–172. https://doi.org/10.1016/j.gca.2016.03.018
Feka, N.Z., Ajonina, G.N., 2011. Drivers causing decline of mangrove in West-Central Africa: a review. Int. J. Biodivers. Sci. Ecosyst. Serv. Manag. 7, 217–230. https://doi.org/10.1080/21513732.2011.634436
Feng, X., Porporato, A., Rodriguez-Iturbe, I., 2013. Changes in rainfall seasonality in the tropics. Nat. Clim. Change 3, 811–815. https://doi.org/10.1038/nclimate1907
Ficken, K.J., Li, B., Swain, D.L., Eglinton, G., 2000. An n-alkane proxy for the sedimentary input of submerged/floating freshwater aquatic macrophytes. Org. Geochem. 31, 745–749. https://doi.org/10.1016/S0146-6380(00)00081-4
Fisk, M.C., Ruether, K.F., Yavitt, J.B., 2003. Microbial activity and functional composition among northern peatland ecosystems. Soil Biol. Biochem. 35, 591–602. https://doi.org/10.1016/S0038-0717(03)00053-1
Flato, G., Marotzke, J., Abiodun, B., Braconnot, P., Chou, S.C., Collins, W., Cox, P., Driouech, F., Emori, S., Eyring, V., 2014. Evaluation of climate models, in: Climate Change 2013: The Physical Science Basis. Contribution of Working Group I to the Fifth Assessment Report of the Intergovernmental Panel on Climate Change. Cambridge University Press, pp. 741–866.
Fleitmann, D., Burns, S.J., Mangini, A., Mudelsee, M., Kramers, J., Villa, I., Neff, U., Al-Subbary, A.A., Buettner, A., Hippler, D., Matter, A., 2007. Holocene ITCZ and Indian monsoon dynamics recorded in stalagmites from Oman and Yemen (Socotra). Quat. Sci. Rev. 26, 170–188. https://doi.org/10.1016/j.quascirev.2006.04.012
Fleitmann, D., Mudelsee, M., Burns, S.J., Bradley, R.S., Kramers, J., Matter, A., 2008. Evidence for a widespread climatic anomaly at around 9.2 ka before present.

Paleoceanography 23. https://doi.org/10.1029/2007PA001519
Fontaine, B., Janicot, S., 1992. Wind-Field Coherence and Its Variations over West Africa. J. Clim. 5, 512–524. https://doi.org/10.1175/1520-0442(1992)005<0512:WFCAIV>2.0.CO;2
Forman, S.L., Wright, D.K., Bloszies, C., 2014. Variations in water level for Lake Turkana in the past 8500 years near Mt. Porr, Kenya and the transition from the African Humid Period to Holocene aridity. Quat. Sci. Rev. 97, 84–101. https://doi.org/10.1016/j.quascirev.2014.05.005
France-Lanord, C., Derry, L.A., 1994. δ13C of organic carbon in the Bengal Fan: Source evolution and transport of C3 and C4 plant carbon to marine sediments. Geochim. Cosmochim. Acta 58, 4809–4814. https://doi.org/10.1016/0016-7037(94)90210-0
Francey, R.J., Allison, C.E., Etheridge, D.M., Trudinger, C.M., ENTING, I.G., Leuenberger, M., Langenfelds, R.L., Michel, E., Steele, L.P., 1999. A 1000-year high precision record of δ13C in atmospheric CO2. Tellus B 51, 170–193. https://doi.org/10.1034/j.1600-0889.1999.t01-1-00005.x
Fritz, S.C., 2008. Deciphering climatic history from lake sediments. J. Paleolimnol. 39, 5–16. https://doi.org/10.1007/s10933-007-9134-x
Frolking, S., Roulet, N.T., 2007. Holocene radiative forcing impact of northern peatland carbon accumulation and methane emissions. Glob. Change Biol. 13, 1079–1088. https://doi.org/10.1111/j.1365-2486.2007.01339.x
Frolking, S., Roulet, N.T., Moore, T.R., Richard, P.J., Lavoie, M., Muller, S.D., 2001. Modeling northern peatland decomposition and peat accumulation. Ecosystems 4, 479–498.
Fuhrmann, A., Mingram, J., Lücke, A., Lu, H., Horsfield, B., Liu, J., Negendank, J.F.W., Schleser, G.H., Wilkes, H., 2003. Variations in organic matter composition in sediments from Lake Huguang Maar (Huguangyan), south China during the last 68 ka: implications for environmental and climatic change. Org. Geochem. 34, 1497–1515. https://doi.org/10.1016/S0146-6380(03)00158-X
Gadea, A., Khazem, M., Gaslonde, T., 2022. Current knowledge on chemistry of Proteaceae family, and biological activities of their bis-5-alkylresorcinol derivatives. Phytochem. Rev. 21, 1969–2005. https://doi.org/10.1007/s11101-022-09821-4
Gagosian, R.B., Peltzer, E.T., 1986. The importance of atmospheric input of terrestrial organic material to deep sea sediments. Org. Geochem. 10, 661–669. https://doi.org/10.1016/S0146-6380(86)80002-X
Gajewski, K., Lézine, A.-M., Vincens, A., Delestan, A., Sawada, M., 2002. Modern climate–vegetation–pollen relations in Africa and adjacent areas. Quat. Sci. Rev. 21, 1611–1631. https://doi.org/10.1016/S0277-3791(01)00152-4
Gao, L., Hou, J., Toney, J., MacDonald, D., Huang, Y., 2011. Mathematical modeling of the aquatic macrophyte inputs of mid-chain n-alkyl lipids to lake sediments: Implications for interpreting compound specific hydrogen isotopic records. Geochim. Cosmochim. Acta 75, 3781–3791. https://doi.org/10.1016/j.gca.2011.04.008
Gao, M., Simoneit, B.R.T., Gantar, M., Jaffé, R., 2007. Occurrence and distribution of novel botryococcene hydrocarbons in freshwater wetlands of the Florida Everglades. Chemosphere 70, 224–236. https://doi.org/10.1016/j.chemosphere.2007.06.056
Garcin, Y., Deschamps, P., Ménot, G., De Saulieu, G., Schefuß, E., Sebag, D., Dupont, L.M., Oslisly, R., Brademann, B., Mbusnum, K.G., Onana, J.-M., Ako, A.A., Epp, L.S., Tjallingii, R., Strecker, M.R., Brauer, A., Sachse, D., 2018. Early anthropogenic impact on Western Central African rainforests 2,600 y ago. Proc. Natl. Acad. Sci. USA 115,

3261–3266.
Garcin, Y., Melnick, D., Strecker, M.R., Olago, D., Tiercelin, J.-J., 2012a. East African mid-Holocene wet–dry transition recorded in palaeo-shorelines of Lake Turkana, northern Kenya Rift. Earth Planet. Sci. Lett. 331–332, 322–334. https://doi.org/10.1016/j.epsl.2012.03.016
Garcin, Y., Schefuß, E., Dargie, G.C., Hawthorne, D., Lawson, I.T., Sebag, D., Biddulph, G.E., Crezee, B., Bocko, Y.E., Ifo, S.A., Mampouya Wenina, Y.E., Mbemba, M., Ewango, C.E.N., Emba, O., Bola, P., Kanyama Tabu, J., Tyrrell, G., Young, D.M., Gassier, G., Girkin, N.T., Vane, C.H., Adatte, T., Baird, A.J., Boom, A., Gulliver, P., Morris, P.J., Page, S.E., Sjögersten, S., Lewis, S.L., 2022. Hydroclimatic vulnerability of peat carbon in the central Congo Basin. Nature 1–6.
Garcin, Y., Schefuß, E., Schwab, V.F., Garreta, V., Gleixner, G., Vincens, A., Todou, G., Séné, O., Onana, J.-M., Achoundong, G., Sachse, D., 2014. Reconstructing C3 and C4 vegetation cover using n-alkane carbon isotope ratios in recent lake sediments from Cameroon, Western Central Africa. Geochim. Cosmochim. Acta 142, 482–500. https://doi.org/10.1016/j.gca.2014.07.004
Garcin, Y., Schwab, V.F., Gleixner, G., Kahmen, A., Todou, G., Séné, O., Onana, J.-M., Achoundong, G., Sachse, D., 2012b. Hydrogen isotope ratios of lacustrine sedimentary n-alkanes as proxies of tropical African hydrology: Insights from a calibration transect across Cameroon. Geochim. Cosmochim. Acta 79, 106–126. https://doi.org/10.1016/j.gca.2011.11.039
Garcin, Y., Vincens, A., Williamson, D., Buchet, G., Guiot, J., 2007. Abrupt resumption of the African Monsoon at the Younger Dryas—Holocene climatic transition. Quat. Sci. Rev. 26, 690–704. https://doi.org/10.1016/j.quascirev.2006.10.014
Garelick, S., Russell, J.M., Dee, S., Verschuren, D., Olago, D.O., 2021. Atmospheric controls on precipitation isotopes and hydroclimate in high-elevation regions in Eastern Africa since the Last Glacial Maximum. Earth Planet. Sci. Lett. 567, 116984.
Gasse, F., 2000. Hydrological changes in the African tropics since the Last Glacial Maximum. Quat. Sci. Rev. 19, 189–211.
Gasse, F., 1977. Evolution of Lake Abhé (Ethiopia and TFAI), from 70,000 b.p. Nature 265, 42–45. https://doi.org/10.1038/265042a0
Gasse, F., Téhet, R., Durand, A., Gibert, E., Fontes, J.-C., 1990. The arid–humid transition in the Sahara and the Sahel during the last deglaciation. Nature 346, 141–146. https://doi.org/10.1038/346141a0
Gasse, F., Van Campo, E., 1994. Abrupt post-glacial climate events in West Asia and North Africa monsoon domains. Earth Planet. Sci. Lett. 126, 435–456. https://doi.org/10.1016/0012-821X(94)90123-6
Gat, J.R., 1996. Oxygen and hydrogen isotopes in the hydrologic cycle. Annu. Rev. Earth Planet. Sci. 24, 225–262. https://doi.org/10.1146/annurev.earth.24.1.225
Georgiou, C.D., Deamer, D.W., 2014. Lipids as Universal Biomarkers of Extraterrestrial Life. Astrobiology 14, 541–549. https://doi.org/10.1089/ast.2013.1134
Ghienne, J.-F., Schuster, M., Bernard, A., Duringer, P., Brunet, M., 2002. The Holocene giant Lake Chad revealed by digital elevation models. Holocene Stud. INQUA Comm. Meet. Sevilla 2000 87, 81–85. https://doi.org/10.1016/S1040-6182(01)00063-5
Giannini, A., Biasutti, M., Held, I.M., Sobel, A.H., 2008. A global perspective on African climate. Clim. Change 90, 359–383. https://doi.org/10.1007/s10584-008-9396-y
Gillespie, R., Street-Perrott, F.A., Switsur, R., 1983. Post-glacial arid episodes in Ethiopia have

implications for climate prediction. Nature 306, 680–683. https://doi.org/10.1038/306680a0
Gillette, D.A., Passi, R., 1988. Modeling dust emission caused by wind erosion. J. Geophys. Res. Atmospheres 93, 14233–14242. https://doi.org/10.1029/JD093iD11p14233
Giresse, P., Maley, J., Chepstow-Lusty, A., 2020. Understanding the 2500 yr BP rainforest crisis in West and Central Africa in the framework of the Late Holocene: Pluridisciplinary analysis and multi-archive reconstruction. Glob. Planet. Change 192, 103257.
Giresse, P., Maley, J., Doumenge, C., Philippon, N., Mahé, G., Chepstow-Lusty, A., Aleman, J., Lokonda, M., Elenga, H., 2018. Paleoclimatic changes are the most probable causes of the rainforest crises 2,600 y ago in Central Africa. Proc. Natl. Acad. Sci. 115, E6672–E6673. https://doi.org/10.1073/pnas.1807615115
Girkin, Nick T, Lopes dos Santos, R.A., Vane, C., Ostle, N., Turner, B.L., Sjögersten, S., 2020. Peat properties, dominant vegetation type and microbial community structure in a tropical peatland. Wetlands 40, 1367–1377.
Girkin, Nicholas T., Vane, C.H., Turner, B.L., Ostle, N.J., Sjögersten, S., 2020. Root oxygen mitigates methane fluxes in tropical peatlands. Environ. Res. Lett. 15, 064013.
Gonfiantini, R., Roche, M.-A., Olivry, J.-C., Fontes, J.-C., Zuppi, G.M., 2001. The altitude effect on the isotopic composition of tropical rains. Chem. Geol. 181, 147–167. https://doi.org/10.1016/S0009-2541(01)00279-0
Goudie, A.S., Middleton, N.J., 2001. Saharan dust storms: nature and consequences. Earth-Sci. Rev. 56, 179–204. https://doi.org/10.1016/S0012-8252(01)00067-8
Griepentrog, M., De Wispelaere, L., Bauters, M., Bodé, S., Hemp, A., Verschuren, D., Boeckx, P., 2019. Influence of plant growth form, habitat and season on leaf-wax n-alkane hydrogen-isotopic signatures in equatorial East Africa. Geochim. Cosmochim. Acta 263, 122–139. https://doi.org/10.1016/j.gca.2019.08.004
Grist, J.P., Nicholson, S.E., 2001. A Study of the Dynamic Factors Influencing the Rainfall Variability in the West African Sahel. J. Clim. 14, 1337–1359. https://doi.org/10.1175/1520-0442(2001)014<1337:ASOTDF>2.0.CO;2
Grossi, V., Caradec, S., Gilbert, F., 2003. Burial and reactivity of sedimentary microalgal lipids in bioturbated Mediterranean coastal sediments. Mar. Chem. 81, 57–69.
Grossi, V., de Mesmay, R., Bardoux, G., Metzger, P., Williamson, D., Derenne, S., 2012. Contrasting variations in the structure and stable carbon isotopic composition of botryococcenes through the last glacial–interglacial transition in Lake Masoko (southern Tanzania). Org. Geochem. 43, 150–155. https://doi.org/10.1016/j.orggeochem.2011.10.003
Grove, J.M., 2012. The little ice age. Routledge.
Gupta, L.P., Kawahata, H., 2006. Downcore diagenetic changes in organic matter and implications for paleoproductivity estimates. Glob. Planet. Change 53, 122–136.
Haflidason, H., Eiriksson, J., Kreveld, S.V., 2000. The tephrochronology of Iceland and the North Atlantic region during the Middle and Late Quaternary: a review. J. Quat. Sci. 15, 3–22. https://doi.org/10.1002/(SICI)1099-1417(200001)15:1<3::AID-JQS530>3.0.CO;2-W
Halamka, T.A., Raberg, J.H., McFarlin, J.M., Younkin, A.D., Mulligan, C., Liu, X.-L., Kopf, S.H., 2023. Production of diverse brGDGTs by Acidobacterium Solibacter usitatus in response to temperature, pH, and O2 provides a culturing perspective on brGDGT proxies and biosynthesis. Geobiology 21, 102–118.

https://doi.org/10.1111/gbi.12525
Han, J., Calvin, M., 1969. Hydrocarbon distribution of algae and bacteria, and microbiologial activity in sediments. Proc. Natl. Acad. Sci. 64, 436–443. https://doi.org/10.1073/pnas.64.2.436
Harris, I., Jones, P.D., Osborn, T.J., Lister, D.H., 2014. Updated high-resolution grids of monthly climatic observations–the CRU TS3. 10 Dataset. Int. J. Climatol. 34, 623–642.
Hart, B.S., Hofmann, M.H., 2022. Revisiting paleoenvironmental analyses and interpretations of organic-rich deposits: The importance of TOC corrections. Org. Geochem. 170, 104434.
Haug, G.H., Hughen, K.A., Sigman, D.M., Peterson, L.C., Röhl, U., 2001. Southward Migration of the Intertropical Convergence Zone Through the Holocene. Science 293, 1304–1308. https://doi.org/10.1126/science.1059725
He, Y., Zhao, C., Zheng, Z., Liu, Z., Wang, N., Li, J., Cheddadi, R., 2015. Peatland evolution and associated environmental changes in central China over the past 40,000 years. Quat. Res. 84, 255–261. https://doi.org/10.1016/j.yqres.2015.06.004
He, Y., Zhao, Q., Sun, D., 2022. Unique distribution pattern and δ13C signature of des-A-triterpenoids from Lake Wuliangsu: Source and paleoenvironmental implications. Org. Geochem. 174, 104509. https://doi.org/10.1016/j.orggeochem.2022.104509
Hede, M.U., Rasmussen, P., Noe-Nygaard, N., Clarke, A.L., Vinebrooke, R.D., Olsen, J., 2010. Multiproxy evidence for terrestrial and aquatic ecosystem responses during the 8.2 ka cold event as recorded at Højby Sø, Denmark. Quat. Res. 73, 485–496. https://doi.org/10.1016/j.yqres.2009.12.002
Heipieper, H.J., Neumann, G., Kabelitz, N., Kastner, M., Richnow, H.H., 2004. Carbon isotope fractionation during cis–trans isomerization of unsaturated fatty acids in Pseudomonas putida. Appl. Microbiol. Biotechnol. 66, 285–290. https://doi.org/10.1007/s00253-004-1734-z
Henderson, G.M., 2002. New oceanic proxies for paleoclimate. Earth Planet. Sci. Lett. 203, 1–13. https://doi.org/10.1016/S0012-821X(02)00809-9
Heubes, J., Kühn, I., König, K., Wittig, R., Zizka, G., Hahn, K., 2011. Modelling biome shifts and tree cover change for 2050 in West Africa. J. Biogeogr. 38, 2248–2258. https://doi.org/10.1111/j.1365-2699.2011.02560.x
Hightower, J.W., Hall, W.K., 1967. Tracer Studies of Acid-Catalyzed Reactions. VI. Deuterium Redistribution and Isotope Effects in n-butene Isomerization over Alumina and Silica-Alumina Catalysts. J. Am. Chem. Soc. 89, 778–787.
Hinrichs, K.-U., 2002. Microbial fixation of methane carbon at 2.7 Ga: Was an anaerobic mechanism possible? Geochem. Geophys. Geosystems 3, 1–10. https://doi.org/10.1029/2001GC000286
Hodgkins, S.B., Richardson, C.J., Dommain, R., Wang, H., Glaser, P.H., Verbeke, B., Winkler, B.R., Cobb, A.R., Rich, V.I., Missilmani, M., Flanagan, N., Ho, M., Hoyt, A.M., Harvey, C.F., Vining, S.R., Hough, M.A., Moore, T.R., Richard, P.J.H., De La Cruz, F.B., Toufaily, J., Hamdan, R., Cooper, W.T., Chanton, J.P., 2018. Tropical peatland carbon storage linked to global latitudinal trends in peat recalcitrance. Nat. Commun. 9, 3640.
Hoffmann, B., Kahmen, A., Cernusak, L.A., Arndt, S.K., Sachse, D., 2013. Abundance and distribution of leaf wax n-alkanes in leaves of Acacia and Eucalyptus trees along a strong humidity gradient in northern Australia. Org. Geochem. 62, 62–67. https://doi.org/10.1016/j.orggeochem.2013.07.003
Hogg, A.G., Heaton, T.J., Hua, Q., Palmer, J.G., Turney, C.S., Southon, J., Bayliss, A., Blackwell,

P.G., Boswijk, G., Bronk Ramsey, C., Pearson, C., Petchey, F., Reimer, P., Reimer, R., Wacker, L., 2020. SHCal20 Southern Hemisphere calibration, 0–55,000 years cal BP. Radiocarbon 62, 759–778.
Holton, J.R., Wallace, J.M., Young, J.A., 1971. On Boundary Layer Dynamics and the ITCZ. J. Atmospheric Sci. 28, 275–280. https://doi.org/10.1175/1520-0469(1971)028<0275:OBLDAT>2.0.CO;2
Hooghiemstra, H., Agwu, C.O., Beug, H.-J., 1986. Pollen and spore distribution in recent marine sediments: a record of NW-African seasonal wind patterns and vegetation belts. Meteor Forschungsergebnisse Reihe C Geol. Geophys. 40, 87–135.
Hooijer, A., Page, S., Canadell, J.G., Silvius, M., Kwadijk, J., Wösten, H., Jauhiainen, J., 2010. Current and future CO2 emissions from drained peatlands in Southeast Asia. Biogeosciences 7, 1505–1514. https://doi.org/10.5194/bg-7-1505-2010
Hooijer, A., Page, S., Jauhiainen, J., Lee, W.A., Lu, X.X., Idris, A., Anshari, G., 2012. Subsidence and carbon loss in drained tropical peatlands. Biogeosciences 9, 1053–1071. https://doi.org/10.5194/bg-9-1053-2012
Hopmans, E.C., Schouten, S., Damsté, J.S.S., 2016. The effect of improved chromatography on GDGT-based palaeoproxies. Org. Geochem. 93, 1–6.
Hoyos-Santillan, J., Lomax, B.H., Large, D., Turner, B.L., Lopez, O.R., Boom, A., Sepulveda-Jauregui, A., Sjögersten, S., 2019. Evaluation of vegetation communities, water table, and peat composition as drivers of greenhouse gas emissions in lowland tropical peatlands. Sci. Total Environ. 688, 1193–1204. https://doi.org/10.1016/j.scitotenv.2019.06.366
Hua, Q., Barbetti, M., Rakowski, A.Z., 2013. Atmospheric radiocarbon for the period 1950–2010. Radiocarbon 55, 2059–2072.
Huang, X., Meyers, P.A., Xue, J., Gong, L., Wang, X., Xie, S., 2015. Environmental factors affecting the low temperature isomerization of homohopanes in acidic peat deposits, central China. Geochim. Cosmochim. Acta 154, 212–228. https://doi.org/10.1016/j.gca.2015.01.031
Huang, X., Meyers, P.A., Xue, J., Zhang, Y., Wang, X., 2016. Paleoclimate significance of n-alkane molecular distributions and δ2H values in surface peats across the monsoon region of China. Palaeogeogr. Palaeoclimatol. Palaeoecol. 461, 77–86. https://doi.org/10.1016/j.palaeo.2016.08.011
Huang, X., Pancost, R.D., Xue, J., Gu, Y., Evershed, R.P., Xie, S., 2018. Response of carbon cycle to drier conditions in the mid-Holocene in central China. Nat. Commun. 9, 1369. https://doi.org/10.1038/s41467-018-03804-w
Huang, X., Wang, C., Zhang, J., wiesenberg, G.L.B., Zhang, Z., Xie, S., 2011. Comparison of free lipid compositions between roots and leaves of plants in the Dajiuhu Peatland, central China. Geochem. J. 45, 365–373. https://doi.org/10.2343/geochemj.1.0129
Huang, X., Xie, S., Zhang, C.L., Jiao, D., Huang, J., Yu, J., Jin, F., Gu, Y., 2008. Distribution of aliphatic des-A-triterpenoids in the Dajiuhu peat deposit, southern China. Stable Isot. Biogeosciences II 39, 1765–1771. https://doi.org/10.1016/j.orggeochem.2008.08.002
Huang, Y., Dupont, L., Sarnthein, M., Hayes, J.M., Eglinton, G., 2000. Mapping of C4 plant input from North West Africa into North East Atlantic sediments. Geochim. Cosmochim. Acta 64, 3505–3513. https://doi.org/10.1016/S0016-7037(00)00445-2
Huang, Y., Murray, M., Eglinton, G., Metzger, P., 1995. Sacredicene, a novel monocyclic C33 hydrocarbon from sediment of Sacred Lake, a tropical freshwater lake, Mount Kenya. Tetrahedron Lett. 36, 5973–5976. https://doi.org/10.1016/0040-4039(95)01156-C

Huang, Y., Street-Perrott, F.A., Metcalfe, S.E., Brenner, M., Moreland, M., Freeman, K.H., 2001. Climate Change as the Dominant Control on Glacial-Interglacial Variations in C3 and C4 Plant Abundance. Science 293, 1647–1651. https://doi.org/10.1126/science.1060143

Huang, Y., Street-Perrott, F.A., Perrott, R.A., Metzger, P., Eglinton, G., 1999. Glacial–interglacial environmental changes inferred from molecular and compound-specific δ13C analyses of sediments from Sacred Lake, Mt. Kenya. Geochim. Cosmochim. Acta 63, 1383–1404. https://doi.org/10.1016/S0016-7037(99)00074-5

Hughen, K.A., Eglinton, T.I., Xu, L., Makou, M., 2004. Abrupt Tropical Vegetation Response to Rapid Climate Changes. Science 304, 1955–1959. https://doi.org/10.1126/science.1092995

Hughen, K.A., Overpeck, J.T., Peterson, L.C., Trumbore, S., 1996. Rapid climate changes in the tropical Atlantic region during the last deglaciation. Nature 380, 51–54. https://doi.org/10.1038/380051a0

Hughes, R.H., Hughes, J.S., 1992. A directory of African wetlands. IUCN.

Huguet, A., Fosse, C., Laggoun-Défarge, F., Delarue, F., Derenne, S., 2013. Effects of a short-term experimental microclimate warming on the abundance and distribution of branched GDGTs in a French peatland. Geochim. Cosmochim. Acta 105, 294–315. https://doi.org/10.1016/j.gca.2012.11.037

Huguet, A., Fosse, C., Laggoun-Défarge, F., Toussaint, M.-L., Derenne, S., 2010. Occurrence and distribution of glycerol dialkyl glycerol tetraethers in a French peat bog. Org. Geochem. 41, 559–572. https://doi.org/10.1016/j.orggeochem.2010.02.015

Huguet, A., Francez, A.-J., Jusselme, M.D., Fosse, C., Derenne, S., 2014. A climatic chamber experiment to test the short term effect of increasing temperature on branched GDGT distribution in Sphagnum peat. Org. Geochem. 73, 109–112. https://doi.org/10.1016/j.orggeochem.2014.05.010

Huguet, C., Hopmans, E.C., Febo-Ayala, W., Thompson, D.H., Sinninghe Damsté, J.S., Schouten, S., 2006. An improved method to determine the absolute abundance of glycerol dibiphytanyl glycerol tetraether lipids. Org. Geochem. 37, 1036–1041. https://doi.org/10.1016/j.orggeochem.2006.05.008

Hulme, M., Doherty, R., Ngara, T., New, M., Lister, D., 2001. African climate change: 1900-2100. Clim. Res. 17, 145–168.

Igri, P.M., Tanessong, R.S., Vondou, D.A., Panda, J., Garba, A., Mkankam, F.K., Kamga, A., 2018. Assessing the performance of WRF model in predicting high-impact weather conditions over Central and Western Africa: an ensemble-based approach. Nat. Hazards 93, 1565–1587. https://doi.org/10.1007/s11069-018-3368-y

Inglis, G.N., Bhattacharya, T., Hemingway, J.D., Hollingsworth, E.H., Feakins, S.J., Tierney, J.E., 2022. Biomarker Approaches for Reconstructing Terrestrial Environmental Change. Annu. Rev. Earth Planet. Sci. 50, 369–394. https://doi.org/10.1146/annurev-earth-032320-095943

Inglis, G.N., Farnsworth, A., Lunt, D., Foster, G.L., Hollis, C.J., Pagani, M., Jardine, P.E., Pearson, P.N., Markwick, P., Galsworthy, A.M.J., Raynham, L., Taylor, Kyle.W.R., Pancost, R.D., 2015. Descent toward the Icehouse: Eocene sea surface cooling inferred from GDGT distributions. Paleoceanography 30, 1000–1020. https://doi.org/10.1002/2014PA002723

Inglis, G.N., Naafs, B.D.A., Zheng, Y., McClymont, E.L., Evershed, R.P., Pancost, R.D., 2018. Distributions of geohopanoids in peat: Implications for the use of hopanoid-based

proxies in natural archives. Geochim. Cosmochim. Acta 224, 249–261. https://doi.org/10.1016/j.gca.2017.12.029
Inglis, G.N., Naafs, B.D.A., Zheng, Y., Schellekens, J., Pancost, R.D., "the T-GRES peat database collaborators," 2019. ^{13}C values of bacterial hopanoids and leaf waxes as tracers for methanotrophy in peatlands. Geochim. Cosmochim. Acta 260, 244–256.
Ingram, H., 1978. Soil layers in mires: function and terminology. J. Soil Sci. 29, 224–227.
Innes, H.E., Bishop, A.N., Head, I.M., Farrimond, P., 1997. Preservation and diagenesis of hopanoids in Recent lacustrine sediments of Priest Pot, England. Role Bact. Process. Sourc. Sediment. Org. Matter 26, 565–576. https://doi.org/10.1016/S0146-6380(97)00017-X
Inubushi, K., Hadi, A., Okazaki, M., Yonebayashi, K., 1998. Effect of converting wetland forest to sago palm plantations on methane gas flux and organic carbon dynamics in tropical peat soil. Hydrol. Process. 12, 2073–2080. https://doi.org/10.1002/(SICI)1099-1085(19981030)12:13/14<2073::AID-HYP720>3.0.CO;2-K
Ise, T., Dunn, A.L., Wofsy, S.C., Moorcroft, P.R., 2008. High sensitivity of peat decomposition to climate change through water-table feedback. Nat. Geosci. 1, 763–766.
Issa, Ohba, T., Chako Tchamabé, B., Padrón, E., Hernández, P., Eneke Takem, E.G., Barrancos, J., Sighomnoun, D., Ooki, S., Nkamdjou, S., Kusakabe, M., Yoshida, Y., Dionis, S., 2014. Gas emission from diffuse degassing structures (DDS) of the Cameroon volcanic line (CVL): Implications for the prevention of CO2-related hazards. J. Volcanol. Geotherm. Res. 283, 82–93. https://doi.org/10.1016/j.jvolgeores.2014.07.001
Jackson, C.R., Liew, K.C., Yule, C.M., 2009. Structural and Functional Changes with Depth in Microbial Communities in a Tropical Malaysian Peat Swamp Forest. Microb. Ecol. 57, 402–412. https://doi.org/10.1007/s00248-008-9409-4
Jacob, H., Sonntag, C., 1991. An 8-year record of the seasonal variation of 2H and 18O in atmospheric water vapour and precipitation at Heidelberg, Germany. Tellus B 43, 291–300. https://doi.org/10.1034/j.1600-0889.1991.t01-2-00003.x
Jacob, J., Disnar, J.-R., Boussafir, M., Spadano Albuquerque, A.L., Sifeddine, A., Turcq, B., 2007. Contrasted distributions of triterpene derivatives in the sediments of Lake Caçó reflect paleoenvironmental changes during the last 20,000 yrs in NE Brazil. Org. Geochem. 38, 180–197. https://doi.org/10.1016/j.orggeochem.2006.10.007
Jahnke, L.L., Summons, R.E., Hope, J.M., Des Marais, D.J., 1999. Carbon isotopic fractionation in lipids from methanotrophic bacteria II: The effects of physiology and environmental parameters on the biosynthesis and isotopic signatures of biomarkers. Geochim. Cosmochim. Acta 63, 79–93.
Janssen, A.B., Janse, J.H., Beusen, A.H., Chang, M., Harrison, J.A., Huttunen, I., Kong, X., Rost, J., Teurlincx, S., Troost, T.A., van Wijk, D., Mooij, W.M., 2019. How to model algal blooms in any lake on earth. Environ. Change Assess. 36, 1–10. https://doi.org/10.1016/j.cosust.2018.09.001
Jauhiainen, J., Takahashi, H., Heikkinen, J.E.P., Martikainen, P.J., Vasander, H., 2005. Carbon fluxes from a tropical peat swamp forest floor. Glob. Change Biol. 11, 1788–1797.
Johnsen, S.J., Clausen, H.B., Dansgaard, W., Fuhrer, K., Gundestrup, N., Hammer, C.U., Iversen, P., Jouzel, J., Stauffer, B., steffensen, J.P., 1992. Irregular glacial interstadials recorded in a new Greenland ice core. Nature 359, 311–313. https://doi.org/10.1038/359311a0
Johnson, T.C., Brown, E.T., McManus, J., Barry, S., Barker, P., Gasse, F., 2002. A High-

Resolution Paleoclimate Record Spanning the Past 25,000 Years in Southern East Africa. Science 296, 113–132. https://doi.org/10.1126/science.1070057
Johnson, T.C., Kelts, K., Eric Odada, 2000. The Holocene History of Lake Victoria. Ambio 29, 2–11.
Jones, M.C., Peteet, D.M., Sambrotto, R., 2010. Late-glacial and Holocene ^{15}N and ^{13}C variation from a Kenai Peninsula, Alaska peatland. Palaeogeogr. Palaeoclimatol. Palaeoecol. 293, 132–143.
Jouzel, J., Alley, R.B., Cuffey, K.M., Dansgaard, W., Grootes, P., Hoffmann, G., Johnsen, S.J., Koster, R.D., Peel, D., Shuman, C.A., Stievenard, M., Stuiver, M., White, J., 1997. Validity of the temperature reconstruction from water isotopes in ice cores. J. Geophys. Res. Oceans 102, 26471–26487. https://doi.org/10.1029/97JC01283
Jungandreas, L., Hohenegger, C., Claussen, M., 2021. Influence of the representation of convection on the mid-Holocene West African Monsoon. Clim Past 17, 1665–1684. https://doi.org/10.5194/cp-17-1665-2021
Junginger, A., Trauth, M.H., 2013. Hydrological constraints of paleo-Lake Suguta in the Northern Kenya Rift during the African Humid Period (15–5kaBP). Glob. Planet. Change 111, 174–188. https://doi.org/10.1016/j.gloplacha.2013.09.005
Kanokratana, P., Uengwetwanit, T., Rattanachomsri, U., Bunterngsook, B., Nimchua, T., Tangphatsornruang, S., Plengvidhya, V., Champreda, V., Eurwilaichitr, L., 2011. Insights into the Phylogeny and Metabolic Potential of a Primary Tropical Peat Swamp Forest Microbial Community by Metagenomic Analysis. Microb. Ecol. 61, 518–528. https://doi.org/10.1007/s00248-010-9766-7
Kaplan, J.O., Folberth, G., Hauglustaine, D.A., 2006. Role of methane and biogenic volatile organic compound sources in late glacial and Holocene fluctuations of atmospheric methane concentrations. Glob. Biogeochem. Cycles 20. https://doi.org/10.1029/2005GB002590
Kaufman, D.S., Broadman, E., 2023. Revisiting the Holocene global temperature conundrum. Nature 614, 425–435. https://doi.org/10.1038/s41586-022-05536-w
Keddy, P.A., Fraser, L.H., Solomeshch, A.I., Junk, W.J., Campbell, D.R., Arroyo, M.T., Alho, C.J., 2009. Wet and wonderful: the world's largest wetlands are conservation priorities. BioScience 59, 39–51.
Keeling, C.D., 1979. The Suess effect: 13Carbon-14Carbon interrelations. Environ. Int. 2, 229–300. https://doi.org/10.1016/0160-4120(79)90005-9
Keely, J.E., Sandquist, D.R., 1992. Carbon: freshwater plants. Plant Cell Environ. 15, 1021–1035. https://doi.org/10.1111/j.1365-3040.1992.tb01653.x
Killops, V.J., Killops, S.D., 2013. Introduction to organic geochemistry. John Wiley & Sons.
Kim, D., Chin, M., Remer, L.A., Diehl, T., Bian, H., Yu, H., Brown, M.E., Stockwell, W.R., 2017. Role of surface wind and vegetation cover in multi-decadal variations of dust emission in the Sahara and Sahel. Atmos. Environ. 148, 282–296. https://doi.org/10.1016/j.atmosenv.2016.10.051
Kindler, P., Guillevic, M., Baumgartner, M., Schwander, J., Landais, A., Leuenberger, M., 2014. Temperature reconstruction from 10 to 120 kyr b2k from the NGRIP ice core. Clim Past 10, 887–902. https://doi.org/10.5194/cp-10-887-2014
Kip, N., van Winden, J.F., Pan, Y., Bodrossy, L., Reichart, G.-J., Smolders, A.J.P., Jetten, M.S.M., Damsté, J.S.S., Op den Camp, H.J.M., 2010. Global prevalence of methane oxidation by symbiotic bacteria in peat-moss ecosystems. Nat. Geosci. 3, 617–621. https://doi.org/10.1038/ngeo939

Kling, G.W., Clark, M.A., Wagner, G.N., Compton, H.R., Humphrey, A.M., Devine, J.D., Evans, W.C., Lockwood, J.P., Tuttle, M.L., Koenigsberg, E.J., 1987. The 1986 Lake Nyos Gas Disaster in Cameroon, West Africa. Science 236, 169–175. https://doi.org/10.1126/science.236.4798.169

Kluber, L.A., Johnston, E.R., Allen, S.A., Hendershot, J.N., Hanson, P.J., Schadt, C.W., 2020. Constraints on microbial communities, decomposition and methane production in deep peat deposits. PloS One 15, e0223744.

Knödler, M., Reisenhauer, K., Schieber, A., Carle, R., 2009. Quantitative Determination of Allergenic 5-Alk(en)ylresorcinols in Mango (Mangifera indica L.) Peel, Pulp, and Fruit Products by High-Performance Liquid Chromatography. J. Agric. Food Chem. 57, 3639–3644. https://doi.org/10.1021/jf803934p

Knoll, A.H., 1999. A New Molecular Window on Early Life. Science 285, 1025–1026. https://doi.org/10.1126/science.285.5430.1025

Kobashi, T., Menviel, L., Jeltsch-Thömmes, A., Vinther, B.M., Box, J.E., Muscheler, R., Nakaegawa, T., Pfister, P.L., Döring, M., Leuenberger, M., Wanner, H., Ohmura, A., 2017. Volcanic influence on centennial to millennial Holocene Greenland temperature change. Sci. Rep. 7, 1441. https://doi.org/10.1038/s41598-017-01451-7

Koga, Y., Akagawa-Matsushita, M., Ohga, M., Nishihara, M., 1993. Taxonomic Significance of the Distribution of Component Parts of Polar Ether Lipids in Methanogens. Syst. Appl. Microbiol. 16, 342–351. https://doi.org/10.1016/S0723-2020(11)80264-X

Koh, L.P., Miettinen, J., Liew, S.C., Ghazoul, J., 2011. Remotely sensed evidence of tropical peatland conversion to oil palm. Proc. Natl. Acad. Sci. 108, 5127–5132. https://doi.org/10.1073/pnas.1018776108

Kohn, M.J., 2010. Carbon isotope compositions of terrestrial C3 plants as indicators of (paleo)ecology and (paleo)climate. Proc. Natl. Acad. Sci. 107, 19691–19695. https://doi.org/10.1073/pnas.1004933107

Konecky, B.L., Russell, J.M., Johnson, T.C., Brown, E.T., Berke, M.A., Werne, J.P., Huang, Y., 2011. Atmospheric circulation patterns during late Pleistocene climate changes at Lake Malawi, Africa. Earth Planet. Sci. Lett. 312, 318–326. https://doi.org/10.1016/j.epsl.2011.10.020

Konecny, K., Ballhorn, U., Navratil, P., Jubanski, J., Page, S.E., Tansey, K., Hooijer, A., Vernimmen, R., Siegert, F., 2016. Variable carbon losses from recurrent fires in drained tropical peatlands. Glob. Change Biol. 22, 1469–1480. https://doi.org/10.1111/gcb.13186

Korhola, A., Ruppel, M., Seppä, H., Väliranta, M., Virtanen, T., Weckström, J., 2010. The importance of northern peatland expansion to the late-Holocene rise of atmospheric methane. Quat. Sci. Rev. 29, 611–617. https://doi.org/10.1016/j.quascirev.2009.12.010

Kovats, E., 1958. Gas chromatographic characterization of organic compounds. I. Retention indexes of aliphatic halides, alcohols, aldehydes, and ketones. Helv Chim Acta 41, 1915.

Kozubek, A., Pietr, S., Czerwonka, A., 1996. Alkylresorcinols are abundant lipid components in different strains of Azotobacter chroococcum and Pseudomonas spp. J. Bacteriol. 178, 4027–4030. https://doi.org/10.1128/jb.178.14.4027-4030.1996

Kozubek, A., Tyman, J.H.P., 1999. Resorcinolic Lipids, the Natural Non-isoprenoid Phenolic Amphiphiles and Their Biological Activity. Chem. Rev. 99, 1–26. https://doi.org/10.1021/cr970464o

Kristen, I., Wilkes, H., Vieth, A., Zink, K.-G., Plessen, B., Thorpe, J., Partridge, T.C., Oberhänsli, H., 2010. Biomarker and stable carbon isotope analyses of sedimentary organic matter from Lake Tswaing: evidence for deglacial wetness and early Holocene drought from South Africa. J. Paleolimnol. 44, 143–160. https://doi.org/10.1007/s10933-009-9393-9

Kröpelin, S., Verschuren, D., Lézine, A.-M., Eggermont, H., Cocquyt, C., Francus, P., Cazet, J.-P., Fagot, M., Rumes, B., Russell, J.M., Darius, F., Conley, D.J., Schuster, M., von Suchodoletz, H., Engstrom, D.R., 2008. Climate-driven ecosystem succession in the Sahara: the past 6000 years. Science 320, 765–768.

Kuhry, P., Vitt, D.H., 1996. Fossil carbon/nitrogen ratios as a measure of peat decomposition. Ecology 77, 271–275.

Kurnianto, S., Warren, M., Talbot, J., Kauffman, B., Murdiyarso, D., Frolking, S., 2015. Carbon accumulation of tropical peatlands over millennia: a modeling approach. Glob. Change Biol. 21, 431–444.

Kutzbach, J., Bonan, G., Foley, J., Harrison, S.P., 1996. Vegetation and soil feedbacks on the response of the African monsoon to orbital forcing in the early to middle Holocene. Nature 384, 623–626. https://doi.org/10.1038/384623a0

Kutzbach, J.E., 1981. Monsoon Climate of the Early Holocene: Climate Experiment with the Earth's Orbital Parameters for 9000 Years Ago. Science 214, 59–61. https://doi.org/10.1126/science.214.4516.59

Lafargue, E., Marquis, F., Pillot, D., 1998. Rock-Eval 6 applications in hydrocarbon exploration, production, and soil contamination studies. Rev. Inst. Fr. Pétrole 53, 421–437.

Lamb, P.J., 1978. Case Studies of Tropical Atlantic Surface Circulation Patterns During Recent Sub-Saharan Weather Anomalies: 1967 and 1968. Mon. Weather Rev. 106, 482–491. https://doi.org/10.1175/1520-0493(1978)106<0482:CSOTAS>2.0.CO;2

Lamit, L.J., Romanowicz, K.J., Potvin, L.R., Lennon, J.T., Tringe, S.G., Chimner, R.A., Kolka, R.K., Kane, E.S., Lilleskov, E.A., 2021. Peatland microbial community responses to plant functional group and drought are depth-dependent. Mol. Ecol. 30, 5119–5136. https://doi.org/10.1111/mec.16125

Lane, C.S., Mora, C.I., Horn, S.P., Orvis, K.H., 2008. Sensitivity of bulk sedimentary stable carbon isotopes to prehistoric forest clearance and maize agriculture. J. Archaeol. Sci. 35, 2119–2132.

Langner, A., Miettinen, J., Siegert, F., 2007. Land cover change 2002–2005 in Borneo and the role of fire derived from MODIS imagery. Glob. Change Biol. 13, 2329–2340. https://doi.org/10.1111/j.1365-2486.2007.01442.x

Large, D.J., Spiro, B., Ferrat, M., Shopland, M., Kylander, M., Gallagher, K., Li, X., Shen, C., Possnert, G., Zhang, G., Darling, W.G., Weiss, D., 2009. The influence of climate, hydrology and permafrost on Holocene peat accumulation at 3500m on the eastern Qinghai–Tibetan Plateau. Quat. Sci. Rev. 28, 3303–3314. https://doi.org/10.1016/j.quascirev.2009.09.006

Larmola, T., Tuittila, E.-S., Tiirola, M., Nykänen, H., Martikainen, P.J., Yrjälä, K., Tuomivirta, T., Fritze, H., 2010. The role of Sphagnum mosses in the methane cycling of a boreal mire. Ecology 91, 2356–2365. https://doi.org/10.1890/09-1343.1

Larrasoaña, J.C., 2021. A review of West African monsoon penetration during Green Sahara periods; implications for human evolution and dispersals over the last three million years. Oxf. Open Clim. Change 1, kgab011. https://doi.org/10.1093/oxfclm/kgab011

Larrasoaña, J.C., Roberts, A.P., Rohling, E.J., 2013. Dynamics of Green Sahara Periods and Their Role in Hominin Evolution. PLOS ONE 8, e76514. https://doi.org/10.1371/journal.pone.0076514

Lebamba, J., Vincens, A., Lézine, A.-M., Marchant, R., Buchet, G., 2016. Forest-savannah dynamics on the Adamawa plateau (Central Cameroon) during the "African humid period" termination: A new high-resolution pollen record from Lake Tizong. Rev. Palaeobot. Palynol. 235, 129–139.

Leblanc, M., 2022. Étude des périodes humides Africaines enregistrées au cours des deux derniers cycles climatiques à partir de la caractérisation de poussières Sahariennes déposées en Méditerranée Occidentale et dans l'océan Atlantique Tropical Nord-Est.

Lehtonen, K., Ketola, M., 1993. Solvent-extractable lipids of Sphagnum, Carex, Bryales and Carex-Bryales peats: content and compositional features vs peat humification. Org. Geochem. 20, 363–380. https://doi.org/10.1016/0146-6380(93)90126-V

Leifeld, J., Menichetti, L., 2018. The underappreciated potential of peatlands in global climate change mitigation strategies. Nat. Commun. 9, 1071. https://doi.org/10.1038/s41467-018-03406-6

Letouzey, R., 1958. Phytogéographie camerounaise, in: Atlas du Cameroun. IRCAM, Yaoundé, p. 6.

Lézine, A.-M., 2017. Vegetation at the time of the African Humid Period, in: Oxford Research Encyclopedia of Climate Science.

Lézine, A.-M., Assi-Kaudjhis, C., Roche, E., Vincens, A., Achoundong, G., 2013. Towards an understanding of West African montane forest response to climate change. J. Biogeogr. 40, 183–196. https://doi.org/10.1111/j.1365-2699.2012.02770.x

Lézine, A.-M., Casanova, J., 1989. Pollen and hydrological evidence for the interpretation of past climates in tropical west Africa during the holocene. Quat. Sci. Rev. 8, 45–55. https://doi.org/10.1016/0277-3791(89)90020-6

Lézine, A.-M., Hély, C., Grenier, C., Braconnot, P., Krinner, G., 2011. Sahara and Sahel vulnerability to climate changes, lessons from Holocene hydrological data. Quat. Sci. Rev. 30, 3001–3012. https://doi.org/10.1016/j.quascirev.2011.07.006

Lézine, A.-M., Izumi, K., Achoundong, G., 2023. Mbi Crater (Cameroon) illustrates the relations between mountain and lowland forests over the past 15,000 years in western equatorial Africa. Interdiscip. Res. Afr. Quat. Landsc. Environ. Change Hum. Act. 657, 67–76. https://doi.org/10.1016/j.quaint.2020.12.014

Liang, J., Russell, J.M., Xie, H., Lupien, R.L., Si, G., Wang, J., Hou, J., Zhang, G., 2019. Vegetation effects on temperature calibrations of branched glycerol dialkyl glycerol tetraether (brGDGTs) in soils. Org. Geochem. 127, 1–11. https://doi.org/10.1016/j.orggeochem.2018.10.010

Liu, H., Liu, W., 2019. Hydrogen isotope fractionation variations of n-alkanes and fatty acids in algae and submerged plants from Tibetan Plateau lakes: Implications for palaeoclimatic reconstruction. Sci. Total Environ. 695, 133925.

Liu, J., Hao, Y., Wang, Z., Ni, F., Wang, Y., Gong, L., Sun, B., Wang, J., 2018. Identification, Quantification, and Anti-inflammatory Activity of 5-n-Alkylresorcinols from 21 Different Wheat Varieties. J. Agric. Food Chem. 66, 9241–9247. https://doi.org/10.1021/acs.jafc.8b02911

Liu, X.-L., Leider, A., Gillespie, A., Gröger, J., Versteegh, G.J., Hinrichs, K.-U., 2010. Identification of polar lipid precursors of the ubiquitous branched GDGT orphan lipids in a peat bog in Northern Germany. Org. Geochem. 41, 653–660.

Liu, Z., Wang, Y., Gallimore, R., Gasse, F., Johnson, T., deMenocal, P., Adkins, J., Notaro, M., Prentice, I.C., Kutzbach, J., Jacob, R., Behling, P., Wang, L., Ong, E., 2007. Simulating the transient evolution and abrupt change of Northern Africa atmosphere–ocean–terrestrial ecosystem in the Holocene. Quat. Sci. Rev. 26, 1818–1837. https://doi.org/10.1016/j.quascirev.2007.03.002

Logan, G.A., Eglinton, G., 1994. Biogeochemistry of the Miocene lacustrine deposit, at Clarkia, northern Idaho, U.S.A. Org. Geochem. 21, 857–870. https://doi.org/10.1016/0146-6380(94)90045-0

Lohmann, F., Trendel, J., Hetru, C., Albrecht, P., 1990. C-29 tritiated β-amyrin: Chemical synthesis aiming at the study of aromatization processes in sediments. J. Label. Compd. Radiopharm. 28, 377–386. https://doi.org/10.1002/jlcr.2580280403

Loisel, J., Gallego-Sala, A.V., Amesbury, M.J., Magnan, G., Anshari, G., Beilman, D.W., Benavides, J.C., Blewett, J., Camill, P., Charman, D.J., Chawchai, S., Hedgpeth, A., Kleinen, T., Korhola, A., Large, D., Mansilla, C.A., Müller, J., van Bellen, S., West, J.B., Yu, Z., Bubier, J.L., Garneau, M., Moore, T., Sannel, A.B.K., Page, S., Väliranta, M., Bechtold, M., Brovkin, V., Cole, L.E.S., Chanton, J.P., Christensen, T.R., Davies, M.A., De Vleeschouwer, F., Finkelstein, S.A., Frolking, S., Gałka, M., Gandois, L., Girkin, N., Harris, L.I., Heinemeyer, A., Hoyt, A.M., Jones, M.C., Joos, F., Juutinen, S., Kaiser, K., Lacourse, T., Lamentowicz, M., Larmola, T., Leifeld, J., Lohila, A., Milner, A.M., Minkkinen, K., Moss, P., Naafs, B.D.A., Nichols, J., O'Donnell, J., Payne, R., Philben, M., Piilo, S., Quillet, A., Ratnayake, A.S., Roland, T.P., Sjögersten, S., Sonnentag, O., Swindles, G.T., Swinnen, W., Talbot, J., Treat, C., Valach, A.C., Wu, J., 2021. Expert assessment of future vulnerability of the global peatland carbon sink. Nat. Clim. Change 11, 70–77. https://doi.org/10.1038/s41558-020-00944-0

Long, M., Entekhabi, D., Nicholson, S.E., 2000. Interannual Variability in Rainfall, Water Vapor Flux, and Vertical Motion over West Africa. J. Clim. 13, 3827–3841. https://doi.org/10.1175/1520-0442(2000)013<3827:IVIRWV>2.0.CO;2

Longo, W.M., Theroux, S., Giblin, A.E., Zheng, Y., Dillon, J.T., Huang, Y., 2016. Temperature calibration and phylogenetically distinct distributions for freshwater alkenones: Evidence from northern Alaskan lakes. Geochim. Cosmochim. Acta 180, 177–196. https://doi.org/10.1016/j.gca.2016.02.019

Loomis, S.E., Russell, J.M., Heureux, A.M., D'Andrea, W.J., Sinninghe Damsté, J.S., 2014. Seasonal variability of branched glycerol dialkyl glycerol tetraethers (brGDGTs) in a temperate lake system. Geochim. Cosmochim. Acta 144, 173–187. https://doi.org/10.1016/j.gca.2014.08.027

Loomis, S.E., Russell, J.M., Ladd, B., Street-Perrott, F.A., Sinninghe Damsté, J.S., 2012. Calibration and application of the branched GDGT temperature proxy on East African lake sediments. Earth Planet. Sci. Lett. 357, 277–288.

Lu, H., Wu, N., Liu, K., Zhu, L., Yang, X., Yao, T., Wang, L., Li, Q., Liu, X., Shen, C., Li, X., Tong, G., Jiang, H., 2011. Modern pollen distributions in Qinghai-Tibetan Plateau and the development of transfer functions for reconstructing Holocene environmental changes. Quat. Sci. Rev. 30, 947–966. https://doi.org/10.1016/j.quascirev.2011.01.008

Mackenzie, A.S., McKenzie, D., 1983. Isomerization and aromatization of hydrocarbons in sedimentary basins formed by extension. Geol. Mag. 120, 417–470. https://doi.org/10.1017/S0016756800027461

Mackenzie, A.S., Patience, R.L., Maxwell, J.R., Vandenbroucke, M., Durand, B., 1980.

Molecular parameters of maturation in the Toarcian shales, Paris Basin, France—I. Changes in the configurations of acyclic isoprenoid alkanes, steranes and triterpanes. Geochim. Cosmochim. Acta 44, 1709–1721. https://doi.org/10.1016/0016-7037(80)90222-7

Magny, M., Peyron, O., Sadori, L., Ortu, E., Zanchetta, G., Vannière, B., Tinner, W., 2012. Contrasting patterns of precipitation seasonality during the Holocene in the south- and north-central Mediterranean. J. Quat. Sci. 27, 290–296. https://doi.org/10.1002/jqs.1543

Makou, M., Eglinton, T., McIntyre, C., Montluçon, D., Antheaume, I., Grossi, V., 2018. Plant wax n-alkane and n-alkanoic acid signatures overprinted by microbial contributions and old carbon in meromictic lake sediments. Geophys. Res. Lett. 45, 1049–1057.

Maley, J., 1991. The African rain forest vegetation and palaeoenvironments during late quaternary. Clim. Change 19, 79–98. https://doi.org/10.1007/BF00142216

Maley, J., 1989. Late Quaternary Climatic Changes in the African Rain Forest : Forest Refugia and the Major Role of Sea Surface Temperature Variations, in: Leinen, M., Sarnthein, M. (Eds.), Paleoclimatology and Paleometeorology: Modern and Past Patterns of Global Atmospheric Transport. Springer Netherlands, Dordrecht, pp. 585–616. https://doi.org/10.1007/978-94-009-0995-3_25

Maley, J., Brenac, P., 1998. Vegetation dynamics, palaeoenvironments and climatic changes in the forests of western Cameroon during the last 28,000 years BP. Rev. Palaeobot. Palynol. 99, 157–187.

Maley, J., Doumenge, C., Giresse, P., Mahé, G., Philippon, N., Hubau, W., Lokonda, M.O., Tshibamba, J.M., Chepstow-Lusty, A., 2018. Late Holocene forest contraction and fragmentation in central Africa. Quat. Res. 89, 43–59. https://doi.org/10.1017/qua.2017.97

Malhi, Y., Farfán Amézquita, F., Doughty, C.E., Silva-Espejo, J.E., Girardin, C.A.J., Metcalfe, D.B., Aragão, L.E.O.C., Huaraca-Quispe, L.P., Alzamora-Taype, I., Eguiluz-Mora, L., Marthews, T.R., Halladay, K., Quesada, C.A., Robertson, A.L., Fisher, J.B., Zaragoza-Castells, J., Rojas-Villagra, C.M., Pelaez-Tapia, Y., Salinas, N., Meir, P., Phillips, O.L., 2014. The productivity, metabolism and carbon cycle of two lowland tropical forest plots in south-western Amazonia, Peru. Plant Ecol. Divers. 7, 85–105. https://doi.org/10.1080/17550874.2013.820805

Marchant, R., Hooghiemstra, H., 2004. Rapid environmental change in African and South American tropics around 4000 years before present: a review. Earth-Sci. Rev. 66, 217–260. https://doi.org/10.1016/j.earscirev.2004.01.003

Martínez-Sosa, P., Tierney, J.E., Meredith, L.K., 2020. Controlled lacustrine microcosms show a brGDGT response to environmental perturbations. Org. Geochem. 145, 104041. https://doi.org/10.1016/j.orggeochem.2020.104041

Martínez-Sosa, P., Tierney, J.E., Stefanescu, I.C., Dearing Crampton-Flood, E., Shuman, B.N., Routson, C., 2021. A global Bayesian temperature calibration for lacustrine brGDGTs. Geochim. Cosmochim. Acta 305, 87–105. https://doi.org/10.1016/j.gca.2021.04.038

Marzi, R., Torkelson, B.E., Olson, R.K., 1993. A revised carbon preference index. Org. Geochem. 20, 1303–1306. https://doi.org/10.1016/0146-6380(93)90016-5

Masson-Delmotte, V., Zhai, P., Pirani, A., Connors, S.L., Péan, C., Berger, S., Caud, N., Chen, Y., Goldfarb, L., Gomis, M.I., 2021. Climate change 2021: the physical science basis. Contrib. Work. Group Sixth Assess. Rep. Intergov. Panel Clim. Change 2.

Mathewes, R.W., Heusser, L.E., 1981. A 12 000 year palynological record of temperature

and precipitation trends in southwestern British Columbia. Can. J. Bot. 59, 707–710. https://doi.org/10.1139/b81-100
Mauquoy, D., van Geel, B., Blaauw, M., van der Plicht, J., 2002. Evidence from northwest European bogs shows 'Little Ice Age' climatic changes driven by variations in solar activity. The Holocene 12, 1–6. https://doi.org/10.1191/0959683602hl514rr
Mauri, A., Davis, B.A.S., Collins, P.M., Kaplan, J.O., 2015. The climate of Europe during the Holocene: a gridded pollen-based reconstruction and its multi-proxy evaluation. Quat. Sci. Rev. 112, 109–127. https://doi.org/10.1016/j.quascirev.2015.01.013
McCarroll, D., Loader, N.J., 2004. Stable isotopes in tree rings. Isot. Quat. Paleoenviron. Reconstr. 23, 771–801. https://doi.org/10.1016/j.quascirev.2003.06.017
McClymont, E.L., Mauquoy, D., Yeloff, D., Broekens, P., Van Geel, B., Charman, D.J., Pancost, R.D., Chambers, F.M., Evershed, R.P., 2008. The disappearance of Sphagnum imbricatum from Butterburn Flow, UK. The Holocene 18, 991–1002.
McDermott, F., Mattey, D.P., Hawkesworth, C., 2001. Centennial-Scale Holocene Climate Variability Revealed by a High-Resolution Speleothem δ18O Record from SW Ireland. Science 294, 1328–1331. https://doi.org/10.1126/science.1063678
McGee, D., deMenocal, P.B., Winckler, G., Stuut, J.B.W., Bradtmiller, L.I., 2013. The magnitude, timing and abruptness of changes in North African dust deposition over the last 20,000yr. Earth Planet. Sci. Lett. 371–372, 163–176. https://doi.org/10.1016/j.epsl.2013.03.054
Melling, L., Hatano, R., Goh, K.J., 2005. Methane fluxes from three ecosystems in tropical peatland of Sarawak, Malaysia. Soil Biol. Biochem. 37, 1445–1453. https://doi.org/10.1016/j.soilbio.2005.01.001
Mertz, O., D'haen, S., Maiga, A., Moussa, I.B., Barbier, B., Diouf, A., Diallo, D., Da, E.D., Dabi, D., 2012. Climate Variability and Environmental Stress in the Sudan-Sahel Zone of West Africa. AMBIO 41, 380–392. https://doi.org/10.1007/s13280-011-0231-8
Metzger, P., Berkaloff, C., Casadevall, E., Coute, A., 1985a. Alkadiene- and botryococcene-producing races of wild strains of Botryococcus braunii. Phytochemistry 24, 2305–2312. https://doi.org/10.1016/S0031-9422(00)83032-0
Metzger, P., Casadevall, E., Coute, A., 1988. Botryococcene distribution in strains of the green alga Botryococcus braunii. Phytochemistry 27, 1383–1388. https://doi.org/10.1016/0031-9422(88)80199-7
Metzger, P., Casadevall, E., Pouet, M.J., Pouet, Y., 1985b. Structures of some botryococcenes: branched hydrocarbons from the b-race of the green alga Botryococcus braunii. Phytochemistry 24, 2995–3002. https://doi.org/10.1016/0031-9422(85)80043-1
Meyers, P.A., 2003. Applications of organic geochemistry to paleolimnological reconstructions: a summary of examples from the Laurentian Great Lakes. Org. Geochem. 34, 261–289. https://doi.org/10.1016/S0146-6380(02)00168-7
Meyers, P.A., Lallier-Vergès, E., 1999. Lacustrine sedimentary organic matter records of Late Quaternary paleoclimates. J. Paleolimnol. 21, 345–372.
Milanković, M., 1920. Théorie mathématique des phénomènes thermiques produits par la radiation solaire. Gauthier-Villars et Cie.
Mille, G., Guiliano, M., Asia, L., Malleret, L., Jalaluddin, N., 2006. Sources of hydrocarbons in sediments of the Bay of Fort de France (Martinique). Chemosphere 64, 1062–1073. https://doi.org/10.1016/j.chemosphere.2005.12.001
Miller, D.R., Habicht, M.H., Keisling, B.A., Castañeda, I.S., Bradley, R.S., 2018. A 900-year New

England temperature reconstruction from in situ seasonally produced branched glycerol dialkyl glycerol tetraethers (brGDGTs). Clim. Past 14, 1653–1667. https://doi.org/10.5194/cp-14-1653-2018
Miller, G.H., Geirsdóttir, Á., Zhong, Y., Larsen, D.J., Otto-Bliesner, B.L., Holland, M.M., Bailey, D.A., Refsnider, K.A., Lehman, S.J., Southon, J.R., Anderson, C., Björnsson, H., Thordarson, T., 2012. Abrupt onset of the Little Ice Age triggered by volcanism and sustained by sea-ice/ocean feedbacks. Geophys. Res. Lett. 39. https://doi.org/10.1029/2011GL050168
Moore, P.D., 1989. The ecology of peat-forming processes: a review. Int. J. Coal Geol. 12, 89–103.
Moreau, C., Caffy, I., Comby, C., Delqué-Količ, E., Dumoulin, J., Hain, S., Quiles, A., Setti, V., Souprayen, C., Thellier, B., Vincent, J., 2013. Research and development of the Artemis 14C AMS Facility: status report. Radiocarbon 55, 331–337.
Morris, P.J., 2021. Wetter is better for peat carbon. Nat. Clim. Change 11, 561–562. https://doi.org/10.1038/s41558-021-01072-z
Moy, C.M., Seltzer, G.O., Rodbell, D.T., Anderson, D.M., 2002. Variability of El Niño/Southern Oscillation activity at millennial timescales during the Holocene epoch. Nature 420, 162–165. https://doi.org/10.1038/nature01194
Muscheler, R., Beer, J., Vonmoos, M., 2004. Causes and timing of the 8200yr BP event inferred from the comparison of the GRIP 10Be and the tree ring Δ14C record. Holocene Clim. Var. - Mar. Perspect. 23, 2101–2111. https://doi.org/10.1016/j.quascirev.2004.08.007
Naafs, B.D.A., Gallego-Sala, A.V., Inglis, G.N., Pancost, R.D., 2017a. Refining the global branched glycerol dialkyl glycerol tetraether (brGDGT) soil temperature calibration. Org. Geochem. 106, 48–56. https://doi.org/10.1016/j.orggeochem.2017.01.009
Naafs, B.D.A., Inglis, G., Blewett, J., McClymont, E.L., Lauretano, V., Xie, S., Evershed, R., Pancost, R., 2019. The potential of biomarker proxies to trace climate, vegetation, and biogeochemical processes in peat: A review. Glob. Planet. Change 179, 57–79.
Naafs, B.D.A., Inglis, G.N., Zheng, Y., Amesbury, M.J., Biester, H., Bindler, R., Blewett, J., Burrows, M.A., Del Castillo Torres, D., Chambers, F.M., 2017b. Introducing global peat-specific temperature and pH calibrations based on brGDGT bacterial lipids. Geochim. Cosmochim. Acta 208, 285–301.
Naafs, B.D.A., Oliveira, A.S.F., Mulholland, A.J., 2021. Molecular dynamics simulations support the hypothesis that the brGDGT paleothermometer is based on homeoviscous adaptation. Geochim. Cosmochim. Acta 312, 44–56. https://doi.org/10.1016/j.gca.2021.07.034
Naeher, S., Cui, X., Summons, R.E., 2022. Biomarkers: Molecular Tools to Study Life, Environment, and Climate. Elements 18, 79–85. https://doi.org/10.2138/gselements.18.2.79
Neumann, K., 2018. Development of Plant Food Production in the West African Savannas: Archaeobotanical Perspectives. https://doi.org/10.1093/acrefore/9780190277734.013.138
Neumann, K., 1989. Holocene vegetation of the Eastern Sahara: charcoal from prehistoric sites. Afr. Archaeol. Rev. 7, 97–116. https://doi.org/10.1007/BF01116839
Neumann, K., Eggert, M.K.H., Oslisly, R., Clist, B., Denham, T., de Maret, P., Ozainne, S., Hildebrand, E., Bostoen, K., Salzmann, U., Schwartz, D., Eichhorn, B., Tchiengué, B., Höhn, A., 2012. Comment on “Intensifying Weathering and Land Use in Iron Age

Central Africa." Science 337, 1040–1040. https://doi.org/10.1126/science.1221747
Ngomanda, A., Neumann, K., Schweizer, A., Maley, J., 2009. Seasonality change and the third millennium BP rainforest crisis in southern Cameroon (Central Africa). Quat. Res. 71, 307–318. https://doi.org/10.1016/j.yqres.2008.12.002
Ngos III, S., Giresse, P., Maley, J., 2003. Palaeoenvironments of Lake Assom near Tibati (south Adamawa, Cameroon). What happened in Tibati around 1700 years BP? J. Afr. Earth Sci. 37, 35–45.
Ngos, S., Giresse, P., 2012. The Holocene sedimentary and pyroclastic accumulations of two crater lakes (Mbalang,Tizong) of the volcanic plateau of Adamawa (Cameroon): Palaeoenvironmental reconstruction. The Holocene 22, 31–42. https://doi.org/10.1177/0959683611409779
Nguetsop, V., Bentaleb, I., Favier, C., Martin, C., Bietrix, S., Giresse, P., Servant-Vildary, S., Servant, M., 2011. Past environmental and climatic changes during the last 7200 cal yr BP in Adamawa plateau (Northern-Cameroun) based on fossil diatoms and sedimentary carbon isotopic records from Lake Mbalang. Clim. Past 7, 1371–1393.
Nguetsop, V.F., Bentaleb, I., Favier, C., Bietrix, S., Martin, C., Servant-Vildary, S., Servant, M., 2013. A late Holocene palaeoenvironmental record from Lake Tizong, northern Cameroon using diatom and carbon stable isotope analyses. Quat. Sci. Rev. 72, 49–62. https://doi.org/10.1016/j.quascirev.2013.04.005
Nichols, J.E., Booth, R.K., Jackson, S.T., Pendall, E.G., Huang, Y., 2006. Paleohydrologic reconstruction based on n-alkane distributions in ombrotrophic peat. Org. Geochem. 37, 1505–1513. https://doi.org/10.1016/j.orggeochem.2006.06.020
Nichols, J.E., Peteet, D.M., Moy, C.M., Castañeda, I.S., McGeachy, A., Perez, M., 2014. Impacts of climate and vegetation change on carbon accumulation in a south-central Alaskan peatland assessed with novel organic geochemical techniques. The Holocene 24, 1146–1155. https://doi.org/10.1177/0959683614540729
Nichols, J.E., Walcott, M., Bradley, R., Pilcher, J., Huang, Y., 2009. Quantitative assessment of precipitation seasonality and summer surface wetness using ombrotrophic sediments from an Arctic Norwegian peatland. Quat. Res. 72, 443–451.
Nicholson, S.E., 2018. The ITCZ and the Seasonal Cycle over Equatorial Africa. Bull. Am. Meteorol. Soc. 99, 337–348. https://doi.org/10.1175/BAMS-D-16-0287.1
Nicholson, S.E., 2009. A revised picture of the structure of the "monsoon" and land ITCZ over West Africa. Clim. Dyn. 32, 1155–1171. https://doi.org/10.1007/s00382-008-0514-3
Nicholson, S.E., 1993. An Overview of African Rainfall Fluctuations of the Last Decade. J. Clim. 6, 1463–1466.
Nicholson, S.E., 1981. Rainfall and Atmospheric Circulation during Drought Periods and Wetter Years in West Africa. Mon. Weather Rev. 109, 2191–2208. https://doi.org/10.1175/1520-0493(1981)109<2191:RAACDD>2.0.CO;2
Nicholson, S.E., Selato, J., 2000. The influence of La Nina on African rainfall. Int. J. Climatol. J. R. Meteorol. Soc. 20, 1761–1776.
Niedermeyer, E.M., Forrest, M., Beckmann, B., Sessions, A.L., Mulch, A., Schefuß, E., 2016. The stable hydrogen isotopic composition of sedimentary plant waxes as quantitative proxy for rainfall in the West African Sahel. Geochim. Cosmochim. Acta 184, 55–70. https://doi.org/10.1016/j.gca.2016.03.034
Niedermeyer, E.M., Schefuß, E., Sessions, A.L., Mulitza, S., Mollenhauer, G., Schulz, M., Wefer, G., 2010. Orbital- and millennial-scale changes in the hydrologic cycle and vegetation in the western African Sahel: insights from individual plant wax δD and

δ13C. Quat. Sci. Rev. 29, 2996–3005. https://doi.org/10.1016/j.quascirev.2010.06.039
Njagi, D.M., Routh, J., Olago, D., Gayantha, K., 2021. A multi-proxy reconstruction of the late Holocene climate evolution in the Kapsabet Swamp, Kenya (East Africa). Palaeogeogr. Palaeoclimatol. Palaeoecol. 574, 110475.
N'nanga, A., Ngos III, S., Ngueutchoua, G., 2019. The late Pleistocene – Holocene paleoclimate reconstruction in the Adamawa plateau (Central Cameroon) inferred from the geochemistry and mineralogy of the Lake Fonjak sediments. J. Afr. Earth Sci. 150, 23–36. https://doi.org/10.1016/j.jafrearsci.2018.09.024
N'nanga, A., Nguetsop, V.F., Tematio, P., Ngos, S., 2021a. Paleoclimate implication on the Lake Fonjak level changes (Adamawa Plateau, Central Cameroon) during the last 13,500 cal yr BP. J. Afr. Earth Sci. 182, 104286.
N'nanga, A., Ngueutchoua, G., Ekomane, E., Tematio, P., 2021b. The Lake Fonjak paleoproductivity controlled by the paleoclimate variations in the Adamawa plateau (Central Cameroon) during the Holocene: implications for sedimentary rate and the organic matter enrichment in Fe-shales. Arab. J. Geosci. 14, 1813. https://doi.org/10.1007/s12517-021-08149-1
Nono, A., Déruelle, B., Demaiffe, D., Kambou, R., 1994. Tchabal Nganha volcano in Adamawa (Cameroon): petrology of a continental alkaline lava series. J. Volcanol. Geotherm. Res. 60, 147–178. https://doi.org/10.1016/0377-0273(94)90066-3
Nott, C.J., Xie, S., Avsejs, L.A., Maddy, D., Chambers, F.M., Evershed, R.P., 2000. n-Alkane distributions in ombrotrophic mires as indicators of vegetation change related to climatic variation. Org. Geochem. 31, 231–235. https://doi.org/10.1016/S0146-6380(99)00153-9
O'Leary, M.H., 1980. [4] Determination of heavy-aton isotope effects on enzyme-catalyzed reactions, in: Purich, D.L. (Ed.), Methods in Enzymology. Academic Press, pp. 83–104. https://doi.org/10.1016/S0076-6879(80)64006-3
Ortiz, J.E., Gallego, J.L.R., Torres, T., Díaz-Bautista, A., Sierra, C., 2010. Palaeoenvironmental reconstruction of Northern Spain during the last 8000calyr BP based on the biomarker content of the Roñanzas peat bog (Asturias). Org. Geochem. 41, 454–466. https://doi.org/10.1016/j.orggeochem.2010.02.003
Ourisson, G., Rohmer, M., Poralla, K., 1987. Prokaryotic Hopanoids and other Polyterpenoid Sterol Surrogates. Annu. Rev. Microbiol. 41, 301–333. https://doi.org/10.1146/annurev.mi.41.100187.001505
Owen, R.B., Barthelme, J.W., Renaut, R.W., Vincens, A., 1982. Palaeolimnology and archaeology of Holocene deposits north-east of Lake Turkana, Kenya. Nature 298, 523–529. https://doi.org/10.1038/298523a0
Paerl, H.W., Hall, N.S., Calandrino, E.S., 2011. Controlling harmful cyanobacterial blooms in a world experiencing anthropogenic and climatic-induced change. Sci. Total Environ. 409, 1739–1745. https://doi.org/10.1016/j.scitotenv.2011.02.001
Paerl, H.W., Huisman, J., 2008. Blooms Like It Hot. Science 320, 57–58. https://doi.org/10.1126/science.1155398
Page, S., Rieley, J., Shotyk, Ø., Weiss, D., 1999. Interdependence of peat and vegetation in a tropical peat swamp forest. Philos. Trans. R. Soc. Lond. B. Biol. Sci. 354, 1885–1897.
Page, S.E., Rieley, J.O., Banks, C.J., 2011. Global and regional importance of the tropical peatland carbon pool. Glob. Change Biol. 17, 798–818. https://doi.org/10.1111/j.1365-2486.2010.02279.x

Palchan, D., Torfstein, A., 2019. A drop in Sahara dust fluxes records the northern limits of the African Humid Period. Nat. Commun. 10, 3803. https://doi.org/10.1038/s41467-019-11701-z

Pancost, R.D., Baas, M., van Geel, B., Sinninghe Damsté, J.S., 2003. Response of an ombrotrophic bog to a regional climate event revealed by macrofossil, molecular and carbon isotopic data. The Holocene 13, 921–932.

Pancost, R.D., Damsté, J.S.S., 2003. Carbon isotopic compositions of prokaryotic lipids as tracers of carbon cycling in diverse settings. Chem. Geol. 195, 29–58.

Pancost, R.D., Steart, D.S., Handley, L., Collinson, M.E., Hooker, J.J., Scott, A.C., Grassineau, N.V., Glasspool, I.J., 2007. Increased terrestrial methane cycling at the Palaeocene–Eocene thermal maximum. Nature 449, 332–335. https://doi.org/10.1038/nature06012

Patricola, C.M., Cook, K.H., 2007. Dynamics of the West African Monsoon under Mid-Holocene Precessional Forcing: Regional Climate Model Simulations. J. Clim. 20, 694–716. https://doi.org/10.1175/JCLI4013.1

Pearson, A., Flood Page, S.R., Jorgenson, T.L., Fischer, W.W., Higgins, M.B., 2007. Novel hopanoid cyclases from the environment. Environ. Microbiol. 9, 2175–2188.

Peiseler, B., Rohmer, M., 1992. Prokaryotic triterpenoids of the hopane series. Bacteriohopanetetrols of new side-chain configuration from Acetobacter species. J. Chem. Res. Synop. Print 298–299.

Peltoniemi, K., Laiho, R., Juottonen, H., Bodrossy, L., Kell, D.K., Minkkinen, K., Mäkiranta, P., Mehtätalo, L., Penttilä, T., Siljanen, H.M.P., Tuittila, E.-S., Tuomivirta, T., Fritze, H., 2016. Responses of methanogenic and methanotrophic communities to warming in varying moisture regimes of two boreal fens. Soil Biol. Biochem. 97, 144–156. https://doi.org/10.1016/j.soilbio.2016.03.007

Penlap, E.K., Matulla, C., Storch, H., Mkankam, F.K., 2004. Downscaling of GCM scenarios to assess precipitation changes in the little rainy season (March-June) in Cameroon. Clim. Res. 26, 85–96.

Penman, H.L., 1956. Estimating evaporation. Eos Trans. Am. Geophys. Union 37, 43–50. https://doi.org/10.1029/TR037i001p00043

Pérez-Angel, L.C., Sepúlveda, J., Molnar, P., Montes, C., Rajagopalan, B., Snell, K., Gonzalez-Arango, C., Dildar, N., 2020. Soil and Air Temperature Calibrations Using Branched GDGTs for the Tropical Andes of Colombia: Toward a Pan-Tropical Calibration. Geochem. Geophys. Geosystems 21, e2020GC008941. https://doi.org/10.1029/2020GC008941

Peterse, F., Hopmans, E.C., Schouten, S., Mets, A., Rijpstra, W.I.C., Sinninghe Damsté, J.S., 2011. Identification and distribution of intact polar branched tetraether lipids in peat and soil. Org. Geochem. 42, 1007–1015. https://doi.org/10.1016/j.orggeochem.2011.07.006

Peterse, F., van der Meer, J., Schouten, S., Weijers, J.W.H., Fierer, N., Jackson, R.B., Kim, J.-H., Sinninghe Damsté, J.S., 2012. Revised calibration of the MBT–CBT paleotemperature proxy based on branched tetraether membrane lipids in surface soils. Geochim. Cosmochim. Acta 96, 215–229. https://doi.org/10.1016/j.gca.2012.08.011

Petrenko, V.V., Smith, A.M., Schaefer, H., Riedel, K., Brook, E., Baggenstos, D., Harth, C., Hua, Q., Buizert, C., Schilt, A., Fain, X., Mitchell, L., Bauska, T., Orsi, A., Weiss, R.F., Severinghaus, J.P., 2017. Minimal geological methane emissions during the Younger Dryas–Preboreal abrupt warming event. Nature 548, 443–446.

https://doi.org/10.1038/nature23316
Ponton, C., West, A.J., Feakins, S.J., Galy, V., 2014. Leaf wax biomarkers in transit record river catchment composition. Geophys. Res. Lett. 41, 6420–6427. https://doi.org/10.1002/2014GL061328
Poudjom Djomani, Y.H., Diament, M., Wilson, M., 1997. Lithospheric structure across the Adamawa plateau (Cameroon) fromgravity studies. Tectonophysics 273, 317–327. https://doi.org/10.1016/S0040-1951(96)00280-6
Powers, L.A., Werne, J.P., Johnson, T.C., Hopmans, E.C., Damsté, J.S.S., Schouten, S., 2004. Crenarchaeotal membrane lipids in lake sediments: A new paleotemperature proxy for continental paleoclimate reconstruction? Geology 32, 613–616. https://doi.org/10.1130/G20434.1
Poynter, J., Eglinton, G., 1990. 14. Molecular composition of three sediments from hole 717c: The Bengal fan, in: Proceedings of the Ocean Drilling Program: Scientific Results. pp. 155–161.
Poynter, J.G., Farrimond, P., Robinson, N., Eglinton, G., 1989. Aeolian-Derived Higher Plant Lipids in the Marine Sedimentary Record: Links with Palaeoclimate, in: Leinen, M., Sarnthein, M. (Eds.), Paleoclimatology and Paleometeorology: Modern and Past Patterns of Global Atmospheric Transport. Springer Netherlands, Dordrecht, pp. 435–462. https://doi.org/10.1007/978-94-009-0995-3_18
Prell, W.L., Kutzbach, J.E., 1987. Monsoon variability over the past 150,000 years. J. Geophys. Res. Atmospheres 92, 8411–8425. https://doi.org/10.1029/JD092iD07p08411
Price, G.D., McKenzie, J.E., Pilcher, J.R., Hoper, S.T., 1997. Carbon-isotope variation in Sphagnum from hummock-hollow complexes: implications for Holocene climate reconstruction. The Holocene 7, 229–233.
Quirk, M.M., Wardroper, A.M.K., Wheatley, R.E., Maxwell, J.R., 1984. Extended hopanoids in peat environments. Chem. Geol. 42, 25–43. https://doi.org/10.1016/0009-2541(84)90003-2
Raberg, J.H., Harning, D.J., Crump, S.E., de Wet, G., Blumm, A., Kopf, S., Geirsdóttir, Á., Miller, G.H., Sepúlveda, J., 2021. Revised fractional abundances and warm-season temperatures substantially improve brGDGT calibrations in lake sediments. Biogeosciences 18, 3579–3603. https://doi.org/10.5194/bg-18-3579-2021
Raghoebarsing, A.A., Smolders, A.J.P., Schmid, M.C., Rijpstra, W.I.C., Wolters-Arts, M., Derksen, J., Jetten, M.S.M., Schouten, S., Sinninghe Damsté, J.S., Lamers, L.P.M., Roelofs, J.G.M., Op den Camp, H.J.M., Strous, M., 2005. Methanotrophic symbionts provide carbon for photosynthesis in peat bogs. Nature 436, 1153–1156. https://doi.org/10.1038/nature03802
Ran, M., Chen, L., 2019. The 4.2 ka BP climatic event and its cultural responses. Quat. Int. 521, 158–167. https://doi.org/10.1016/j.quaint.2019.05.030
Randall, D.A., Wood, R.A., Bony, S., Colman, R., Fichefet, T., Fyfe, J., Kattsov, V., Pitman, A., Shukla, J., Srinivasan, J., 2007. Climate models and their evaluation, in: Climate Change 2007: The Physical Science Basis. Contribution of Working Group I to the Fourth Assessment Report of the IPCC (FAR). Cambridge University Press, pp. 589–662.
Rao, Z., Guo, H., Wei, S., Cao, J., Jia, G., 2022. Influence of water conditions on peat brGDGTs: A modern investigation and its paleoclimatic implications. Chem. Geol. 606, 120993. https://doi.org/10.1016/j.chemgeo.2022.120993
Rasmussen, S.O., Andersen, K.K., Svensson, A.M., Steffensen, J.P., Vinther, B.M., Clausen,

H.B., Siggaard-Andersen, M.-L., Johnsen, S.J., Larsen, L.B., Dahl-Jensen, D., Bigler, M., Röthlisberger, R., Fischer, H., Goto-Azuma, K., Hansson, M.E., Ruth, U., 2006. A new Greenland ice core chronology for the last glacial termination. J. Geophys. Res. Atmospheres 111. https://doi.org/10.1029/2005JD006079

Rea, D.K., 1994. The paleoclimatic record provided by eolian deposition in the deep sea: The geologic history of wind. Rev. Geophys. 32, 159–195. https://doi.org/10.1029/93RG03257

Regnery, J., Püttmann, W., Koutsodendris, A., Mulch, A., Pross, J., 2013. Comparison of the paleoclimatic significance of higher land plant biomarker concentrations and pollen data: A case study of lake sediments from the Holsteinian interglacial. Org. Geochem. 61, 73–84. https://doi.org/10.1016/j.orggeochem.2013.06.006

Reich, P.B., 1995. Phenology of tropical forests: patterns, causes, and consequences. Can. J. Bot. 73, 164–174. https://doi.org/10.1139/b95-020

Renssen, H., 2022. Climate model experiments on the 4.2 ka event: The impact of tropical sea-surface temperature anomalies and desertification. The Holocene 32, 378–389. https://doi.org/10.1177/09596836221074031

Renssen, H., Brovkin, V., Fichefet, T., Goosse, H., 2006. Simulation of the Holocene climate evolution in Northern Africa: The termination of the African Humid Period. Impact Rapid Environ. Chang. Hum. Ecosyst. 150, 95–102. https://doi.org/10.1016/j.quaint.2005.01.001

Renssen, H., Brovkin, V., Fichefet, T., Goosse, H., 2003. Holocene climate instability during the termination of the African Humid Period. Geophys. Res. Lett. 30. https://doi.org/10.1029/2002GL016636

Renssen, H., Goosse, H., Fichefet, T., Campin, J.-M., 2001. The 8.2 kyr BP event simulated by a Global Atmosphere—Sea-Ice—Ocean Model. Geophys. Res. Lett. 28, 1567–1570. https://doi.org/10.1029/2000GL012602

Renssen, H., Mairesse, A., Goosse, H., Mathiot, P., Heiri, O., Roche, D.M., Nisancioglu, K.H., Valdes, P.J., 2015. Multiple causes of the Younger Dryas cold period. Nat. Geosci. 8, 946–949. https://doi.org/10.1038/ngeo2557

Reusch, R., Sadoff, H., 1979. 5-n-Alkylresorcinols from encysting Azotobacter vinelandii: isolation and characterization. J. Bacteriol. 139, 448–453. https://doi.org/10.1128/jb.139.2.448-453.1979

Reynaud-Farrera, I., Maley, J., Wirrmann, D., 1996. Végétation et climat dans les forêts du Sud-Ouest Cameroun depuis 4770 ans BP: analyse pollinique des sédiments du Lac Ossa. CR Acad Sci Paris 322, 749–755.

Reynolds, C.S., 2006. The ecology of phytoplankton. Cambridge University Press.

Rieley, J., Page, S., 2016. Tropical Peatland of the World, in: Osaki, M., Tsuji, N. (Eds.), Tropical Peatland Ecosystems. Springer Japan, Tokyo, pp. 3–32. https://doi.org/10.1007/978-4-431-55681-7_1

Ries-Kautt, M., Albrecht, P., 1989. Hopane-derived triterpenoids in soils. Chem. Geol. 76, 143–151. https://doi.org/10.1016/0009-2541(89)90133-2

Roehm, C.L., 2005. Respiration in wetland ecosystems. Respir. Aquat. Ecosyst. 83–102.

Rohling, E.J., Pälike, H., 2005. Centennial-scale climate cooling with a sudden cold event around 8,200 years ago. Nature 434, 975–979. https://doi.org/10.1038/nature03421

Rohmer, M., Bouvier-Nave, P., Ourisson, G., 1984. Distribution of Hopanoid Triterpenes in Prokaryotes. Microbiology. https://doi.org/10.1099/00221287-130-5-1137

Rommerskirchen, F., Plader, A., Eglinton, G., Chikaraishi, Y., Rullkötter, J., 2006.

Chemotaxonomic significance of distribution and stable carbon isotopic composition of long-chain alkanes and alkan-1-ols in C4 grass waxes. Stable Isot. Biogeosciences 37, 1303–1332. https://doi.org/10.1016/j.orggeochem.2005.12.013
Rosa-Putra, S., Nalin, R., Domenach, A.-M., Rohmer, M., 2001. Novel hopanoids from Frankia spp. and related soil bacteria. Eur. J. Biochem. 268, 4300–4306. https://doi.org/10.1046/j.1432-1327.2001.02348.x
Rosenthal, Y., Lohmann, G.P., 2002. Accurate estimation of sea surface temperatures using dissolution-corrected calibrations for Mg/Ca paleothermometry. Paleoceanography 17, 16–1.
Ross, A.B., 2012. Present Status and Perspectives on the Use of Alkylresorcinols as Biomarkers of Wholegrain Wheat and Rye Intake. J. Nutr. Metab. 2012, 462967. https://doi.org/10.1155/2012/462967
Ross, A.B., Shepherd, M.J., Schüpphaus, M., Sinclair, V., Alfaro, B., Kamal-Eldin, A., Åman, P., 2003. Alkylresorcinols in Cereals and Cereal Products. J. Agric. Food Chem. 51, 4111–4118. https://doi.org/10.1021/jf0340456
Rozanski, K., Araguás-Araguás, L., Gonfiantini, R., 1993. Isotopic patterns in modern global precipitation. Clim. Change Cont. Isot. Rec. 78, 1–36.
Rubino, M., Etheridge, D.M., Trudinger, C.M., Allison, C.E., Battle, M.O., Langenfelds, R.L., Steele, L.P., Curran, M., Bender, M., White, J.W.C., Jenk, T.M., Blunier, T., Francey, R.J., 2013. A revised 1000 year atmospheric δ13C-CO2 record from Law Dome and South Pole, Antarctica. J. Geophys. Res. Atmospheres 118, 8482–8499. https://doi.org/10.1002/jgrd.50668
Rummukainen, M., 2010. State-of-the-art with regional climate models. WIREs Clim. Change 1, 82–96. https://doi.org/10.1002/wcc.8
Rupp, D., Kane, E.S., Dieleman, C., Keller, J.K., Turetsky, M., 2019. Plant functional group effects on peat carbon cycling in a boreal rich fen. Biogeochemistry 144, 305–327. https://doi.org/10.1007/s10533-019-00590-5
Russell, J.M., Johnson, T.C., 2007. Little Ice Age drought in equatorial Africa: Intertropical Convergence Zone migrations and El Niño–Southern Oscillation variability. Geology 35, 21–24. https://doi.org/10.1130/G23125A.1
Russell, N.J., Fukunaga, N., 1990. A comparison of thermal adaptation of membrane lipids in psychrophilic and thermophilic bacteria. FEMS Microbiol. Lett. 75, 171–182. https://doi.org/10.1016/0378-1097(90)90530-4
Sachse, D., Billault, I., Bowen, G.J., Chikaraishi, Y., Dawson, T.E., Feakins, S.J., Freeman, K.H., Magill, C.R., McInerney, F.A., Van Der Meer, M.T.J., Polissar, P., Robins, R.J., Sachs, J.P., Schmidt, H.-L., Sessions, A.L., White, J.W.C., West, J.B., Kahmen, A., 2012. Molecular paleohydrology: interpreting the hydrogen-isotopic composition of lipid biomarkers from photosynthesizing organisms. Annu. Rev. Earth Planet. Sci. 40, 221–249.
Sachse, D., Radke, J., Gleixner, G., 2006. δD values of individual n-alkanes from terrestrial plants along a climatic gradient – Implications for the sedimentary biomarker record. Org. Geochem. 37, 469–483. https://doi.org/10.1016/j.orggeochem.2005.12.003
Sachse, D., Radke, J., Gleixner, G., 2004. Hydrogen isotope ratios of recent lacustrine sedimentary n-alkanes record modern climate variability. Geochim. Cosmochim. Acta 68, 4877–4889. https://doi.org/10.1016/j.gca.2004.06.004
Saenger, A., Cécillon, L., Sebag, D., Brun, J.-J., 2013. Soil organic carbon quantity, chemistry and thermal stability in a mountainous landscape: A Rock–Eval pyrolysis survey. Org.

Geochem. 54, 101–114.
Salzmann, U., 2000. Are modern savannas degraded forests?-A Holocene pollen record from the Sudanian vagetation zone of NE Nigeria. Veg. Hist. Archaeobotany 9, 1–15. https://doi.org/10.1007/BF01295010
Salzmann, U., Hoelzmann, P., 2005. The Dahomey Gap: an abrupt climatically induced rain forest fragmentation in West Africa during the late Holocene. The Holocene 15, 190–199. https://doi.org/10.1191/0959683605hl799rp
Salzmann, U., Hoelzmann, P., Morczinek, I., 2002. Late Quaternary Climate and Vegetation of the Sudanian Zone of Northeast Nigeria. Quat. Res. 58, 73–83. https://doi.org/10.1006/qres.2002.2356
Sauer, P.E., Eglinton, T.I., Hayes, J.M., Schimmelmann, A., Sessions, A.L., 2001. Compound-specific D/H ratios of lipid biomarkers from sediments as a proxy for environmental and climatic conditions11Associate editor: N. E. Ostrom. Geochim. Cosmochim. Acta 65, 213–222. https://doi.org/10.1016/S0016-7037(00)00520-2
Savenije, H.H.G., 1995. New definitions for moisture recycling and the relationship with land-use changes in the Sahel. J. Hydrol. 167, 57–78. https://doi.org/10.1016/0022-1694(94)02632-L
Schaaff, V., Sebag, D., Makou, M., Grossi, V., Antheaume, I., Hamelin, B., Garcin, Y., Ngounou Ngatcha, B., Deschamps, P., Ménot, G., 2023. Modeling the decomposition signal and correcting bulk organic data from a peat deposit, a case study at low latitudes (Cameroon). Org. Geochem. 179, 104589. https://doi.org/10.1016/j.orggeochem.2023.104589
Scheffer, M., van Nes, E.H., 2007. Shallow lakes theory revisited: various alternative regimes driven by climate, nutrients, depth and lake size. Hydrobiologia 584, 455–466. https://doi.org/10.1007/s10750-007-0616-7
Schefuß, E., Kuhlmann, H., Mollenhauer, G., Prange, M., Pätzold, J., 2011. Forcing of wet phases in southeast Africa over the past 17,000 years. Nature 480, 509–512. https://doi.org/10.1038/nature10685
Schefuß, E., Ratmeyer, V., Stuut, J.-B.W., Jansen, J.H.F., Sinninghe Damsté, J.S., 2003. Carbon isotope analyses of n-alkanes in dust from the lower atmosphere over the central eastern Atlantic. Geochim. Cosmochim. Acta 67, 1757–1767. https://doi.org/10.1016/S0016-7037(02)01414-X
Schefuß, E., Schouten, S., Schneider, R.R., 2005. Climatic controls on central African hydrology during the past 20,000 years. Nature 437, 1003–1006.
Schellekens, J., Buurman, P., 2011. n-Alkane distributions as palaeoclimatic proxies in ombrotrophic peat: The role of decomposition and dominant vegetation. Geoderma 164, 112–121. https://doi.org/10.1016/j.geoderma.2011.05.012
Schepanski, K., Tegen, I., Macke, A., 2009. Saharan dust transport and deposition towards the tropical northern Atlantic. Atmos Chem Phys 9, 1173–1189. https://doi.org/10.5194/acp-9-1173-2009
Schlosser, E., Oerter, H., Masson-Delmotte, V., Reijmer, C., 2008. Atmospheric influence on the deuterium excess signal in polar firn: implications for ice-core interpretation. J. Glaciol. 54, 117–124. https://doi.org/10.3189/002214308784408991
Schmerk, C.L., Bernards, M.A., Valvano, M.A., 2011. Hopanoid production is required for low-pH tolerance, antimicrobial resistance, and motility in Burkholderia cenocepacia. J. Bacteriol. 193, 6712–6723.
Schouten, S., Hoefs, M.J.L., Sinninghe Damsté, J.S., 2000a. A molecular and stable carbon

isotopic study of lipids in late Quaternary sediments from the Arabian Sea. Org. Geochem. 31, 509–521. https://doi.org/10.1016/S0146-6380(00)00031-0
Schouten, S., Hopmans, E.C., Damsté, J.S.S., 2013. The organic geochemistry of glycerol dialkyl glycerol tetraether lipids: A review. Org. Geochem. 54, 19–61. https://doi.org/10.1016/j.orggeochem.2012.09.006
Schouten, S., Hopmans, E.C., Pancost, R.D., Damsté, J.S.S., 2000b. Widespread occurrence of structurally diverse tetraether membrane lipids: Evidence for the ubiquitous presence of low-temperature relatives of hyperthermophiles. Proc. Natl. Acad. Sci. 97, 14421–14426. https://doi.org/10.1073/pnas.97.26.14421
Schouten, S., Van Der Meer, M.T.J., Hopmans, E.C., Rijpstra, W.I.C., Reysenbach, A.-L., Ward, D.M., Sinninghe Damsté, J.S., 2007. Archaeal and Bacterial Glycerol Dialkyl Glycerol Tetraether Lipids in Hot Springs of Yellowstone National Park. Appl. Environ. Microbiol. 73, 6181–6191. https://doi.org/10.1128/AEM.00630-07
Schrag, D.P., DePaolo, D.J., Richter, F.M., 1995. Reconstructing past sea surface temperatures: Correcting for diagenesis of bulk marine carbonate. Geochim. Cosmochim. Acta 59, 2265–2278.
Schwab, V.F., Garcin, Y., Sachse, D., Todou, G., Séné, O., Onana, J.-M., Achoundong, G., Gleixner, G., 2015. Effect of aridity on δ13C and δD values of C3 plant- and C4 graminoid-derived leaf wax lipids from soils along an environmental gradient in Cameroon (Western Central Africa). Org. Geochem. 78, 99–109. https://doi.org/10.1016/j.orggeochem.2014.09.007
Schwartz-Narbonne, R., Schaeffer, P., Lengger, S.K., Blewett, J., Martin Jones, D., Motsch, E., Crombie, A., Jetten, M.S.-M., Mikkelsen, D., Normand, P., Nuijten, G.H.L., Pancost, R.D., Rush, D., 2023. Bacterial physiology highlighted by the δ13C fractionation of bacteriohopanetetrol isomers. Org. Geochem. 181, 104617. https://doi.org/10.1016/j.orggeochem.2023.104617
Sebag, D., Disnar, J.-R., Guillet, B., Di Giovanni, C., Verrecchia, E.P., Durand, A., 2006. Monitoring organic matter dynamics in soil profiles by 'Rock-Eval pyrolysis': bulk characterization and quantification of degradation. Eur. J. Soil Sci. 57, 344–355.
Sebag, D., Verrecchia, E., Cécillon, L., Adatte, T., Albrecht, R., Aubert, M., Bureau, F., Cailleau, G., Copard, Y., Decaens, T., Disnar, J.-R., Hetényi, M., Nyilas, T., Trombino, L., 2016. Dynamics of soil organic matter based on new Rock-Eval indices. Geoderma 284, 185–203.
Sene, K.J., Plinston, D.T., 1994. A review and update of the hydrology of Lake Victoria in East Africa. Hydrol. Sci. J. 39, 47–63. https://doi.org/10.1080/02626669409492719
Sereno, P.C., Garcea, E.A.A., Jousse, H., Stojanowski, C.M., Saliège, J.-F., Maga, A., Ide, O.A., Knudson, K.J., Mercuri, A.M., Stafford, T.W., Jr., Kaye, T.G., Giraudi, C., N'siala, I.M., Cocca, E., Moots, H.M., Dutheil, D.B., Stivers, J.P., 2008. Lakeside Cemeteries in the Sahara: 5000 Years of Holocene Population and Environmental Change. PLOS ONE 3, e2995. https://doi.org/10.1371/journal.pone.0002995
Servant, M., Servant-Vildary, S., 1980. L'environnement quaternaire du bassin du Tchad. Sahara Nile 133, 162.
Sessions, A.L., Burgoyne, T.W., Schimmelmann, A., Hayes, J.M., 1999. Fractionation of hydrogen isotopes in lipid biosynthesis. Org. Geochem. 30, 1193–1200. https://doi.org/10.1016/S0146-6380(99)00094-7
Shanahan, T.M., McKay, N.P., Hughen, K.A., Overpeck, J.T., Otto-Bliesner, B., Heil, C.W., King, J., Scholz, C.A., Peck, J., 2015. The time-transgressive termination of the African

Humid Period. Nat. Geosci. 8, 140–144.
Shanahan, T.M., Overpeck, J.T., Sharp, W.E., Scholz, C.A., Arko, J.A., 2007. Simulating the response of a closed-basin lake to recent climate changes in tropical West Africa (Lake Bosumtwi, Ghana). Hydrol. Process. 21, 1678–1691. https://doi.org/10.1002/hyp.6359
Shanahan, T.M., Overpeck, J.T., Wheeler, C.W., Beck, J.W., Pigati, J.S., Talbot, M.R., Scholz, C.A., Peck, J., King, J.W., 2006. Paleoclimatic variations in West Africa from a record of late Pleistocene and Holocene lake level stands of Lake Bosumtwi, Ghana. Palaeogeogr. Palaeoclimatol. Palaeoecol. 242, 287–302. https://doi.org/10.1016/j.palaeo.2006.06.007
Shimamura, T., Momose, K., 2007. Reciprocal interactions between carbon storage function and plant species diversity in a tropical peat swamp forest. Asian Afr. Area Stud. 6, 279–296.
Sigurdsson, H., Devine, J.D., Tchua, F.M., Presser, F.M., Pringle, M.K.W., Evans, W.C., 1987. Origin of the lethal gas burst from Lake Monoun, Cameroun. J. Volcanol. Geotherm. Res. 31, 1–16. https://doi.org/10.1016/0377-0273(87)90002-3
Singarayer, J.S., Valdes, P.J., Friedlingstein, P., Nelson, S., Beerling, D.J., 2011. Late Holocene methane rise caused by orbitally controlled increase in tropical sources. Nature 470, 82–85. https://doi.org/10.1038/nature09739
Sinninghe Damsté, J.S., Hopmans, E.C., Pancost, R.D., Schouten, S., Geenevasen, J.A., 2000. Newly discovered non-isoprenoid glycerol dialkyl glycerol tetraether lipids in sediments. Chem. Commun. 1683–1684.
Sinninghe Damsté, J.S., Rijpstra, W.I.C., Foesel, B.U., Huber, K.J., Overmann, J., Nakagawa, S., Kim, J.J., Dunfield, P.F., Dedysh, S.N., Villanueva, L., 2018. An overview of the occurrence of ether- and ester-linked iso-diabolic acid membrane lipids in microbial cultures of the Acidobacteria: Implications for brGDGT paleoproxies for temperature and pH. Org. Geochem. 124, 63–76. https://doi.org/10.1016/j.orggeochem.2018.07.006
Sinninghe Damsté, J.S., Rijpstra, W.I.C., Hopmans, E.C., Foesel, B.U., Wüst, P.K., Overmann, J., Tank, M., Bryant, D.A., Dunfield, P.F., Houghton, K., Stott, M.B., 2014. Ether- and Ester-Bound iso-Diabolic Acid and Other Lipids in Members of Acidobacteria Subdivision 4. Appl. Environ. Microbiol. 80, 5207–5218. https://doi.org/10.1128/AEM.01066-14
Sinninghe Damsté, J.S., Rijpstra, W.I.C., Hopmans, E.C., Weijers, J.W.H., Foesel, B.U., Overmann, J., Dedysh, S.N., 2011. 13,16-Dimethyl Octacosanedioic Acid (iso-Diabolic Acid), a Common Membrane-Spanning Lipid of Acidobacteria Subdivisions 1 and 3. Appl. Environ. Microbiol. 77, 4147–4154. https://doi.org/10.1128/AEM.00466-11
Sinninghe Damsté, J.S., Van Duin, A.C.T., Hollander, D., Kohnen, M.E.L., De Leeuw, J.W., 1995. Early diagenesis of bacteriohopanepolyol derivatives: Formation of fossil homohopanoids. Geochim. Cosmochim. Acta 59, 5141–5157. https://doi.org/10.1016/0016-7037(95)00338-X
Skonieczny, C., Paillou, P., Bory, A., Bayon, G., Biscara, L., Crosta, X., Eynaud, F., Malaizé, B., Revel, M., Aleman, N., Barusseau, J.-P., Vernet, R., Lopez, S., Grousset, F., 2015. African humid periods triggered the reactivation of a large river system in Western Sahara. Nat. Commun. 6, 8751. https://doi.org/10.1038/ncomms9751
Skrzypek, G., Jezierski, P., Szynkiewicz, A., 2010. Preservation of primary stable isotope signatures of peat-forming plants during early decomposition—observation along an

altitudinal transect. Chem. Geol. 273, 238–249.
Smith, F.A., Freeman, K.H., 2006. Influence of physiology and climate on δD of leaf wax n-alkanes from C3 and C4 grasses. Geochim. Cosmochim. Acta 70, 1172–1187. https://doi.org/10.1016/j.gca.2005.11.006
Smittenberg, R.H., Baas, M., Schouten, S., Damste, J.S.S., 2005. The demise of the alga Botryococcus braunii from a Norwegian fjord was due to early eutrophication. The Holocene 15, 133–140. https://doi.org/10.1191/0959683605hl786rp
Stout, S.A., 1992. Aliphatic and aromatic triterpenoid hydrocarbons in a Tertiary angiospermous lignite. Org. Geochem. 18, 51–66. https://doi.org/10.1016/0146-6380(92)90143-L
Strack, M., Waddington, J.M., Tuittila, E.-S., 2004. Effect of water table drawdown on northern peatland methane dynamics: Implications for climate change. Glob. Biogeochem. Cycles 18. https://doi.org/10.1029/2003GB002209
Street-Perrott, F.A., Marchand, D.S., Roberts, N., Harrison, S.P., 1989. Global lake-level variations from 18,000 to 0 years ago: A palaeoclimate analysis. United States. https://doi.org/10.2172/5609291
Strobel, P., Kasper, T., Frenzel, P., Schittek, K., Quick, L., Meadows, M., Mäusbacher, R., Haberzettl, T., 2019. Late Quaternary palaeoenvironmental change in the year-round rainfall zone of South Africa derived from peat sediments from Vankervelsvlei. Quat. Sci. Rev. 218, 200–214.
Sukumar, R., Ramesh, R., Pant, R., Rajagopalan, G., 1993. A ^{13}C record of late Quaternary climate change from tropical peats in southern India. Nature 364, 703–706.
Sultan, B., Janicot, S., 2000. Abrupt shift of the ITCZ over West Africa and intra-seasonal variability. Geophys. Res. Lett. 27, 3353–3356. https://doi.org/10.1029/1999GL011285
Sun, Q., Chu, G., Liu, M., Xie, M., Li, S., Ling, Y., Wang, X., Shi, L., Jia, G., Lü, H., 2011. Distributions and temperature dependence of branched glycerol dialkyl glycerol tetraethers in recent lacustrine sediments from China and Nepal. J. Geophys. Res. Biogeosciences 116. https://doi.org/10.1029/2010JG001365
Talbot, M.R., Delibrias, G., 1977. Holocene variations in the level of Lake Bosumtwi, Ghana. Nature 268, 722–724. https://doi.org/10.1038/268722a0
Talbot, M.R., Johannessen, T., 1992. A high resolution palaeoclimatic record for the last 27,500 years in tropical West Africa from the carbon and nitrogen isotopic composition of lacustrine organic matter. Earth Planet. Sci. Lett. 110, 23–37.
Talbot, M.R., Livingstone, D.A., Palmer, P.G., Maley, J., Melack, J.M., Delibrias, G., Gulliksen, S., 1984. Preliminary results from sediment cores from Lake Bosumtwi, Ghana, in: Palaeoecology of Africa. Routledge, pp. 173–192.
Tanyileke, G., Ntchantcho, R., Fantong, W.Y., Aka, F.T., Hell, J.V., 2019. 30 years of the Lakes Nyos and Monoun gas disasters: A scientific, technological, institutional and social adventure. J. Afr. Earth Sci. 150, 415–424. https://doi.org/10.1016/j.jafrearsci.2018.11.022
Teller, J.T., Leverington, D.W., 2004. Glacial Lake Agassiz: A 5000 yr history of change and its relationship to the δ18O record of Greenland. GSA Bull. 116, 729–742. https://doi.org/10.1130/B25316.1
ten Haven, H.L., Peakman, T.M., Rullkötter, J., 1992. Early diagenetic transformation of higher-plant triterpenoids in deep-sea sediments from Baffin Bay. Geochim.

Cosmochim. Acta 56, 2001–2024. https://doi.org/10.1016/0016-7037(92)90326-E
Thauer, R.K., 1998. Biochemistry of methanogenesis: a tribute to Marjory Stephenson:1998 Marjory Stephenson Prize Lecture. Microbiology,.
Thompson, A.J., Tabor, C.R., Poulsen, C.J., Skinner, C.B., 2021. Water isotopic constraints on the enhancement of the mid-Holocene West African monsoon. Earth Planet. Sci. Lett. 554, 116677. https://doi.org/10.1016/j.epsl.2020.116677
Thompson, K., Hamilton, A.C., 1983. Peatland and Swamps of the African Continent. Gore AJP. Mires: Swamp, Bog, Fen and Moor, B: Regional Studies. Elsevier, Amsterdam.
Thompson, K., Shewry, P.R., Woolhouse, H.W., 1979. Papyrus swamp development in the Upemba Basin, Zaïre: studies of population structure in Cyperus papyrus stands. Bot. J. Linn. Soc. 78, 299–316. https://doi.org/10.1111/j.1095-8339.1979.tb02573.x
Thompson, L.G., Mosley-Thompson, E., Davis, M.E., Henderson, K.A., Brecher, H.H., Zagorodnov, V.S., Mashiotta, T.A., Lin, P.-N., Mikhalenko, V.N., Hardy, D.R., Beer, J., 2002. Kilimanjaro Ice Core Records: Evidence of Holocene Climate Change in Tropical Africa. Science 298, 589–593. https://doi.org/10.1126/science.1073198
Tierney, J.E., deMenocal, P.B., 2013. Abrupt Shifts in Horn of Africa Hydroclimate Since the Last Glacial Maximum. Science 342, 843–846. https://doi.org/10.1126/science.1240411
Tierney, J.E., deMenocal, P.B., Zander, P.D., 2017a. A climatic context for the out-of-Africa migration. Geology 45, 1023–1026. https://doi.org/10.1130/G39457.1
Tierney, J.E., Lewis, S.C., Cook, B.I., LeGrande, A.N., Schmidt, G.A., 2011a. Model, proxy and isotopic perspectives on the East African Humid Period. Earth Planet. Sci. Lett. 307, 103–112. https://doi.org/10.1016/j.epsl.2011.04.038
Tierney, J.E., Pausata, F.S.R., deMenocal, P.B., 2017b. Rainfall regimes of the Green Sahara. Sci. Adv. 3, e1601503. https://doi.org/10.1126/sciadv.1601503
Tierney, J.E., Russell, J.M., Huang, Y., 2010. A molecular perspective on Late Quaternary climate and vegetation change in the Lake Tanganyika basin, East Africa. Quat. Sci. Rev. 29, 787–800. https://doi.org/10.1016/j.quascirev.2009.11.030
Tierney, J.E., Russell, J.M., Huang, Y., Damsté, J.S.S., Hopmans, E.C., Cohen, A.S., 2008. Northern Hemisphere Controls on Tropical Southeast African Climate During the Past 60,000 Years. Science 322, 252–255. https://doi.org/10.1126/science.1160485
Tierney, J.E., Russell, J.M., Sinninghe Damsté, J.S., Huang, Y., Verschuren, D., 2011b. Late Quaternary behavior of the East African monsoon and the importance of the Congo Air Boundary. Quat. Sci. Rev. 30, 798–807. https://doi.org/10.1016/j.quascirev.2011.01.017
Timmermann, A., Oberhuber, J., Bacher, A., Esch, M., Latif, M., Roeckner, E., 1999. Increased El Niño frequency in a climate model forced by future greenhouse warming. Nature 398, 694–697. https://doi.org/10.1038/19505
Tinner, W., Lotter, A.F., 2001. Central European vegetation response to abrupt climate change at 8.2 ka. Geology 29, 551–554. https://doi.org/10.1130/0091-7613(2001)029<0551:CEVRTA>2.0.CO;2
Tipple, B.J., Berke, M.A., Doman, C.E., Khachaturyan, S., Ehleringer, J.R., 2013. Leaf-wax n-alkanes record the plant–water environment at leaf flush. Proc. Natl. Acad. Sci. 110, 2659–2664. https://doi.org/10.1073/pnas.1213875110
Too, C.C., Keller, A., Sickel, W., Lee, S.M., Yule, C.M., 2018. Microbial community structure in a Malaysian tropical peat swamp forest: the influence of tree species and depth. Front. Microbiol. 9, 2859.

Tossou, M.G., Akoègninou, A., Ballouche, A., Sowunmi, M.A., Akpagana, K., 2008. The history of the mangrove vegetation in Bénin during the Holocene: A palynological study. J. Afr. Earth Sci. 52, 167–174. https://doi.org/10.1016/j.jafrearsci.2008.07.007

Toth, L.T., Aronson, R.B., 2019. The 4.2 ka event, ENSO, and coral reef development. Clim Past 15, 105–119. https://doi.org/10.5194/cp-15-105-2019

Trendel, J.M., Lohmann, F., Kintzinger, J.P., Albrecht, P., Chiarone, A., Riche, C., Cesario, M., Guilhem, J., Pascard, C., 1989. Identification of des-A-triterpenoid hydrocarbons occurring in surface sediments. Tetrahedron 45, 4457–4470. https://doi.org/10.1016/S0040-4020(01)89081-5

Tripathi, B.M., Song, W., Slik, J.W.F., Sukri, R.S., Jaafar, S., Dong, K., Adams, J.M., 2016. Distinctive Tropical Forest Variants Have Unique Soil Microbial Communities, But Not Always Low Microbial Diversity. Front. Microbiol. 7.

Turetsky, M.R., Benscoter, B., Page, S., Rein, G., van der Werf, G.R., Watts, A., 2015. Global vulnerability of peatlands to fire and carbon loss. Nat. Geosci. 8, 11–14. https://doi.org/10.1038/ngeo2325

Turner, B.F., Gardner, L.R., Sharp, W.E., 1996. The hydrology of Lake Bosumtwi, a climate-sensitive lake in Ghana, West Africa. J. Hydrol. 183, 243–261. https://doi.org/10.1016/0022-1694(95)02982-6

Upton, A., Vane, C.H., Girkin, N., Turner, B.L., Sjögersten, S., 2018. Does litter input determine carbon storage and peat organic chemistry in tropical peatlands? Geoderma 326, 76–87.

Vago, J.L., Westall, F., Pasteur Instrument Teams, L.S.S.W.G., and Other Contributors, Coates, A.J., Jaumann, R., Korablev, O., Ciarletti, V., Mitrofanov, I., Josset, J.-L., De Sanctis, M.C., Bibring, J.-P., Rull, F., Goesmann, F., Steininger, H., Goetz, W., Brinckerhoff, W., Szopa, C., Raulin, F., Westall, F., Edwards, H.G.M., Whyte, L.G., Fairén, A.G., Bibring, J.-P., Bridges, J., Hauber, E., Ori, G.G., Werner, S., Loizeau, D., Kuzmin, R.O., Williams, R.M.E., Flahaut, J., Forget, F., Vago, J.L., Rodionov, D., Korablev, O., Svedhem, H., Sefton-Nash, E., Kminek, G., Lorenzoni, L., Joudrier, L., Mikhailov, V., Zashchirinskiy, A., Alexashkin, S., Calantropio, F., Merlo, A., Poulakis, P., Witasse, O., Bayle, O., Bayón, S., Meierhenrich, U., Carter, J., García-Ruiz, J.M., Baglioni, P., Haldemann, A., Ball, A.J., Debus, A., Lindner, R., Haessig, F., Monteiro, D., Trautner, R., Voland, C., Rebeyre, P., Goulty, D., Didot, F., Durrant, S., Zekri, E., Koschny, D., Toni, A., Visentin, G., Zwick, M., van Winnendael, M., Azkarate, M., Carreau, C., the ExoMars Project Team, 2017. Habitability on Early Mars and the Search for Biosignatures with the ExoMars Rover. Astrobiology 17, 471–510. https://doi.org/10.1089/ast.2016.1533

van Bree, L.G.J., Rijpstra, W.I.C., Al-Dhabi, N.A., Verschuren, D., Sinninghe Damsté, J.S., de Leeuw, J.W., 2016. Des-A-lupane in an East African lake sedimentary record as a new proxy for the stable carbon isotopic composition of C3 plants. Org. Geochem. 101, 132–139. https://doi.org/10.1016/j.orggeochem.2016.09.003

van der Lubbe, H.J.L., Krause-Nehring, J., Junginger, A., Garcin, Y., Joordens, J.C.A., Davies, G.R., Beck, C., Feibel, C.S., Johnson, T.C., Vonhof, H.B., 2017. Gradual or abrupt? Changes in water source of Lake Turkana (Kenya) during the African Humid Period inferred from Sr isotope ratios. Quat. Sci. Rev. 174, 1–12. https://doi.org/10.1016/j.quascirev.2017.08.010

van Schaik, C.P., Terborgh, J.W., Wright, S.J., 1993. The Phenology of Tropical Forests: Adaptive Significance and Consequences for Primary Consumers. Annu. Rev. Ecol. Syst. 24, 353–377. https://doi.org/10.1146/annurev.es.24.110193.002033

van Winden, J.F., Reichart, G.-J., McNamara, N.P., Benthien, A., Damsté, J.S.Sinninghe., 2012. Temperature-Induced Increase in Methane Release from Peat Bogs: A Mesocosm Experiment. PLOS ONE 7, e39614. https://doi.org/10.1371/journal.pone.0039614
Véquaud, P., Thibault, A., Derenne, S., Anquetil, C., Collin, S., Contreras, S., Nottingham, A.T., Sabatier, P., Werne, J.P., Huguet, A., 2022. FROG: A global machine-learning temperature calibration for branched GDGTs in soils and peats. Geochim. Cosmochim. Acta 318, 468–494. https://doi.org/10.1016/j.gca.2021.12.007
Vincens, A., Buchet, G., Servant, M., and ECOFIT Mbalang collaborators, 2010. Vegetation response to the "African Humid Period" termination in Central Cameroon (7° N)–new pollen insight from Lake Mbalang. Clim. Past 6, 281–294.
Vincens, A., Schwartz, D., Bertaux, J., Elenga, H., de Namur, C., 1998. Late Holocene Climatic Changes in Western Equatorial Africa Inferred from Pollen from Lake Sinnda, Southern Congo. Quat. Res. 50, 34–45. https://doi.org/10.1006/qres.1998.1979
Vinçon-Laugier, A., Cravo-Laureau, C., Mitteau, I., Grossi, V., 2017. Temperature-Dependent Alkyl Glycerol Ether Lipid Composition of Mesophilic and Thermophilic Sulfate-Reducing Bacteria. Front. Microbiol. 8.
Vinther, B.M., Clausen, H.B., Johnsen, S.J., Rasmussen, S.O., Andersen, K.K., Buchardt, S.L., Dahl-Jensen, D., Seierstad, I.K., Siggaard-Andersen, M.-L., Steffensen, J.P., Svensson, A., Olsen, J., Heinemeier, J., 2006. A synchronized dating of three Greenland ice cores throughout the Holocene. J. Geophys. Res. Atmospheres 111. https://doi.org/10.1029/2005JD006921
Vogts, A., Moossen, H., Rommerskirchen, F., Rullkötter, J., 2009. Distribution patterns and stable carbon isotopic composition of alkanes and alkan-1-ols from plant waxes of African rain forest and savanna C3 species. Org. Geochem. 40, 1037–1054. https://doi.org/10.1016/j.orggeochem.2009.07.011
Vogts, A., Schefuß, E., Badewien, T., Rullkötter, J., 2012. n-Alkane parameters from a deep sea sediment transect off southwest Africa reflect continental vegetation and climate conditions. Org. Geochem. 47, 109–119. https://doi.org/10.1016/j.orggeochem.2012.03.011
Volkman, J.K., Barrett, S.M., Blackburn, S.I., Mansour, M.P., Sikes, E.L., Gelin, F., 1998. Microalgal biomarkers: A review of recent research developments. Org. Geochem. 29, 1163–1179. https://doi.org/10.1016/S0146-6380(98)00062-X
Von Grafenstein, U., Erlenkeuser, H., Brauer, A., Jouzel, J., Johnsen, S.J., 1999. A Mid-European Decadal Isotope-Climate Record from 15,500 to 5000 Years B.P. Science 284, 1654–1657. https://doi.org/10.1126/science.284.5420.1654
von Wettstein-Knowles, P., 1979. Genetics and biosynthesis of plant epicuticular waxes. Adv. Biochem. Physiol. Plant Lipids 1–26.
Wake, L.V., Hillen, L.W., 1980. Study of a "bloom" of the oil-rich alga Botryococcus braunii in the Darwin River Reservoir. Biotechnol. Bioeng. 22, 1637–1656. https://doi.org/10.1002/bit.260220808
Waldrop, M.P., Firestone, M.K., 2006. Response of Microbial Community Composition and Function to Soil Climate Change. Microb. Ecol. 52, 716–724. https://doi.org/10.1007/s00248-006-9103-3
Wang, G., Alo, C.A., 2012. Changes in Precipitation Seasonality in West Africa Predicted by RegCM3 and the Impact of Dynamic Vegetation Feedback. Int. J. Geophys. 2012, 597205. https://doi.org/10.1155/2012/597205
Wang, J.J., Dodla, S.K., DeLaune, R.D., 2015. Characteristics and Functions of Labile Organic

Carbon in Coastal Wetland Soils of the Mississippi River Deltaic Plain, in: Labile Organic Matter—Chemical Compositions, Function, and Significance in Soil and the Environment. John Wiley & Sons, Ltd, pp. 315–336.
Wang, M., Zheng, Z., Man, M., Hu, J., Gao, Q., 2017. Branched GDGT-based paleotemperature reconstruction of the last 30,000years in humid monsoon region of Southeast China. Chem. Geol. 463, 94–102. https://doi.org/10.1016/j.chemgeo.2017.05.014
Wang, X.-F., Yakir, D., 2000. Using stable isotopes of water in evapotranspiration studies. Hydrol. Process. 14, 1407–1421. https://doi.org/10.1002/1099-1085(20000615)14:8<1407::AID-HYP992>3.0.CO;2-K
Wang, Y.V., Larsen, T., Leduc, G., Andersen, N., Blanz, T., Schneider, R.R., 2013. What does leaf wax δD from a mixed C3/C4 vegetation region tell us? Hydrog. Isot. 111, 128–139. https://doi.org/10.1016/j.gca.2012.10.016
Wang, Z., Liu, S., Huang, C., Liu, Y., Bu, Z., 2017. Impact of land use change on profile distributions of organic carbon fractions in peat and mineral soils in Northeast China. Catena 152, 1–8.
Webb, T., 1986. Is vegetation in equilibrium with climate? How to interpret late-Quaternary pollen data. Vegetatio 67, 75–91. https://doi.org/10.1007/BF00037359
Weete, J.D., 1976. Algal and fungal waxes. Chem. Biochem. Nat. Waxes 349–418.
Wei, G., Xie, L., Sun, Y., Lu, Y., Liu, Y., 2012. Major and trace elements of a peat core from Yunnan, Southwest China: implications for paleoclimatic proxies. J. Asian Earth Sci. 58, 64–77.
Weijers, J.W., Schouten, S., Hopmans, E.C., Geenevasen, J.A., David, O.R., Coleman, J.M., Pancost, R.D., Sinninghe Damsté, J.S., 2006. Membrane lipids of mesophilic anaerobic bacteria thriving in peats have typical archaeal traits. Environ. Microbiol. 8, 648–657.
Weijers, J.W., Schouten, S., van der Linden, M., van Geel, B., Sinninghe Damsté, J.S., 2004. Water table related variations in the abundance of intact archaeal membrane lipids in a Swedish peat bog. FEMS Microbiol. Lett. 239, 51–56.
Weijers, J.W.H., Panoto, E., van Bleijswijk, J., Schouten, S., Rijpstra, W.I.C., Balk, M., Stams, A.J.M., Damsté, J.S.S., 2009. Constraints on the Biological Source(s) of the Orphan Branched Tetraether Membrane Lipids. Geomicrobiol. J. 26, 402–414. https://doi.org/10.1080/01490450902937293
Weijers, J.W.H., Schefuß, E., Schouten, S., Damsté, J.S.S., 2007a. Coupled Thermal and Hydrological Evolution of Tropical Africa over the Last Deglaciation. Science 315, 1701–1704. https://doi.org/10.1126/science.1138131
Weijers, J.W.H., Schouten, S., van den Donker, J.C., Hopmans, E.C., Sinninghe Damsté, J.S., 2007b. Environmental controls on bacterial tetraether membrane lipid distribution in soils. Geochim. Cosmochim. Acta 71, 703–713. https://doi.org/10.1016/j.gca.2006.10.003
Weijers, J.W.H., Steinmann, P., Hopmans, E.C., Schouten, S., Sinninghe Damsté, J.S., 2011. Bacterial tetraether membrane lipids in peat and coal: Testing the MBT–CBT temperature proxy for climate reconstruction. Org. Geochem. 42, 477–486. https://doi.org/10.1016/j.orggeochem.2011.03.013
Welander, P.V., Coleman, M.L., Sessions, A.L., Summons, R.E., Newman, D.K., 2010. Identification of a methylase required for 2-methylhopanoid production and implications for the interpretation of sedimentary hopanes. Proc. Natl. Acad. Sci. 107, 8537–8542. https://doi.org/10.1073/pnas.0912949107

Welander, P.V., Hunter, R.C., Zhang, L., Sessions, A.L., Summons, R.E., Newman, D.K., 2009. Hopanoids Play a Role in Membrane Integrity and pH Homeostasis in *Rhodopseudomonas palustris* TIE-1. J. Bacteriol. 191, 6145–6156. https://doi.org/10.1128/JB.00460-09

Westrich, J.T., Berner, R.A., 1984. The role of sedimentary organic matter in bacterial sulfate reduction: The G model tested 1. Limnol. Oceanogr. 29, 236–249.

Whiticar, M.J., 1999. Carbon and hydrogen isotope systematics of bacterial formation and oxidation of methane. Chem. Geol. 161, 291–314.

Wickens, G.E., 1975. Quaternary plant fossils from the Jebel Marra volcanic complex and their palaeoclimatic interpretation. Palaeogeogr. Palaeoclimatol. Palaeoecol. 17, 109–122. https://doi.org/10.1016/0031-0182(75)90049-8

Williams, R.T., Crawford, R.L., 1983. Microbial diversity of Minnesota peatlands. Microb. Ecol. 9, 201–214. https://doi.org/10.1007/BF02097737

Wilmshurst, J.M., McGlone, M.S., Leathwick, J.R., Newnham, R.M., 2007. A pre-deforestation pollen-climate calibration model for New Zealand and quantitative temperature reconstructions for the past 18 000 years BP. J. Quat. Sci. 22, 535–547. https://doi.org/10.1002/jqs.1135

Winsborough, C., Basiliko, N., 2010. Fungal and Bacterial Activity in Northern Peatlands. Geomicrobiol. J. 27, 315–320. https://doi.org/10.1080/01490450903424432

Woodhouse, A.D., Oung, J.-N., Philp, R.P., Weston, R.J., 1992. Triterpanes and ring-A degraded triterpanes as biomarkers characteristic of Tertiary oils derived from predominantly higher plant sources. Org. Geochem. 18, 23–31. https://doi.org/10.1016/0146-6380(92)90140-S

Wooller, M.J., Pohlman, J.W., Gaglioti, B.V., Langdon, P., Jones, M., Walter Anthony, K.M., Becker, K.W., Hinrichs, K.-U., Elvert, M., 2012. Reconstruction of past methane availability in an Arctic Alaska wetland indicates climate influenced methane release during the past ~12,000 years. J. Paleolimnol. 48, 27–42. https://doi.org/10.1007/s10933-012-9591-8

Wright, D.K., 2017. Humans as Agents in the Termination of the African Humid Period. Front. Earth Sci. 5.

Wright, E.L., Black, C.R., Cheesman, A.W., Drage, T., Large, D., Turner, B.L., Sjögersten, S., 2011. Contribution of subsurface peat to CO2 and CH4 fluxes in a neotropical peatland. Glob. Change Biol. 17, 2867–2881. https://doi.org/10.1111/j.1365-2486.2011.02448.x

Wright, S.J., 1996. Phenological Responses to Seasonality in Tropical Forest Plants, in: Mulkey, S.S., Chazdon, R.L., Smith, A.P. (Eds.), Tropical Forest Plant Ecophysiology. Springer US, Boston, MA, pp. 440–460. https://doi.org/10.1007/978-1-4613-1163-8_15

Wright, S.J., van Schaik, C.P., 1994. Light and the Phenology of Tropical Trees. Am. Nat. 143, 192–199. https://doi.org/10.1086/285600

Wynn-Williams, D.D., 1982. Simulation of seasonal changes in microbial activity of maritime antarctic peat. Soil Biol. Biochem. 14, 1–12. https://doi.org/10.1016/0038-0717(82)90069-4

Xiao, W., Xu, Y., Ding, S., Wang, Y., Zhang, X., Yang, H., Wang, G., Hou, J., 2015. Global calibration of a novel, branched GDGT-based soil pH proxy. Org. Geochem. 89–90, 56–60. https://doi.org/10.1016/j.orggeochem.2015.10.005

Xie, S., Nott, C.J., Avsejs, L.A., Maddy, D., Chambers, F.M., Evershed, R.P., 2004. Molecular

and isotopic stratigraphy in an ombrotrophic mire for paleoclimate reconstruction. Geochim. Cosmochim. Acta 68, 2849–2862. https://doi.org/10.1016/j.gca.2003.08.025

Yacoub, A.N., Sylvestre, F., Moussa, A., Hoelzmann, P., Alexandre, A., Dinies, M., Chalié, F., Vallet-Coulomb, C., Paillès, C., Darius, F., Sonzogni, C., Couapel, M., Mazur, J.-C., Kröpelin, S., 2023. The African Holocene Humid Period in the Tibesti mountains (central Sahara, Chad): Climate reconstruction inferred from fossil diatoms and their oxygen isotope composition. Quat. Sci. Rev. 308, 108099. https://doi.org/10.1016/j.quascirev.2023.108099

Yu, J.-H., O'Reilly, S.Y., Zhou, M.-F., Griffin, W.L., Wang, L., 2012. U–Pb geochronology and Hf–Nd isotopic geochemistry of the Badu Complex, Southeastern China: Implications for the Precambrian crustal evolution and paleogeography of the Cathaysia Block. Precambrian Geol. China 222–223, 424–449. https://doi.org/10.1016/j.precamres.2011.07.014

Yunana, D.A., Shittu, A.A., Ayuba, S., Bassah, E.J., Joshua, W.K., 2017. Climate change and lake water resources in Sub-Saharan Africa: case study of lake Chad and lake Victoria. Niger. J. Technol. 36, 648–654.

Zabolotneva, A.A., Shatova, O.P., Sadova, A.A., Shestopalov, A.V., Roumiantsev, S.A., 2022. An Overview of Alkylresorcinols Biological Properties and Effects. J. Nutr. Metab. 2022, 4667607. https://doi.org/10.1155/2022/4667607

Żarnowska, E.D., Żarnowski, R., Kozubek, A., 2000. Alkylresorcinols in Fruit Pulp and Leaves of Ginkgo biloba L. Zeitschrift für Naturforschung C 55, 881–885. https://doi.org/10.1515/znc-2000-11-1206

Zarnowski, R., Kozubek, A., Pietr, S.J., 1999. Effect of rye 5-n-alkylresorcinols on in vitro growth of phytopathogenic Fusarium and Rhizoctonia fungi. Bull. Pol. Acad. Sci. 47, 231–235.

Zarnowski, R., Suzuki, Y., Esumi, Y., Pietr, S.J., 2000. 5-n-Alkylresorcinols from the green microalga Apatococcus constipatus. Phytochemistry 55, 975–977. https://doi.org/10.1016/S0031-9422(00)00219-3

Zech, M., Zech, R., Rozanski, K., Gleixner, G., Zech, W., 2015. Do n-alkane biomarkers in soils/sediments reflect the δ2H isotopic composition of precipitation? A case study from Mt. Kilimanjaro and implications for paleoaltimetry and paleoclimate research. Isotopes Environ. Health Stud. 51, 508–524. https://doi.org/10.1080/10256016.2015.1058790

Zhang, C., Woodworth, P., Gu, G., 2006. The seasonal cycle in the lower troposphere over West Africa from sounding observations. Q. J. R. Meteorol. Soc. 132, 2559–2582. https://doi.org/10.1256/qj.06.23

Zhang, L., Wu, Z., Chen, J., Liu, D., Chen, P., 2022. Spatiotemporal patterns and drivers of net primary production in the terrestrial ecosystem of the Dajiuhu Basin, China, between 1990 and 2018. Ecol. Inform. 72, 101839. https://doi.org/10.1016/j.ecoinf.2022.101839

Zhang, Y., Huang, X., Wang, R., Naafs, B.D.A., 2020. The distribution of long-chain n-alkan-2-ones in peat can be used to infer past changes in pH. Chem. Geol. 544, 119622. https://doi.org/10.1016/j.chemgeo.2020.119622

Zhang, Y.G., Zhang, C.L., Liu, X.-L., Li, L., Hinrichs, K.-U., Noakes, J.E., 2011. Methane Index: A tetraether archaeal lipid biomarker indicator for detecting the instability of marine gas hydrates. Earth Planet. Sci. Lett. 307, 525–534.

https://doi.org/10.1016/j.epsl.2011.05.031
Zhao, B., Zhang, Y., Huang, X., Qiu, R., Zhang, Z., Meyers, P.A., 2018. Comparison of n-alkane molecular, carbon and hydrogen isotope compositions of different types of plants in the Dajiuhu peatland, central China. Org. Geochem. 124, 1–11. https://doi.org/10.1016/j.orggeochem.2018.07.008
Zheng, Y., Li, Q., Wang, Z., Naafs, B.D.A., Yu, X., Pancost, R.D., 2015. Peatland GDGT records of Holocene climatic and biogeochemical responses to the Asian Monsoon. Org. Geochem. 87, 86–95. https://doi.org/10.1016/j.orggeochem.2015.07.012
Zheng, Y., Singarayer, J.S., Cheng, P., Yu, X., Liu, Z., Valdes, P.J., Pancost, R.D., 2014. Holocene variations in peatland methane cycling associated with the Asian summer monsoon system. Nat. Commun. 5, 4631. https://doi.org/10.1038/ncomms5631
Zheng, Y., Zhou, W., Liu, Z., Chen, Q., Yu, X., Liu, X., 2010. Compositions of aliphatic des-A-triterpenes in the Hani peat deposit, Northeast China and its biological significance. Chin. Sci. Bull. 55, 2275–2281. https://doi.org/10.1007/s11434-010-3229-x
Zielhofer, C., von Suchodoletz, H., Fletcher, W.J., Schneider, B., Dietze, E., Schlegel, M., Schepanski, K., Weninger, B., Mischke, S., Mikdad, A., 2017. Millennial-scale fluctuations in Saharan dust supply across the decline of the African Humid Period. Quat. Sci. Rev. 171, 119–135. https://doi.org/10.1016/j.quascirev.2017.07.010

A. Appendix 1:

The following pages present the code used for the modeling in chapter 3 for TOC values, the same code is used for $\delta^{13}C$ and C/N after replacing the corresponding terms. The code needs to be adapted depending on the chosen form of the function. The moving average method was used in the chapter, but three methods were tested and are presented here.

```
import pandas as pd
import matplotlib.pyplot as plt
import numpy as np
import csv
from scipy.optimize import curve_fit

from sklearn.preprocessing import MinMaxScaler #For data normalization
import statsmodels.api as sm #For data smoothing (Lowess)
from scipy.signal import savgol_filter #For data smoothing (Sawitzky-Golay)

## Objective function
def function(x,a,b,c,d):
    return a*np.log(b*x+c)+d
def function2(x,a,b,c):
    return a*np.log(b*x)+c

## Entering the file and dataplot
fig = plt.figure()

print('Attention ! Your columns has to be named as age, depth, %C,...')
filename=input('What is your file name (/!\Dont forget the.csv) ?')

data=pd.read_csv(filename, delimiter=";")
data.plot.scatter(x='age', y='%C', marker='+') # for scatter point

print('Please, save and/or close figure files to continue')
plt.legend()
plt.show()

## Normalization (between 0 and 1) of the data
# Normalization of y-data
minmaxscale = MinMaxScaler().fit(data['%C'].values.reshape(-1,1))
data['%Cstd']=minmaxscale.transform(data['%C'].values.reshape(-1,1))
# Normalization of x-data
minmaxscale = MinMaxScaler().fit(data['age'].values.reshape(-1,1))
data['agestd']=minmaxscale.transform(data['age'].values.reshape(-1,1))
data['agestd']=data['agestd']+0.001

## Curve fit - normalized data
fig2 = plt.figure()
data.plot.scatter(x='agestd', y='%Cstd', marker='+') # for scatter point
Column_agestd = data.columns.get_loc("agestd") #Finding the right columns for the age
Column_percentC = data.columns.get_loc("%Cstd") #Finding the right columns for the percentC
datav=data.to_numpy()

#Based on whole dataset
xdata0=datav[:,Column_agestd]
ydata0=datav[:,Column_percentC]
```

```
xdata0=np.array(xdata0, dtype=[('O', float)]).astype(float) # in case the values are not considered as float by default
ydata0=np.array(ydata0, dtype=[('O', float)]).astype(float)

# Estimating optimizing parameters #if needed if encountering the error "Optimal parameters not found: Number of calls to function has reached maxfev = 800" or possibility to change the "maxfev" parameter
a0=ydata0[0]
amax=max(ydata0)
th=xdata0[np.searchsorted(-ydata0+a0, -0.5*amax)]
b0 = np.log(2)/th

popt, _ = curve_fit(function, xdata0, ydata0, p0=(a0,b0,0,0))
#popt, _ = curve_fit(function, xdata0, ydata0)
#popt, _ = curve_fit(function2, xdata0, ydata0)
a, b, c ,d= popt
#a, b, c = popt

print('y=%.5f*np.log(%.5f*x+%.5f)+%.5f'%(a,b,c,d))
#print('y=%.5f*np.log(%.5f*x)+%.5f'%(a,b,c))

residuals0 = ydata0- function(xdata0, *popt) # for r2 calculation
#residuals0 = ydata0- function2(xdata0, *popt) # for r2 calculation

ss_res0 = np.sum(residuals0**2)
ss_tot0 = np.sum((ydata0-np.mean(ydata0))**2)
r_squared0 = 1 - (ss_res0 / ss_tot0)
print(r_squared0)

poptr2 = (a, b, c , d, r_squared0) # list for the legend
#poptr2 = (a, b, c , r_squared0) # list for the legend

plt.plot(xdata0, function(xdata0, *popt), 'r--',label='f(x)=%5.3f*ln(%5.3f*x+%.5f) + %5.3f, r\u00B2=%5.3f' % tuple(poptr2), linewidth=3)
#plt.plot(xdata0, function2(xdata0, *popt), 'r--',label='f(x)=%5.3f*ln(%5.3f*x) + %5.3f, r\u00B2=%5.3f' % tuple(poptr2), linewidth=3)

#Based on data with f'(x)>1
max_age = abs((a*b-c)/b) # Finding the age corresponding to f'(x)>1 – function 1
#max_age = abs(a) # Finding the age corresponding to f'(x)>1 – function 2
line_max_age = 0
while xdata0[line_max_age] <= max_age : #Finding the corresponding line
   line_max_age = line_max_age + 1
xdata1=datav[0:line_max_age,Column_agestd] #Selecting only these lines in the dataset
ydata1=datav[0:line_max_age,Column_percentC]

# Estimating optimizing parameters #if needed if encountering the error "Optimal parameters not found: Number of calls to function has reached maxfev = 800" or possibility to change the "maxfev" parameter
b0=0.5**((ydata0[1]-ydata0[0])/(ydata0[1]-ydata0[2])) #Using the 3 first lines to estimate a, b and c, considering d=0
a0=(ydata0[1]-ydata0[2])/np.log(1/2)
#c0=ydata0[0]/a0
#or c0=ydata0[0] #depending on what is working the best

popt, _ = curve_fit(function2, xdata1, ydata1, p0=(a0,b0,0))
#popt, _ = curve_fit(function, xdata1, ydata1)
#popt, _ = curve_fit(function2, xdata1, ydata1)
```

```
a, b, c, d= popt
#a, b, c= popt

print('y=%.5f*np.log(%.5f*x+%.5f)+%.5f'%(a,b,c,d))
#print('y=%.5f*np.log(%.5f*x)+%.5f'%(a,b,c))

residuals1 = ydata1- function(xdata1, *popt) # for r2 calculation
#residuals1 = ydata1- function2(xdata1, *popt) # for r2 calculation
ss_res1 = np.sum(residuals1**2)
ss_tot1 = np.sum((ydata1-np.mean(ydata1))**2)
r_squared1 = 1 - (ss_res1 / ss_tot1)
print(r_squared1)

residuals1 = ydata0- function(xdata0, *popt) # for r2 calculation
#residuals1 = ydata0- function2(xdata0, *popt) # for r2 calculation
ss_res1 = np.sum(residuals1**2)
ss_tot1 = np.sum((ydata0-np.mean(ydata0))**2)
r_squared1 = 1 - (ss_res1 / ss_tot1)
print(r_squared1)


poptr2 = (a, b, c, d, r_squared1) # list for the legend
#poptr2 = (a, b, c, r_squared1) # list for the legend

plt.plot(xdata0, function(xdata0, *popt), 'g-.',label='f(x)=%5.3f*ln(%5.3f*x+%.5f) +%5.3f, r\u00B2=%5.3f' %
tuple(poptr2), linewidth=3)
#plt.plot(xdata0, function2(xdata0, *popt), 'g-.',label='f(x)=%5.3f*ln(%5.3f*x) +%5.3f, r\u00B2=%5.3f' %
tuple(poptr2), linewidth=3)

print('Please, save and/or close figure files to continue')

plt.legend()
plt.show()

## Correction

#data['corr%Cstd']=data['%Cstd']-a*np.log(b*data['agestd']+c)-d
data['corr%Cstd']=data['%Cstd']-a*np.log(b*data['agestd'])-c

fig3 = plt.figure()
#data.plot.line(x='agestd', y='corr%Cstd', label='data', style='--+', linewidth=3) # for scatter point with dashed
line
data.plot.line(x='agestd', y='corr%Cstd', style='--+') # for scatter point with dashed line

#data.plot.scatter(x='agestd', y='corr%Cstd', label='Normalized data', marker='+', s=40) # for scatter point
 # for scatter point // data.plot(x='agestd', y='corr%Cstd') # for solid line
print(data['corr%Cstd'])
print('Please, save and/or close figure files to continue')
plt.show()

## Datasmoothing
fig4 = plt.figure()
data.plot.line(x='age', y='corr%Cstd', label='data', style='+') # for scatter point with dashed line

# LOWESS method
lowess = sm.nonparametric.lowess(data['corr%Cstd'], data['age'], frac=0.1)
data['lowess']=lowess[:,1]
```

```
plt.plot(lowess[:, 0], lowess[:, 1], 'g-', label='Lowess method')

# Moving average box by convolution
datav=data.to_numpy()
Column_percentCcorr = data.columns.get_loc("corr%Cstd") #Finding the right columns for the percentC

def smooth(y, box_pts): #The higher box_pts is, the smoother the signal is
    box = np.ones(box_pts)/box_pts
    y_smooth = np.convolve(y, box, mode='same')
    return y_smooth

plt.plot(datav[:,Column_age], smooth(datav[:,Column_percentCcorr],2), 'b-', label='Moving average box by
convolution')
plt.plot(datav[:,Column_age], smooth(datav[:,Column_percentCcorr],3), 'r-', label='Moving average box by
convolution')

data['movingaverage2']=smooth(datav[:,Column_percentCcorr],2)
data['movingaverage3']=smooth(datav[:,Column_percentCcorr],3)

# Savitzky-Golay method
window_size = 11
ysavit = savgol_filter(data['corr%Cstd'], window_size, 5) # window size must be odd, polynomial order 5
plt.plot(datav[:,Column_age], ysavit, label='Savitzky-Golay method')
data['SGw11poly5']=ysavit

filename=input('How do you want to name your file (Don\'t forger the .csv) ')
data.to_csv(filename, sep=';')

plt.legend()
plt.title('Smoothing')
plt.show()
```